



저작자표시-비영리-변경금지 2.0 대한민국

이용자는 아래의 조건을 따르는 경우에 한하여 자유롭게

- 이 저작물을 복제, 배포, 전송, 전시, 공연 및 방송할 수 있습니다.

다음과 같은 조건을 따라야 합니다:



저작자표시. 귀하는 원저작자를 표시하여야 합니다.



비영리. 귀하는 이 저작물을 영리 목적으로 이용할 수 없습니다.



변경금지. 귀하는 이 저작물을 개작, 변형 또는 가공할 수 없습니다.

- 귀하는, 이 저작물의 재이용이나 배포의 경우, 이 저작물에 적용된 이용허락조건을 명확하게 나타내어야 합니다.
- 저작권자로부터 별도의 허가를 받으면 이러한 조건들은 적용되지 않습니다.

저작권법에 따른 이용자의 권리는 위의 내용에 의하여 영향을 받지 않습니다.

이것은 [이용허락규약\(Legal Code\)](#)을 이해하기 쉽게 요약한 것입니다.

[Disclaimer](#)

공학박사 학위논문

Fine control of tyrosinase
dependent monophenol oxidation:
Production of catechol derivatives and
development of functional hydrogels

티로시나아제를 이용한 모노페놀류 산화반응의 정밀제어:
카테콜형 구조 물질 생산과 기능성 하이드로겔의 개발

2017년 8월

서울대학교 대학원
바이오엔지니어링 협동과정
이 상 혁

Fine control of tyrosinase dependent monophenol oxidation:

Production of catechol derivatives and
development of functional hydrogels

A Thesis

Submitted to the Faculty of Seoul National University

by

Sang-Hyuk Lee

In Partial Fulfillment of the Requirements
For the Degree of Doctor of Philosophy

Advisor: Professor Byung-Gee Kim, Ph. D.

August 2017

Interdisciplinary Program of Bioengineering
Seoul National University

Abstract

Fine control of tyrosinase dependent monophenol oxidation:

Production of catechol derivatives and
development of functional hydrogels

Sang-Hyuk Lee

Interdisciplinary Program of Bioengineering

The Graduated School of Engineering

Seoul National University

Tyrosinase, a type III copper containing polyphenol oxidase, is an essential enzyme that involves the synthesis of melanin, dark pigments found in most living organisms, for example, hairs of mammals and inks of cephalopods. The natural pigmentation is processed from small phenolic molecules, for instance, from one of the essential amino acids, L-tyrosine, via two different oxidative reactions of tyrosinase, which are consecutive and inseparable. Previous studies on this oxidase

are mainly focused on searching inhibitors of the pigmentation reactions for the purpose of skin whitening and prevention of fruit browning. However, not much effort has been exerted to guide how to control this enzyme for developing it as a highly valuable catalyst.

In this thesis, the two oxidative reactions of tyrosinase were studied intensively, and methodologies for shifting the three different states of tyrosinase (*deoxy*-tyrosinase, *oxy*-tyrosinase, and *met*-tyrosinase) and for controlling the inseparable two reactions (monophenolase and catecholase activity) were suggested. This thesis can be broadly divided into two themes in accordance with two applications depending on the types of the oxidation mechanisms. Simply put, one is inhibiting reactions related to the production of melanin by-product, and another is accelerating the reactions. The first theme, the selective inhibition, suggests universal instructions in the usage of tyrosinase in the regio-selective *ortho*-hydroxylation of monophenols to produce functional catechol derivatives, which are valuable in the markets of food additives, cosmetic ingredients, and even in the markets of fine drugs. And the second theme includes the fabricating methods of hydrogel from natural biomacromolecules and the development of it as sprayable/injectable sticky hydrogel for minimally invasive treatments.

The first theme is present in the three chapters of this thesis, Chapter 2, 3 and 4. These chapters are composed of a long journey of designing new reaction paths for inhibiting the second oxidation of tyrosinase, searching or constructing novel tyrosinases, and improving the yield and productivity of the production of *ortho*-hydroxylated monophenol phytochemicals, from the enzyme engineering in lab scale to the mass production up to 400 L reaction. As a result, approximately

1.2 kg of *ortho*-hydroxylated isoflavones, 3'-ODI and orobol, were successfully synthesized with $3.17 \text{ g}\cdot\text{L}^{-1}\cdot\text{h}^{-1}$ of productivity. The total yield (considering both conversion and recovery yield) for this reaction reached the theoretical values, over 99 %, and the products were extremely purely recovered with over 99% of purity. Furthermore, it was demonstrated that the methods could generally be applicable in hydroxylation of various phenolic phytochemicals such as phloretin, resveratrol, naringenin, apigenin, daidzin, polydatin, glycitin, genistin, etc.

Contrary to the previous chapters (Chapter 2, 3, and 4) that are for inhibiting the second oxidative reaction, Chapter 5 and 6 are comprised of the studies for accelerating the tyrosinase activity for enzymatic crosslinking of macromolecules. Previously, tyrosinase from *Agaricus bisporus* was generally utilized for the enzymatic crosslinking for preparing hydrogels because of easy availability; the mushroom tyrosinase is the only tyrosinase which is commercially available. However, the applications of tyrosinase from *A. bisporus* in enzymatic crosslinking have been limited due to the low degree of crosslinking as a result of the steric hindrances between tyrosinase and macromolecules. Through the studies for previous chapters, it was found that the tyrosinase from *Streptomyces avermitilis* has a flat surface that is evolved for binding to a helper protein. Thus, the new tyrosinase from *S. avermitilis* was brought up for resolving the steric hindrance when crosslinking macromolecules. In these chapters, the method for preparing the tyrosinase-mediated hydrogel (composed of porcine gelatin, hyaluronic acid, and elastin-like polypeptide) is present, which showed significantly increased mechanical properties regarding storage modulus (strength) and adhesion work (stickiness). Especially, the adhesion work of this stick

hydrogel made by gelatin and tyramine-conjugated hyaluronic acid was remarkable, which is $21.34 \text{ J}\cdot\text{m}^{-2}$, compared to previously studied catechol-conjugated polymers including mussel foot proteins, which in the range of 0.12 to $7 \text{ J}\cdot\text{m}^{-2}$.

Keywords: tyrosinase, monooxygenase, type III copper protein, *ortho*-hydroxylation, catechol derivatives, daidzein, 3'-*ortho*-dihydroxyisoflavone, enzymatic crosslinking, hydrogel

Student number: 2012-20934

Contents

Abstract	i
Contents	v
List of Tables	xi
List of Figures	xii
Chapter 1. Introduction	1
1.1 Mechanism of tyrosinase	2
1.1.1 Copper metalloproteins.....	2
1.1.2 The active site of tyrosinase and the structural comparison of type III copper-containing proteins.	5
1.1.3 Rate-determining step of tyrosinase reaction.....	12
1.1.4 Inhibitors of tyrosinase and the suicidal inactivation	17
1.2 Application of tyrosinases	21
1.2.1 Production of catechol derivatives.....	21
1.2.2 Tyrosinase as a crosslinking agent.....	28
1.2.3 Miscellaneous	31
1.2.3.1 Melanin synthesis and its usages	31
1.2.3.2 Waste water treatment	34
1.3 The scope of thesis	35
Chapter 2. Heterologous expression of tyrosinase (SAV1137) from <i>Streptomyces avermitilis</i> MA4680 in <i>Echerichia coli</i> and its application for <i>ortho</i>-hydroxylation of resveratrol to produce piceatannol.....	40
2.1 Abstract	41

2.2 Introduction	42
2.3 Materials and Methods	46
2.3.1 Materials	46
2.3.2 Construction of plasmids for the recombinant tyrosinase and a glucose dehydrogenase.	46
2.3.3 Expression and preparation of recombinant tyrosinase and glucose dehydrogenase (GDH) for reaction.	47
2.3.4 Constructing mutants of MelC1 and MelC2.....	48
2.3.5 Oxidation reaction of resveratrol in <i>E. coli</i>	48
2.3.6 Effects of NADH on the production of piceatannol through tyrosinase reaction.	49
2.3.7 Screening for mutants with high specificity in piceatannol production	51
2.3.8 Kinetics characterization of wild-type and I41Y on L-tyrosine, L-DOPA, resveratrol, and piceatannol.	55
2.3.9 Preparing samples for kinetic values of MelC2.....	55
2.3.10 Computational modeling	56
2.3.11 Analytical methods	57
2.4 Results and Discussion.....	63
2.4.1 Expression of tyrosinase, MelC2, in <i>E. coli</i>	63
2.4.2 Effect of NADH in the reaction system.....	65
2.4.3 Saturation mutagenesis of helper protein, MelC1 at Y91.....	68
2.4.5 Model prediction and characterization of mutants	77
2.5 Conclusion.....	84
Chapter 3. Using tyrosinase as a monophenol monooxygenase: a combined strategy for effective inhibition of melanin formation	87
3.1 Abstract	88
3.2 Introduction.....	90
3.3 Materials and Methods.....	95

3.3.1 Materials	95
3.3.2 Construction of plasmids for recombinant tyrosinases.....	95
3.3.3 Conditions for cell cultures and reactions	97
3.3.4 Computational modeling	98
3.3.5 Identification of products.....	98
3.4 Results and Discussion.....	100
3.4.1 Comparison of Tys from three different organisms for the <i>ortho</i> -hydroxylation of daidzein.....	100
3.4.2 Protecting the diol moiety of 3'-ODI by borate ester bonds.....	104
3.4.4 Whole cell biocatalysis of daidzein by BM_Ty to produce 3'-ODI	116
3.4.5 <i>ortho</i> -Hydroxylation of monophenols by tyrosinase.....	127
3.4.6 <i>ortho</i> -Hydroxylation of benzopyrone ring of isoflavones by tyrosinase; 6- and 8- hydroxylation.....	141
3.4.7 Calculation of k_1 and k_2 of BM_Ty on daidzein	149
3.4.8 Calculation of oxygen transfer rate and coefficient of the 5 mL reaction in a 50 mL reactor without additional oxygen transfer.....	154
3.4.9 Calculation of oxygen transfer rate and coefficient of the 400 mL reaction in a 1 L reactor with a continuous air flow rate of $12 \text{ L} \cdot \text{min}^{-1}$	155
3.4.10 Mass production of 3'-ODI and orobol	160
3.4.10.1 Enzyme expression for scale-up studies.	160
3.4.10.2 The optimization of the reaction conditions.....	164
3.4.10.3 The optimization of the purification of products.	170
3.4.10.4 Overall process of the mass production of catechol derivatives.	174
3.5 Conclusion.....	178
Chapter 4. A novel tyrosinase from <i>Burkholderia thailandensis</i> active active at acidic pH and its application for the <i>ortho</i>-hydroxylation of glyco-conjugated monophenolic phytochemicals	179
4.1 Abstract	180
4.2 Introduction	181

4.3 Materials and Methods	185
4.3.1 Materials	185
4.3.2 Construction of a cladogram of bacterial Tys	185
4.3.3 Plasmid construction.....	186
4.3.4 Expression and purification of tyrosinases	189
4.3.5 Purification of tyrosinase from <i>Agaricus bisporus</i> , mushroom tyrosinase	189
4.3.6 Measurement of tyrosinase activities.....	190
4.3.7 <i>ortho</i> -Hydroxylation of monophenol glycosides	191
4.3.8 HPLC and LC/MS analysis	191
4.4 Result and Discussion	193
4.4.1 Reactivity depending on pH and measurements of kinetic parameters. ...	193
4.4.2 <i>ortho</i> -Hydroxylation of monophenol phyrochemicals by BT_Ty.....	197
4.4.2.1 <i>ortho</i> -Hydroxylation of monophenol gycosides	197
4.4.2.2 <i>ortho</i> -Hydroxylation of monophenol aglycones	207
4.4.3 Structural analysis of BT_Ty	211
4.4.3.1 The morphology of BT_Ty based on the X-ray crystallography	211
4.4.3.2 Residues related to inter-interactions for maintaining the homo- tetrameric structure.	218
4.4.3.3 Residues related to intra-interactions between cap and body domains.	222
4.4.3.4 Identifying residues that enhance the Ty activity even at acidic pH. .	227
4.4 Conclusion.....	233
Chapter 5. Tissue adhesive, rapid forming, and sprayable ECM hydrogel via recombinant tyrosinase crosslinking	234
5.1 Abstract	235
5.2 Introduction.....	236
5.3 Materials and Methods.....	239

5.3.1 Materials	239
5.3.2 Preparation of enzymes.....	239
5.3.2.1 Expression and purification of recombinant tyrosinases.....	239
5.3.2.2 Purification of mushroom tyrosinase.	242
5.3.4 Measurement of the specific activity of tyrosinase.	243
5.3.5 Fabricating HG_gels.....	243
5.3.5.1 Synthesis of modified HA.....	243
5.3.5.2 Preparation of HG_gels.....	244
5.3.6 Characterization of the tyrosinase-mediated hydrogels.....	245
5.3.6.1 Measurement of the swelling ratio of hydrogels.....	245
5.3.6.2 Rheological analysis.	245
5.3.6.3 Evaluation of gelation time of HG_gel.....	246
5.3.6.4 Scanning electron microscopy (SEM) analysis.....	246
5.3.7 Biocompatibility and tissue adhesiveness.	247
5.3.7.1 Live/Dead assay.	247
5.3.7.2 Synthesis of fluorescein isothiocyanate (FITC) conjugated gelatin...247	
5.3.7.3 Immunofluorescence assay.	247
5.3.7.4 Adhesion test of HG_gel to mouse skin tissue <i>ex vivo</i>	248
5.3.7.5 Imaging HG_gels coated on Mouse Cardiac.	248
5.4 Results and Discussion.....	250
5.4.1 Structure of tyrosinase from <i>Streptomyces avermitilis</i>	250
5.4.2 The activities of tyrosinases from various organisms to macromolecules	253
5.4.3 Preparation of hydrogel	259
5.4.5 Swelling and in vitro degrading properties.....	264
5.4.6 The measurement of stickiness of HG_gel.....	270
5.4.7 Biocompatibility and the applications for organ coating	272
5.4.8 List of supplementary videos (Links to Google Drive).....	275
5.5 Conclusion.....	276
Chapter 6. Elastin-like polypeptide for fabricating functional hydrogel	277
6.1 Abstract	278

6.2 Introduction	279
6.3 Materials and Methods	282
6.3.1 Nomenclature.....	282
6.3.2 Construction of plasmids for expressing ELPs.....	282
6.3.3 Expression of ELP in <i>E. coli</i> and purification by ITC.....	286
6.3.4 Preparation of the ECM hydrogel, HGE_gel (HG_gel + ELP)	288
6.3.5 Hydroxylation of Tyr residue of VY24V20.....	288
6.3.6 Preparation of mussel mimicking ELP hydrogel	289
6.3.7 Synthesis of reduced graphene oxide (rGO).....	289
6.3.8 Preparation of rGO hydrogel and a thin rGO film.....	290
6.4 Results and Discussion.....	291
6.4.1 Expression and purification of ELPs.	291
6.4.2 VY24V20 as a crosslinker of ECM hydrogel, HG_gel	294
6.4.3 Introducing DOPA moiety into gelatin and VY24V20 for mimicking the mussel foot protein	297
6.4.4 Synthesis of rGO, and fabrication of rGO-ELP hydrogel.....	299
6.5 Conclusion.....	303
Chapter 7. Overall Conclusion.....	305
7.1 From the design of reaction paths to the mass production of functional catechol derivatives	306
7.2 Expanding the scope of target products and searching novel tyrosinase with different substrate specificity.....	311
7.3 Enzymatic crosslinking for fabricating hydrogels and polymerization for producing dark pigments.....	318
Reference.....	320
Abstract in Korean.....	339

List of Tables

Table 1.1. Summary of tyrosinase inhibitory activity of compounds.....	19
Table 2.1. Primer list for cloning SA_Ty and GDH.....	58
Table 2.2. The list of primers for mutants of MelC1.....	59
Table 2.3. The list of primers for mutants of MelC2.....	61
Table 2.4. Absorbance of melanin at 340 nm after induction of MelC2 and Y91 mutants of MelC1.	72
Table 2.5. Kinetics constants of wild type MelC2 and I41Y.....	73
Table 2.6. Result of site-saturated mutagenesis	76
Table 3.1. Primer list for cloning SA_Ty and BM_Ty	96
Table 3.2. Kinetic constants of tyrosinase from <i>B. megaterium</i> on daidzein.	103
Table 3.3. The effect of ascorbic acid on the reaction rate of tyrosinase.	115
Table 3.4. Reaction conditions.	126
Table 3.5. Measuring D.O. for calculating oxygen transfer rate of a 50 mL reactor.	156
Table 3.6. Measuring D.O. for calculating oxygen transfer rate of a 400 mL reactor.	157
Table 3.7. The composition of complex media used in this study.....	163
Table 4.1. The primer list for cloning tyrosinase from <i>Burkholderia thailandensis</i>	188
Table 4.2. Kinetic parameters of Tys.....	196
Table 5.1. A list of primers for cloning bacterial tyrosinases.....	241
Table 5.2. Identity and similarity matrix generated by pairwise alignment.	252
Table 6.1. Primer list for N-term head and C-term tail groups of ELP	284
Table 6.2. The list of ELPs expressed and purified in this study	293

List of Figures

Figure 1.1 General structures and characteristics of copper-containing proteins.....	4
Figure 1.2. The general reaction mechanism of tyrosinase.....	7
Figure 1.3. A resonance effect of arene ring with an electron-withdrawing group. ..	8
Figure 1.4. Imposed image of the oxygen binding pocket of type III copper proteins.	11
Figure 1.5. The movements of electrons in the monophenolase activity of Ty.....	14
Figure 1.6. The orbital configuration of Ty_{oxy} , $[Cu^{++}_2O_2]^{2+}$	15
Figure 1.7. Structure-supported deprotonation scenario.	16
Figure 1.8. The hypothetical paths for the suicidal inactivation.	20
Figure 1.9. The representative examples of functional catechol derivatives.....	22
Figure 1.10. The first commercial synthesis process of L-DOPA synthesis.	26
Figure 1.11. A schematic figure of repressing the catecholase activity.....	27
Figure 1.12. Mechanism of the enzymatic reaction mediated by tyrosinase, advantages and drawbacks.....	30
Figure 1.13. The brief structures of different types of melanin.....	33
Figure 1.15. The schematic figure of the two different themes of this thesis.	39
Figure 2.1. Schematic figure of the NADH regenerating system in piceatannol production by MelC2.....	45
Figure 2.2. The colorimetric assay method for screening mutants.....	53
Figure 2.3. Residues around the active site of MelC2.....	54
Figure 2.4. Assay of melanin formation.....	64
Figure 2.5. Concentration of piceatannol depending on the concentration of NADH.	66
Figure 2.6. Time profile of hydroxylation of 500 μ M resveratrol with or without the NADH regenerating system.....	67
Figure 2.7. Homology models of (a) MelC1 and (b) MelC2.	70
Figure 2.8. SDS-PAGE gel image of MelC2 expressed with Y91 mutants of MelC1.	

.....	71
Figure 2.9. Pymol images of homology models.....	79
Figure 2.10. Docking result of WT and I41Y on resveratrol and piceatannol.	80
Figure 2.11. Docking result of WT and I41Y on tyrosine and L-Dopa.....	82
Figure 2.12. The structure of wild type (I218) and I218S mutants of MelC2 were compared.....	83
Figure 3.1. Effective strategy for suppressing byproduct formation of the Ty reaction to selectively produce functional diphenols.....	94
Figure 3.2. Different tyrosinase activities for the <i>o</i> -hydroxylation of daidzein and docking simulation of each enzyme on daidzein.	102
Figure 3.3. HPLC data after 30 min of the Ty reaction with/without acid hydrolysis.	105
Figure 3.4. The concentration of 3'-ODI produced by tyrosinase from daidzein with various initial concentrations of boric acid.....	106
Figure 3.5. Auto-oxidation of 3'-ODI in buffer at pH 9.....	107
Figure 3.6. Effect of hydroxylamine and L-ascorbic acid (LAA) in the Ty reaction.	111
Figure 3.7. Rate changes depending on various concentrations of L-ascorbic acid.	113
Figure 3.8. Docking simulation of tyrosinase from <i>B. megaterium</i> (3NM8) with ascorbic acid.....	114
Figure 3.9. HPLC result of the Ty reaction for producing 3'-ODI.....	118
Figure 3.10. The time profile of the concentration of daidzein and 3'-ODI in the 400 mL fed-batch reaction.	119
Figure 3.11. ¹ HNMR analysis of the substrate (daidzein) and the product (3'-ODI).	123
Figure 3.12. GC/MS analysis of the product from daidzein.	125
Figure 3.13. HPLC analysis of the production of resveratrol (a) and genistein (b).	128
Figure 3.14. ¹ HNMR of the hydroxylated product from resveratrol.....	132
Figure 3.15. ¹ HNMR of the hydroxylated product from genistein.....	136
Figure 3.16. GC/MS analysis of the product from resveratrol.....	138

Figure 3.17. GC/MS analysis of the product from genistein.....	140
Figure 3.18. The physiological effects of catechol derivatives <i>ortho</i> -hydroxylated from daidzein	144
Figure 3.19. The suicide inactivation mechanism depending on the basicity of substrates.....	145
Figure 3.20. <i>ortho</i> -hydroxylation of formononetin to produce 6- or 8-hydroxylated isoflavones.	146
Figure 3.21. The full scan of the product after 20 hours of reaction.....	147
Figure 3.22. The fragmentation of 6-hydroxylated formononetin.	148
Figure 3.23. The simplified graph showing changes in the concentration of substrate, intermediate, and product.	151
Figure 3.24. An example for calculating k_1 and k_2	152
Figure 3.25. Plots for calculating k_1 and k_2	153
Figure 3.26. A graph for measuring $k_{v,l}$ of a 50 mL reactor.....	158
Figure 3.27. A graph for measuring $k_{v,l}$ of a 400 mL reactor.	159
Figure 3.28. Comparison of tyrosinase as different inducers, IPTG, and lactose.	161
Figure 3.29. The expression level of tyrosinase at certain time periods in the lactose broth.....	162
Figure 3.30. Monitoring of dissolved oxygen level during the reaction.	166
Figure 3.31. 3 L reaction of hydroxylation of daidzein with the optimized condition.	167
Figure 3.32. The formation of boron ester bond with genistein and boric acid. ...	169
Figure 3.33. Purification with organic solvent extraction	171
Figure 3.34. Purification by using differences in the solubility depending on pH.	172
Figure 3.35. Purification of piceatannol with Amberlite.....	173
Figure 3.36. The process optimized for the production and purification of 3'-ODI and Orobol from daidzein and genistein, respectively.	176
Figure 3.37. The process optimized for the production and purification of piceatannol from resveratrol.	177
Figure 4.1. Cladogram of 499 bacterial tyrosinases.....	187
Figure 4.2. The optimal pH of Ty reaction.....	195

Figure 4.3. HPLC data of 1 mM daidzin in the presence of boric acid.....	199
Figure 4.4. The substrate specificity of tyrosinase from different organisms.	201
Figure 4.5. The reaction profiles of <i>ortho</i> -hydroxylation of monophenol glycosides.	202
Figure 4.6. LC/MS data of the initial substrate, daidzin, and the hydroxylated product, 3'-hydroxy daidzin.....	203
Figure 4.7. LC/MS data of the initial substrate, glycitin, and the hydroxylated product, 3'-hydroxy glycitin.	204
Figure 4.8. LC/MS data of the initial substrate, genistin, and the hydroxylated product, 3'-hydroxy genistin.....	205
Figure 4.9. LC/MS data of the initial substrate, polydatin, and the hydroxylated product, astringin.	206
Figure 4.10. The substrate specificity of tyrosinases to naringenin, kaempferol, and quercetin.....	209
Figure 4.11. <i>ortho</i> -Hydroxylation of monophenol aglycones by BT_Ty w/o boric acid.....	210
Figure 4.12. The structural comparison of type III copper containing polyphenol oxidases.....	213
Figure 4.13. The measurement of T_m of BT_Ty.	214
Figure 4.14. The X-ray crystallography of BT_Ty, and the result of size-exclusive chromatography depending on pH.....	215
Figure 4.15. The existence of a cap domain that blocks the active site of BT_Ty.	216
Figure 4.16. Identification of the active site, and electrostatic intra-interactions b/w cap and body domains.....	217
Figure 4.17. The residues that have inter-interactions for maintaining the homo- tetrameric structure.	220
Figure 4.18. The results of alanine scanning of residues that have inter-interactions b/w monomers.....	221
Figure 4.19. The residues that have intra-interactions b/w cap and body domains, and the result of alanine scanning on the residues.	225
Figure 4.20. SDS-PAGE gel images of BT_Ty mutants.	226
Figure 4.21. A residue that has a hydrogen bond with hydroxyl group of	

monophenols.....	230
Figure 4.22. The alanine scanning of residues that have interactions to monophenol substrates.....	231
Figure 4.23. Introducing the residue, Asn, has a hydrogen bond to monophenol to other tyrosinase.....	232
Figure 5.1. Schematic illustration of fabrication of SA_Ty mediated HG_gel.	238
Figure 5.2. The structural comparison of tyrosinase from different organisms. ...	251
Figure 5.3. SDS-PAGE gel image of the purified tyrosinases.....	254
Figure 5.4. Detection of tyramine moiety on HA by UV spectroscopy and ¹ H NMR.	255
Figure 5.5. The reaction profiles of Tys on free tyrosine, gelatin, and HA_t.....	257
Figure 5.6. The initial oxidation rates of tyrosinase from three different organisms	258
Figure 5.7. The changes in viscosity of HG_gel depending on the concentration of NaCl.....	262
Figure 5.8. The images of HG_gel after injecting and spraying.	263
Figure 5.9. Storage modulus of gels w/ or w/o enzymatic crosslinking.....	266
Figure 5.10. Gelation time measured by a rheometer.....	267
Figure 5.11. Swelling ratios of gels after crosslinking, and degrading rates of the gels.....	268
Figure 5.12. SEM images of HG_gel after tyrosinase crosslinking.	269
Figure 5.13. The tacking tests for measuring stickiness of gels.....	271
Figure 5.14. Biocompatibility test of HG_gel.....	273
Figure 5.15. Histological evaluation of in vivo degradation and stability of HG_gel.	274
Figure 6.1. The schematic figure of three building blocks of fabricating functional hydrogel.	281
Figure 6.2. Schematic figure of constructing plasmid for ELP elongation and C-term tail group.....	285
Figure 6.3. Schematic figure of inverse transition cycling for purifying ELPs	287
Figure 6.4. Rheology test of gelatin-hyaluronic acid hydrogel incorporating ELPs.	296

Figure 6.5. The image of ELP gel containing DOPA residues as pH changes in the presence of ferric ions	298
Figure 6.6. The result of powder X-ray diffraction	301
Figure 6.7. The images of the rGO-ELP hydrogel.	302
Figure 7.1. A simplified reaction scheme for efficient <i>ortho</i> -hydroxylation by tyrosinase.	310
Figure 7.2. The position of tyrosinase domain	312
Figure 7.3. The hypothetical reasons for the suicide inactivation	315
Figure 7.4. Chemicals subjected in this thesis for the substrate of <i>ortho</i> -hydroxylation	316
Figure 7.5. Possible substrates for <i>ortho</i> -hydroxylation by tyrosinase.....	317

Chapter 1.

Introduction

1.1 Mechanism of tyrosinase

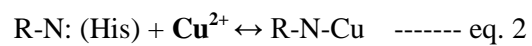
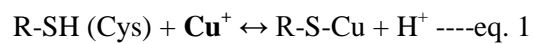
1.1.1 Copper metalloproteins

All living organisms on this planet are composed of complex mixtures of organic and inorganic chemicals. The fundamental composition of macromolecules, such as amino acid, carbohydrates, lipids, and nucleotides that are building blocks of supporting materials of cells and are also catalyzing metabolites from energy sources for lives are mainly organic. However, chemical and biological functions of lives can be more sophisticated by ligating with inorganic elements such as copper, iron, zinc, etc. It was previously hypothesized that the expansion of biological roles of copper had been led by a decrease in the solubility of iron by oxygenation of oceans after the rise of photosynthetic organisms such as cyanobacteria 2.4-2.3 billion years ago (Festa and Thiele 2011).

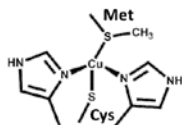
In general, the usages of copper in biology are not prevalent comparing to magnesium, iron, and manganese, but a trace amount of copper is essential, for example, because the last enzyme in the respiratory electron transport chain is cytochrome c oxidase, which is one of the copper-containing proteins. The copper containing metalloproteins have been classified into five groups depending on the ligated components and the structural configurations as shown in Figure 1.1.

The types of ligands may vary in accordance with the ionized states of copper ions, reduced copper ions (Cu^+ , $[\text{Ar}]4s^03d^{10}$) or oxidized copper ions (Cu^{2+} , $[\text{Ar}]4s^03d^9$) or the transition of both states. Cuprous ions have an affinity for thiol and thioether groups while cupric ions prefer coordinated bonds with the deprotonated nitrogen of imidazole groups (Tarkhanova, Gantman et al. 2010, Wu, Fernandez-Lima et al. 2010). It is because of the protonation state and free lone

electrons of functional groups (at neutral pH), and the reaction of the coordinated bonds are briefly formulated below. The copper ions have the empty 4s and 4p orbitals thus a lone pair electron could share the orbital spontaneously.

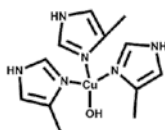


Type I (T1Cu)



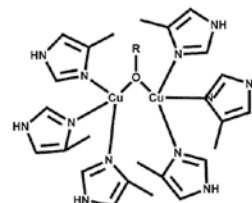
- amicyanin, plastocyanin, azurin, nitrite reductase
- mononuclear
- distorted tetrahedral
- strong absorbance at 600 nm
- 2 His, 1 Cys, and 1 Met

Type II (T2Cu)



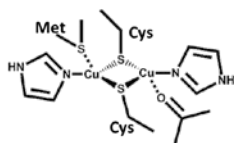
- superoxide dismutase, amine oxidase, laccase
- mononuclear
- distorted tetragonal
- weak absorbance at 700 nm
- 3 His

Type III (T3Cu)



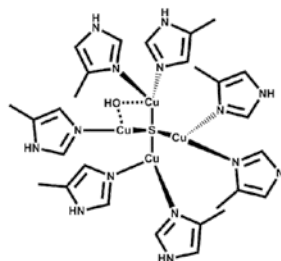
- tyrosinase, hemocyanin, catechol oxidase, laccase
- binuclear
- tetragonal
- weak absorbance at 700 nm
- non-detectable by EPR
- 6 His

Cu_A



- cytochrome c oxidase, N₂O reductase, menaquinol NO reductase
- binuclear
- trigonal planar
- strong absorbance at 480 & 530nm
- 2 His, 2 Cys

Cu_Z



- N₂O reductase
- tetranuclear
- tetracopper cluster
- strong absorbance at 640 nm
- 7 His

Figure 1.1 General structures and characteristics of copper-containing proteins.

1.1.2 The active site of tyrosinase and the structural comparison of type III copper-containing proteins.

The type III copper containing proteins utilize the both oxidation states of copper ions, Cu^+ and Cu^{2+} , depending on ligand bindings. The active site of type III copper proteins has a well-conserved four alpha helices, and the structure makes a distinctive feature of type III copper proteins. In the bundle of alpha helices, two copper ions ($[\text{Cu}^+_2]^{2+}$) are ligated by six π -histidines (protonated at δ -amine) (*deoxy-state*), and normally, a copper ion held by first three histidines that are located N-term is called copper A, Cu_A , and another copper ion is called copper B, Cu_B (Bijelic, Pretzler et al. 2015). The copper ions form spontaneously ($\mu\text{-}\eta^2\text{:}\eta^2\text{-peroxo}$)-dicopper(II) complex with one oxygen molecule (*oxy-state*, $[\text{Cu}^{++}_2\text{O}_2]^{2+}$) in aerobic condition, driven by the electrostatically destabilization of the *deoxy* structure (Yoon, Fujii et al. 2009, Chiang, Keown et al. 2016, Hamann, Herzigkeit et al. 2017). The formation of the dicopper(II) complex is reversible so hemocyanin (Hc), one of the type III copper containing proteins, function as an oxygen carrier in arthropods and mollusks.

Tyrosinase (Ty) is also a type III copper containing proteins but, unlike Hc, Ty shows oxidoreductase activities. It is classified as a polyphenol oxidase (PPO) since the substrate specificity is limited to only phenolic compounds. Ty catalyzes the two-step consecutive oxidation reactions; *o*-hydroxylation of monophenols to catechols, phenolase activity, also called cresolase activity (k_1), and the subsequent dehydrogenation of catechols to *o*-quinones, catecholase activity, also known as diphenolase activity (k_2) (Figure 1.2).(Goldfeder, Kanteev et al. 2013, Kanteev, Goldfeder et al. 2015) The *o*-quinones produced by Ty are unstable. Thus the non-

enzymatic polymerization of *o*-quinones (with or without amines and/or thiols), melanin formation, occurs spontaneously in the most living organisms from bacteria to humans.(Kanteev, Goldfeder et al. 2015) In the phenolase reaction, k_1 , the C-H bond right next to the hydroxyl group of monophenols is selectively hydroxylated by electrophilic substitution, namely, *o*-hydroxylation. (Because of the nature of phenols, as shown in Figure 1.3, the *ortho*-position of the compounds could be subjected to the electrophilic substitution.)

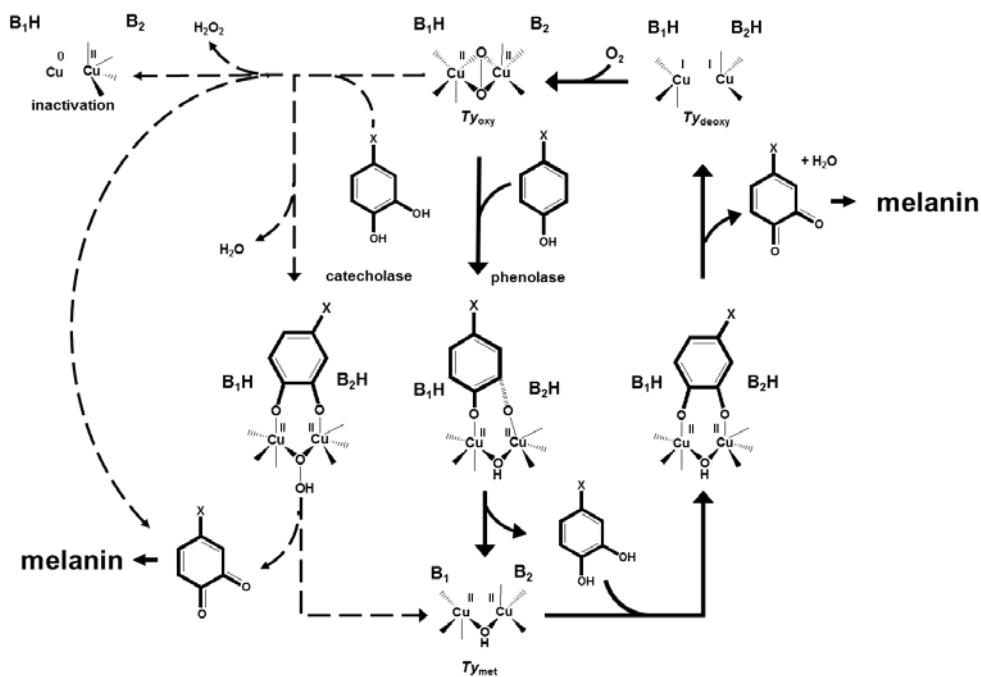


Figure 1.2. The general reaction mechanism of tyrosinase.

Reaction cycle of tyrosinase including the changes of the position of protons and the oxidation state of copper ions in each path. B₁ and B₂ represent water and basic residue nearby the active site. The bold straight line is dominant function of tyrosinase, and the dotted line are the minor reactions under certain conditions

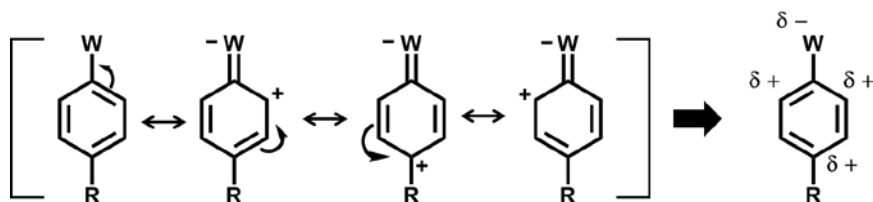


Figure 1.3. A resonance effect of arene ring with an electron-withdrawing group.

The electronegative atom (W), for example, an oxygen atom of a hydroxyl group, adjacent to the pi bonds tends to deactivate the aromatic ring by decreasing the electron density through a resonance withdrawing effect. The resonance only reduces the electron density at the *ortho*- and *para*- positions. Therefore, the *ortho*-position is easily subjected to electrophilic substitution.

As the oxygen of the hydroxyl group of the monophenols activates one of the copper ions of Ty_{oxy}, [Cu⁺⁺₂O₂]²⁺ (nucleophilic attack), the hydroperoxide group of the complex attacks the *ortho* position of monophenols (electrophilic attack), producing catechols and an oxo-bridged dicopper (II) complex (*met*-state, [Cu⁺⁺₂(OH)]³⁺) (Muñoz-Muñoz, Berna et al. 2012, Hamann, Herzigkeit et al. 2017). Ty_{met} cannot oxidize the monophenols but selectively oxidizes catechols to *o*-quinones, and then becomes Ty_{deoxy} again, i.e., dicopper (I) without molecular oxygen. The Ty oxidation cycle is recurrently circulated after Ty_{oxy} is regenerated from Ty_{deoxy} by molecular oxygen (Mirica, Vance et al. 2005, Muñoz-Muñoz, Berna et al. 2012, Ramsden and Riley 2014). Ty becomes inactivated when *o*-diphenols or external reductants are not available during the reaction despite the presence of the monophenolic substrate. Monophenols with low pka value frequently cause an irreversible inactivation by the reduction of copper ions to copper metals. This inactivation will be discussed in depth at the next session 1.1.4 Inhibition of tyrosinase and the suicidal inactivation. Without *o*-diphenols or reducing agents, the oxidation cycle of Ty cannot be completed since the oxygen atom of the oxo-bridged dicopper(II) complex of Ty_{met} is not easily reduced. An initial lag period of Ty reaction on monophenols is often observed because Ty_{met} is the most common resting state of Ty (Yamazaki and Itoh 2003, Ramsden and Riley 2014).

The side-on $\mu\text{-}\eta^2\text{:}\eta^2\text{-peroxo}$ -bridged Cu₂O₂ oxy structure of Ty is crucial for the both oxidations of monophenols and catechols; however, not all of the type III copper proteins can catalyze the polyphenol oxidation as Ty because of diverse neighboring residues (Decker and Tucek 2000, Yoon, Fujii et al. 2009). As shown in Figure 1.4, the secondary and tertiary structure of the core domains is well

conserved. However, catechol oxidase (Cox) only performs the latter oxidations, k_2 (Decker and Tuzcek 2000, Molitor, Mauracher et al. 2016, Solem, Tuzcek et al. 2016). Recent studies on the structural comparison of Ty and Cox have revealed that an absence of one asparagine residues in Cox are the direct evidence of the difference in their activities since the water molecule activated by the asparagine and an adjacent glutamate in Ty protonates the monophenols for initializing the *ortho*-hydroxylation as stated above (Goldfeder, Kanteev et al. 2014, Solem, Tuzcek et al. 2016). And the substrate specificity of k_1 of aurone synthase from *Coreopsis grandiflora* (CG_Aus) differ from Ty, which hydroxylation is limited only to a particular chalcone, isoliquiritigenin, but not to L-tyrosine and tyramine because of bulky gate residues and substrate binding residues (Molitor, Mauracher et al. 2016). Hemocyanin (Hc) also has the peroxo-bridged copper complex held by six histidines but, as stated earlier, Hc only functions as an oxygen carrier in arthropods and mollusks. In previous studies, k_2 of Hc were partially recovered upon artificial activations such as N-term truncations, and it was concluded that the low accessibility of the active site of Hc to the substrates by the sterical hindrance precisely turns off the phenolic oxidations for controlling the biological events (Zlateva, Di Muro et al. 1996, Decker and Rimke 1998, Salvato, Santamaria et al. 1998). However, the factors that govern the substrate specificity and the rate of activities of type III copper proteins are not clearly unraveled yet.

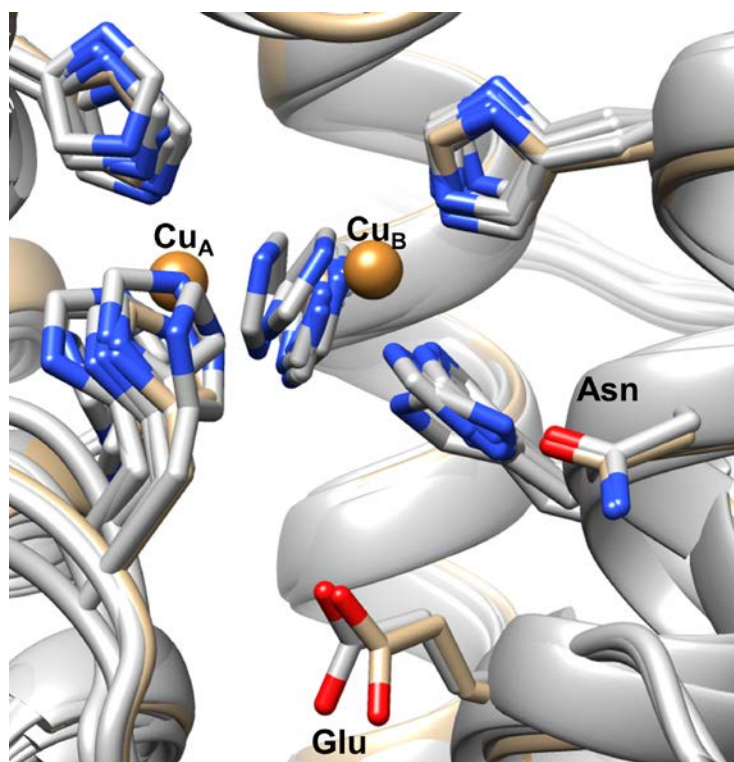


Figure 1.4. Imposed image of the oxygen binding pocket of type III copper proteins.

Hc, Cox, Aus, and Ty are imposed in this figure, and the image shows that the secondary and tertiary structure of the core domain are well conserved, including the histidine residues that hold the copper ions. Asn and Glu are well-known residues for water capturing that are essential for monophenolase activity; however, the roles of the residue regarding monophenolase activity are still controversial.

1.1.3 Rate-determining step of tyrosinase reaction

The reaction mechanism of Ty is complicated, and thus the studies for identifying the rate-determining step of this reaction was critical in terms of the application of the enzyme, for example, for the purpose of enhancing the oxidation rate. As stated earlier, the major three states of Ty exist depending on the configuration of two copper ions and oxygen molecule. In this section, two states (*oxy*- and *deoxy*-) among three Ty states will be discussed because the states involved in both oxygen binding and the initial monophenolase activity.

Firstly, the *deoxy*-state of type III copper proteins (before oxygen binding) is unstable because of the electrostatic repulsion of the two cuprous ions as maintained the close distance of the range of 3 to 5 Å by the histidines at the core active site. The destabilization drives the oxygen binding, and the oxygen leads the oxidation of cuprous ions of deoxy state to cupric ions. The *oxy*-state is relatively stable, and it was previously proved by calculating the total energy differences of *oxy*- and *deoxy*-states. For example, the density functional theory calculations indicate that O₂ binding in Hc is approximately 9 kcal·mol⁻¹. Thus, the binding of oxygen in the core active site of Ty is not a rate-determining step.

There are two major steps in monophenolase activity; the deprotonation of monophenols and the O₂ cleavage of dicopper peroxo complex (Figure 1.5). Solomon et al (Ross and Solomon 1990, Solomon, Chen et al. 2001) observed the O-O stretch of dicopper peroxo complex with Raman spectroscopy. In *oxy*-state, the vibration of O-O stretch (which is typically detected at 800 cm⁻¹) was observed at 750 cm⁻¹, which indicate the O-O bonds is still existed but weakened. This result is also supported by the orbital configuration of dicopper peroxo complex of *oxy*-

state as shown in Figure 1.6. The peroxide sigma donor bond produces one intense charge transfer transition, the peroxo π_{σ}^* to Cu $d_{x^2-y^2}$. The interaction stabilizes the sigma bonds, and this implies that the O₂ is not cleavage in oxy-state. The nucleophilic attack by the hydroxyl group of phenolic substrates on a copper ion in Ty_{oxy} initiates Ty reaction by transferring a proton from the hydroxyl group of the substrate to the peroxide group of Ty_{oxy}. The protonation states of the Ty_{oxy} and phenolic substrates were monitored by performing the reaction in D₂O and by deuterium substituted L-tyrosine, and it was concluded that this deprotonation step of substrate is known as the rate-limiting step of the Ty reaction (Peñalver, Rodríguez-López et al. 2003, Fenoll, Peñalver et al. 2004, Muñoz-Muñoz, Berna et al. 2012).

Recently, the structural comparison of Ty from *Bacillus megaterium* and Coxs from sweet potato revealed that the conserved water capturing residues serve as the deprotonating base, which is only found in Tys but is absent in Coxs. The water capturing residues could be Glu, Asn, Asp, etc. that could form hydrogen bonds with a water molecule (Figure 1.7). The hydrogen bonds can activate it by increasing in the dipole moment and basicity of the water molecule. Removing one of the hydrophilic residues in Ty, the monophenolase activity was selectively repressed. Again, this could be another evidence for emphasizing the importance of the initial deprotonation step of monophenols for Ty's activity.

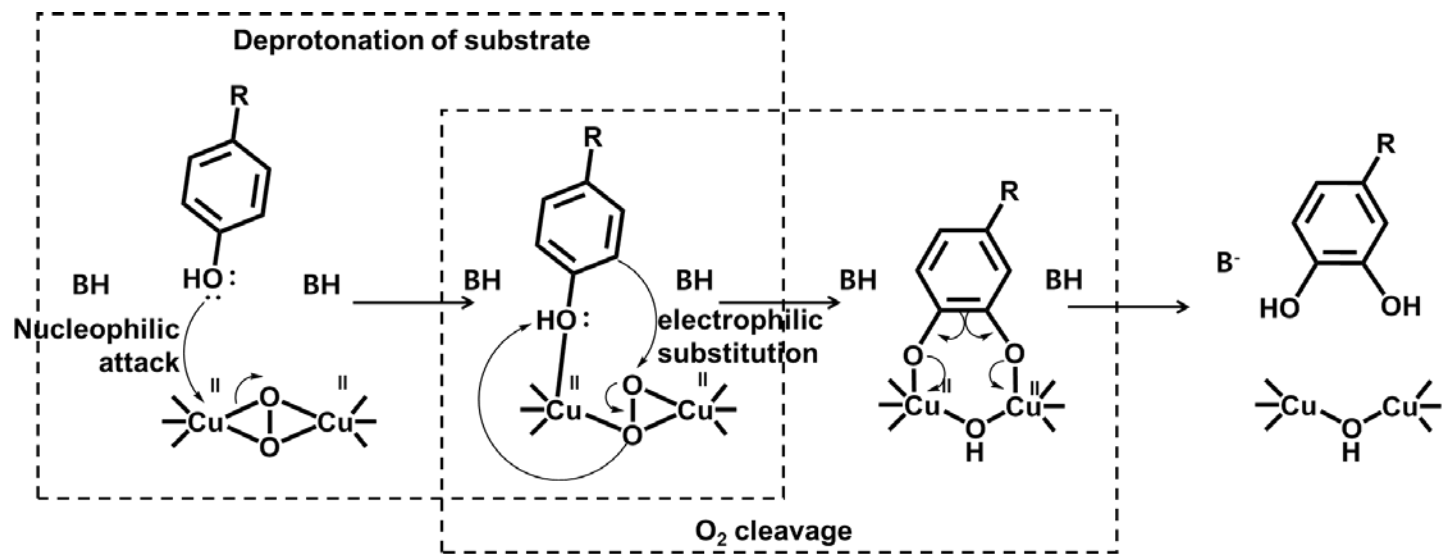


Figure 1.5. The movements of electrons in the monophenolase activity of Ty.

The deprotonation and O₂ cleavage step of Ty_{oxy} during the monophenolase activity. The rate-determining step of the reaction is the deprotonation of monophenols.

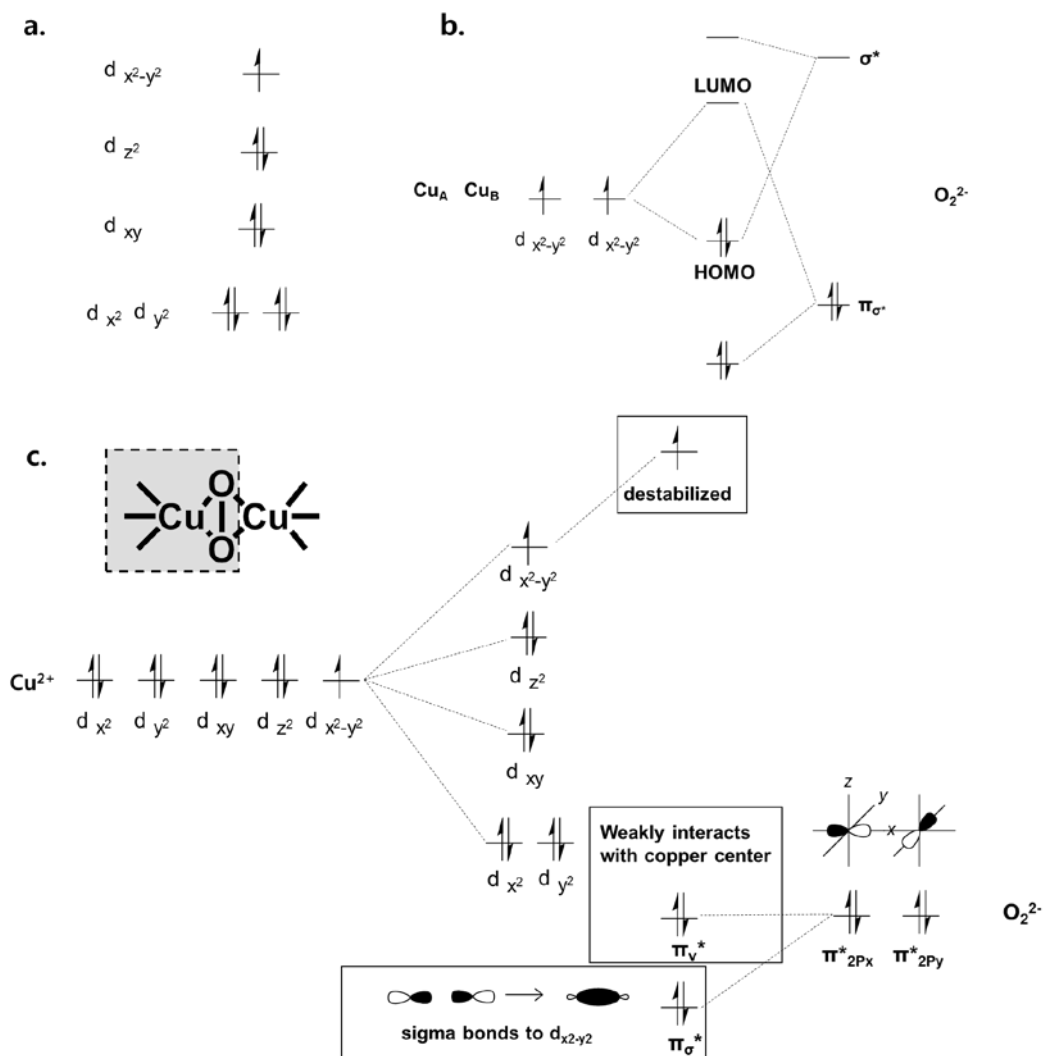


Figure 1.6. The orbital configuration of Ty_{oxy} , $[Cu^{++}_2O_2]^{2+}$

(a) The degenerated orbital energy state of a cupric ion for square pyramidal configuration. (b) The orbital configuration of oxy-state. The oxy-state has no EPR signal since the magnetic coupling between the two copper ions is $S = 1/2$ (c) One side of bicopper peroxo bridge. The peroxide sigma donor bond produces one intense charge transfer transition, the peroxo π_{σ^*} to $Cu d_{x^2-y^2}$.

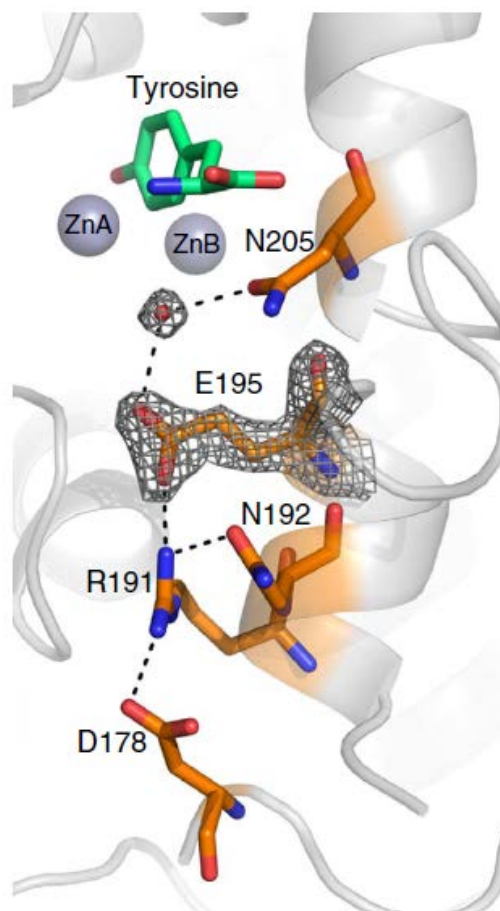


Figure 1.7. Structure-supported deprotonation scenario.

Zn ions were used instead of copper ions for inactivating the oxidation of Ty in order only to see the ligand binding states. The dashed lines are all less than 3\AA . This figure was slightly modified from Figure 4 of a previous report (Goldfeder, Kanteev et al. 2014) with permission (License Number: Nature Publishing Group 4110590683168).

1.1.4 Inhibitors of tyrosinase and the suicidal inactivation

As stated earlier, Ty is a key enzyme in melanin synthesis in all living organism, and the melanin plays important roles in protecting cells from ultraviolet damages and in removing reactive oxygen species. However, studies in the retardation of Ty activity is continuously growing as the techniques for Ty inactivation could draw tremendous revenue in markets of cosmetics, and food industry. Not only the inactivation of Ty is directly linked to the skin whitening but also the suppressing the pigmentation may prevent the excessive level of epidermal pigmentation which frequently causes various dermatological disorders in a human being, such as aging spot and melasma. Furthermore, unfavorable browning of vegetables and fruits by Ty causes a decrease in nutritional quality by oxidation essential amino acid, and in product quality, which consequently causes economical loss.

Kim et al. (Kim and Uyama 2005) reviewed on inhibitors from natural and synthetic sources. And the representative inhibitors are briefly listed in Table 1.1. Natural polyphenols such as catechins and (iso)flavonoids are well known Ty inhibitors due to the structural similarity with L-tyrosine, and L-DOPA (L-3,4-dihydroxyphenyl alanine). Catechins that has catechol moieties normally inhibit the monophenolase activity competitively by tightly binding to copper ions, and flavonols that have 3-hydroxy-4-keto-moiety are also inhibited the Ty activity by binding to copper ions. Interestingly, the flavanols such as quercetin and kaempferol can chelate copper ions in Ty_{met} while kojic acid only chelates copper ions in Ty_{oxy} (Cabanès, Chazarra et al. 1994). Recently, X-ray crystallography of Ty from *Bacillus megaterium* with kojic acid was successfully supported the mixed-type inhibition mechanism of kojic acid (Deri, Kanteev et al. 2016).

Beside the normal inhibitions mechanism such as (non-, un-) competitive inhibition because of structural similarity, the issues on the irreversible inactivation of Ty, so-called “suicide inactivation,” were firstly brought by Land et al. (Land, Ramsden et al. 2007) by presenting indirect evidences for the reduction of copper ions. The mechanism of the suicide inactivation suggested is briefly presented in Figure 1.8. The stabilization of O⁻ of a hydroxyl group (which does not form a bond to the copper ion) by electronegative atoms which act as strong electron-withdrawing group could result in failing to send two electrons to peroxide from the dihydroxy substrate to reduce a water molecule. The electrons end up reducing the copper ion, and this is the dead-end of the enzyme unless alternative copper ion is given. The R1 and R2 were substituted to fluorines for maximizing the electron-withdrawing effects, and it was demonstrated that the phenols with fluorines dramatically induced the suicide inactivation of Ty (Munoz-Munoz, Garcia-Molina et al. 2010). However, the frequency of inactivation due to reducing copper ions has not yet been quantified, and the correlation between electronegativity of R1 and R2 with the reduction of copper ions is not clear yet. Thus, additional copper ions in the reaction could just abolish the suicide inactivation of Ty.

Table 1.1. Summary of tyrosinase inhibitory activity of compounds.*

Compounds	Type of inhibition	Inhibition target	IC50 (mM)
Flavanols			
(-)-Epigallocatechin	competitive	monophenolase	0.035
(-)-Epicatechin gallate	competitive	monophenolase	0.017
(-)-Epigallocatechin gallate	competitive	monophenolase	0.034
Flavonols			
Quercetin	competitive	diphenolase	0.07
Kaempferol	competitive	diphenolase	0.23
Morin	competitive	diphenolase	2.32
Flavones			
Luteolin	noncompetitive	diphenolase	0.19
Luteoilin 7-O-glucoside	noncompetitive	diphenolase	0.5
Isoflavans			
Glabridin	noncompetitive	diphenolase	0.004
Glabrene	mixed-type	diphenolase	7.6
Isoliquiritigenin	mixed-type	diphenolase	0.047
Other compounds			
Kojic acid	mixed-type	diphenolase	0.014
Anisaldehyde	noncompetitive	diphenolase	0.32
Cuminaldehyde	noncompetitive	diphenolase	0.05
Cinnamaldehyde	noncompetitive	diphenolase	0.98

*This table is slightly modified from Table 2 of a previous report (Kim and Uyama 2005) with permission; License Number: Springer 4107650048677

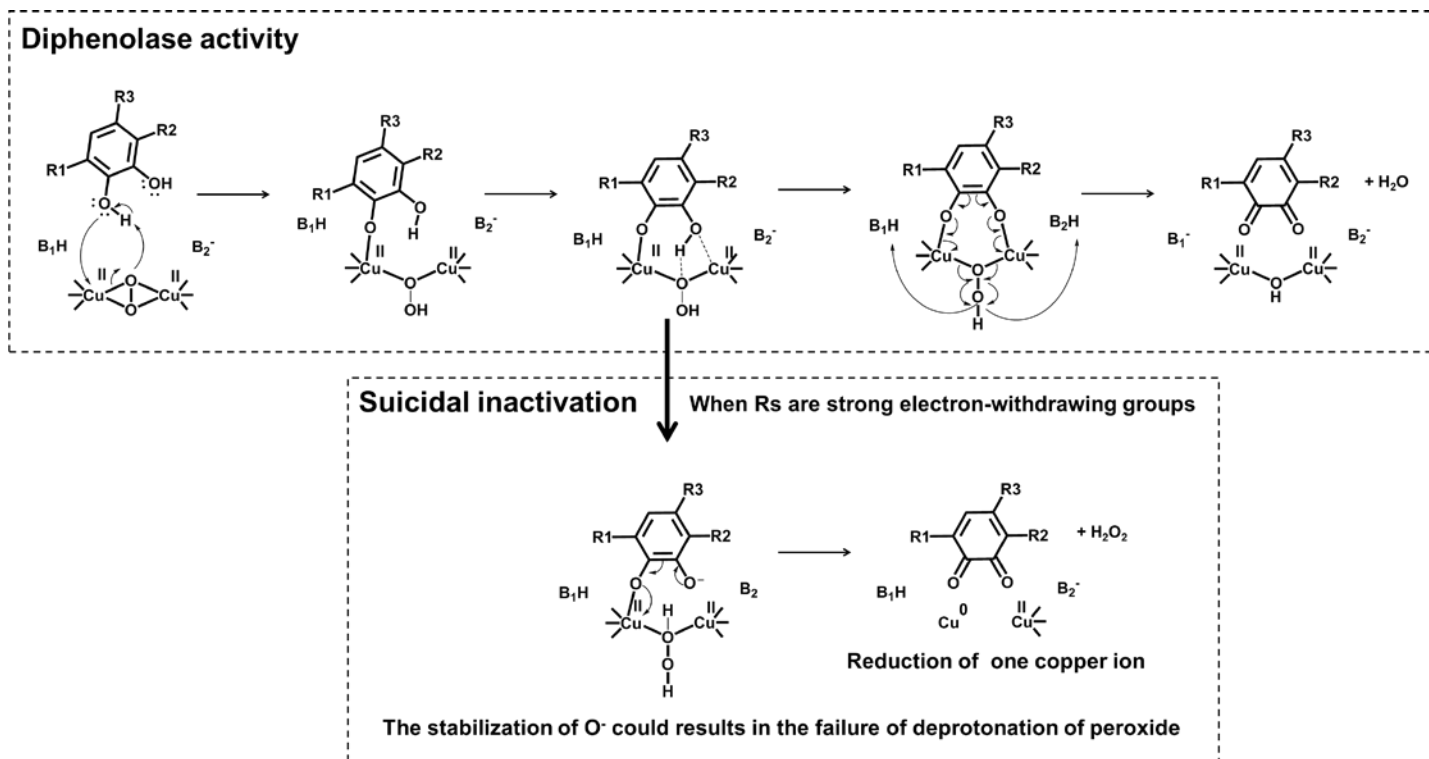


Figure 1.8. The hypothetical paths for the suicidal inactivation.

B_1 and B_2 represent bases around the active site. The tendency of stabilizing $O^{\bullet-}$ of the hydroxyl group increases as increasing of the electronegativity of R_1 and R_2 , and consequently causes higher frequency of suicide inactivation of Ty.

1.2 Application of tyrosinases

1.2.1 Production of catechol derivatives

Phenolic phytochemicals have attracted considerable interest about human health because these natural substances may have the potential to prevent multiple chronic diseases including cancer. Especially, *ortho*-dihydroxylated phenolic phytochemicals such as hydroxytyrosol (olive oil) (Bisignano, Tomaino et al. 1999), luteolin (artichoke and broccoli) (Miean and Mohamed 2001), piceatannol (grape and wine) (Larrosa, Tomás-Barberán et al. 2004), esculetin (chicory) (Hazra, Sarkar et al. 2002), and *ortho*-dihydroxy isoflavones (fermented soybean paste) (Park, Park et al. 2008) are functional compounds in foods and drinks that are generally regarded as healthy. For example, 7,3',4'-trihydroxyisoflavone (3'-ODI), one of the *ortho*-dihydroxylated isoflavones (ODIs), is not present in soybeans but a trace amount of ODIs is found in aged soybean paste, which is known to be converted from daidzein during fermentation (Park, Park et al. 2008)a. The anti-oxidative effect of 3'-ODI is quite comparable to that of L-ascorbic acid (Park, Park et al. 2008), and the biological effects of 3'-ODI on skin whitening (Park, Kim et al. 2010), and its cancer chemoprotection activities (Lee, Lee et al. 2011, Lee, Bode et al. 2011, Lo, Wang et al. 2012), have marked it as a multifunctional bioactive substance.

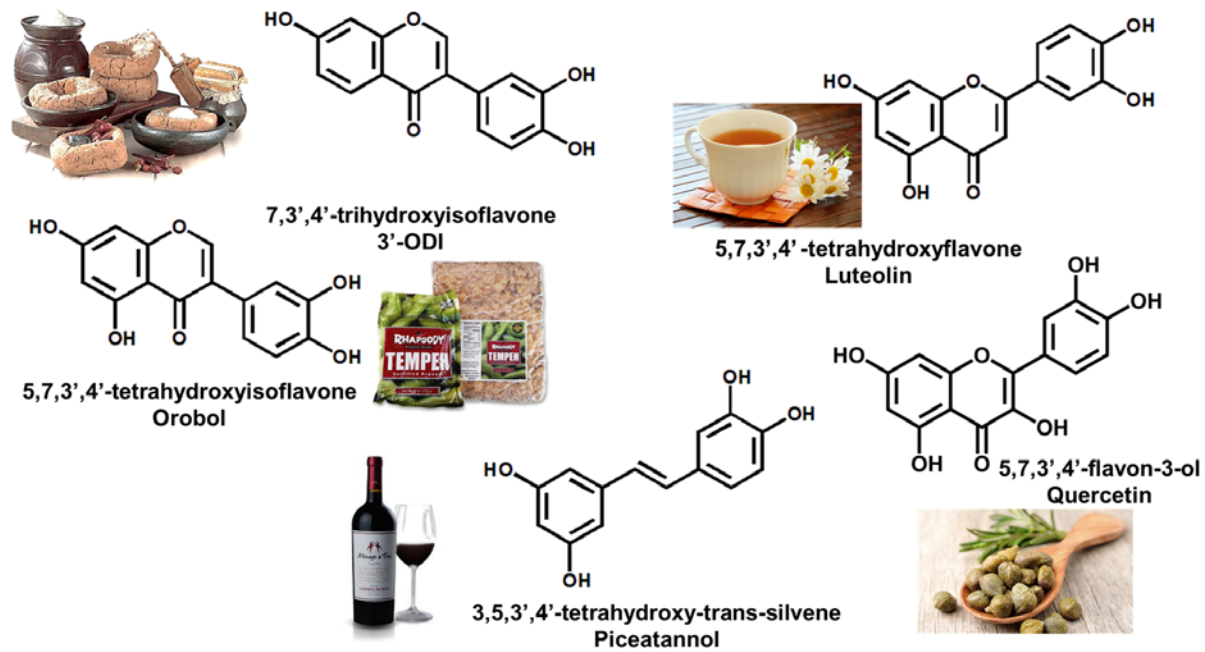


Figure 1.9. The representative examples of functional catechol derivatives

Ty governs two consecutive reactions, phenolase activity, and catecholase activity. The two reactions are inevitably linked to a complete cycle of Ty reactions. However, there are tremendous studies for controlling the two reactions separately. The first phenolase activity could be utilized for the production of catechol derivatives such as L-DOPA, a precursor of the neurotransmitters such as dopamine and norepinephrine and epinephrine. Since the L-DOPA could cross the blood-brain barrier, which dopamine cannot diffuse in, L-DOPA is used for increasing the level of dopamine in the treatment of Parkinson's disease. The first commercial production of L-DOPA was Monsanto process developed by William S. Knowles, won the Nobel Prize in Chemistry 2001. The four major synthesis steps lead the production of L-DOPA, and the reaction is present in Figure 1.10. However, the synthesis method is costly consuming through several synthesis and purification steps, and cannot be universally applied for the production of various catechol derivatives, for example, *ortho*-dihydroxy isoflavones.

The *regio*-specific hydroxylation could be performed by a simple one-step reaction of an enzyme, specifically oxygenase such as cytochrome P450 and Ty. Previously, cytochrome P450s (CYPs) were utilized to lead the *o*-hydroxylation of daidzein to produce 3'-ODI (Seeger, Gonzalez et al. 2003, Choi, Jung et al. 2012, Choi, Jung et al. 2013). Choi *et al.* (Choi, Jung et al. 2012) constructed an artificial self-sufficient CYP which was a combination of the heme domain of CYP105D7 and the reductase domain of CYP102D. The fused CYP exhibited enhanced electron transfer efficiency; however, these enzymes are found inappropriate for industrial use because of their low productivities, low yields and the requirement for cofactor regeneration systems.

Ty is also an attractive enzyme for the hydroxylation of monophenols, and various attempts were previously reported for the production of functional catechols such as L-DOPA, 3'-hydroxytyrosol, and piceatannol. However, none of the processes were industrially developed yet because the two consecutive reactions are not easy to separate and thus the catechol derivatives are also oxidized form the Ty. Thus, researchers have focused on resolving the restriction, inseparable consecutive reaction, by enzyme engineering and process engineering.

For controlling the inseparable reaction, the direct evolution of Ty from *B. megaterium* was performed by the adjusting adjacent residues of the enzyme that could alter the substrate specificity of Ty. Ben-Yosef et al. generated a random mutant library by error-prone PCR and screened a mutant, R209H, which the ratio of monophenolase and catecholase activities is enhanced from 0.12 to 0.31 (Shuster Ben-Yosef, Sendovski et al. 2010). And Goldfeder et al. (Goldfeder, Kanteev et al. 2013) analyzed the structure of the Ty, and found that a V218 is pointed to the copper ions in the active site. By site-saturation mutagenesis of V218, a mutant library was constructed and, screened another mutant, V218F. This mutant exhibited a 9-fold higher ratio of monophenolase and catecholase activities. The ratio was calculated based on the V_{\max} of monophenolase and catecholase activities, and it was 0.8; the wild type was calculated to be 0.09. However, the catalytic efficiency of the monophenolase activity of the mutant was significantly decreased from 80.0 to 11.9 $\text{mM}^{-1}\cdot\text{s}^{-1}$, and also the catecholase activity was decreased from 55.1 to 19.1 $\text{mM}^{-1}\cdot\text{s}^{-1}$. The author concluded that the flexibility of copper ions could enhance the ratio, but the explanation was not enough to clarify the increment.

Secondly, the addition of additives could effectively suppress the catecholase activity. For example, the boron in boric acid can form boron ester bonds with the arene diol of the catechols, and thus the catecholic intermediate could be protected by the second Ty oxidation. Yamazaki et al. (Yamazaki and Itoh 2003) introduced boric acid to completely inhibit the catecholase activity while the first monophenolase activity keeps intact for the measurement of monophenolase activity independently. There was one problem when protecting the intermediate from being oxidized by Ty; that is the incompleteness of Ty reaction cycle because of the formation of boron ester complex also has the effect of extracting the catecholic intermediate from the reaction system, and thus there is no substance capable of reducing Ty_{met} to Ty_{oxy} . The author resolves the problem by using hydroxylamine a strong reducing agent for reducing Ty_{met} to convert it to Ty_{deoxy} . The excessive amount of the reducing agent successfully circulates the Ty reaction cycle despite the absence of catecholic intermediates. However, the amine functional group in hydroxylamine could form a covalent bond to the unstable quinonic by-product of Ty reaction and produce another form of by-products. Therefore, the method is limited to the measurement of kinetics only.

Before this method, the kinetics of the monophenolase activity was measured by the formation of dopachrome, a product of catecholase activity, under the assumption that the first oxidation reaction is a rate-determining step of Ty. In the article, the consumption of oxygen was monitored, and this method could guide the valid approach for measuring monophenolase separately for the first time. Still, there is no general solution for the usage of Ty as a monooxygenase for the production of catechol derivatives.

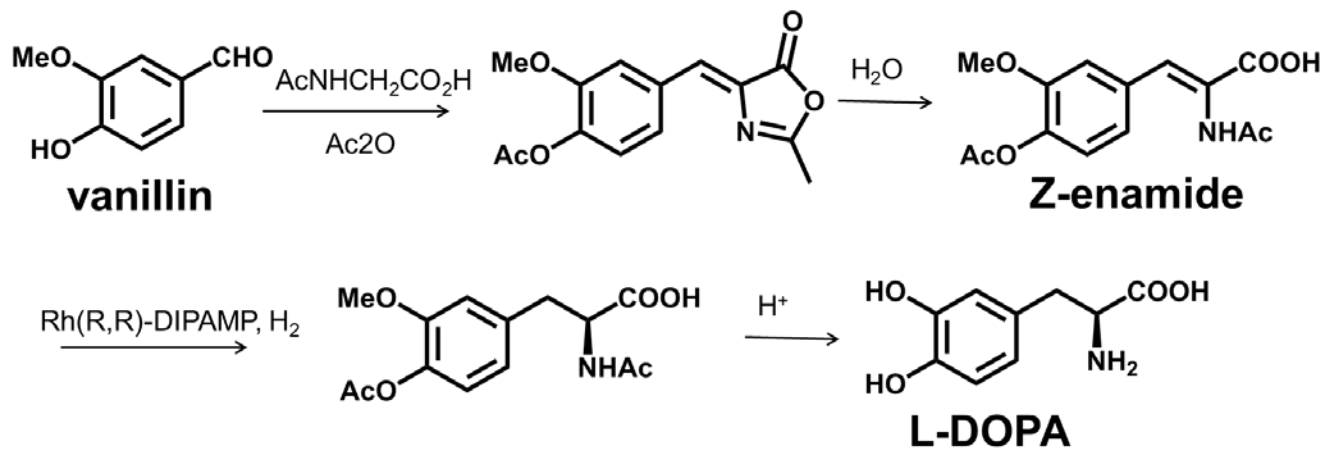


Figure 1.10. The first commercial synthesis process of L-DOPA synthesis.

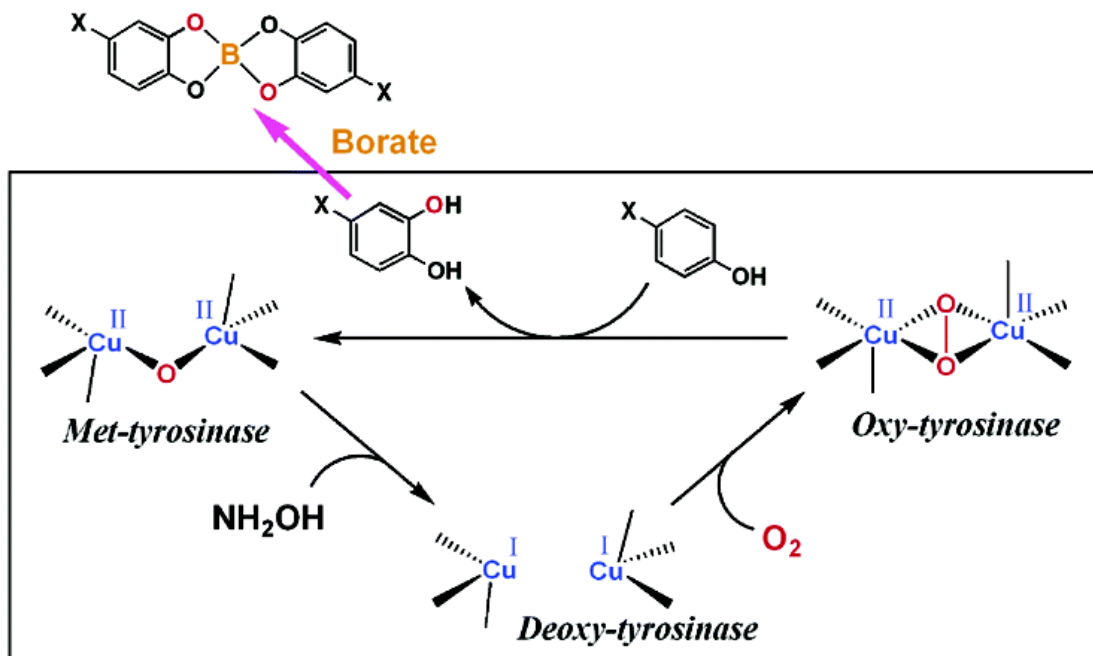


Figure 1.11. A schematic figure of repressing the catecholase activity.

This strategy for measuring monophenolase activity selectively allowed the separation of the two oxidative reactions of tyrosinase. The figure was reprinted from a previous article (Yamazaki and Itoh 2003).

1.2.2 Tyrosinase as a crosslinking agent

Tyrosinase (Ty) as a polyphenol oxidase also plays a leading role in the formation of mussel adhesive protein (Hwang, Zeng et al. 2010, Lee, Messersmith et al. 2011). The subsequent oxidation of catechols to produce quinones under physiological conditions (Decker, Dillinger et al. 2000, Lee, Baek et al. 2016). The reactive quinones promptly form covalent bonds with amines, thiols, or other phenolic moieties by non-enzymatic reactions; oxidative phenol coupling reaction, Michael addition, and Maillard reaction (Chen, Embree et al. 2002, Lee, Lee et al. 2011).

Chen et al. (Chen, Embree et al. 2002, Chen, Embree et al. 2003) compared Ty and transglutaminase (which crosslinks lysine and glutamine) by making gels with gelatin and chitosan (Figure 1.12). They concluded that the gelation rate of the gel mixture by Ty is faster than transglutaminase. However, the hydrogels crosslinked with Ty were only formed when chitosan is co-existed in the gelatin solution and was mechanically weaker than a gel made by transglutaminase.

In the most of previous studies including the studies by Chen et al, Ty from *Agaricus bisporus* has been widely utilized for the hydroxylation of phenolic moieties on macromolecules such as gelatin (Le Thi, Lee et al. 2017), mussel protein(Hwang, Gim et al. 2007), silk fibroin (Freddi, Anghileri et al. 2006) because of its easy availability. However, applications of Ty from *A. bisporus* based crosslinking has been limited due to the low degree of crosslinking as a result of the steric hindrance between Ty from *A. bisporus* and macromolecules (Freddi, Anghileri et al. 2006, Hwang, Gim et al. 2007, Le Thi, Lee et al. 2017). Later in this thesis, Chapter 6, the reasons for the low degree of crosslinking of Ty from *A.*

bisporus will be discussed by comparing the structures of Ty from various organisms.

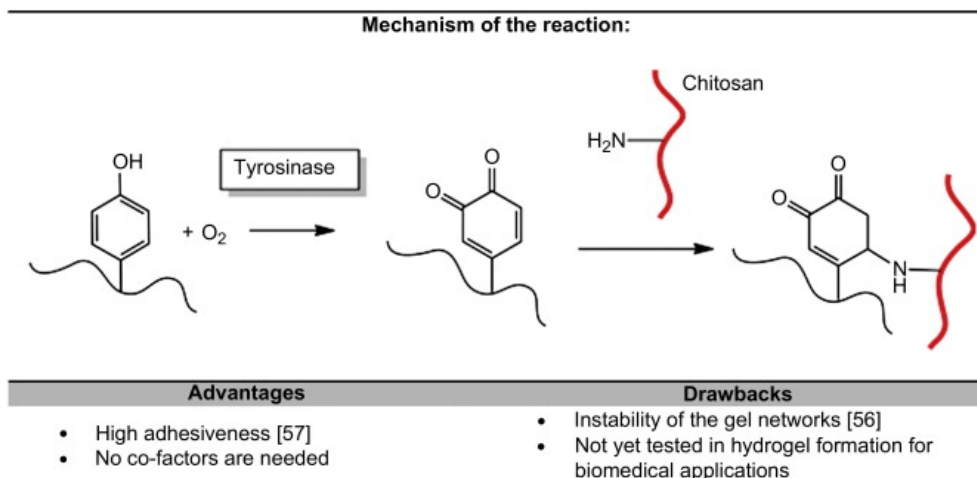


Figure 1.12. Mechanism of the enzymatic reaction mediated by tyrosinase, advantages and drawbacks.

The figure was reprinted from Fig 2. of a previous article (Teixeira, Feijen et al. 2012) with permission; License Number: Elsevier, 4111161129527.

1.2.3 Miscellaneous

1.2.3.1 Melanin synthesis and its usages

In nature, the final product of the consecutive two oxidations from L-tyrosine by Ty is dopaquinone, which is unstable and thus spontaneously form covalent bonds with amines, thiols, or other phenolic moieties by non-enzymatic reactions; oxidative phenol coupling reaction, Michael addition, and Maillard reaction (Chen, Embree et al. 2002, Lee, Lee et al. 2011). Cephalopod ink is one of the representative forms of melanin. The ink is also one of the dark pigment induced by Ty in most species of cephalopod (as an escaping tool). The composition of the ink was the mixture of 5,6-dihydroxyindole (DHI) and 5,6-dihydroxyindol-e-carboxylic acid (DHICA), which are all derived from dopaquinone. The color of human hair is also a form of melanin, which varies depending on the components of the melanin beside DHI and DHICA, for instance, L-cysteine. The color and properties of the pigments vary as the different compositions. The pigments can be called in a more accurate way such as eumelanin, pheomelanin, and neuromelanin. Eumelanin is the one like the dark cephalopod ink composed with DHI and DHICA. Pheomelanin has a similar composition with eumelanin, but L-cysteine is present and involved in the polymerization. Neuromelanin is a dark insoluble pigment found in the brain of human. (The biological function is not clearly defined yet.)

When the aromatic rings are connected and bridged together by crosslinking, the pi electrons of the multimeric arene rings could absorb the light of various wavelengths, and this is the main reason why the melanin, a biological pigment induced by Ty, is dark. From a different point of view, the dense pi-

electron cloud of the melanins can allow melanin be developed as electronic materials, which is completely biocompatible. However, melanin is not readily dispersible in an aqueous solution as graphene, thus not easy for fabricating.

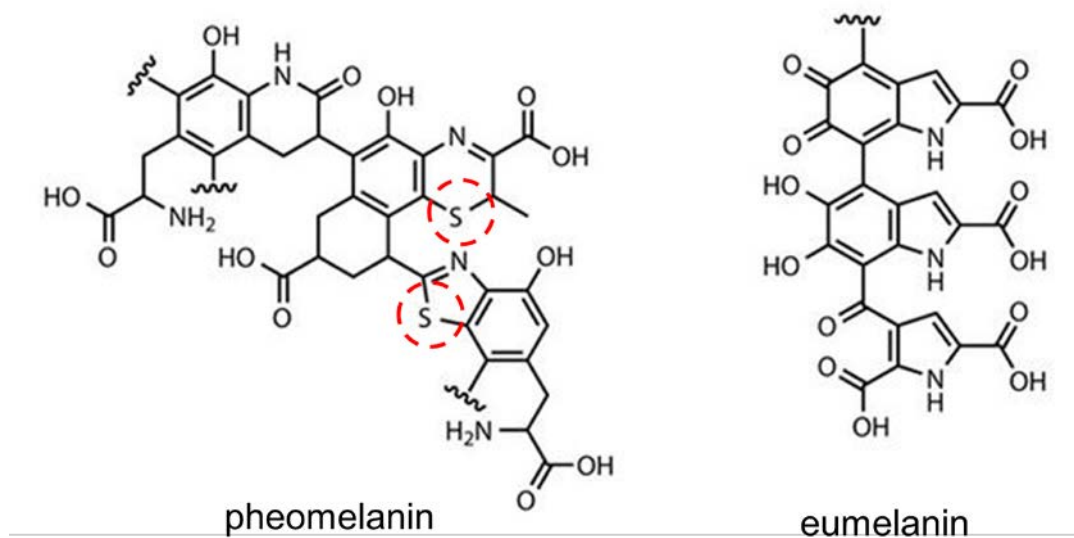


Figure 1.13. The brief structures of different types of melanin.

Depending on the initial substrates, the types of melanin can be classified. The two types of melanin present in this figure is the representative structure of melanin found in nature. The structure of neuromelanin, other well-known melanin found in brain of Human being, is not identified clearly yet.

1.2.3.2 Waste water treatment

Wada et al. (Wada, Ichikawa et al. 1993, Wada, Ichikawa et al. 1995) tried to treat waste water with Ty as the enzyme can oxidize phenols. They successfully demonstrate the potent usage of Ty as a water treatment agent by removing 100% phenol in 2h with immobilized Ty with chitosan; however, the stability of Ty matters in wastewater.

The stability of Ty when treating the phenol waste could enhance by the cross-linked enzyme aggregates (CLEAs). Xu et al. ((Xu and Yang 2013) made the stable Ty from mushroom, *A. bisporus*, by CLEA, and used it for removing phenol. They successfully demonstrated that the waste water after treating Ty could be non-toxic to a living organism, herein, *Hydra sinensis*.

1.3 The scope of thesis

The aim of this thesis is mainly to study the two different types of the oxidative reaction of phenolic compounds by tyrosinase. This thesis can be broadly divided into two themes depending on the types of the oxidation mechanism. Simply put, one is inhibiting reactions related to the production of melanin by-product, and another is accelerating the reactions. The brief schematic figure is illustrated in Figure 1.14. The first theme is focused on the *regio*-selective *ortho*-hydroxylation of monophenols to produce functional catechol derivatives, which are valuable in the markets of food additives, cosmetic ingredients, and even in the markets of fine drugs. And the second theme includes the fabricating methods of hydrogel from natural biomacromolecules and the development of it as sprayable/injectable sticky hydrogel for minimally invasive treatments.

The first three chapters of this thesis, Chapter 2, 3 and 4, are composed of a long journey of designing the new reaction paths, searching novel tyrosinases, and improving the yield and productivity of the production of *ortho*-hydroxylated monophenolic phytochemicals, from the enzyme engineering in lab scale to the mass production up to 400 L reaction. Chapter 2 is a full reprint of a previously published article with a minor revision in which the production of piceatannol from resveratrol by tyrosinase from *Streptomyces avermitilis* (SA_Ty) is mainly discussed. The chapter includes a screening method for finding a tyrosinase mutant that has higher ratio of monophenolase and catecholase activity, which is advantageous for accumulating catecholic intermediates (herein, piceatannol), and a strategy for continuously regenerating reducing agent, NADH, for protecting the product, piceatannol, from being oxidized by catecholase activity of tyrosinase.

Through the studies and results of research in this chapter, it was realized that the most important direction of the studies for enhancing the yield and productivity of the production of catechol derivatives is the screening affordable reducing agents for the mass production, and the screening more efficient enzymes, specifically, the enzymes having higher k_1/k_2 ratio and different substrate specificity for broadening the scopes of catechol derivatives.

Chapter 3 is a full reprint of a previously published article with a minor revision in which suggests more broadly applicable reaction paths for the *ortho*-hydroxylation of monophenolic compounds by tyrosinase. In this chapter, tyrosinase from *Bacillus megaterium* (BM_Ty) is studied, and the two additives, boric acid, and L-ascorbic acid, were added in the reaction. The boron in boric acid is for the protecting the catecholic product from the oxidations by tyrosinase and dissolved oxygen, and L-ascorbic acid is for back-reducing o-quinones, and circulating tyrosinase reaction cycle. After optimizing the reaction conditions, the *ortho*-hydroxylation of daidzein, genistein, and resveratrol was successfully performed, and the produced substances, 7,3',4'-trihydroxy isoflavone (3'-ODI), 7,5,3',4'-tetrahydroxy isoflavone (orobol), and piceatannol, were identified as expected. The strategy was further subjected to the scale-up study, and the process was applicable in 400 L reaction with theoretical yield. Moreover, the hydroxylated phytochemicals were developed as functional ingredients of cosmetics. However, the method also has several limitations. One is that the dissociation constant of the formation of catechols and boric acid less than one, which means the formation is entirely dependent on the concentration of boric acid, which is not dissolved above 500 mM. The unbinding product was oxidized spontaneously by dissolved oxygen

during the reaction.

In Chapter 4, a novel tyrosinase from *Burkholderia thailandensis* (BT_Ty) was characterized and used it as another tool for *ortho*-hydroxylation of monophenols that could not be hydroxylated by the previous method, the method present in Chapter 3. The usage of boric acid and the optimum reaction pH of other tyrosinases could be problematic for producing and purifying the catechol derivatives because, for example, boric acid are not separable with glycosides, and the catechol derivatives are oxidized in neutral-to-basic pH by dissolved oxygen. This new enzyme was active only at acidic pH (where other tyrosinase is commonly inactivated) with the highest catalytic efficiency among tyrosinases reported so far. The target products, catechol derivatives, are found to be stable in such low pH solution. Thus, the *ortho*-hydroxylation using this tyrosinase did not require boric acid which was added for the protection of catechols. This reaction system was efficient for the *ortho*-hydroxylation of monophenol glycosides, daidzin, glycitin, genistin, polydatin, and phlorizin as well as several aglycones, phloretin, resveratrol, and daidzein.

Contrary to the previous chapters (Chapter 2, 3, and 4), Chapter 5 is comprised of the studies for accelerating the catecholase activity for enzymatic crosslinking of macromolecules. Previously, mushroom tyrosinase, tyrosinase from *Agaricus bisporus* (AB_Ty) was utilized for the enzymatic crosslinking for preparing hydrogels because of easy availability because the tyrosinase is only commercially available. However, applications of AB_Ty based crosslinking has been limited due to the low degree of crosslinking as a result of the steric hindrance between AB_Ty and macromolecules (Freddi, Anghileri et al. 2006, Hwang, Gim

et al. 2007, Le Thi, Lee et al. 2017). In this chapter, tyrosinase from *S. avermitilis* (SA_Ty) was utilized since the enzyme has a flat surface that is evolved for binding to a helper protein of the SA_Ty. And, through this chapter, the method for preparing the tyrosinase-mediated hydrogel is present, which showed significantly increased mechanical properties in terms of storage modulus (strength) and storage energy (stickiness).

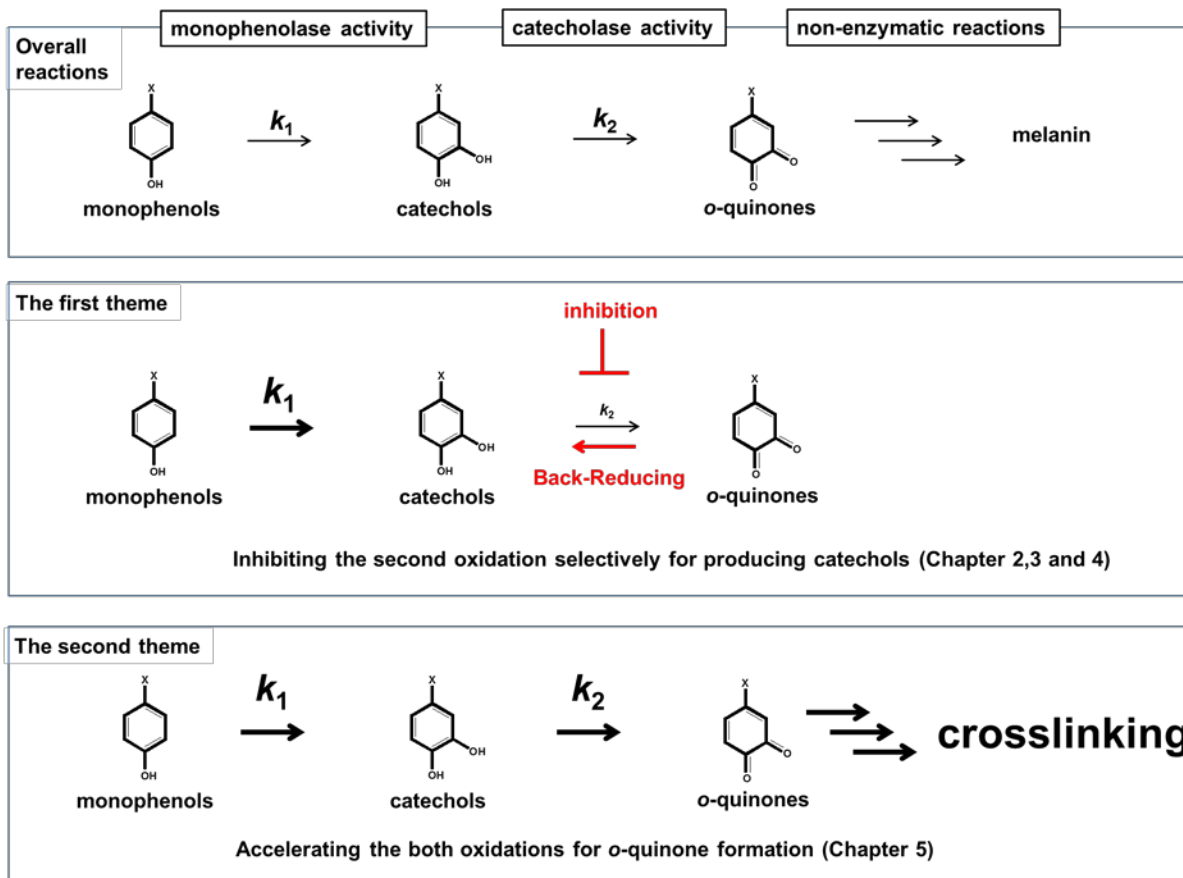


Figure 1.14. The schematic figure of the two different themes of this thesis.

Chapter 2.

**Heterologous expression of tyrosinase (SAV1137)
from *Streptomyces avermitilis* MA4680 in *Echerichia
coli* and its application for *ortho*-hydroxylation of
resveratrol to produce piceatannol**

2.1 Abstract

Recombinant tyrosinase from *Streptomyces avermitilis* MA4680, MelC2 (gi:499291317), was heterologously expressed in *E. coli* BL21 (DE3). The expression level of active MelC2 was increased by the codon-optimized MelC1 caddie protein (KP198295.1). By performing saturation mutagenesis of the Y91 residue of MelC1, it was found that aromatic residues such as Y, F, and W at the 91st position help produce a correctly folded conformation of MelC2. The recombinant MelC2 was utilized as a biocatalyst to convert trans-resveratrol into piceatannol. In order to improve the product yield through suppression of the formation of melanin, a by-product, an increase in the ratio of monooxygenation (k_1) to dioxygenation (k_2) of MelC2 is desirable. This was achieved by a combination of protein engineering and regeneration of NADH with glucose dehydrogenase (GDH). Saturation mutagenesis was performed at 15 residues within 8 Å radius from copper ions of MelC2. A total of 2,760 mutants were examined (99.7 % probability for NNK codon) and I41Y, a mutant, was screened. The ratio of k_1 to k_2 of the mutant increased sevenfold on tyrosine and fivefold on resveratrol when compared to wild-type MelC2. As a result, the overall product yield from 500 μM resveratrol in 50 mL reaction was 15.4 % (77.4 μM piceatannol), 1.7 times higher than wild type. When I41Y was incorporated with the NADH regeneration system, the total product yield was 58.0 %, an eightfold increase (290.2 μM of piceatannol).

Keywords: tyrosinase, *Streptomyces avermitilis*, resveratrol, piceatannol

2.2 Introduction

Tyrosinase is one of the type III copper-containing oxygenases, which performs both monooxygenation of monophenolic compounds and subsequent oxidation (called dioxygenation) of intermediate diphenolic compounds into quinonic compounds (Bright, Wood et al. 1963). Depending on the initial substrates, the quinonic compounds eventually lead to the formation of several types of melanin (Fairhead and Thöny-Meyer 2012). Under an excess amount of catechol, which acts as an inhibitor of dioxygenation, tyrosinase is an efficient enzyme for the conversion of *trans*-resveratrol into piceatannol (Lee, Kim et al. 2012). Furthermore, tyrosinase can hydroxylate tyrosol to *ortho*-hydroxytyrosol in the presence of ascorbic acid, suggesting that the quinonic products can be quickly reduced to diphenolic compounds with an appropriate reducing reagent (Espin, Varon et al. 2000). Although the roles of the additional reagents such as catechol and ascorbic acid are different, the yield of diphenolic compounds from the reaction is substantially dependent on their concentrations.

The first 3-D tyrosinase structure from *Streptomyces castaneoglobisporus* was revealed by Matoba et al. (Matoba, Kumagai et al. 2006), and other tyrosinase crystal structures from *Agaricus bisporus*, *Bacillus megaterium*, and *Marsupenaeus japonicus* (Matoba, Kumagai et al. 2006, Sendovski, Kanteev et al. 2010, Ismaya, Rozeboom et al. 2011, Rolff, Schottenheim et al. 2011, Masuda, Momoji et al. 2014, Mauracher, Molitor et al. 2014) are available on the RCSB. According to structures of 3WKY (Masuda, Momoji et al. 2014) and 1WS2 (Matoba, Kumagai et al. 2006), two copper ions are located in the active site of tyrosinase and tightly bind molecular oxygen (μ - η^2 : η^2 -peroxodicopper complex).

The position of each copper is firmly fixed by three histidine residues, maintaining approximately 3.5 Å between the two coppers (Palavicini, Granata et al. 2005, Hoffmann, Citek et al. 2013). The formation of the $\mu\text{-}\eta^2\text{:}\eta^2\text{-peroxodicopper}$ complex is critical for actual tyrosinase activity, while the diverse peptide frames restrict the substrate specificity of tyrosinase (Sendovski, Kanteev et al. 2011, Goldfeder, Kanteev et al. 2014). The catalytic efficiency of tyrosinase (k_{cat}/K_m) on L-tyrosine and L-3,4-dihydroxyphenylalanine (L-Dopa), and the ratio of monooxygenation and dioxygenation (k_1/k_2) of tyrosinase, can be changed through modification of residues near the entrance of its active site and the residues related to the flexibility of His residues coordinating the copper ions (Goldfeder, Kanteev et al. 2013). However, tyrosinase activity and the k_1/k_2 ratio both depend on the structure of each enzyme and substrate.

In this study, we have systemically carried out saturation mutagenesis on both MelC1 (gi:499291316) and MelC2 (gi:499291317) from *S. avermitilis* based on a 3D homology model. This allowed us to estimate what residues are critical in increasing the ratio of k_1 to k_2 on resveratrol to produce higher amounts of piceatannol, a known potent anticancer drug (Piotrowska, Kucinska et al. 2012). The mutagenesis studies demonstrate that the saturation mutagenesis of one tyrosine residue of MelC1 fitting into the active site of MelC2 influences the folding and solubility of tyrosinase. Moreover, site-saturation mutagenesis of a few residues of MelC2 involved in accessibility of the substrate to the copper ions, is critical for the increase in the k_1/k_2 ratio of MelC2 tyrosinase and the subsequent production of diphenolic compounds, herein piceatannol. In addition, we incorporated glucose dehydrogenase (GDH) into the tyrosinase reaction system to

continuously regenerate NADH, thus preventing further oxidation of piceatannol by reducing the oxidized quinone form of piceatannol back to piceatannol (Figure 2.1) (Iyanagi and Yamazaki 1970, Carlson and Miller 1985, Brown, Male et al. 1994)

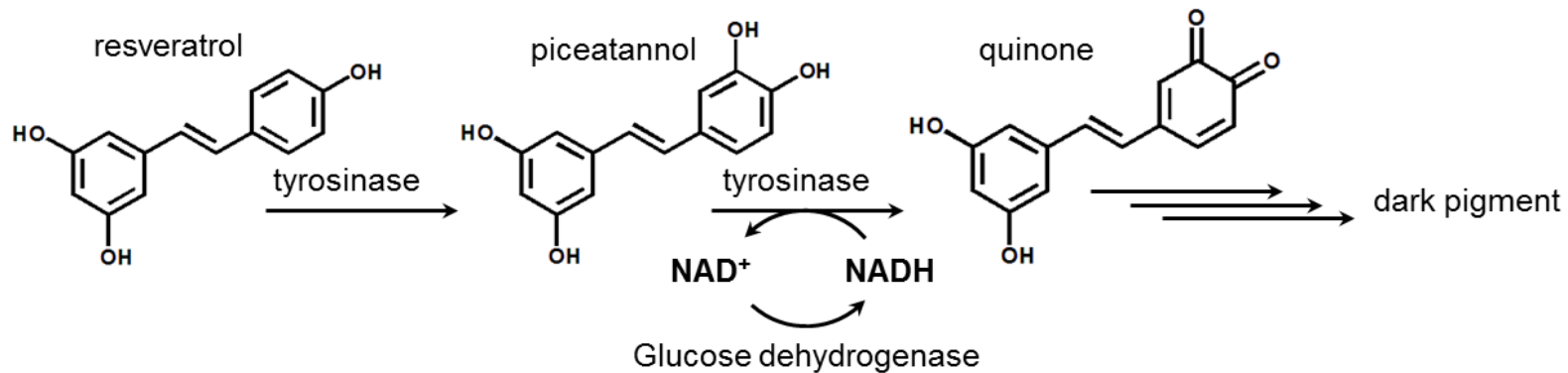


Figure 2.1. Schematic figure of the NADH regenerating system in piceatannol production by MelC2.

2.3 Materials and Methods

2.3.1 Materials

Restriction enzymes, T4-DNA ligase, DNA polymerase, and reagents for genetic engineering were purchased from Invitrogen Life Technology. L-tyrosine disodium salt hydrate, L-3,4-dihydroxyphenylalanine, resveratrol, and piceatannol were purchased from Sigma-Aldrich (Yongin, Korea). *Streptomyces avermitilis* MA4680, ATCC 31267, was purchased from the Korean Culture Center of Microorganisms (KCCM, Seoul, Korea). The NAD⁺/NADH quantitation colorimetric Kit (Cat#K337-100) was purchased from Biovision Inc. (Milpitas, CA., U.S.) Ni-NTA agarose (nickel-charged resin for His-tag purification) was purchased from Qiagen Korea Ltd. (Seoul, Korea). Primers (Table 2.1), reagents, and plasmids information on recombinant tyrosinase construction and glucose dehydrogenase are presented in Supplementary Material.

2.3.2 Construction of plasmids for the recombinant tyrosinase and a glucose dehydrogenase.

Genomic DNA was extracted from *S. avermitilis* with G-spin genomic DNA extract kit (Intron, Korea), and PCR was performed for amplifying the genes of tyrosinase. The genes of tyrosinase helper proteins, melC1(gi:499291316) and melD1(gi:499295506), were synthesized by Bioneer (Daejeon, Korea); Gene Designer by DNA 2.0 was used to design the gene sequence following the frequent *E.coli* codon usage (the accession numbers of the codon optimized melC1 and

melD1 are KP198295.1 and KP198296.1, respectively). The genes of tyrosinase helper protein were inserted into MCS1 of pETDuet (Novagen, USA), and the genes of tyrosinase into MCS2. His-tag was introduced at the N-terminal of the MelC2. GDH gene from *Bacillus subtilis* was amplified and inserted into the multiple cloning site of pET28a. The primers are listed in Table C1.

2.3.3 Expression and preparation of recombinant tyrosinase and glucose dehydrogenase (GDH) for reaction.

The recombinant plasmid was transformed into *E. coli* BL21 (DE3) by heat shock, and the engineered strain was spread on plates of solid Luria-Bertani (LB) media. A colony on the plate was inoculated into a test tube with 3 mL of LB broth with 25 µg/ml of ampicillin, and the test tube was placed into an incubator at 37 °C and at 200 rpm overnight. 0.5 mL of cell culture was transferred into a 250 mL flask with 50 mL of fresh LB with 25 µg·ml⁻¹ of ampicillin, and the flask was incubated at 37 °C at 200 rpm for about 2.5 hr. When OD at 600 nm (OD_{600nm}) of the cell cultures reached approximately 0.6, 0.2 mM IPTG and 1 mM CuSO₄ (i.e. final concentrations) were added. The cell culture was placed in an incubator at 18 °C at 200 rpm for 24 hrs. Cell pellets from 50 mL of cell culture (Cell OD_{600nm} was 1.35) was collected by centrifugation (approximately 5 g of wet cell weight) and washed with 5 mL of 50 mM tris-HCl buffer at pH 7.5. After cell lysis by ultra-sonication, 5 mL of soluble fraction of crude cell soup was collected after centrifugation at 16000 rpm for 30 min. The expressed enzymes were purified by general His-tag purification for kinetic measurements.

The experimental steps for expressing GDH are identical to heterologous expression of tyrosinase except for the antibiotic selection marker (50 $\mu\text{g}\cdot\text{ml}^{-1}$ of kanamycin was used), concentration of inducers (only 0.2 mM IPTG was added) and incubation conditions (at 37 °C for 5 hr). After disturbing cell walls by ultrasonication, 5 mL of soluble fraction of crude cell soup was collected from 50 mL cell culture.

2.3.4 Constructing mutants of MelC1 and MelC2.

We changed Y91 of MelC1 to 19 other residues by altering the codon of Y91 when designing primers (Table 2.3). For site-directed mutagenesis, we used NNK codon at target residues of MelC2 (Table 2.4). SolgTM Pfu DNA polymerase (SolGent Co., Ltd.) was used and the condition for PCR with the primers was primary denaturing at 95 °C for 2 min, 25 cycles of denaturing (at 95 °C for 20 sec), annealing (50-60°C for 20 sec, depending on T_m of primers), and extension (at 72 °C for 20 sec). The final extension was held at 72 °C for 5 min. After PCR, FastDigest DpnI (Thermo science) was used for removing the template plasmid.

2.3.5 Oxidation reaction of resveratrol in *E. coli*.

The recombinant tyrosinase was heterologously expressed in *E. coli* BL21 (DE3), and the crude cell extract was prepared as stated in Supplementary Material. 0.15 U of tyrosinase cell extract, 10 μM CuSO₄ and 500 μM resveratrol were used in the tyrosinase reaction. (The unit of MelC2 solution was calculated using 1 mM of L-tyrosine at 37°C with UV spectroscopy at 475 nm, measuring dopachrome

production with $\epsilon_{\text{dopachrome at } 475\text{nm}} = 3600 \text{ M}^{-1} \text{ cm}^{-1}$)(Goldfeder, Kanteev et al. 2013). 10 μM CuSO_4 was added for all tyrosinase reactions in this study for prevention of possible suicidal activity (Munoz-Munoz, Garcia-Molina et al. 2010). Otherwise, we have specified the reaction conditions. The control reaction was performed without tyrosinase but with the same amount of cell extract. Only the empty vector, pETDuet, was transformed into *E. coli* BL21 for the control reaction. The reaction mixture was kept in a shaking incubator at 200 rpm and 30 °C. Reaction samples of 100 μL were collected at certain time points and, the samples were extracted with 400 μL of ethyl acetate. The ethyl acetate layer was transferred into clean tubes and evaporated thoroughly, with the residual powder dissolved in methanol for further analysis. The product was analyzed by HPLC and the product was identified with GC/MS.

2.3.6 Effects of NADH on the production of piceatannol through tyrosinase reaction.

Firstly, the concentration of NADH was varied from 0 mM to 4 mM in the *in vitro* hydroxylation reaction system (500 μM resveratrol in 50mL reaction volume) to find the appropriate concentration of NADH. NADH regeneration was also optimized by using GDH. To do that, GDH from *B. subtilis* was heterologously expressed in *E. coli* BL21 (DE3) (Hilt et al. 1991). The unit of GDH was calculated using UV-spectroscopy (SPECTROstar Nano, BMG LABTECH, Ortenberg, Germany); NADH at 339 nm has an extinction coefficient of $6220 \text{ M}^{-1} \text{ cm}^{-1}$ (Alonso et al. 2014). In a 96 well micro-titer plate, a total of 200 μL reaction mixture was

prepared with 1 mM of glucose and NAD⁺. And 1 μ L of cell extract was added right before measuring NADH production. In this study, one unit of GDH is defined as the amount of GDH that produces 1 μ mol NADH in one minute in 200 μ L of reaction mixture at 37°C at pH 8. 0 to 3.6 U of GDH, with 0 to 4 mM of glucose and NAD⁺ added in the tyrosinase reaction to optimize the NADH regeneration system.

2.3.4 Saturation mutagenesis of MelC1 and comparison of MelC2 expression level

Saturation mutagenesis was performed on the Y91 residue of MelC1. The Y91 of MelC1 was changed to the other 19 amino acids. The primer sequences are listed in Table 2.2. After 24 hours of induction, the supernatant of the cell culture media where melanin was dissolved was collected, and the absorbance at 340 nm was measured. The MelC2 expression level-dependent on MelC1 was compared on the SDS-PAGE gel. Briefly, 5g of wet cells were collected from the culture media (washed with 10 mL PBS buffer twice) and cell walls were disturbed with an ultrasonicator (Vibra-Cell™ VCX 130, Sonics & Materials. INC., CT, USA). The soluble fraction of the cell mixtures was collected after spinning at 16000 rpm for 30 min. 10 μ L of each soluble fraction was mixed with 2X SDS loading dye with 200 mM dithiothreitol (Cold Spring Harb Protoc. 2006). Then 7 μ L of samples were loaded on 12 % tris-glycine SDS-polyacrylamide gel. The image of the gel was taken after staining with Coomassie Blue.

2.3.7 Screening for mutants with high specificity in piceatannol production

The candidate residues for the mutagenesis were selected from the results of homology modeling (More details are available in Supplementary Material). Saturation mutagenesis was done on the 15 residues within an 8Å distance from the copper ions of MelC2 (Figure 2.3). Genes corresponding to MelC2 were amplified with primers containing NNK codon (Nov 2012). The primer sequences are listed in Table 2.3. Roughly 200 colonies from each library of MelC2 were randomly selected and inoculated into sterilized 96-deep-well plates with 500 µL LB and 25 µg·mL⁻¹ of ampicillin (Amp) and incubated at 37 °C overnight. 5 µL of subculture was transferred into sterilized 96-deep-well plates with fresh 500µL LB/Amp and incubated at 37 °C. When optical density (O.D.) of the cell cultures reached approximately 0.6 at 600 nm, 0.2 mM IPTG and 1 mM CuSO₄ (i.e., final concentrations) were added. The 96-deep-well plates were placed into an 18 °C shaker (200 rpm) for 17 hrs. The cells were spun down at 4000 rpm for 10 min after induction. The supernatant of each well was carefully removed, and 100 µL of the supernatant was transferred to new 96-well plates. UV spectrometry (at 340 nm) was used to approximately evaluate the ability of the mutants to produce melanin.

100 µL of lysozyme (0.5 mg·mL⁻¹ lysozymes in 5 mM phosphate buffer pH at 7.0) was added into the wells with pellets for cell lysis. 10 µM of CuSO₄, 5U of GDH, 10 µL of 100 mM glucose and NAD⁺, and 0.1 µL of 100 mM of resveratrol were added to each well (total 200 µL), and the plates were placed on a 37 °C shaker (200 rpm) for 10 min. We set up the total reaction time based on the point that reaches the maximum yield of the diphenolic compound. 100 µL of 5

mM FeCl₃ in 50 mM Tris buffer (pH 7.5) was added to stop the reaction. Then, piceatannol was detected by the conjugation of ferric ions, displaying a dark green color (Figure 2.2).

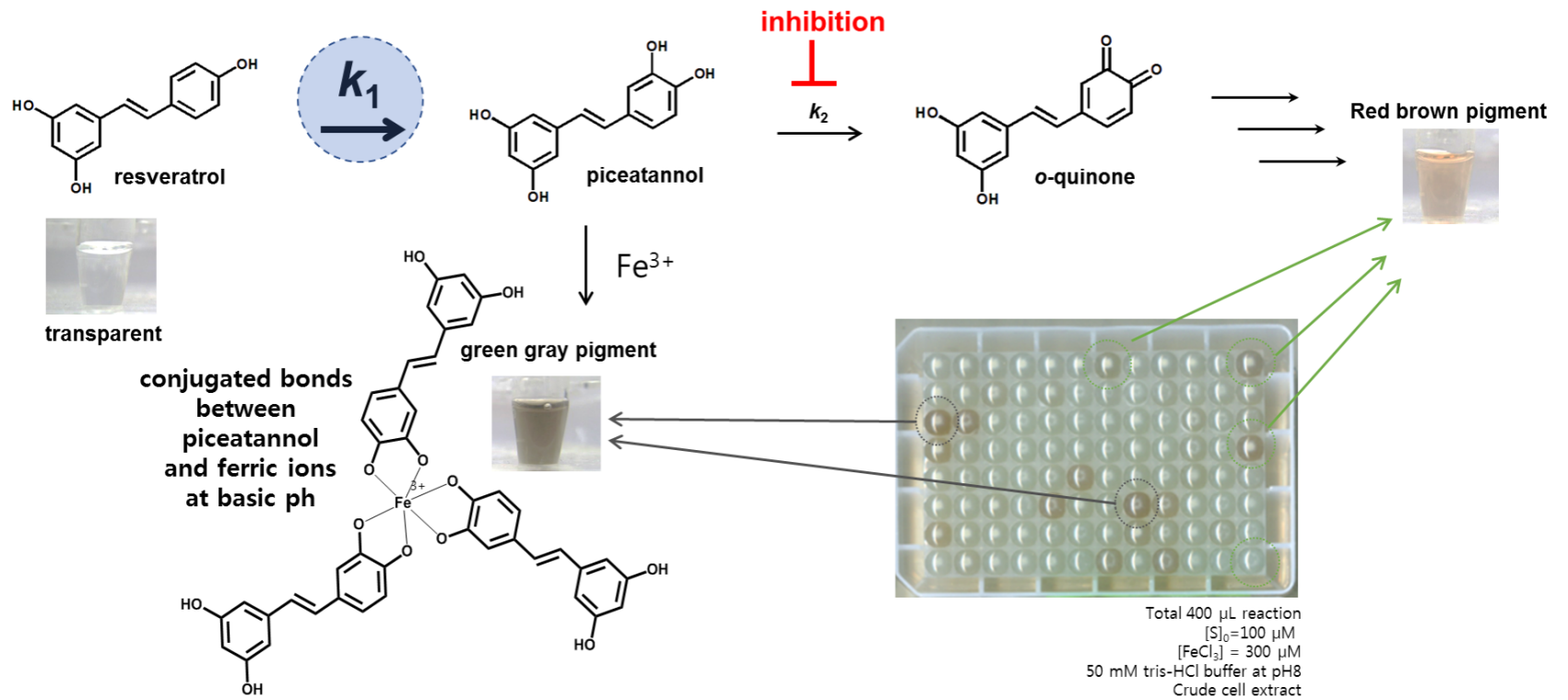


Figure 2.2. The colorimetric assay method for screening mutants.

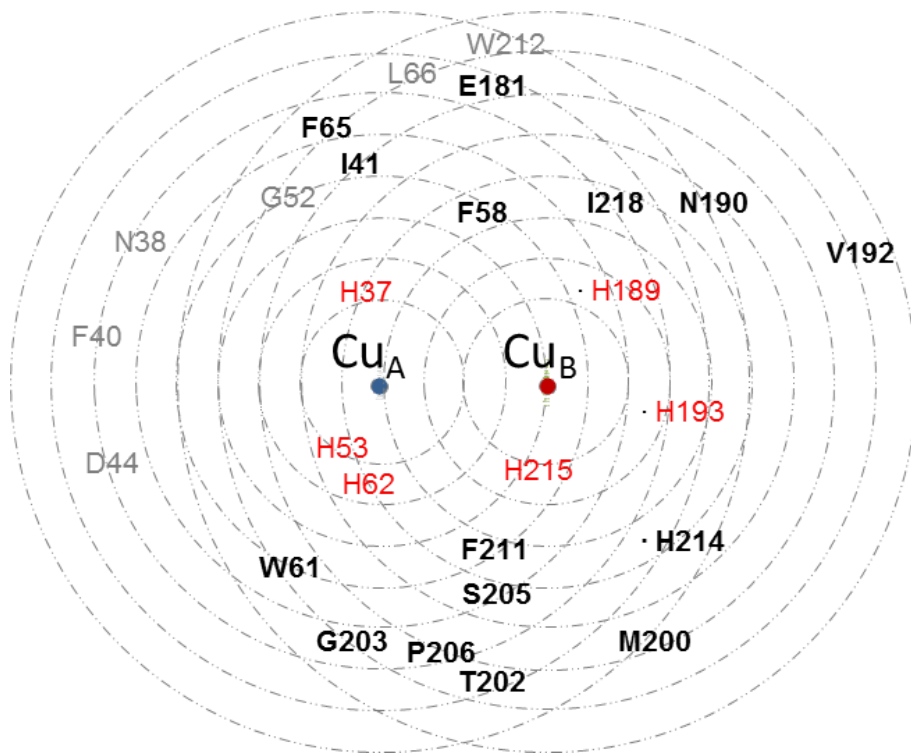


Figure 2.3. Residues around the active site of MelC2.

H37, H53, H62, H189, H193 and H215 are critical residues that hold copper ions.

The radius of each dashed circle is 1 Å. Total 15 residues (bold characters) in 8 Å from the copper ions of MelC2 were subjected to mutagenesis in this study.

2.3.8 Kinetics characterization of wild-type and I41Y on L-tyrosine, L-DOPA, resveratrol, and piceatannol.

MelC2 and the MelC2 mutants were His-tag purified for the kinetics measurements according to the protocol provided by Qiagen. (Qiagen. 2003) The formation of dopachrome was used to measure the kinetics of the enzymes on L-tyrosine and L-DOPA by UV spectroscopy at 475nm ($\epsilon_{\text{dopachrome at 475nm}}=3600 \text{ M}^{-1} \text{ cm}^{-1}$) (Goldfeder et al. 2013). 0.1 to 2 mM of L-tyrosine and L-DOPA was tested with $5 \mu\text{g}\cdot\text{mL}^{-1}$ (170 nM) of His-tag purified enzyme (Qiagen 2003) in 200 μL 50 mM tri-HCl buffer at pH 8 at room temperature. The kinetics of tyrosinases on resveratrol and piceatannol were monitored by HPLC. 10 to 300 μM of the substrate was tested with $25 \mu\text{g}\cdot\text{mL}^{-1}$ (85 nM) of His-tag purified enzyme in 100 μL 50 mM tri-HCl buffer at pH 8 at room temperature. All control reactions were performed under the same reaction condition but without MelC2. After 2 min the reaction was stopped by adding 400 μL ethyl acetate. Then 200 μL ethyl acetate layer was transferred into a new tube. The solvent was evaporated, and 100 μL of methanol was added into the residual powder right before HPLC analysis. (Samples were prepared as stated in Supplementary Material). A total of ten trials were repeated, and the average initial velocities on each initial substrate concentration were plotted using a regression wizard in SigmaPlot 10.0. (one site saturation equation was used)

2.3.9 Preparing samples for kinetic values of MelC2.

All samples were prepared right before measuring the kinetics. First, 20 mg L-Dopa was dissolved in 400 μL of 0.5 M HCl, and then 394 μL of $50 \text{ mg}\cdot\text{ml}^{-1}$ L-

DOPA were added in 50 mL of 50 mM tris-HCl buffer at pH 8 to make 2 mM L-DOPA solution. L-tyrosine disodium salt hydrate was used to prepare 2 mM L-tyrosine solution. With 50 mM tris-HCl buffer at pH 8, the samples were diluted to 100 μ M, 200 μ M, 400 μ M, 600 μ M, 800 μ M, 1.2 mM, 1.5 mM and 2 mM in a 96-well microplate for measuring kinetics. 22.8 mg of resveratrol and 24.4 mg of piceatannol were dissolved in 1 mL of MeOH to make 100 mM samples. With 50 mM tris-HCl buffer at pH 8, the samples were diluted to 18.75 μ M, 37.5 μ M, 75 μ M, 150 μ M, and 300 μ M. Above 500 μ M, resveratrol was precipitated in 50 mM tris-HCl buffer at pH 8.

2.3.10 Computational modeling

MelC1 from *Streptomyces castaneoglobisporus* and *S. avermitillis* were aligned with 85.5 % identity, 92.4% similarity and 0.4% gaps. Thus the crystal structure of MelC1 from *S. castaneoglobisporus*, 1WX2, was used as a template for modeling MelC1 from *S. avermitillis* and mutants with Modeler 9.11. (1WX2 is available on RCSB protein data bank) AutoDock Vina 1.1.2 (Trott et al. 2010) and MGLTools 1.5.6. were used for docking simulation. Chimera 1.10rc and PyMOL were used for visualizing the results. Polar hydrogens were added to all protein structures prior to docking simulation by Python Molecule Viewer 1.5.6. The center of the grid box was fixed at the position of CuA of MelC2, and the grid sizes of x, y and z axis were set to 30 Å. Exhaustiveness was set to 8 as default and the docking number was 10 with an energy range of 3.

2.3.11 Analytical methods

Time-dependent consumption of substrates and formation of products were monitored by HPLC. The HPLC analysis was performed on an Autochro-3000 (Young Lin, Seoul, Korea) connected with a UV/Vis detector and a C18 column (4.6 mm × 150 mm). The HPLC analysis conditions were as follows: 1) resveratrol and piceatannol – mobile phase, 30% acetonitrile in H₂O containing 0.1% trifluoroacetic acid; flow rate: 1 mL/min; detection wavelength, 325 nm; 2) daidzein and 3'-hydroxydaidzein – mobile phase, 25% acetonitrile in H₂O containing 0.1% trifluoroacetic acid; flow rate, 1 mL/min; detection wavelength, 254 nm.

GC/MS was used to identify all metabolites. All hydroxyl groups of the dried sample extracted with ethyl acetate were converted to TMS (trimethylsilyl) derivatives by heating for 30 min at 60 °C with BSTFA. GC/MS was performed on a Thermo Scientific Trace GC Ultra instrument connected to a Thermo Scientific ITQ1100 MS spectrometer (Rockford, IL, USA) with a TR-5ms SQC capillary column (30 m × 0.25 mm i.d., 0.25 μm film thickness). The GC/MS analysis was carried out as follows: injector temperature, 250 °C; temperature gradient: 150 °C hold for 1 min, 10 °C/min up to 300 °C, 300 °C hold for 5 min; MS operating mode: 70 eV electron ionization mode.

Table 2.1. Primer list for cloning SA_Ty and GDH

Primer	Sequence (5' → 3')
MeIC1_F	GAA CCATGG AGTTAACCCGGCGT
MeIC1_R	GAC AAGCTT TTAATTAAACGG
MeID1_F	GAA CCATGG TGACGTTAGCACCTG
MeID1_R	GAC AAGCTT TTAGGCATGTACTC
MeIC2_F	GAA CCATGG ATGACCGTACGCAA
MeIC2_R	GAC AAGCTT GACGGTGTAGAACG
GDH_F	GAT GAATTC ATGTATCCGGATTAAAAGG
GDH_R	GCA CTCGAG TTAACCGCGGCCT

Table 2.2. The list of primers for mutants of MelC1

Site (MelC1)		Primer sequence
Y91R	Forward	GTC GTA TCC CAT CGT GAC CCC GTT GC
	Reverse	GCA ACG GGG TCA CGA TGG GAT ACG AC
Y91N	Forward	GTC GTA TCC CAT AAT GAC CCC GTT GC
	Reverse	GCA ACG GGG TCA TTA TGG GAT ACG AC
Y91D	Forward	GTC GTA TCC CAT GAT GAC CCC GTT GC
	Reverse	GCA ACG GGG TCA TCA TGG GAT ACG AC
Y91C	Forward	GTC GTA TCC CAT TGC GAC CCC GTT GC
	Reverse	GCA ACG GGG TCG CAA TGG GAT ACG AC
Y91E	Forward	GTC GTA TCC CAT GAA GAC CCC GTT GC
	Reverse	GCA ACG GGG TCT TCA TGG GAT ACG AC
Y91Q	Forward	GTC GTA TCC CAT CAG GAC CCC GTT GC
	Reverse	GCA ACG GGG TCC TGA TGG GAT ACG AC
Y91G	Forward	GTC GTA TCC CAT GGC GAC CCC GTT G
	Reverse	CAA CGG GGT CGC CAT GGG ATA CGA C
Y91H	Forward	GTC GTA TCC CAT CAC GAC CCC GTT G
	Reverse	CAA CGG GGT CGT GAT GGG ATA CGA C
Y91I	Forward	GTC GTA TCC CAT ATT GAC CCC GTT GC
	Reverse	GCA ACG GGG TCA ATA TGG GAT ACG AC
Y91L	Forward	GTC GTA TCC CAT CTG GAC CCC GTT GC
	Reverse	GCA ACG GGG TCC AGA TGG GAT ACG AC
Y91K	Forward	GTC GTA TCC CAT AAA GAC CCC GTT GC
	Reverse	GCA ACG GGG TCT TTA TGG GAT ACG AC
Y91M	Forward	GTC GTA TCC CAT ATG GAC CCC GTT GC
	Reverse	GCA ACG GGG TCC ATA TGG GAT ACG AC
Y91P	Forward	GTC GTA TCC CAT CCG GAC CCC GTT GC
	Reverse	GCA ACG GGG TCC GGA TGG GAT ACG AC
Y91S	Forward	GTC GTA TCC CAT AGC GAC CCC GTT G
	Reverse	CAA CGG GGT CGC TAT GGG ATA CGA C
Y91T	Forward	GTC GTA TCC CAT ACC GAC CCC GTT G
	Reverse	CAA CGG GGT CGG TAT GGG ATA CGA C
Y91W	Forward	GTC GTA TCC CAT TGG GAC CCC GTT GCA AC
	Reverse	GTT GCA ACG GGG TCC CAA TGG GAT ACG AC
Y91V	Forward	GTC GTA TCC CAT GTG GAC CCC GTT GC
	Reverse	GCA ACG GGG TCC ACA TGG GAT ACG AC

Y91F	Forward	GTC GTA TCC CAT TTT GAC CCC GTT GCA AC
	Reverse	GTT GCA ACG GGG TCA AAA TGG GAT ACG AC
Y91A	Forward	GTC GTA TCC CAT GCG GAC CCC GTT GC
	Reverse	GCA ACG GGG TCC GCA TGG GAT ACG AC

Table 2.3. The list of primers for mutants of MelC2

NNK and MNN codons were used for constructing mutant libraries, where N = A/C/G/T, B = C/G/T, S = C/G, K = G/T, and M = A/C. (Nov 2012)

Site (MelC2)		Primer sequence
F58	Forward	GTT CGC CTT CCN NKC TGC CCT GGC AC
	Reverse	GTG CCA GGG CAG MNN GGA AGG CGA AC
F211	Forward	CCC AAC GAC CCG GTC NNK TGG CTC CAC CAC GCC
	Reverse	GGC GTG GTG GAG CCA MNN GAC CGG GTC GTT GGG
H214	Forward	GTC TTC TGG CTC NNK CAC GCC TAC ATC
	Reverse	GAT GTA GGC GTG MNN GAG CCA GAA GAC
I218	Forward	CAC CAC GCC TAC NNK GAC AGG CTC TG
	Reverse	CAG AGC CTG TCM NNG TAG GCG TGG TG
N190	Forward	GGT GTG AAC CTG CAC NNK CGC GTC CAC GTC TGG
	Reverse	CCA GAC GTG GAC GCG MNN GTG CAG GTT CAC ACC
S205	Forward	ATG GCC ACC GGG GTC NNK CCC AAC GAC CCG GTC
	Reverse	GAC CGG GTC GTT GGG MNN GAC CCC GGT GGC CAT
M200	Forward	TGG GTC GGC GGC CAG NNK GCC ACC GGG GTC TCC
	Reverse	GGA GAC CCC GGT GGC MNN CTG GCC GCC GAC CCA
I41	Forward	ACC CAC AAC GCC TTC NNK ATG GGC GAC ACC GAC
	Reverse	GTC GGT GTC GCC CAT MNN GAA GGC GTT GTG GGT
W61	Forward	CCT TCC TTC CTG CCC NNK CAC CGC AGA TTT TTG
	Reverse	CAA AAA TCT GCG GTG MNN GGG CAG GAA GGA AGG
F65	Forward	CCC TGG CAC CGC AGA NNK TTG ATC GAG TTC GAG
	Reverse	CTC GAA CTC GAT CAA MNN TCT GCG GTG CCA GGG
E181	Forward	TTC CGC AAC CAT CTC NNK GGC TGG CGC GGT GTG
	Reverse	CAC ACC GCG CCA GCC MNN GAG ATG GTT GCG GAA
V192	Forward	AAC CTG CAC AAC CGC NNK CAC GTC TGG GTC GGC
	Reverse	GCC GAC CCA GAC GTG MNN GCG GTT GTG CAG GTT
T202	Forward	GGC GGC CAG ATG GCC NNK GGG GTC TCC CCC AAC

	Reverse	GTT GGG GGA GAC CCC MNN GGC CAT CTG GCC GCC
G203	Forward	GGC CAG ATG GCC ACC NNK GTC TCC CCC AAC GAC
	Reverse	GTC GTT GGG GGA GAC MNN GGT GGC CAT CTG GCC
P206	Forward	GCC ACC GGG GTC TCC NNK AAC GAC CCG GTC TTC
	Reverse	GAA GAC CGG GTC GTT MNN GGA GAC CCC GGT GGC

2.4 Results and Discussion

2.4.1 Expression of tyrosinase, MelC2, in *E. coli*

MelC2 expressed using the T7 promoter of pET plasmid formed mostly inclusion bodies despite the optimization of IPTG induction conditions (data not shown). Since the presence of MelC1 tyrosinase helper protein in *Streptomyces* strains is known to be essential in assisting the folding of MelC2 during translation (Fairhead et al. 2012), MelC1 and MelC2 were co-expressed. However, the expression level of MelC2 was still poor and melanin formation by MelC2 was not significantly increased (Figure 2.4).

SDS-PAGE electrophoresis then confirmed that MelC1 was not expressed well in the same expression system. We speculated that the biggest problem, in this case, is the significant differences in codon usage between *S. avermitilis* and *E. coli*. To overcome the problem, first, MelC1 was synthesized following the codon usage of *E. coli*. (Sharp et al. 1988) When the codon optimized MelC1 (*i.e.* MelC*) and MelC2 were cloned into pET Duet plasmid and expressed together, the cell culture broth became dark after 7 hours of induction with 0.2 mM IPTG at 18 °C. When the codon-optimized helper protein from another operon (*i.e.* MelD*) was co-expressed on agar plates with 0.2 mM IPTG and 1 mM CuSO₄, its effect was not as great as that of MelC1* (Figure 2.4), suggesting that helper protein also has partner specificity.

Our results suggest that soluble expression of the helper protein MelC1 with codon-optimization was the key to achieving successful expression of MelC2 in *E. coli*. Interestingly, the codon optimization of MelC2 was not essential for its soluble and active expression.

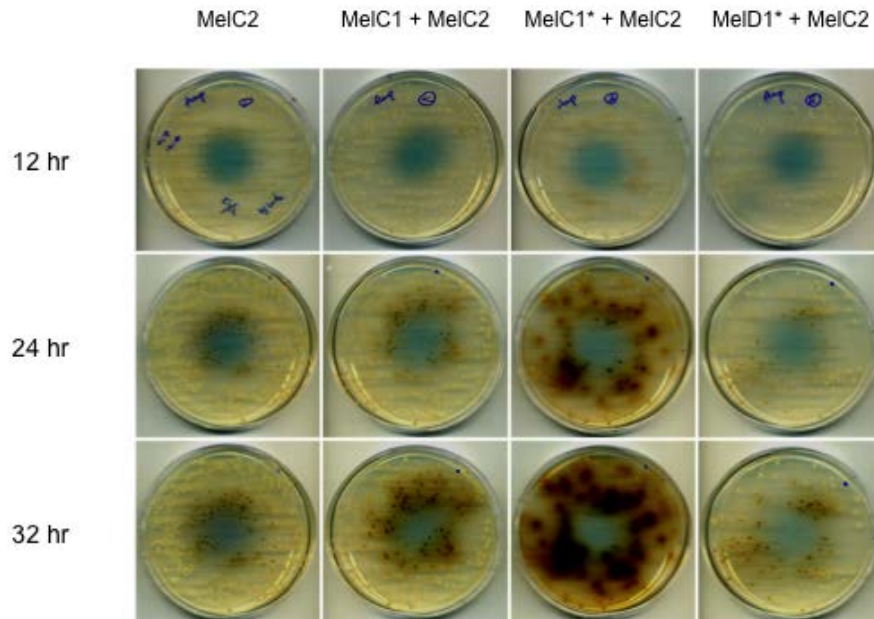


Figure 2.4. Assay of melanin formation.

MeIC2 was co-expressed with helper proteins from *S. avermitilis* MA4680, MeIC1 and MeID1; * indicates codon optimized helper protein. When MeIC2 was co-expressed with MeIC1*, the dark melanin was detected only after 12 hours of induction, and the plate significantly showed the darkest color among the variants.

2.4.2 Effect of NADH in the reaction system.

One molecular NAD(P)H donates two electrons to two molecular quinones, and converts the quinonic compound, 4-(3,5-dihydroxystyryl)cyclohexa-3,5-diene-1,2-dione, back to piceatannol (Iyanagi et al. 1970). As shown in Figure 2.5, the total amount of piceatannol increased as the initial concentration of NADH in the reaction increased; however, more than 2 mM of NADH did not improve the yield of piceatannol significantly. Without NADH, 35.5 μM of piceatannol was produced from 500 μM resveratrol. The additions of 1 mM, 2 mM, 3 mM and 4 mM of NADH resulted in 76.4 μM , 108.1 μM , 110.1 μM and 113.2 μM of piceatannol, respectively.

Furthermore, GDH was utilized to maintain the initial concentration of NADH during the reaction. The effect of GDH expression was effective only after cell lysis since glucose is phosphorylated *in vivo* as it enters the host cell via a glucose specific PTS transporter. The total amounts of piceatannol were increased threefold when 5U of GDH, 4 mM of glucose, and 2 mM of NAD^+ were added in 50 mL reaction. (The optimal unit of GDH and the concentrations of glucose and NAD^+ were determined prior to the experiments.) The maximum concentration of piceatannol was 108.3 μM , which is three times higher than that in the same reaction without NADH. (Figure 2.6)

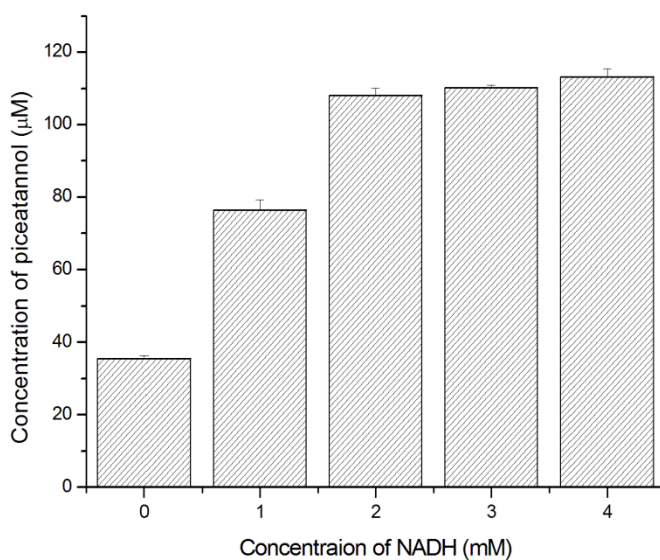


Figure 2.5. Concentration of piceatannol depending on the concentration of NADH.

The total production of piceatannol increased proportionally as the concentration of NADH increased. But 2 mM or more of NADH did not cause significant improvement in piceatannol production from 500 µM resveratrol by 170 nM MelC2 in 50mL reaction volume at 37°C. 50 mM of tris-HCl buffer at pH 8 was used. 10 µM CuSO₄ was added in the reaction for preventing possible suicide inactivation. 100µL of samples were collected after 5, 10, 15, 20, 30, and 60 min of reaction. The product, piceatannol, was extracted from 100µL of samples by 400µL of ethyl acetate. After removing ethyl acetate, the residual powder was dissolved in MeOH and the quantity of piceatannol produced was analyzed by HPLC. The maximum amount of piceatannol produced from each condition was plotted.

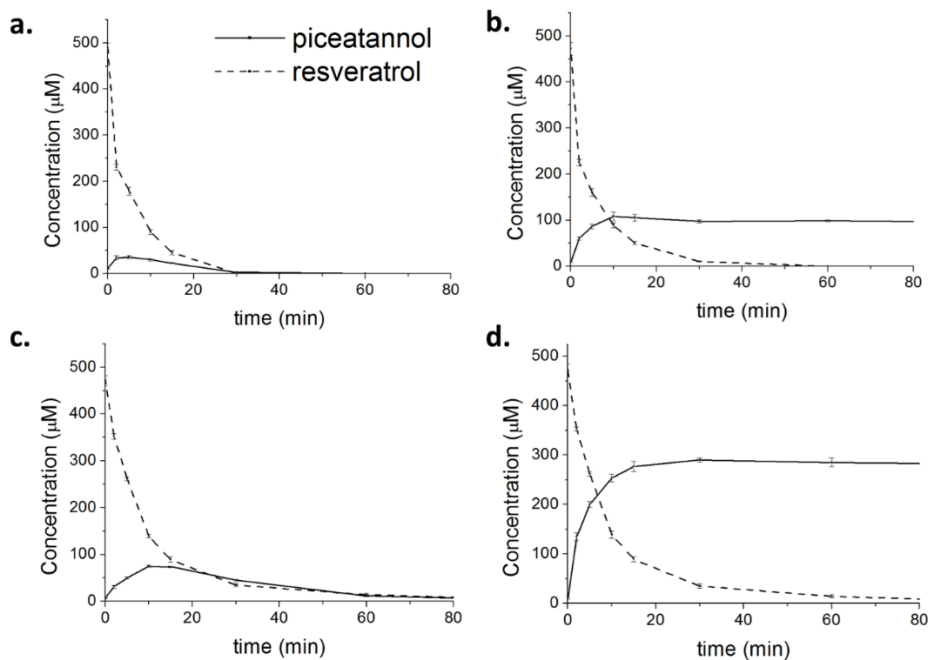


Figure 2.6. Time profile of hydroxylation of 500 μM resveratrol with or without the NADH regenerating system.

The concentration of resveratrol and piceatannol was monitored by HPLC. 0.15 U of tyrosinase cell extract and 10 μM CuSO_4 were used in this 50 mL reaction. (a) Without incorporating GDH, the maximum concentration of piceatannol by MelC2 was 35.8 μM . (b) 5U of GDH, 4 mM glucose, and 2 mM of NAD^+ were added in the reaction buffer, and NADH production was led for 10 min before hydroxylation. The maximum concentration of piceatannol by MelC2 was 108.3 μM . (c) Without GDH, the maximum concentration of piceatannol produced by I41Y was 77 μM . (d) After incorporating 5U of GDH with 4 mM glucose and 2 mM NAD^+ , the piceatannol produced by I41Y was not oxidized easily and the total amount of piceatannol produced was maintained at 290 μM .

2.4.3 Saturation mutagenesis of helper protein, MelC1 at Y91

Using PDB 1WX2 as a template, the structures of predicted homology models of MelC1 (green) and MelC2 (red) are shown in Figure 2.7 (more information on the modeling is in Supplementary Material). The Y91 residue points outward from the MelC1, so that it is likely to fit into the entrance of the MelC2 active site just like the pin of a thumbtack. The role of the tyrosine (Y91) is known to help both the position of the two copper ions inside MelC2 and the correct folding conformation (Chen et al. 1992). To see the effects of the Y91 residue of MelC1 on the activity of MelC2 in detail, single point saturation mutagenesis of MelC1 was performed.

The expression levels of MelC2 were compared indirectly on SDS-PAGE gel (Figure 2.8) and by the amount of melanin produced after induction (Table 2.4). As shown in the SDS-PAGE gel of Figure 2.8, significant amounts of MelC2 were expressed soluble when Y91F, Y91H, Y91K, Y91W mutants and the wild type of MelC1 were co-expressed. Cell culture media of those mutants turned brown after 5 h of cultivation after induction, indicating intact MelC2 function. The common features of the four variants (Y91F, Y91H, Y91K and Y91W) are either aromatic or positively charged amino acids with long chain lengths. However, the culture media became dark after 10 to 17 h when the Y91 variants were substituted with A, C, L, M, N, R and S, though they were slow to form melanin, with expression levels of MelC2 not clearly visible on SDS-PAGE gel.

The other mutants did not show significant color changes and the clear expression levels of MelC2 were not observed on SDS-PAGE gel. When soluble MelC2 was observed at 30kDa (arrow (c) in Figure 2.8), unknown bands over 240kDa at the top of the SDS-PAGE appeared (arrow (a) in Figure 2.8). Generally,

tyrosinase converts tyrosine residues on various proteins into their quinone form, and this quinone can form covalent bonds with some other residues possessing an amine group, thiol group, or monophenolic ring (Thalman et al. 2002). Thus, the (a) band in Figure 2.8 appeared to be cross-linked proteins due to non-specific crosslinking of polypeptides by MelC2. The (b) band in Figure 2.8 between 35kDa and 50kDa, and also found in the lane of *E. coli* with the empty pETDuet vector, disappeared when MelC2 tyrosinase was expressed, and the culture media became dark. The identification of the protein bands is beyond the scope of this study but it is assumed that the (b) band may have tyrosine residues which can be activated by MelC2 for inter- and/or intramolecular crosslinking. As a result, it became larger in size, and appeared at the top of the SDS-PAGE gel, the (a) band.

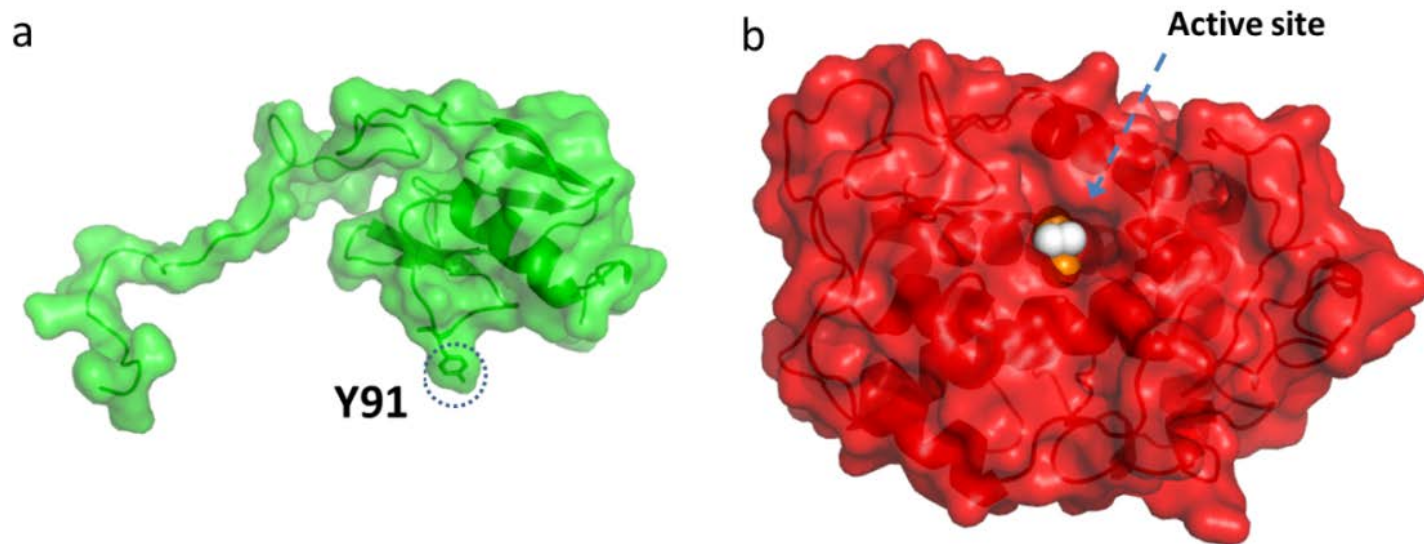


Figure 2.7. Homology models of (a) MelC1 and (b) MelC2.

Y91 of MelC1 perturbs in the active site of MelC2. In (b), orange and white spheres are copper ions and oxygens, respectively.

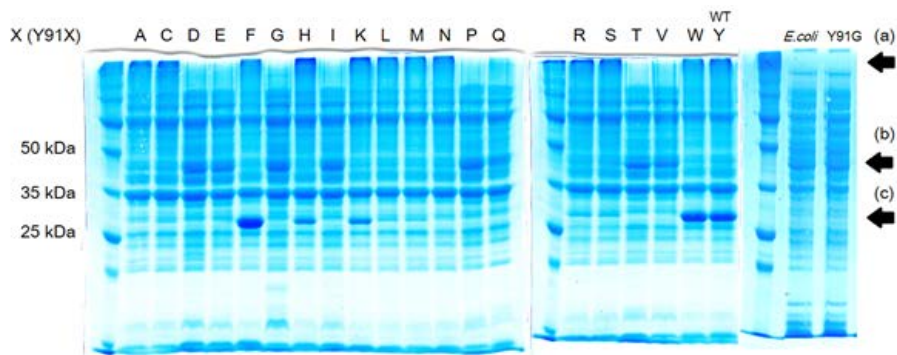


Figure 2.8. SDS-PAGE gel image of MelC2 expressed with Y91 mutants of MelC1.

MelC2 was co-expressed with MelC1 mutants. The expression levels of MelC2 were compared on SDS-PAGE gel. ‘*E. coli*’ means the protein bands of *E.coli* without MelC2. Arrow (a) is assumed to be bands of cross-linked proteins, arrow (b) represents a band of unknown proteins from *E. coli*, and arrow (c) represents the band of MelC2. Only the supernatants of the cell extract after centrifugation were used for loading to SDS-PAGE gel

Table 2.4. Absorbance of melanin at 340 nm after induction of MelC2 and Y91 mutants of MelC1.

After 24 hours of induction with 0.2 mM of IPTG and 1 mM of CuSO₄ in incubator at 18°C, the cell culture soup was spun down at 4000 rpm for 10 min. Supernatant samples were collected and the amount of melanin in the supernatant of each mutant was compared by measuring the absorbance at 340 nm.

Y91X	Abs	Y91X	Abs	Y91X	Abs	Y91X	Abs
A	0.124	G	0.074	M	0.112	S	0.111
C	0.116	H	0.167	N	0.088	T	0.071
D	0.076	I	0.077	P	0.073	V	0.067
E	0.078	K	0.149	Q	0.080	W	0.181
F	0.291	L	0.136	R	0.140	Y	0.228

Table 2.5. Kinetics constants of wild type MelC2 and I41Y

		V_{\max} ($\mu\text{mol}\cdot\text{min}^{-1}\cdot\text{mg}^{-1}$)		K_m (mM)		k_{cat}/K_m ($\mu\text{mol}\cdot\text{min}^{-1}\cdot\text{mg}^{-1}\cdot\text{mM}^{-1}$)	$V_{\max_mono}/$ V_{\max_Di}	$(k_{\text{cat}}/K_m)_{mono}/$ $(k_{\text{cat}}/K_m)_{Di}$
WT	L-tyrosine	1.05	$\pm 3.70\cdot 10^{-2}$	0.589	$\pm 5.63\cdot 10^{-2}$	1.79	0.108	0.515
	L-Dopa	9.67	± 1.85	2.79	$\pm 7.89\cdot 10^{-1}$	3.47		
I41Y	L-tyrosine	2.98	$\pm 9.52\cdot 10^{-2}$	0.152	$\pm 2.91\cdot 10^{-2}$	19.6	0.833	30.7
	L-Dopa	3.57	$\pm 4.02\cdot 10^{-1}$	5.60	± 1.75	0.639		
WT	resveratrol	1.98	± 0.119	0.0949	$\pm 1.39\cdot 10^{-2}$	20.9	0.225	0.358
	piceatannol	8.80	± 0.633	0.150	$\pm 2.26\cdot 10^{-2}$	58.4		
I41Y	resveratrol	5.15	± 0.362	0.0726	$\pm 1.36\cdot 10^{-2}$	70.9	1.23	11.4
	piceatannol	4.18	± 0.313	0.6721	$\pm 1.38\cdot 10^{-1}$	6.22		

Total ten trials were repeated and the average initial velocities of each initial substrate concentration were plotted and the standard errors were obtained by regression wizard of SigmaPlot 10.0. (one site saturation equation was used)

2.4.4 Saturation mutagenesis of MelC2 and production of piceatannol by I41Y mutant.

A total of 2,760 mutants, which are constructed by single point saturation mutagenesis of 15 different sites of MelC2 (Figure 2.3), were compared for piceatannol production. F58, F211, W61, F65, and E181 were omitted from the screening, because these residues appeared to be important for maintaining MelC2 activity. When changing these residues to other amino acids, most of the mutants did not produce melanin. (Table 2.6) The remaining 10 mutant libraries were subjected to the screening step. In the presence of ferric ions, the reaction mixture turned to a dark greenish color due to chelating ferric ion and piceatannol. Mutants showing the darker green colors (i.e. expected to have higher k_1/k_2 than wild type) were found in I218, N190, M200, I41, and T202 libraries; therefore, 50 mutants overall (10 mutants from each library) were selected, and their sequences were identified.

It was found that I41Y (eight out of ten), N190R (four out of ten), M200C (six out of ten), T202S (five out of ten), and I218S (five out of ten) were the major mutants. The results of the saturation mutagenesis of MelC2 were summarized in Table 2.5. After His-tag purification, the reaction profiles of the five mutants were monitored by HPLC, and kinetic parameters of the wild type and the I41Y mutant were measured (Table 2.5). The rates of other mutants such as N190R, M200C, and T202S were not measured because of their low activities. There is a possibility that k_1 and k_2 both get slower though k_1/k_2 may improve. This is the limitation of our screening method. In the case of the I218S mutant, the ratio of k_1/k_2 is similar to that of the wild type but both k_1 and k_2 were two times lower than those of wild

type (data not shown). The structural comparison between wild type and I218S is depicted in Figure 2.12. I41Y mutant is the only mutant that has higher k_1/k_2 , maintaining the same order of k_1 and k_2 as wild type. The ratio of k_1 to k_2 of the I41Y mutant increased sevenfold on tyrosine and fivefold on resveratrol, when compared with wild type MelC2. The ratio of the catalytic efficiency, k_{cat}/K_m , of monophenolase and phenolase activity is significantly increased on both L-tyrosine and resveratrol because of higher K_m of I41Y on L-Dopa and piceatannol (Table 2.5).

In addition, the overall amount of piceatannol produced from its reaction (500 μM resveratrol in 50mL) was 1.7 times higher, resulting in a 15.4 % yield (77.4 μM of piceatannol). Furthermore, by incorporating the NADH regeneration system, the total yield of piceatannol was 58.0 % (290.2 μM of piceatannol), a more than threefold increase of piceatannol (Figure 2.6). As a result, by constructing mutants and introducing GDH a total eightfold increase was achieved.

Table 2.6. Result of site-saturated mutagenesis

In the first screening, 'O' means that the percentage of mutants releasing melanin exceeds 16%, and the second step was performed subsequently. On the other hand, 'X' means that the library was not subjected to the second step, because the number of mutants releasing melanin was below 16%, suggesting that the residue is essential for tyrosinase activity. In the second screening, 'O' means that mutants show higher activity than wild type, and 'X' means that mutants generally do not show darker green than wild type.

Distance(Å) from Cu to C _α of residues	Amino acid	% of the mutants showing melanin synthesis	First step screening (melanin formation)	Second step screening (with substrate after cell lysis)	Major mutants' Sequencing result
5	F58	4	X	-	-
	F211	12	X	-	-
	H214	16	O	X	-
	I218	26	O	O	I218S
6	N190	39	O	O	N190R
	S205	46	O	X	-
7	M200	19	O	O	M200C
8	I41	57	O	O	I41Y
	W61	8	X	-	-
	F65	9	X	-	-
	E181	6	X	-	-
	V192	22	O	X	-
	T202	16	O	O	T202S
	G203	78	O	X	-
	P206	44	O	X	-

2.4.5 Model prediction and characterization of mutants

To analyze the five mutants (N190R, M200C, T202S, I218S, and I41Y) selected above, homology modeling was performed, and an enzyme-substrate docking simulation was attempted using AutoDock Vina 1.1.2 (Trott et al. 2010) with MGLTools 1.5.6. The models of N190R, M200C, and T202S appeared to have narrower entrances for resveratrol than their wild type (Figure 2.9). The results from modeling corresponded well with the results of the actual experiments. All five mutations changed the conformation of H193 in MelC2 (i.e. one of the histidines holding the copper ion). In the I41Y model, it was slightly harder for piceatannol to approach the two copper ions than resveratrol, because Tyr blocks the proper position of piceatannol needed to bind with the copper ions (Figure 2.10).

This hindrance appeared to increase K_m and resulted in the increased k_1/k_2 ratio. When I218 residue was changed into a relatively smaller amino acid, i.e. serine, the homology modeling of the I218S mutant showed that the conformations of H189 and H215 were changed in MelC2 (Figure 2.12). The smaller size of the R group offers more space for H215, and the oxygen of S218 pulls the H189 by hydrogen bonding. These factors are likely to affect the motion of Cu_B , just as earlier published studies have indicated (Chen et al. 1992; Goldfeder et al. 2013). The changes in Cu_B motion affected negatively on the values of both k_1 and k_2 without changing the k_1/k_2 ratio (Brenner et al. 2008).

Based on this finding, we concluded that the conformation of the residues positioned near the entrance of the active site is critical for changing the ratio of k_1/k_2 , while the residue changes altering the position of the two copper ions at the

core active site may cause low tyrosinase activity.

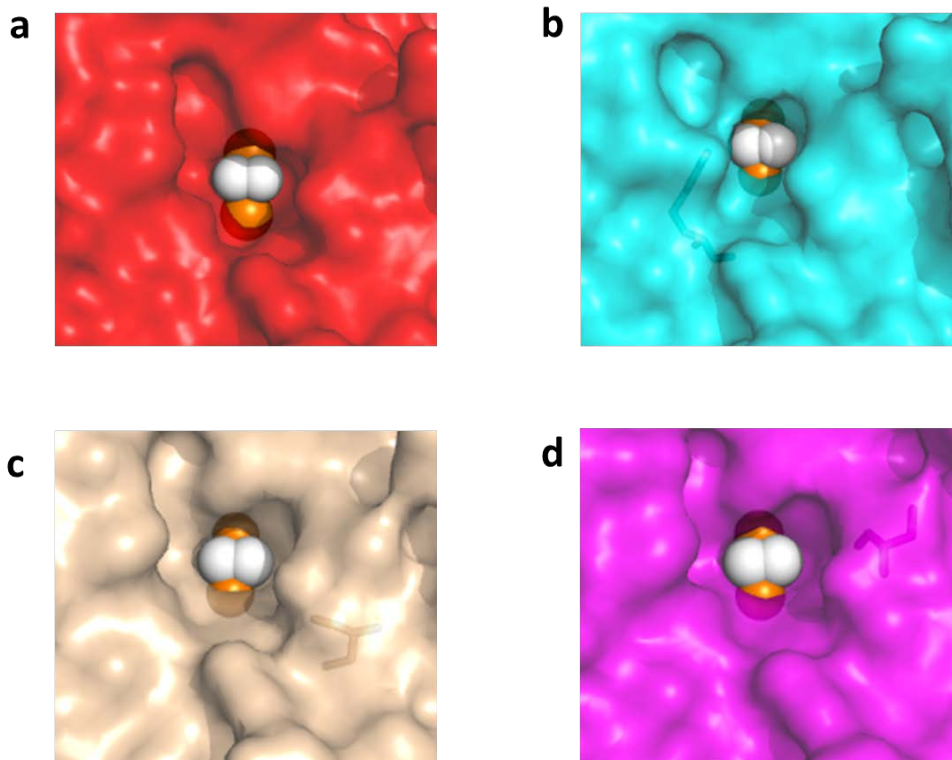


Figure 2.9. Pymol images of homology models.

(a) MeIC2, (b) N190R, (c) M200C, and (d) T202S. Orange spheres are copper ions and white spheres are oxygens. The entrance to copper ions of (b), (c) and (d) get narrowed and blocked by neighboring peptide frames. We assume that it causes the low activity on resveratrol.

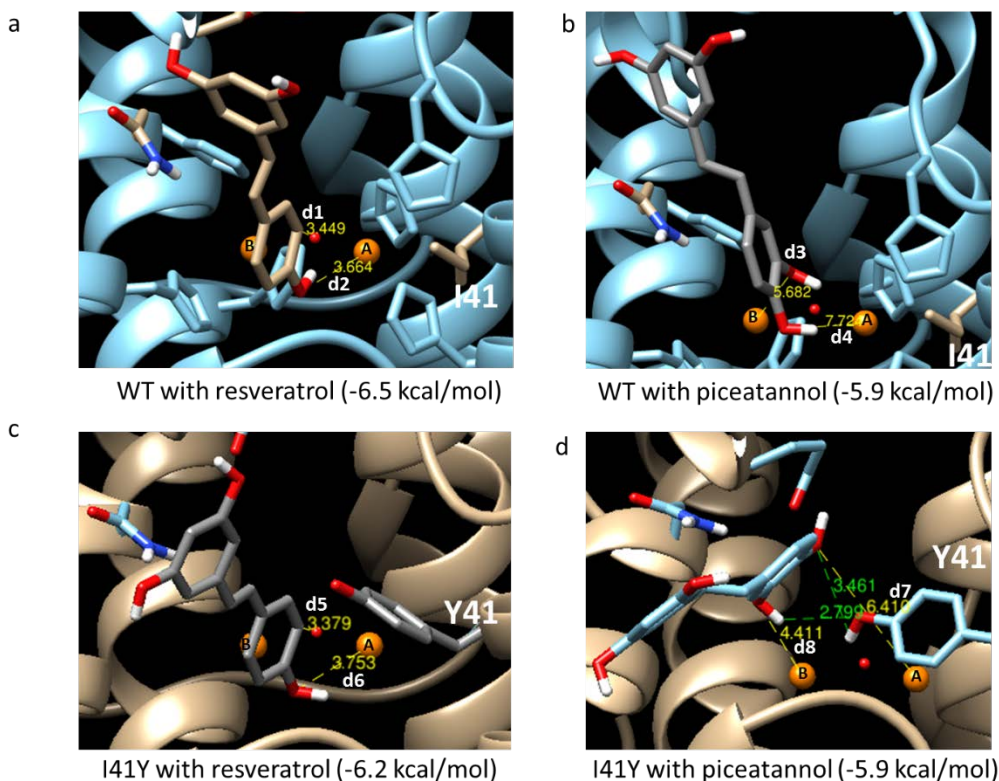


Figure 2.10. Docking result of WT and I41Y on resveratrol and piceatannol.

1WX2 was used as a template for modeling WT and I41Y. Orange spheres are copper ions, and the small red sphere is an oxygen molecule in the met-form tyrosinase. The energy values are the minimum docking score of each model. d1 (a) and d6 (c) are the distances between the oxygen molecules in the met-form model, and d2 (a) and d5 (c) are the distances between CuA and the hydroxyl group of L-tyrosine. d3, d4, d7 and d8 are the distance between the copper ions and the hydroxyl groups of L-Dopa. Unlike (a), (b) and (c), the aromatic ring of L-Dopa in I41Y (d) tilted 90 degrees because Y41 pointed toward the substrate, hindering access of the hydroxyl group to CuA. (b) d3 and d4 is relatively larger than d1, d2, d5, and d6. And this supports the higher K_m of MelC2 on piceatannol. (d) The tendency of the tyrosine residue working on catechol moiety is identical when

compared to Figure 2.11. The distance between the hydrogen of the hydroxyl group in tyrosine and the oxygen of *m*-OH in L-Dopa is 2.79Å (green lines, possible hydrogen bonds).

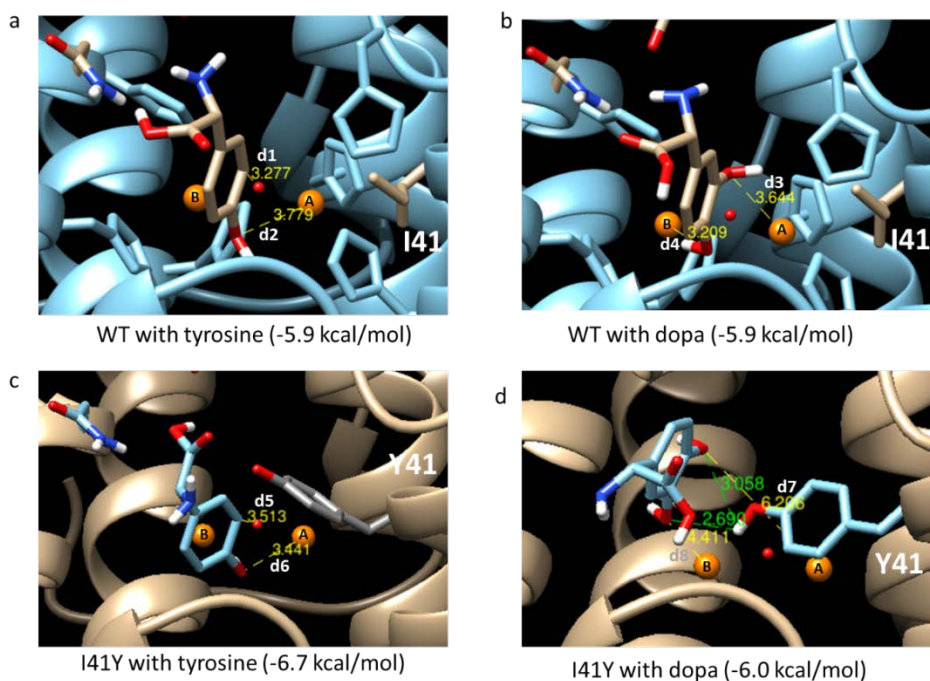


Figure 2.11. Docking result of WT and I41Y on tyrosine and L-Dopa.

Orange spheres are copper ions, and the small red spheres are oxygen molecules in *met*-form tyrosinase. d1 (a) and d5 (c) are the distances between the oxygen molecules in the *met*-form model, and d2 (a) and d6 (c) are the distance between Cu_A and the hydroxyl group of L-tyrosine. d3, d4, d7 and d8 are the distances between copper ions and hydroxyl groups of L-Dopa. Unlike (a), (b) and (c), the aromatic ring of L-Dopa in I41Y (d) tilted 90 degrees because Y41 pointed toward the substrate, hindering the access of the hydroxyl group to Cu_A. (d) The distance between the hydrogen of the hydroxyl group in tyrosine and the oxygen of *m*-OH in L-Dopa is 2.69 Å (green lines, possible hydrogen bonds).

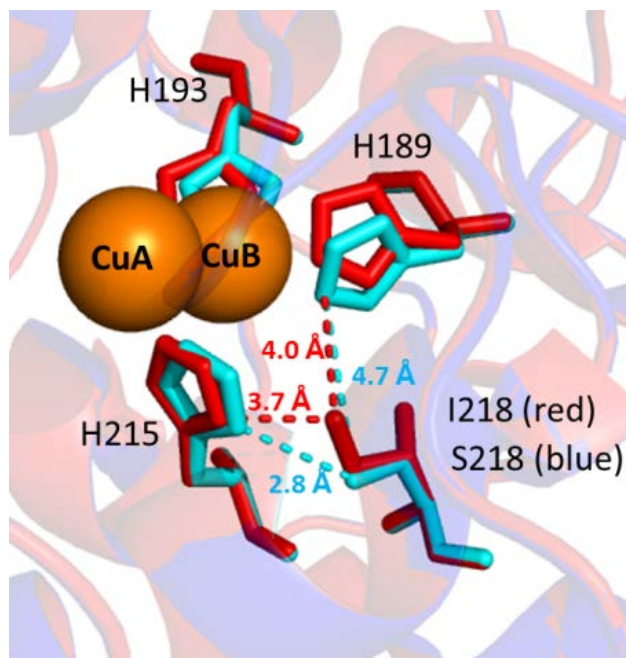


Figure 2.12. The structure of wild type (I218) and I218S mutants of MelC2 were compared.

Orange spheres are copper ions. Red stick structures represent wild type and blue stick structures represent the I218S mutant. The size of residue and the hydrogen bond of the R group with histidines changed the stability of Cu_B by allowing more space.

2.5 Conclusion

Streptomyces avermitilis tyrosinase, MelC2, was heterologously expressed in *E.coli* via codon optimization of tyrosinase helper protein, MelC1. Through the saturation mutagenesis of MelC1, it was demonstrated that Y91 of MelC1 was critical for the expression of active MelC2, and that other aromatic amino acids (F, W) could replace Y91. Furthermore, we found that I41Y mutant has higher selectivity (k_1/k_2) for monophenolic compounds through the saturation mutagenesis of 15 residues of MelC2. Turnover number of MelC2 on L-tyrosine ($1.05 \mu\text{mol}\cdot\text{min}^{-1}\cdot\text{mg}^{-1}$) and on L-Dopa ($3.47 \mu\text{mol}\cdot\text{min}^{-1}\cdot\text{mg}^{-1}$) is ten times faster than of tyrosinase from *Rastonia solanacearum* (Hernandez-Romero, Sanchez-Amat et al. 2006), and similar with tyrosinase from *B. megaterium* (BMty) (Shuster Ben-Yosef, Sendovski et al. 2010). The 41st residue is located at the entrance of the active site of MelC2 above the copper complex. The position is somewhat identical with R209 of BMty, which is known to play a role in substrate binding orientation. (Sendovski et al 2010) It has been reported that R209H mutants of BMty have a threefold greater activity ratio ($V_{\text{max_mono}}/V_{\text{max_Di}}$), 0.31, on L-tyrosine and L-Dopa (Shuster Ben-Yosef, Sendovski et al. 2010). However, I41Y mutants of MelC2, screened in this study, turned out to have an eightfold increased activity ratio of 0.83. It is shown that the Y41 slightly blocked the access of piceatannol to Cu_A while maintaining monooxygenase activity.

By incorporating GDH for NADH regeneration, the *in vitro* *E.coli* cell extract system efficiently enhanced the total yield of the reaction. The current yield and productivity of piceatannol production using the I41Y mutant of MelC2 is remarkable, when we compare it with the P450 reaction systems for the same

reaction: e.g. BM3 mutants from *B. megaterium* can produce 4.0 pM piceatannol·min⁻¹ from 100 μM resveratrol with less than 5% yield in 250 μL reaction (Kim et al. 2009), whereas the tyrosinase mutant in our study resulted in 14.5 μM piceatannol·min⁻¹ from 500 μM resveratrol with 58% yield in 50 mL, suggesting that this tyrosinase system is far superior to P450 system for this *ortho*-hydroxylation. Recently, FADH₂-utilizing monooxygenase from *E. coli* (HpaB) was reported as a *ortho*-hydroxylator of resveratrol with remarkable reaction specificity ($k_{\text{cat}}/K_m = 6.4 \cdot 10^5 \text{ M}^{-1}\text{S}^{-1}$) and high yield (close to 100%, 5 μM piceatannol·min⁻¹) (Lin et al. 2014). However, its productivity is still much lower than that of our tyrosinase due to the diffusion rate of piceatannol into cell. The non-heme monooxygenase (or P450) system works well with the whole cell reaction, but is not efficient if target substrates cannot penetrate the cell wall. This is because the enzyme requires electron transfer partners such as ferredoxin reductase (Fpr) and ferredoxin (Fdx), and reducing power cofactors such as FADH₂ and NAD(P)H. Thus, in this case, the *in vitro* reaction is superior the *in vivo* reaction. Lin et al. (Lin and Yan 2014) also concluded that since the hydroxylation of large substrates is not efficient enough, accurate structural data of HpaB would be helpful in expanding its substrate specificity with protein engineering. On the other hand, many attempts were made to improve its enzymatic properties since the crystal structures and reaction mechanisms of several tyrosinases have been well investigated (Goldfeder, Kanteev et al. 2014).

As tyrosinase is ubiquitous among a diverse range of organisms from bacteria to fungi, and has a relatively broad substrate specificity, high hydroxylation rate and good stability, tyrosinase and its mutants have great

potential for the production of various functional catechol-like compounds. To improve the selectivity of tyrosinase for such monophenolic compounds, tyrosinase can be engineered to a certain extent, which requires thorough understanding of its reaction mechanism and di-copper ions scaffold structure. In order to achieve this understanding, saturation mutagenesis of combinatorial residues near the core active site and structural studies of the various tyrosinase mutants from mutagenesis are currently being conducted. In this study, we demonstrated a potential of tyrosinase in terms of *ortho*-specific hydroxylation of monophenolic compounds. The combination of a tyrosinase screening method and an NADH regenerating system could be used widely for easy screening of monophenolic candidate substrates for the production of various natural diphenolic compounds

Chapter 3.

**Using tyrosinase as a monophenol monooxygenase:
a combined strategy for effective inhibition of
melanin formation**

3.1 Abstract

Tyrosinase is a binuclear copper-containing metalloprotein that leads the fast and regio-selective *o*-hydroxylation of monophenols to *o*-diphenols. However, the subsequent second oxidation to produce *o*-quinones, i.e., melanin precursors, from the *o*-diphenols has restricted its use to the production of functional *o*-diphenol derivatives. Herein, we present a combined strategy for the effective inhibition of melanin formation in tyrosinase reaction, which allows the use of tyrosinase as a monophenol monooxygenase. The *o*-diphenolic products were protected from being oxidized in the tyrosinase reaction by borate ions and L-ascorbic acid (LAA). Borate-*o*-diphenol complexes were favorably formed at high pH and consequentially protected the *o*-diphenolic products from the catecholase activity of tyrosinase. LAA not only directly reduced the byproduct, *o*-quinones, into *o*-diphenols but also assisted the completion of the tyrosinase reaction cycle by removing a hydroxyl group attached to the copper metal cluster at the active site of the *met*-form tyrosinase. The regio-selective *o*-hydroxylation of 7,4'-dihydroxyisoflavone (daidzein) to produce 7,3',4'-trihydroxyisoflavone (3'-ODI) was successfully carried out by whole *E. coli* cell biotransformation with heterologously expressed tyrosinase. The yield of this *o*-hydroxylation of 5 mM daidzein in one-pot 400 mL reaction was ca. 100 % in 90 min and the productivity was 16.3 mg 3'-ODI · L⁻¹ · h⁻¹ · DCW mg⁻¹, which is considerably higher than that of other monooxygenases. The method effectively abolished melanin synthesis, so that the *o*-diphenolic product remained stable without enzyme inactivation. Other monophenolic phytochemicals such as resveratrol and genistein could be subjected to the same strategy. After one hour, 1 mM of genistein and resveratrol were both

converted to orobol and piceatannol, respectively, with ca. 95 % conversion yield. The *ortho*-hydroxylation was not limited only to the simple monophenols but also to the dibenzyl group such as coumarin rings in formononetin though it required more reaction time because of its nature (The extraction of electrons from structures that have more than one aromatic rings attached and have more variable and stable resonance structures require more energy).

These results support the strong potential of tyrosinase as a monooxygenase for regio-selective *o*-hydroxylation of various monophenolic compounds. Furthermore, the optimized conditions were applied into scale-up studies as well. Up to 400 L reaction was performed, and, as a result, 3 g · L⁻¹ of each daidzein, genistein, and piceatannol (1.2 kg each) was successfully bioconverted to corresponding *ortho*-hydroxylated catechol derivatives with over 95 % conversion yield.

Keywords: tyrosinase, 7,3',4'-trihydroxyisoflavone, isoflavone, monooxygenase, *ortho*-hydroxylation

3.2 Introduction

The potential health benefits of phenolic phytochemicals include the prevention of numerous chronic diseases such as cancer. Especially, *o*-dihydroxylated phenolic phytochemicals such as hydroxytyrosol (olive oil) (Bisignano, Tomaino et al. 1999), luteolin (artichoke and broccoli) (Miean and Mohamed 2001), piceatannol (grape and wine) (Larrosa, Tomas-Barberan et al. 2004), esculetin (chicory) (Hazra, Sarkar et al. 2002), and *o*-dihydroxyisoflavones (ODIs; fermented soybean paste) (Park, Park et al. 2008, Park, Kim et al. 2010) are functional compounds in foods and drinks that are generally regarded as healthy. For example, 7,3',4'-trihydroxyisoflavone (3'-ODI), one of the *o*-dihydroxyisoflavones (ODIs), is not usually detected in soybeans but trace amounts are found in aged soybean paste, which is known to be converted from daidzein during fermentation (Park, Park et al. 2008). The anti-oxidative effect of 3'-ODI is comparable to that of L-ascorbic acid (LAA), and the biological effects of 3'-ODI on skin whitening (Park, Kim et al. 2010), and its cancer chemoprotectant activities (Lee, Lee et al. 2011, Lo, Wang et al. 2012) have highlighted it as a multifunctional bioactive substance.

Previously, cytochrome P450s (CYPs) were utilized to lead the *o*-hydroxylation of daidzein to produce 3'-ODI (Seeger, Gonzalez et al. 2003, Choi, Jung et al. 2012, Choi, Jung et al. 2013). Choi et al. (2012) constructed an artificial self-sufficient CYP which was a combination of the heme domain of CYP105D7 and the reductase domain of CYP102D. The fused CYP exhibited enhanced electron transfer efficiency; however, these enzymes are found only limited industrial use because of their low productivities, low yields and requirement for cofactor regeneration systems.

Tyrosinases (Ty) are type III copper-containing proteins that are ubiquitously distributed in bacteria and eukaryotes (Munoz-Munoz, Garcia-Molina et al. 2010, Rolff, Schottenheim et al. 2011). Ty catalyzes a two-step oxidation of monophenols: *o*-hydroxylation of monophenols to *o*-diphenols, monophenolase activity (k_1), and the subsequent oxidation to produce *o*-quinones, precursors for melanin formation, catecholase activity (k_2) (Yamazaki and Itoh 2003, Mirica, Vance et al. 2005, Muñoz-Muñoz, Berna et al. 2012). Two copper ions essential for Ty activity are firmly held by six histidines at the core active site and form a (μ - η^2 : η^2 -peroxo)-dicopper (II) complex with dioxygen (*oxy*-Ty) (Yamazaki and Itoh 2003, Muñoz-Muñoz, Berna et al. 2012). The distance between the two copper ions is well conserved throughout the type III copper-containing protein family but the diverse peptide frames restrict the access of substrates to the active site for precise control of its own biological activity (Rolff, Schottenheim et al. 2011, Goldfeder, Kanteev et al. 2014). Due to such spatial restriction, the substrate specificity of Ty is distinct and the k_1/k_2 ratio differs depending on the initial substrates (Goldfeder, Kanteev et al. 2013).

In the monophenolase reaction, the C-H bond right next to the hydroxyl group of monophenols is selectively hydroxylated by electrophilic substitution, namely, *o*-hydroxylation. Briefly, the deprotonated oxygen of the monophenol disturbs the (μ - η^2 : η^2 -peroxo)-dicopper (II) complex of *oxy*-Ty by bridging to one of the copper ions (nucleophilic attack), after which the hydroperoxide group of the complex attacks the ortho position of the monophenols (electrophilic attack) to produce the *o*-diphenols and the oxo-bridged dicopper (II) complex (*met*-Ty)(Muñoz-Muñoz, Berna et al. 2012). *met*-Ty subsequently oxidizes *o*-diphenols

to *o*-quinones and becomes the third form of Ty (*deoxy*-Ty), i.e., dicopper (I) without molecular oxygen. The Ty oxidation cycle is recurrently circulated after oxy-Ty is regenerated from *deoxy*-Ty by molecular oxygen (Mirica, Vance et al. 2005, Muñoz-Muñoz, Berna et al. 2012, Ramsden and Riley 2014). Ty becomes inactivated when *o*-diphenols or external reductants are not available during the reaction despite the presence of the monophenolic substrate. Without *o*-diphenols or reducing agents, the oxidation cycle of Ty cannot be completed since the oxygen atom of the oxo-bridged dicopper(II) complex of met-Ty is not easily reduced. An initial lag period of Ty reaction on monophenols is often observed because met-Ty is the most common resting state of Ty (Yamazaki and Itoh 2003, Ramsden and Riley 2014).

Over the entire cycle of the Ty reaction with monophenols, it is difficult to detect the monooxygenated intermediates, *o*-diphenols, because the subsequent catecholase reaction is relatively faster than the monophenolase reaction (Goldfeder, Kanteev et al. 2013). Therefore, many researchers have attempted to engineer Ty in order to increase the k_1/k_2 ratio (Shuster Ben-Yosef, Sendovski et al. 2010, Goldfeder, Kanteev et al. 2013), and/or to back-reduce the *o*-quinones to *o*-diphenols by using reducing agents such as NADH (Garcia-Molina, Munoz-Munoz et al. 2010), glutathione (Villarama and Maibach 2005), or LAA (Ros, Rodríguez-López et al. 1993). However, the k_1/k_2 ratio of the engineered Ty was not significantly enhanced, and the reducing agents were incapable of accumulating and maintaining a high amount of *o*-diphenols because of the low electron transfer efficiency and the fast oxidation of the reducing agents at high pH under aerobic conditions.

Based upon these aforementioned previous studies on Ty mechanisms, we have attempted to overcome the limitation of Ty, melanin formation, and to develop a method for regio-selective *o*-hydroxylation of monophenols by Ty. This study presents a combined strategy in which the Ty reaction was systematically optimized for selectively producing 3'-ODI from daidzein (Figure 3.1). Arrows 1, 2, and 3 in Figure 3.1 are the normal cyclic paths of the Ty reaction on monophenols. However, here, three additional reactions were introduced while maintaining only the intact monophenolase activity: the formation of borate-*o*-diphenol complexes, the addition of reducing reagents for transforming met-Ty into *deoxy*-Ty, and the reduction (i.e., back-titration) of *o*-quinones to *o*-diphenols (arrows 4, 5, and 6 in Figure 3.1). *Ortho*-hydroxylated products were well protected by the formation of borate ester bonds with boric acid (Pizer and Babcock 1977, Springsteen and Wang 2002, Maeda, Fujii et al. 2008, He, Fullenkamp et al. 2011), which consequently shifted the equilibrium toward the formation of *o*-diphenolic products. LAA not only reduced *o*-quinones back to *o*-diphenols (Ros, Rodríguez-López et al. 1993) but also helped the complete circulation of the Ty cycle. The additional reactions effectively abolished the melanin synthesis, leading to the successful *o*-hydroxylation of the *o*-diphenolic product, i.e., 3'-ODI. Furthermore, we demonstrated that the same principle can be applied to the *o*-hydroxylation of other monophenolic phytochemicals, such as genistein and resveratrol.

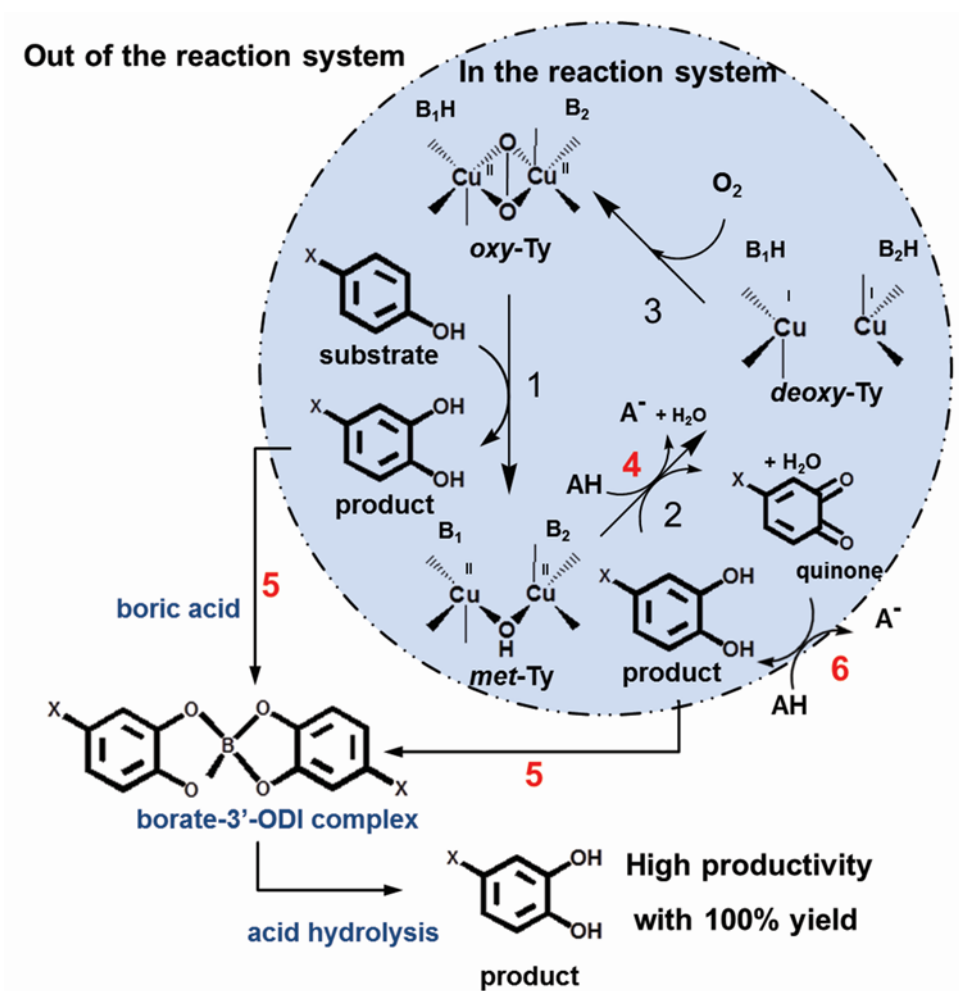


Figure 3.1. Effective strategy for suppressing byproduct formation of the Ty reaction to selectively produce functional diphenols.

3.3 Materials and Methods

3.3.1 Materials

Restriction enzymes were purchased from Thermo Scientific (Seoulin Bioscience Co LTD, Seongnam, Korea). T4 DNA ligase, DNA polymerase, and reagents for the genetic engineering were purchased from Invitrogen Life Technology (Seoul, Korea). Daidzein, resveratrol, piceatannol and all other reagents were purchased from Sigma-Aldrich (Yongin, Korea). Tyrosinase from *Agaricus bisporus* (AB) was used as purchased from Sigma-Aldrich (Yongin, Korea, Catalog Number: T3824). *Bacillus megaterium* (BM), ATCC 10778, and *Streptomyces avermitilis* (SA) MA4680, ATCC 31267, were purchased from the Korean Culture Center of Microorganisms (KCCM, Seoul, Korea).

3.3.2 Construction of plasmids for recombinant tyrosinases.

Genomic DNA was extracted from BM and SA cells with G-spin genomic DNA extract kit (Intron, Korea), and PCR was performed to amplify the genes of tyrosinase. The primer list is in Table 3.1. The gene of Ty helper protein (SA_MelC1, KP198295.1) was inserted into MCS1 of pETDuet (Novagen, USA), and the gene of Ty (SA_MelC2, gi:499291317) into MCS2. His-tag was introduced at the C-terminal of SA_MelC2, but not at SA_MelC1. Ty from BM was amplified and inserted into the multiple cloning site of pET28a.

Table 3.1. Primer list for cloning SA_Ty and BM_Ty

Primer	Sequence (5' → 3')
SA_Ty_melC1_F	GAA CCATGG AGTTAACCCGGCGT
SA_Ty_melC1_R	GAC AAGCTT TTAATTAAACGG
SA_Ty_melC2_F	GAA CCATGG ATGACCGTACGCAA
SA_Ty_melC2_R	GAC AAGCTT GACGGTGTAGAACG
BM_Ty_F	GAT GAATTC ATGAGTAACAAGTA
BM_Ty_R	GCA GTCGAC TGAGGAACGTTTTGA

3.3.3 Conditions for cell cultures and reactions

The recombinant plasmids were transformed into *E. coli* BL21 (DE3) by heat shock, and the strain was spread on a plate of Luria-Bertani (LB) agar with proper antibiotic selection markers (25 $\mu\text{g}\cdot\text{ml}^{-1}$ of ampicillin or 50 $\mu\text{g}\cdot\text{ml}^{-1}$ of kanamycin depending on plasmids). A colony on the plate was inoculated into a test tube with 3 mL of LB broth with antibiotic selection markers, and the cells were cultured in an incubator at 37 °C and 200 rpm overnight. After 0.5 mL of cell culture was transferred into a 250 mL flask with 50 mL of fresh LB with the antibiotic selection marker, the cells were incubated at 37 °C and 200 rpm for 2.5 hr. When OD at 600 nm (OD_{600nm}) of the cell cultures reached approximately 0.6, 0.2 mM IPTG and 1 mM CuSO₄ (i.e., final concentrations) were added. The cells were continuously cultured in an incubator at 18 °C at 200 rpm for 24 hrs. Cell pellets from 50 mL of cell culture (Cell OD_{600nm} was 6.35) were collected by centrifugation (approximately 5 g of wet cell weight) and washed with 5 mL of 50 mM tris-HCl buffer at pH 8. If necessary, the cell wall was disturbed by ultra-sonication. After centrifugation at 16000 rpm for 30 min, 5 mL of soluble fraction of crude cell soup was collected. The unit was calculated by measuring the light absorption of dopachrome at 475 nm ($\epsilon = 3600 \text{ M}^{-1}\cdot\text{cm}^{-1}$) with UV-spectroscopy (SPECTROstar Nano, BMG LABTECH, Ortenberg, Germany). If necessary, the expressed enzymes were purified by the general His-tag purification for kinetic measurements. The concentration of purified enzymes was calculated by the general Bradford assay (Zor and Selinger 1996). The Ty reaction conditions are presented in each figure legend, and Tables D2 and D3.

3.3.4 Computational modeling

Homology modeling of SA_MelC2 was performed with Modeller 9.11. Ty from *Streptomyces castaneoglobisporus*, 1WX2, was used as a template for modeling Ty from SA with Modeler 9.11. 1WX2 is available on RCSB. 3NM8 (Ty from BM) and 2Y9W (Ty from AB) were used to compare the Ty structures. AutoDock Vina 1.1.2 and MGLTools 1.5.6. were used for docking simulation. Chimera 1.10rc was used to visualize the results.

3.3.5 Identification of products

HPLC analysis

The HPLC analysis was performed on CMB-20A (Shimadzu, Seoul, Korea) connected with a UV/Vis detector (SPD-20A) and a SunFire™ C18 5 μM 4.6 x 150 mm column was used. For the HPLC analysis, 100 μL of sample was extracted by ethyl acetate. The mobile phase was 25% acetonitrile in H₂O containing 0.1% trifluoroacetic acid, the flow rate was 1 mL/min, and the detection wavelengths were 254 nm for daidzein and 3'-ODI, 268nm for genistein and orobol, and 325 nm for resveratrol and piceatannol. The same analytic conditions are applied for this study.

GC analysis

After 100 μL of sample was extracted by 400 μL of ethyl acetate, all hydroxyl groups of the product were converted to TMS (trimethylsilyl) derivatives with

BSTFA. GC/MS was performed on a Thermo Scientific Trace GC Ultra instrument connected with a Thermo Scientific ITQ1100 MS spectrometer (Rockford, IL, USA) and with a TR-5ms SQC capillary column (30 m × 0.25 mm i.d., 0.25 μm film thickness). The GC/MS analysis of daidzein and resveratrol was carried out as follows: injector temperature, 250 °C; temperature gradient: holding initial temperature at 100 °C for 1 min, gradually increasing temperature up to 250 °C by 30 °C/min, holding at 250 °C for 10 min, gradually increasing temperature up to 275 °C by 1 °C/min, and holding at 275 °C for 2 min; and MS operating mode: 70 eV electron ionization mode. For genistein: injector temperature, 250 °C; temperature gradient: holding initial temperature at 100 °C for 1 min, gradually increasing temperature up to 250 °C by 30 °C/min, holding at 250 °C for 5 min, gradually increasing temperature up to 290 °C by 5 °C/min, and holding at 290 °C for 5 min; and MS operating mode: 70 eV electron ionization mode.

3.4 Results and Discussion

3.4.1 Comparison of Tys from three different organisms for the *ortho*-hydroxylation of daidzein

The peroxo dicopper complex of Ty is the key intermediate structure for the hydroxylation of substrates, and the diverse peptide sequences of Ty family (including catechol oxidase) determine their substrate specificities (Rolff et al., 2011; Goldfeder et al., 2014). Because of the variation, the substrate specificity of Tys is distinct and the k_1/k_2 ratio also differs depending on the initial substrates. To determine the appropriate Ty for producing 3'-ODI from daidzein, the reaction profiles of Ty from *B. megaterium* (BM_Ty), *A. bisporus* (AB_Ty) and *S. avermitillis* (SA_Ty) were monitored via HPLC.

The concentration time profiles of the product (3'-ODI) produced and the substrate (daidzein) consumed are plotted in Figure 3.2. SA_Ty and BM_Ty were heterologously expressed in *E. coli* and purified by a general protocol of His-tag purification while AB_Ty was used as supplied from Sigma-Aldrich. SA_Ty was previously reported to be a good tool for converting resveratrol to piceatannol (Lee et al., 2012) but showed the lowest activity for daidzein (Figure 3.2-a), and less than 50 μM of 3'-ODI (less than 10% conversion yield) was detected in the reaction mixture after 30 min. In the case of BM_Ty, approximately 94.8 μM of 3'-ODI (18.9 % conversion yield) was observed after 10 min of reaction, although eventually all of 3'-ODI was oxidized to form dark melanin (Figure 3.2-b). AB_Ty produced the lowest amount of 3'-ODI among the three different Tys (Figure 3.2-c), and the results were well correlated with the docking simulations. The docking score of AB_Ty on daidzein was -5.9 kcal/mol, which was the worst case, and

daidzein could not access the copper ions at the active site, as shown in Figure 3.2-f. The docking score of BM_Ty on daidzein was -8.9 kcal/mol, the best score, and one of the copper ions (CuB) of BM_Ty had the closest contact (i.e., 2.3 Å) with *p*-OH on the B-ring of daidzein. The conformation of daidzein at the active site of SA_Ty was similar to that of BM_Ty but the distance between CuB and *p*-OH was longer and the docking score was 1.8 kcal/mol higher than that of BM_Ty (Figure 3.2). Thus, BM_Ty was used for further hydroxylation of daidzein to produce 3'-ODI. The specificity constant (k_{cat}/K_m) of BM_Ty for daidzein was $1.32 \times 10^7 \text{ M}^{-1} \cdot \text{s}^{-1}$ (Table 3.4).

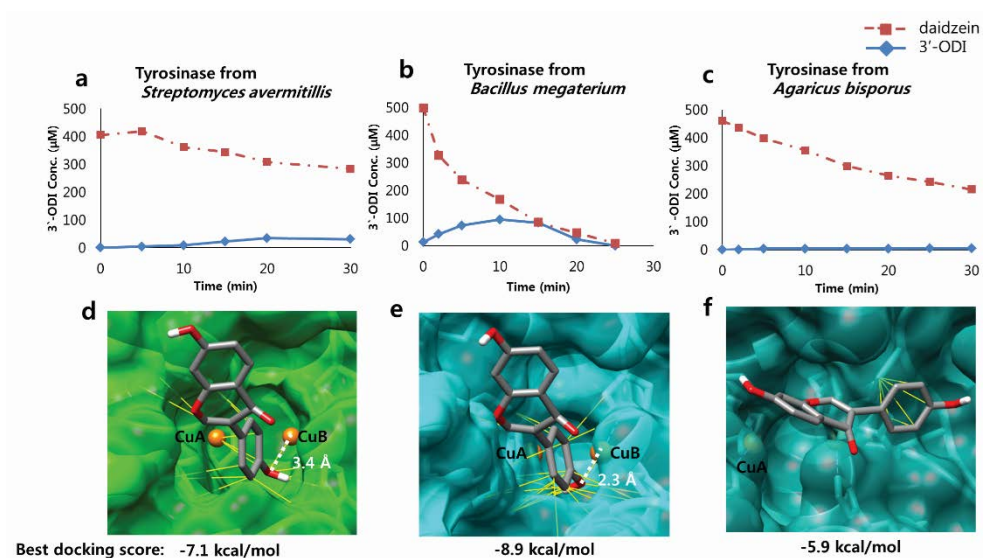


Figure 3.2. Different tyrosinase activities for the *o*-hydroxylation of daidzein and docking simulation of each enzyme on daidzein.

In 5 mL reaction, 10 U of enzyme was used to hydroxylate 500 μM of daidzein. 50 mM tris-HCl buffer at pH 8 and 10 mM of hydroxylamine (for removing the initial lag period) were used in this reaction. (e) Daidzein is positioned relatively stably in the active site of BM_Ty. The conformation of (e) is similar to that of (d) but has better docking score and better contacts with residues near the active site. (f) The entrance of the active site of *A. bisporus* (AB) tyrosinase is deeper and narrower than that of the other two enzymes so that daidzein cannot have correct binding conformations.

Table 3.2. Kinetic constants of tyrosinase from *B. megaterium* on daidzein.

The total reaction volume was 100 μL , and the range of initial concentration of daidzein was 100 μM to 1 mM. For the reaction, 500 mM borate buffer at pH 9 and 10 mM of NH_2OH were used (Yamazaki et al., 2003). The reaction was performed in 1.5 mL tubes at room temperature. The reaction was halted by adding 400 μL of ethyl acetate and 20 μL of 1M HCl. The organic layer was analyzed on HPLC to measure the amount of daidzein left from the reaction. The kinetic constants were calculated based on the triplet sets of the experiment. The average initial velocities of each initial substrate concentration were plotted and the standard errors were obtained by regression wizard of SigmaPlot 10.0. (one site saturation equation was used)

$[\text{E}]_0, \text{nM}$	200
$V_{\text{max}}, \mu\text{M}\cdot\text{min}^{-1}$	26.9 ± 2.29
$K_{\text{m}}, \mu\text{M}$	$6.11 \times 10^2 \pm 1.05 \times 10^2$
$k_{\text{cat}}, \text{s}^{-1}$	8.06×10^3
$k_{\text{cat}}/K_{\text{m}}, \text{M}^{-1}\cdot\text{s}^{-1}$	1.32×10^7

3.4.2 Protecting the diol moiety of 3'-ODI by borate ester bonds

The *o*-diphenolic product, 3'-ODI, was protected and removed from the Ty reaction system by using boric acid, which can form borate ester bonds with *o*-diols (arrow 5 in Figure 3.1). Boron in boric acid has three bonds with oxygen, forming a trigonal planar configuration (sp^2), but it adopts a tetrahedral configuration (sp^3) when a pair of electrons from a Lewis base is available (Griffith et al., 1996; Maeda et al., 2008). As the diol moiety of 3'-ODI acts as a Lewis base, boron can form borate ester bonds with one or two aromatic diols depending on the pH (He et al., 2011; Maeda et al., 2008; Pizer et al., 1977; Springsteen et al., 2002). The equilibrium constant of the complex formation is less than $10^{-2}\cdot M^{-2}$ (Figure 3.4). In this study, therefore, 500 mM borate buffer at pH 9 was used to form borate-3'-ODI complex (500 mM of borate solution is almost saturated at room temperature, and Ty shows intact activities in such buffer condition).

The complex was water soluble and not extracted by ethyl acetate. 3'-ODI was only extracted and detected on HPLC after acidic hydrolysis of the borate ester bonds with 1 M of HCl (Figure 3.3). Furthermore, borate buffer at pH 9 enhanced the solubility of daidzein. At neutral pH, approximately 200 μM of daidzein was dissolved in water with 0.5 v% of DMSO, and 3 mM of daidzein with 0.5 v% of DMSO became soluble in water at pH 9. The pKa values of C7-OH and C4'-OH are predicted to be 6.48 and 8.96, respectively. 3'-ODI is easily oxidized at room temperature in 50 mM tris-HCl buffer at pH 9 by dissolved oxygen (D.O.). However, 3'-ODI remained stable in borate buffer at pH 9 (Figure 3.5).

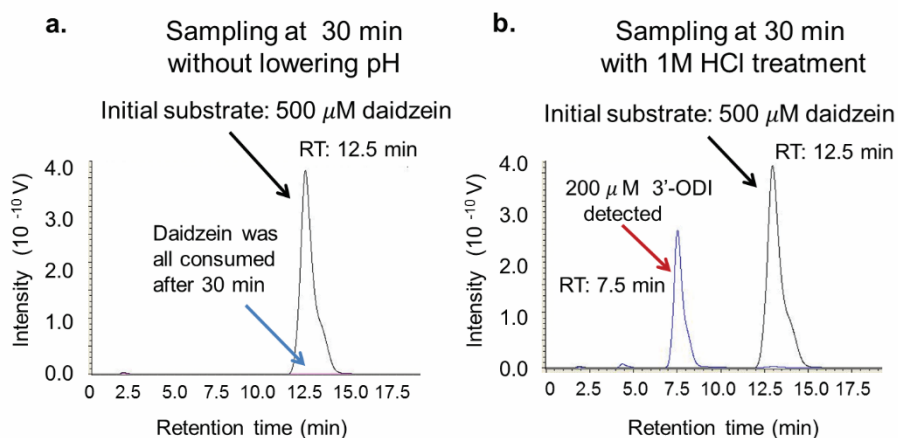


Figure 3.3. HPLC data after 30 min of the Ty reaction with/without acid hydrolysis.

pH was maintained at 9 during the reaction. Two samples at 30 min after the initiation of the reaction were prepared, with or without additional acid hydrolysis. 3'-ODI was not extracted by ethyl acetate from the reaction mixture at pH 9 (a) but was well extracted by ethyl acetate after the addition of 1M HCl (b). The conditions for the HPLC analysis are described in the Supplementary Material.

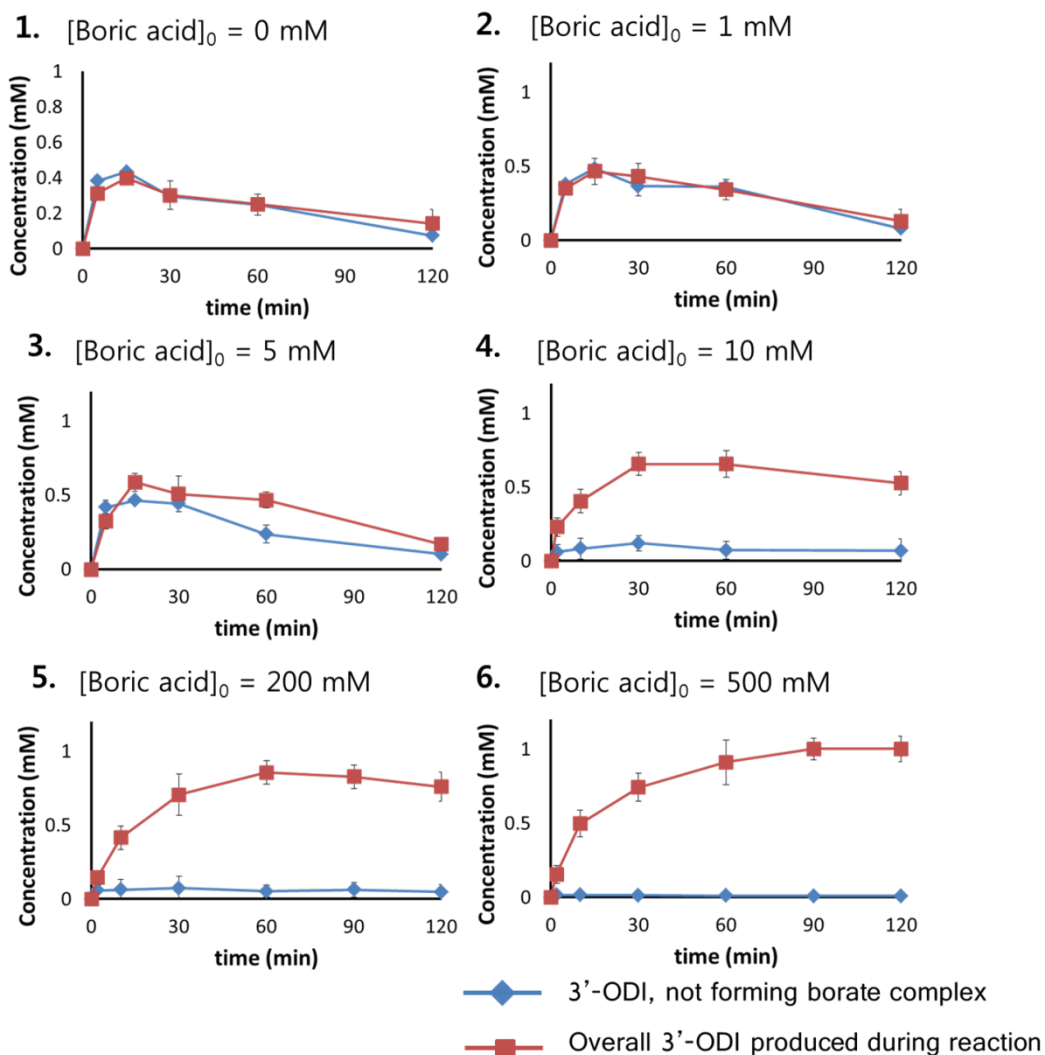


Figure 3.4. The concentration of 3'-ODI produced by tyrosinase from daidzein with various initial concentrations of boric acid.

Red lines show the overall concentration of 3'-ODI produced during reaction. The blue lines show the concentration of 3'-ODI that did not form conjugated bonds with borate. Boric acid was added in 100 mM tris-HCl buffer and the pH was maintained at 9 by adding 6 N NaOH solution.

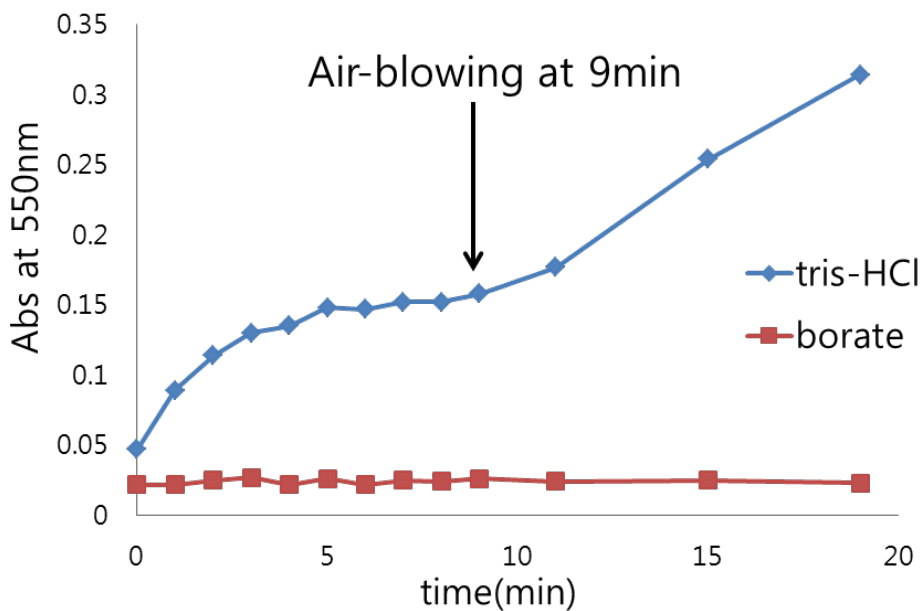


Figure 3.5. Auto-oxidation of 3'-ODI in buffer at pH 9.

In high pH of solution, diphenols are easily deprotonated since the pka values are generally below 9, which causes oxidation of diphenols to yield unstable quinonic compounds (*o*-quinones). Since the Ty reaction condition of producing 3'-ODI is held at pH 9, losses due to the auto-oxidation of 3'-ODI were measured. After 1mM of N-methylbenzothiazolone hydrazine (MBTH) was used to detect the amount of *o*-quinones produced via UV-spectroscopy at 550nm, 500 μ M of 3'-ODI with 0.5 v% of DMSO and 1mM of MBTH were added in a glass cuvette containing 1mL of buffer at pH 9, and the absorbance at 550nm of MBTH-*o*-quinone was measured. In 50 mM of tris-HCl buffer, 3'-ODI was significantly oxidized. After 5 min, the production of MBTH-*o*-quinone reached a steady state but then increased once air was blown through the pipetting. However, 3'-ODI remained stable in 50 mM borate buffer at pH 9.

3.4.3 Effects and roles of L-ascorbic acid (LAA) in the Ty reactions

Lee *et al.* (2012) previously used 1 mM catechol in SA_Ty reaction to inhibit the second oxidation of piceatannol by its catecholase activity after the first *o*-hydroxylation of resveratrol. The additive, catechol, whose accessibility to the active site of SA_Ty is more efficient than that of resveratrol, functioned as a competitive inhibitor, leading to an overall 70% conversion yield of piceatannol from 100 μ M resveratrol. However, the further oxidized products, *o*-quinones, were continuously generated from piceatannol after the first *o*-hydroxylation, and eventually converted into melanin. According to Yamazaki *et al.* (2003), hydroxylamine was an efficient reducing reagent for the reduction of *met*-Ty (arrow 4 in Figure 3.1), which completes the Ty oxidation cycle. Apparently, hydroxylamine is a substitute for catechol in the *o*-hydroxylation of resveratrol (Lee *et al.*, 2012). However, the amine group of hydroxylamine forms a covalent bond with *o*-quinones, leading to melanin formation (Yin 2013). Therefore, it is not an ideal reducing agent for protecting 3'-ODI from the second oxidation to maximize the yield of 3'-ODI production. The reaction solution was initially clear but became yellow after 10-min reaction due to amine-quinone adducts (data not shown). Moreover, only half of the daidzein was converted to 3'-ODI when 10 mL of 10 mM hydroxylamine was added (Figure 3.6-b).

In this study, LAA was used for the completion of the Ty cycle (arrow 4 in Figure 3.1), and for reducing *o*-quinones back to *o*-diphenols (arrow 6 in Figure 3.1). LAA can act like hydroxylamine in terms of helping the completion of the Ty cycle despite LAA being known as an inhibitor of Ty. LAA affects the k_2 value but

does not have a direct effect on k_1 (Muñoz-Muñoz et al., 2014). However, the lag period of the Ty reaction disappeared when LAA was added in the beginning of the reaction (Figure 3.6). Ros *et al.* (1993) hypothesized that the lag period depends only on the concentration of L-3,4-dihydroxyphenylalanine (L-Dopa), and that LAA acts only as a reducing reagent to maintain a certain concentration of L-Dopa. They concluded that the lag period increases when the initial concentration of LAA is higher than that of tyrosine. However, their conclusion is unwarranted because they monitored the reaction by measuring the amounts of dopachrome produced and oxygen consumed, not the amount of L-Dopa directly. However, LAA not only consumes D.O. in solution but also reduces dopachrome back to L-Dopa. The monophenolase reaction cannot be correctly measured unless the amount of tyrosine or L-Dopa is measured during the reaction. Thus, measuring D.O. and dopachrome concentrations is not an appropriate solution for monitoring the monophenolase activity of Ty when LAA is present.

Thus, k_1 was calculated based on the amounts of the *o*-diphenolic product, 3'-ODI, and the initial substrate, daidzein, quantitated by HPLC. The k_1 of Ty increased as the initial LAA concentration increased up to 2 mM (Figure 3.7). Above 2 mM, k_1 of Ty ($[E]_0 = 130$ nM) at 1 mM of daidzein was not increased. The k_1 values were identical when L-Dopa and hydroxylamine were used (data not shown). However, the k_1 with LAA was 2.5 times lower than that with hydroxylamine (Figure 3.6). If LAA cannot affect *met*-Ty directly, and 3'-ODI is the only remaining factor for the completion of Ty cycles, k_1 should be the same. Indeed, *o*-diphenols do not exist as free form anymore at 500 mM borate buffer, but as a borate ester complex (Figure 3.4-6) (Yamazaki et al., 2003). Furthermore, the

suicide inactivation of Ty (an inactivation path from *met*-Ty) described by several reports (Muñoz-Muñoz et al., 2010) is not observed without additional Cu^{2+} ions during the reaction. Thus, it is hypothesized that LAA can reduce *met*-Ty directly by easy access to the active site, and the difference in k_1 is attributed to the difference in the size of the reducing agents or their reduction potentials. The accessibility of LAA to the core active site of Ty was verified by docking simulation (Figure 3.8). The conformation of the penta-ring of LAA in the best fit model is similar to the aromatic ring of L-tyrosine and L-Dopa in the crystal structure in a previously published study (Goldfeder et al., 2014).

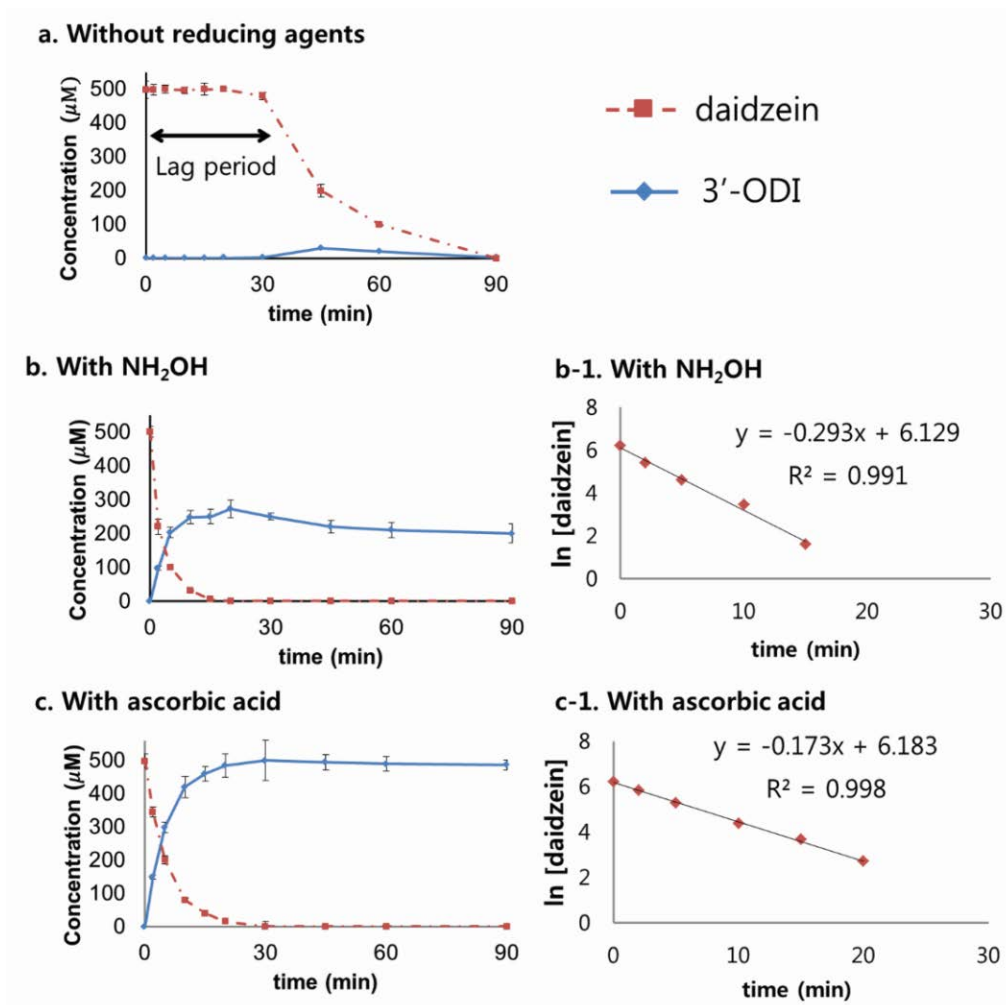


Figure 3.6. Effect of hydroxylamine and L-ascorbic acid (LAA) in the Ty reaction.

500 μM daidzein and 128 nM of His-tag purified Ty were used in a 5 mL reaction volume at 37 $^{\circ}\text{C}$. (a) A lag period was observed when 500 mM tris-HCl buffer at pH 9 was used and (a-1) no reaction occurred when 500 mM borate buffer at pH 9 was used in the absence of reducing agents. And 500 mM borate buffer at pH 9 and 10 mM of hydroxylamine (b) and LAA (c) were used, respectively. (a) A 30-min lag period was observed without any reducing agent. (b) No lag period but only 273 μM of 3'-ODI was detected (54.6% yield). k_1 was 0.293 min^{-1} (b-1). (c) No lag

period was observed and all of the 500 μM daidzein was converted into 3'-ODI (100% yield). k_1 was 0.173 min^{-1} , which is slower than that of (b) (c-1). The experiments were repeated in triplicate.

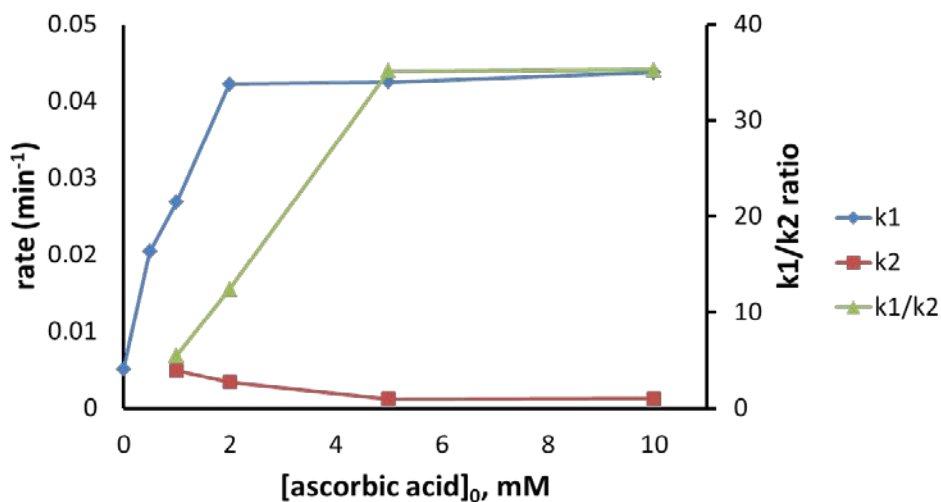


Figure 3.7. Rate changes depending on various concentrations of L-ascorbic acid.

The conditions for the reaction are as follows: total reaction volume is 5 mL, 500 mM borate buffer at pH 9, 1 mM daidzein, 130 nM of enzyme and the temperature was maintained at 37 °C. All the rates obtained from this graph are listed in Table 3.4.

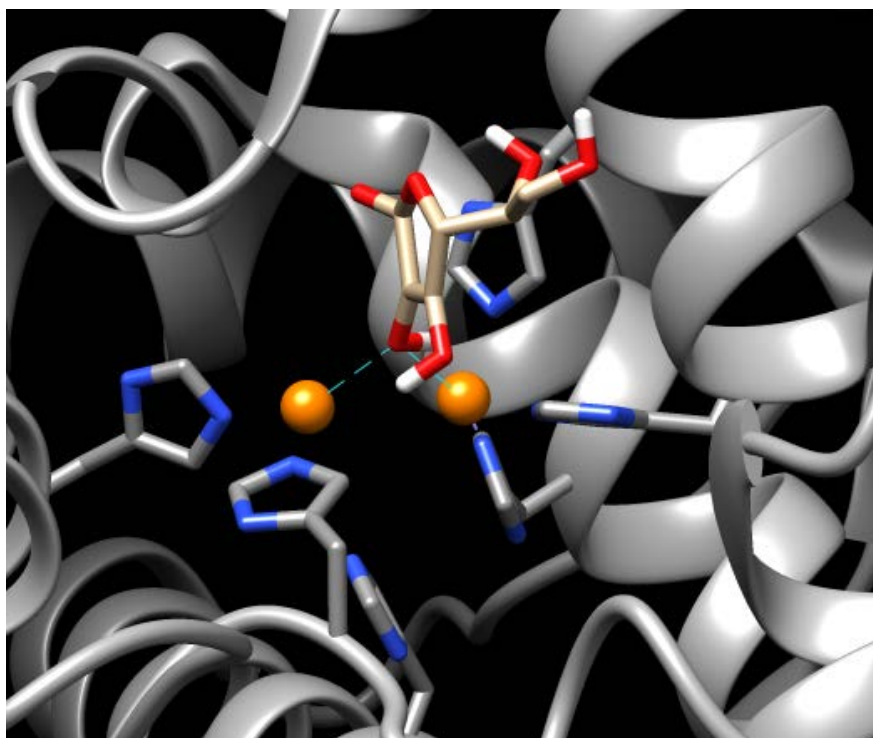


Figure 3.8. Docking simulation of tyrosinase from *B. megaterium* (3NM8) with ascorbic acid.

The crystal structure of tyrosinase from *B. megaterium* (3NM8) is available at RCSB database. ChemDraw Ultra 8.0 and Chem3D Ultra 8.0 were used for making the PDB file of ascorbic acid. The structure of ascorbic acid was modified with inbuilt minimize energy function of Chem3D. AutoDock Vina 1.1.2 and MGLTools 1.5.6. were used for docking simulation. Grid spacing, exhaustiveness and energy range were set as default, which are 3.75 Å, 8 and 3, respectively. X-Score was used to select the best fit conformation. Chimera 1.10rc was used for visualizing the results.

Table 3.3. The effect of ascorbic acid on the reaction rate of tyrosinase.

To measure the first hydroxylation of daidzein, 500 mM of borate was used to make tyrosinase fully focus on phenolase activity as previously studied (Yamazaki and Itoh 2003). Instead of hydroxylamine, L-ascorbic acid was added for circulating the Ty cycle. The method for measuring k_1 and k_2 is stated in “Calculation of k_1 and k_2 of BM_Ty on daidzein,” later in this supporting information.

[ascorbic acid] ₀ , mM	0	0.5	1	2	5	10
t_{ss} , min	-	-	72.29 ± 0.45	62.23 ± 0.63	83.74 ± 1.22	81.39 ± 0.98
[B] _{ss} , mM	-	-	0.786 ± 0.077	0.896 ± 0.090	1 ± 0.0970	1 ± 0.0851
k_1 , min ⁻¹	5.085×10^{-3}	2.041×10^{-2}	2.687×10^{-2}	4.222×10^{-2}	4.250×10^{-2}	4.378×10^{-2}
k_2 , min ⁻¹	-	-	4.901×10^{-3}	3.405×10^{-3}	1.210×10^{-3}	1.241×10^{-3}

3.4.4 Whole cell biocatalysis of daidzein by BM_Ty to produce 3'-ODI

The *o*-hydroxylation of daidzein to produce 3'-ODI was successfully performed by *E. coli* cell biotransformation, with the overproduction of BM_Ty. Figure 3.9-a shows the HPLC raw data of the 400 mL whole cell reaction for producing 3'-ODI from 5 mM daidzein. Initially a peak at retention time (RT) 12.5 min was detected, but another peak at RT 7.5 min rose as the initial peak at 12.5 min decreased. Figure 3.9-b shows the time profile of 3'-ODI produced and daidzein consumed during the reaction. The yield of this *ortho*-hydroxylation of 5 mM daidzein in one-pot 400 mL reaction volume was ca. 100 % in 90 min, and the productivity was $0.055 \text{ mM}\cdot\text{min}^{-1}$ (equivalent to $16.3 \text{ mg } 3'\text{-ODI}\cdot\text{L}^{-1}\cdot\text{h}^{-1}\cdot\text{DCW mg}^{-1}$) (Figure 3.9). The highest titer of 3'-ODI in a fed-batch bioprocess was $1.93 \text{ g } 3'\text{-ODI}\cdot\text{L}^{-1}$ in 200 min (Figure 3.10). The product was identified with GC/MS and $^1\text{HNMR}$. (Figure 3.11, Figure 3.12).

The 400 mL reaction in the 1 L reactor was sealed during the BM_Ty reaction to control the amount of oxygen in the reaction because D.O. is also a critical factor in the Ty reaction. The saturated D.O. level was $400 \text{ }\mu\text{M}$ (6.40 ppm) in 400 mL borate buffer pH 9 at 37°C (in the presence of 5 mM daidzein) but D.O. was significantly decreased down to $125 \text{ }\mu\text{M}$ (2 ppm) when 20 mM of LAA was added in the reaction mixture. The overall volumetric oxygen transfer coefficient of the 400 mL reaction mixture, $k_{v,l}$, was 0.46 min^{-1} , and the oxygen transfer rate in the 400 mL reaction volume at a constant airflow rate of $12 \text{ L}\cdot\text{min}^{-1}$ was $74 \text{ }\mu\text{mol of O}_2\cdot\text{min}^{-1}$ (Detailed calculations are available in Supplementary Material). Approximately 6.7 mmole of oxygen was dissolved into the reaction mixture for 90

min, indicating that it was sufficient for converting 5 mM of daidzein in the 400mL reaction, which is equivalent to 2 mmoles of daidzein.

To increase the productivity, the airflow rate or amount of cells was increased two-fold independently, but the total conversion yield and productivity were decreased down to 63% and to $0.050 \text{ mM}\cdot\text{min}^{-1}$, respectively, although the substrate consumption rate became 1.5-fold faster (Data not shown). It appeared that LAA and 3'-ODI were oxidized easily as the D.O. level increased, which is faster than the formation of 3'-ODI-borate complex and/or the reduction of quinones back to 3'-ODI by LAA.

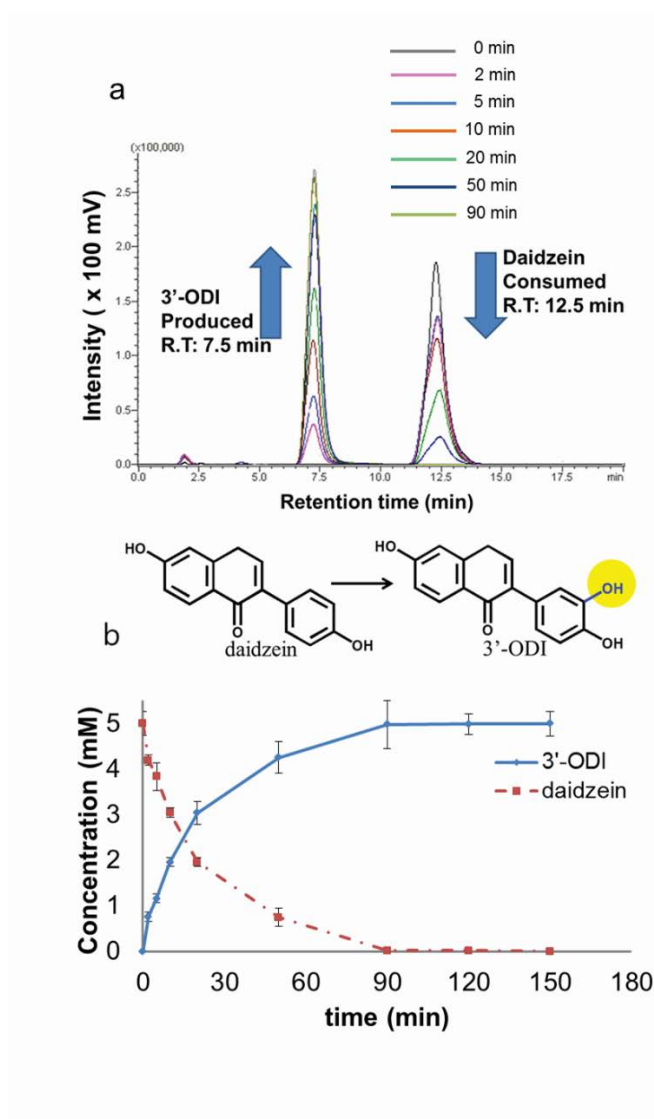


Figure 3.9. HPLC result of the Ty reaction for producing 3'-ODI.

This is an HPLC result from the 400 mL whole cell reaction at 5 mM daidzein. The reaction conditions are presented in Table 3.4. (a) A peak of retention time at 7.5 min. (b) Time profile of daidzein consumption and 3'-ODI production. The experiments were repeated in triplicate.

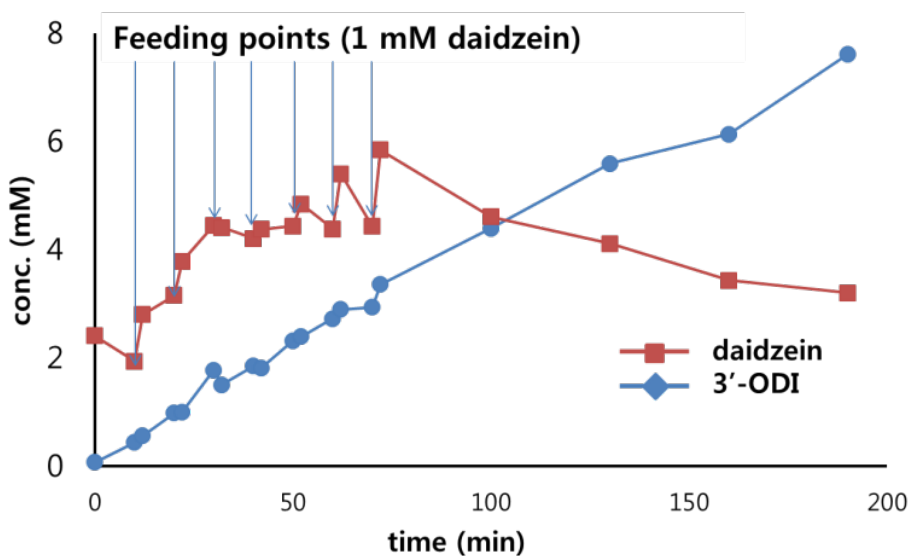
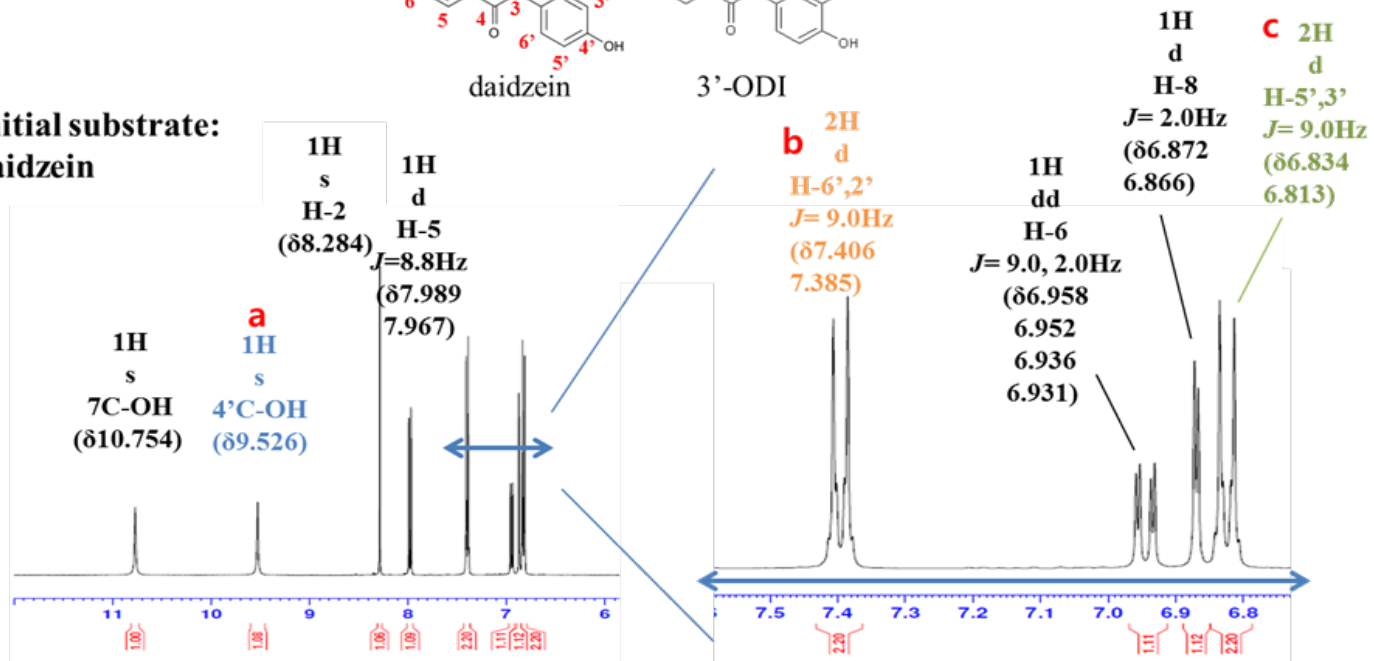
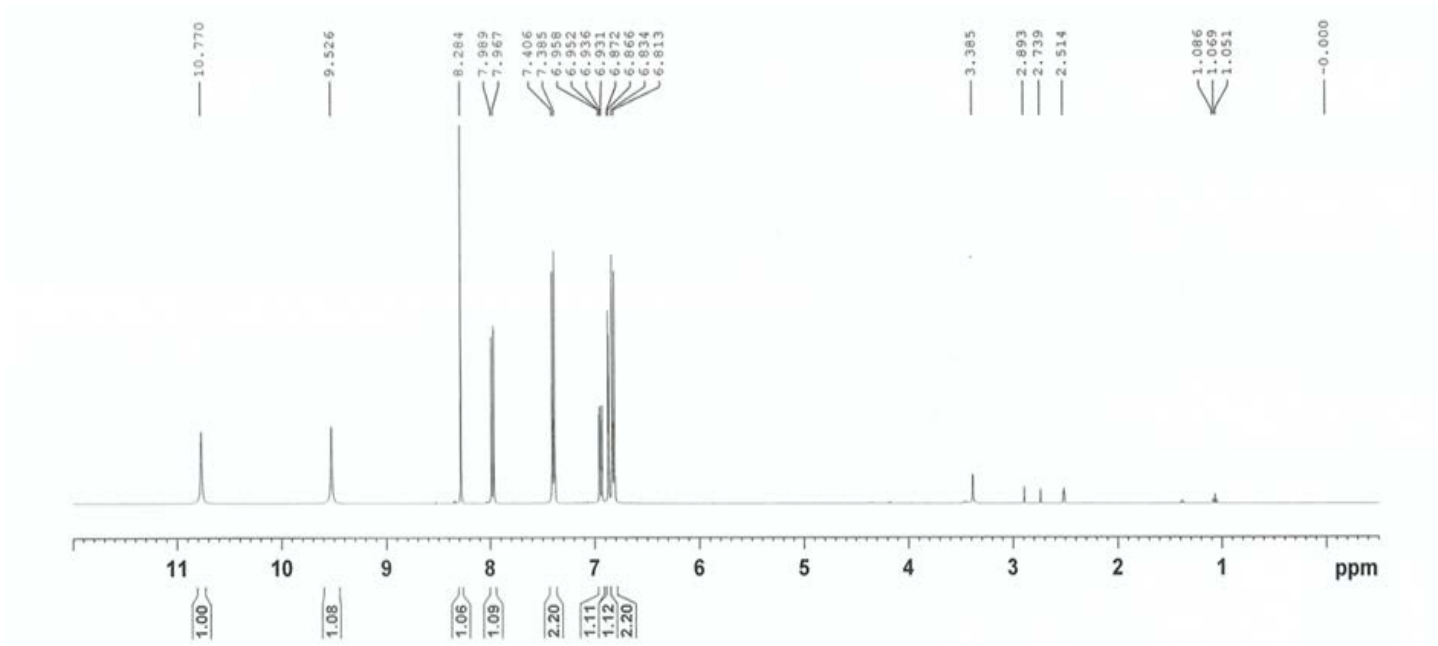


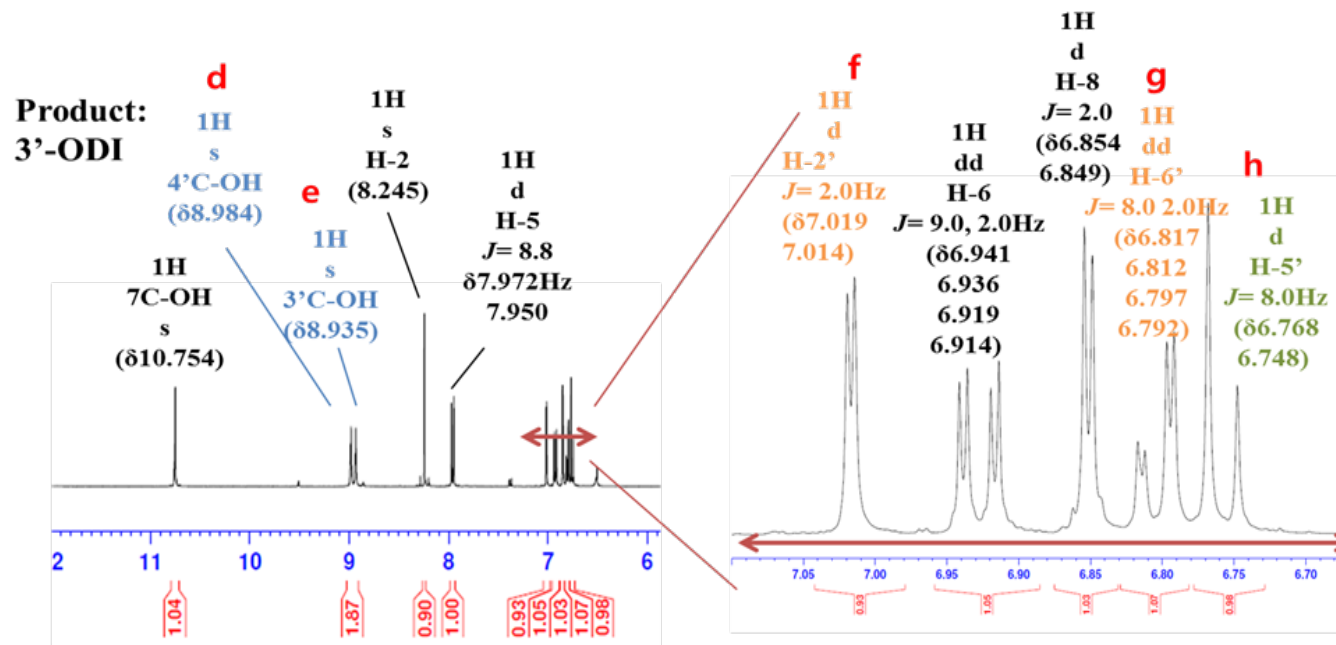
Figure 3.10. The time profile of the concentration of daidzein and 3'-ODI in the 400 mL fed-batch reaction.

The reaction conditions are listed as follows: 400 mL total reaction volume in a 1 L bioreactor, 500 mM borate buffer at pH 9, and 3 mM of dadizein. Approximately 2 g of wet cell was used (final OD at 600nm of the reaction mixture was 0.8). After 10 mM ascorbic acid was added initially, 1mM daidzein and 2 mM ascorbic acid were added every 10 min for 70 min. The temperature was maintained at 37°C. The total concentration of daidzein fed was 10 mM and 12 L·min⁻¹ of air was continuously blown from the bottom of the reactor. The oxygen transfer rate of the reactor was calculated and is further described later in this supporting data, “Calculation of Oxygen transfer rate and coefficient in the 400 mL reaction with the continuous air flow rate of 12 L·min⁻¹.” The yield of 3'-ODI production for 190 min was 70~75% (7.6 mM 3'-ODI), and 3.2 mM daidzein was left

Initial substrate:
daidzein







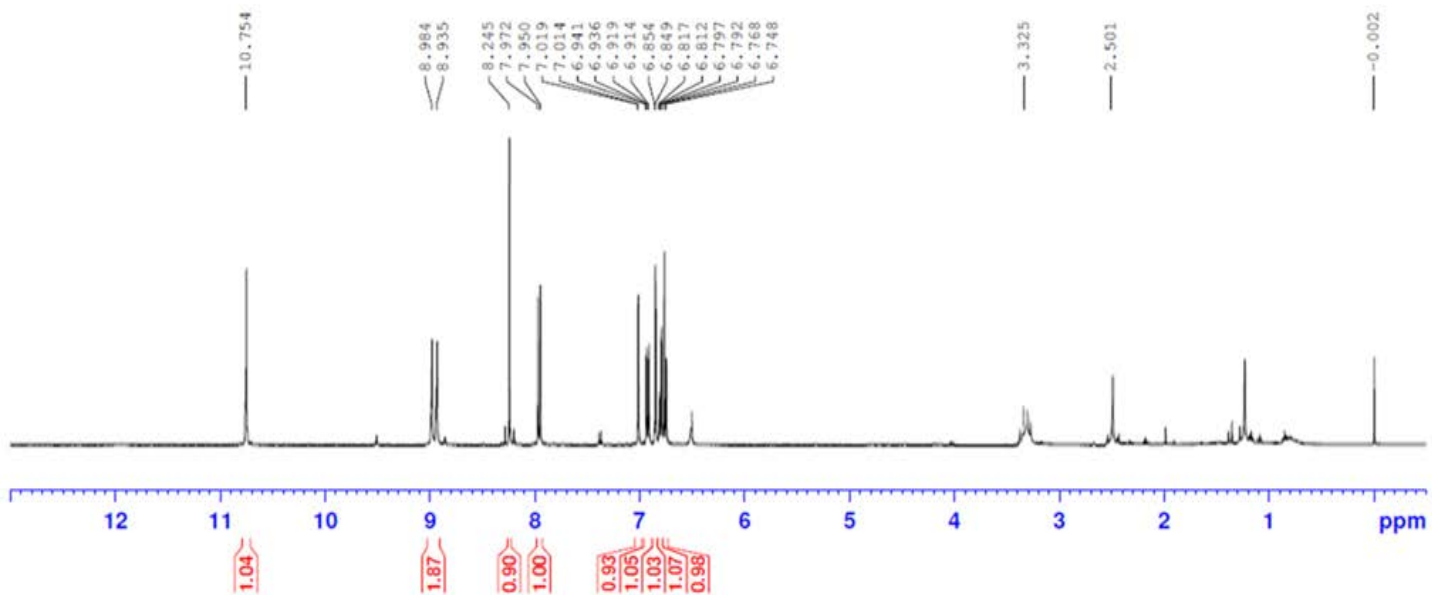
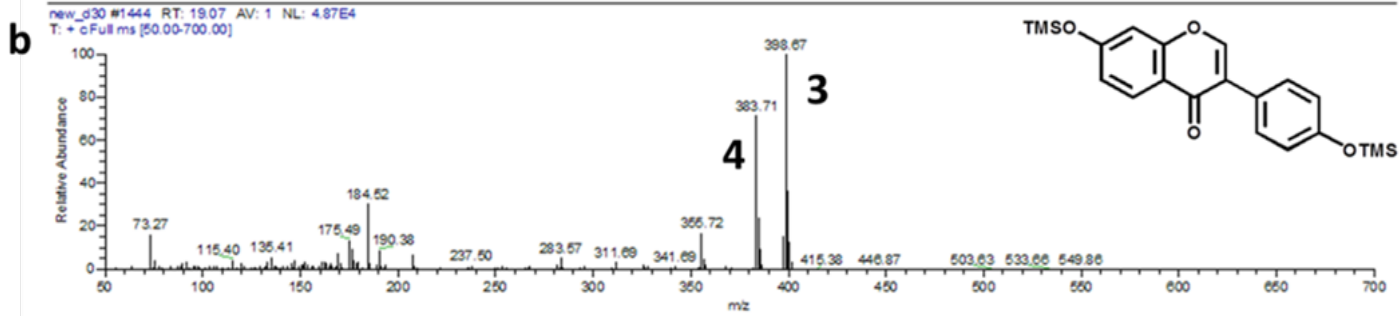
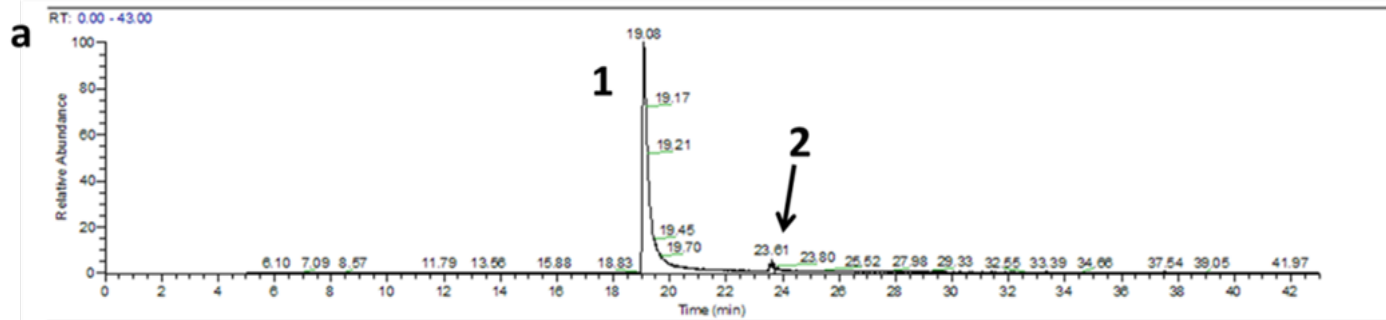


Figure 3.11. ^1H NMR analysis of the substrate (daidzein) and the product (3'-ODI).

Daidzein was dissolved in DMSO- d_6 as it was shipped from Sigma-Aldrich. The peaks of ^1H NMR of the initial substrate, daidzein, and the product, 3'-ODI, are identical except the peaks a, b, c, d, e, f and g. Product was extracted by diethyl ether from the reaction mixture and the top layer was evaporated. The residual powder and daidzein were dissolved in DMSO- d_6 and ^1H NMR spectra were measured at 400 MHz at 25 $^\circ\text{C}$. The ^1H NMR spectroscopic data were stated in ppm (δ) from the internal standard (TMS, 0.0 ppm). ^1H NMR (DMSO- d_6 with 0.05% v/v TMS, 400 MHz) spectrum of 3'-ODI is: δ 10.75 (1H, s, C7-OH), 8.98 (1H, s, C3'-OH), 8.94 (1H, s, C4'-OH), 8.25 (1H, s, H2), 7.97 (1H, d, $J = 8.8$ Hz H5) 7.02 (1H, d, $J = 2$ Hz, H2'), 6.94 (1H, dd, $J = 8.8$ and 2 Hz, H6), 6.85 (1H, d, $J = 2.0$ Hz, H5'), 6.82 (1H, dd, $J = 8.0$ and 2.0 Hz, H6'), 6.77 (1H, d, $J = 8.0$ Hz, H5')

Sampling at 0 min



Sampling at 60 min

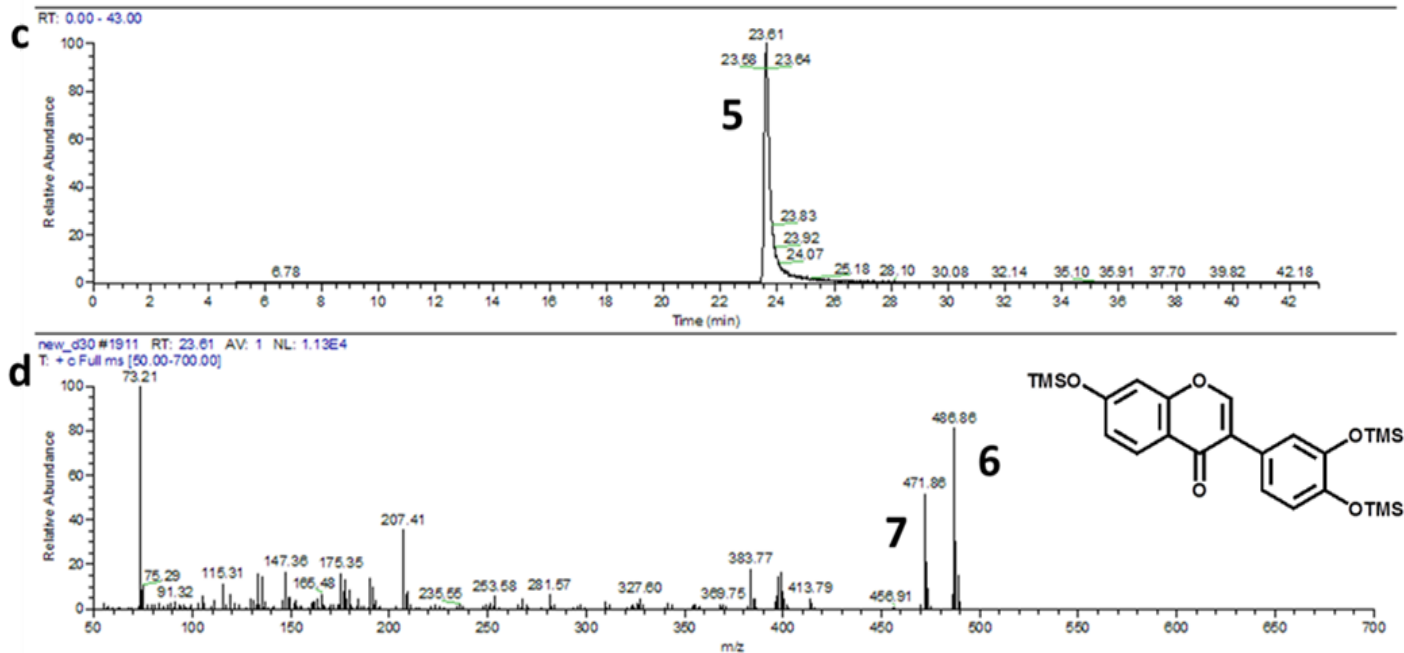


Figure 3.12. GC/MS analysis of the product from daidzein.

Sampling was started right after the enzyme was added in the reaction: (a) and (c) show the chromatography of the sample, and (b) and (d) show the mass spectra of the peaks (1) and (5), respectively. The peak (1) at 19.08 min is daidzein and the peak (2) and (5) which appear at 23.61 min is 3'-ODI. After 60 min of the reaction, peak (1) disappeared and only peak (5) was detected. The detected cation for the product, monohydroxylated daidzein, was $[M+1]^+$ ion of m/z 486.86 (6), which corresponds to the summation of three trimethylsilyl groups and 3'-ODI, and $[M+1]^+$ ion of m/z 471.86 (7), which indicates the loss of one phenolic silyl ether group.

Table 3.4. Reaction conditions.

At a reaction temperature of 37°C, 500 mM borate buffer at pH 9 was used. The detailed calculation of the oxygen transfer coefficient of reactors is addressed later in this supporting material.

Total reaction volume, mL	5	400
[daidzein] ₀ , mM	5	5
[L-ascorbic acid] ₀ , mM	20	20
Wet cell weight, g	0.1	2
Air flow rate, NL·min ⁻¹	Not controlled	12
Oxygen transfer coefficient, min ⁻¹	0.22	0.467

*NL (normal liter): L at 1 atm at 25°C

3.4.5 *ortho*-Hydroxylation of monophenols by tyrosinase.

To investigate the application of a similar *o*-hydroxylation reaction to other monophenolic phytochemicals such as resveratrol and genistein, they were subjected to the same reaction strategy. Resveratrol (1 mM) and genistein (1 mM) were completely *o*-hydroxylated to piceatannol and orobol, respectively, in 5 mL whole cell reaction in one hr with > 95 % conversion yield, suggesting that our approach is commonly applicable to the *o*-hydroxylation of all the compounds with mono-phenolic structure unless the substrate specificity is limited (Figure 3.13). The molecular weight of the products was measured by GC/MS, and the hydroxylated positions were identified with ¹HNMR (Figure 3.13-Figure 3.17).

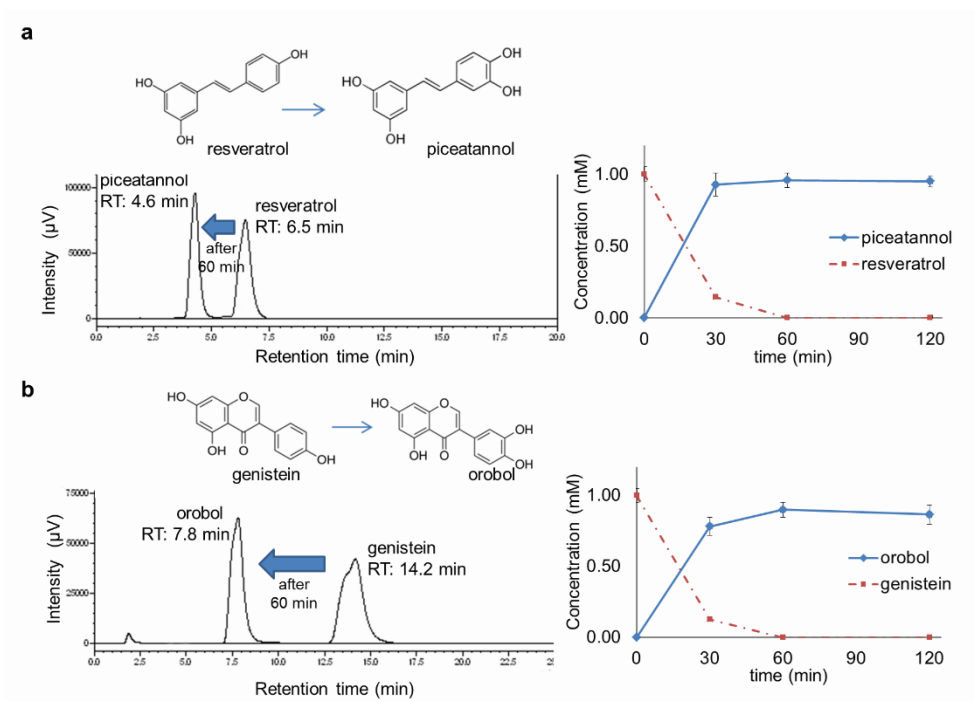
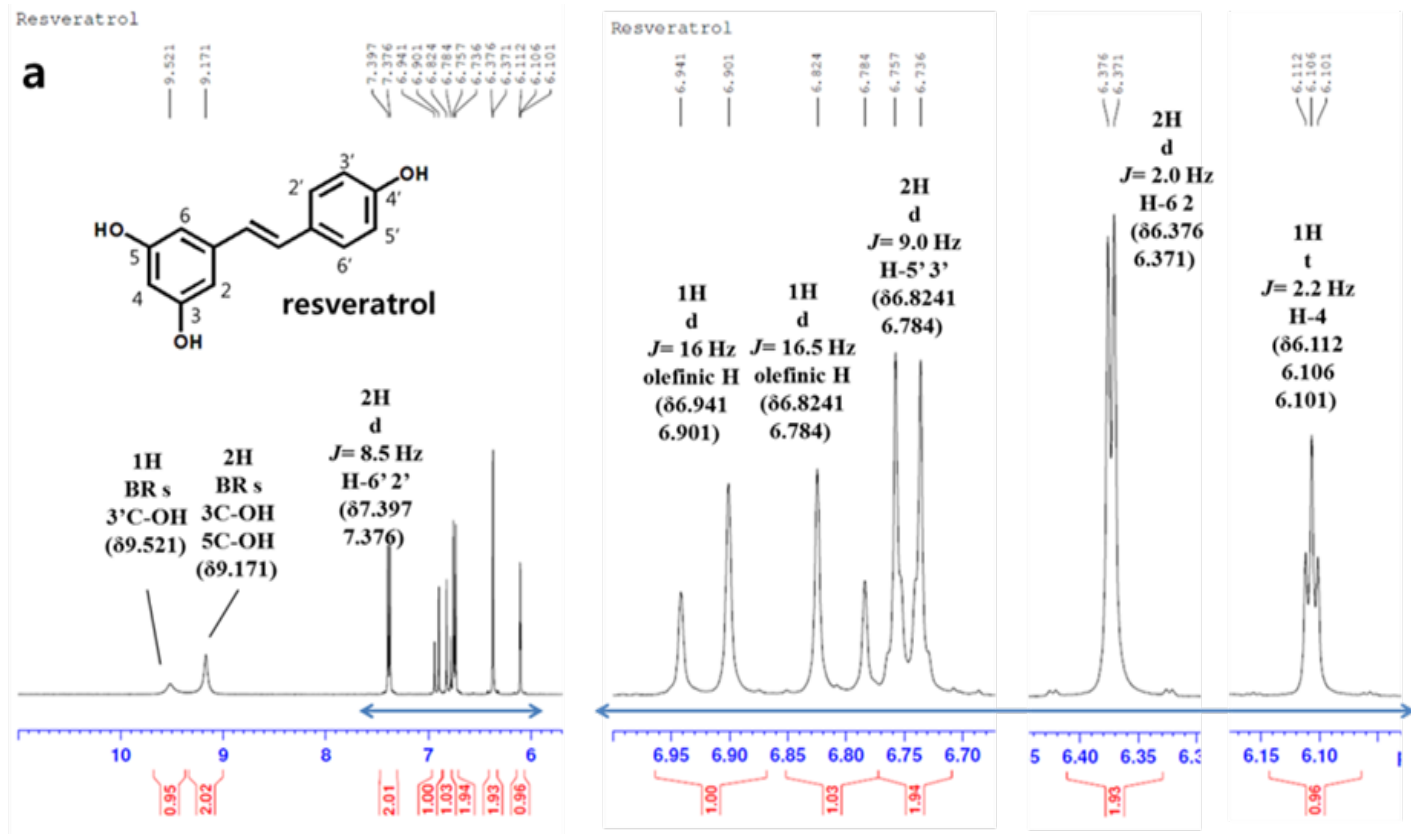
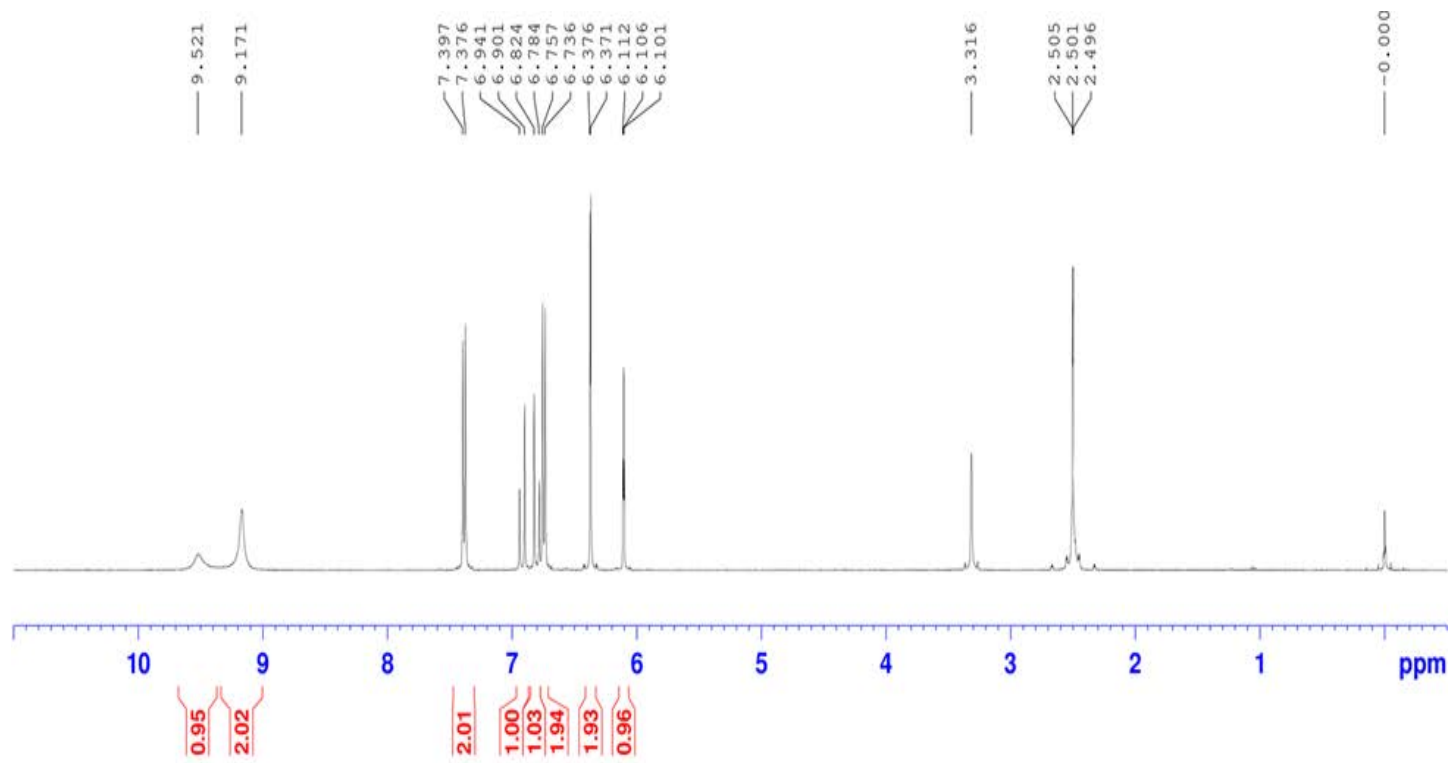
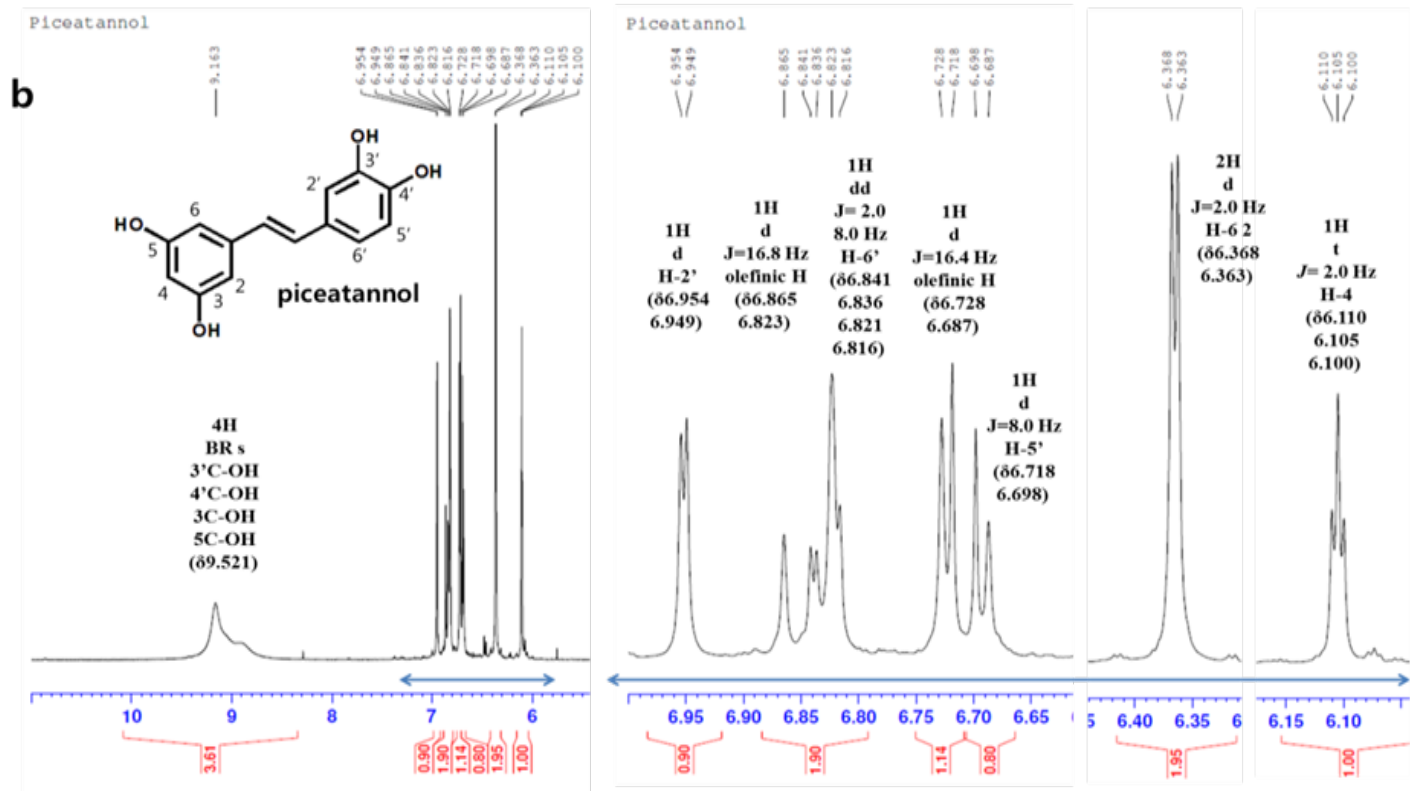


Figure 3.13. HPLC analysis of the production of resveratrol (a) and genistein (b).

After 60 min of Ty reaction on 1mM resveratrol and genistein, all initial substrates were consumed and new peaks appear that correspond to piceatannol (a) and orobol (b). Conditions for this 5 mL reaction are as following; 500 mM borate buffer at pH 9, 10 mM L-ascorbic acid (LAA), 10 mg of wet cells, 1 mM of substrate (resveratrol or genistein), in 37°C water bath.







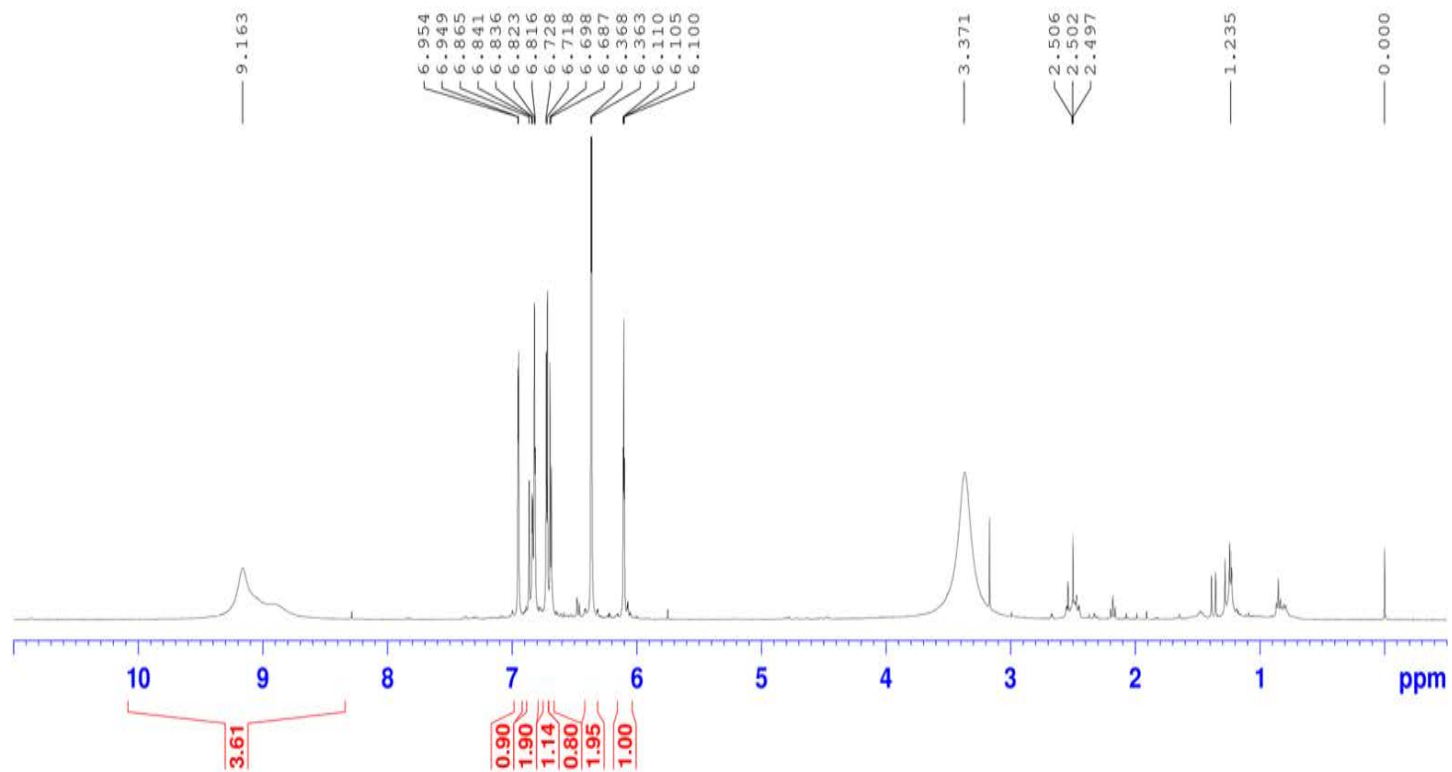
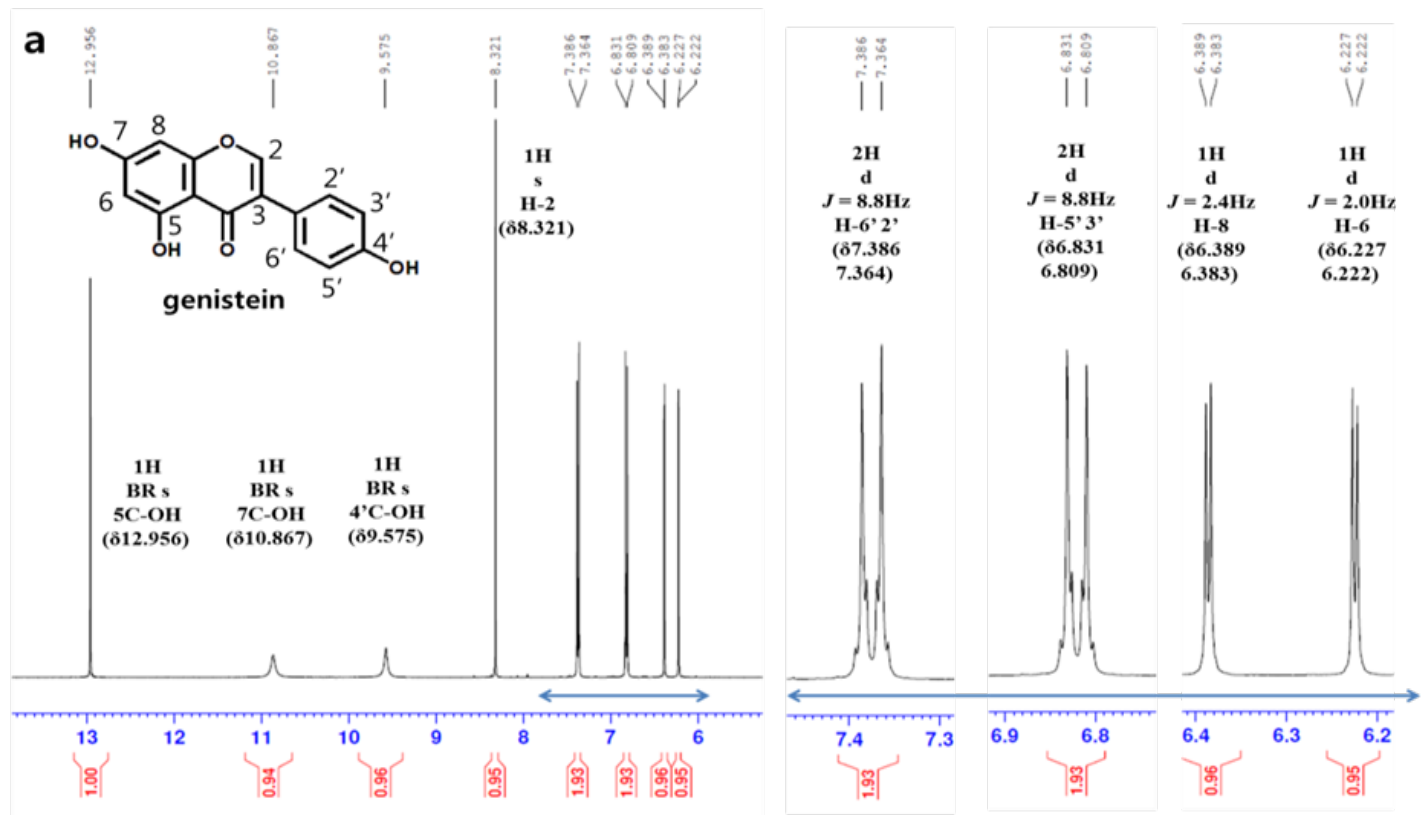
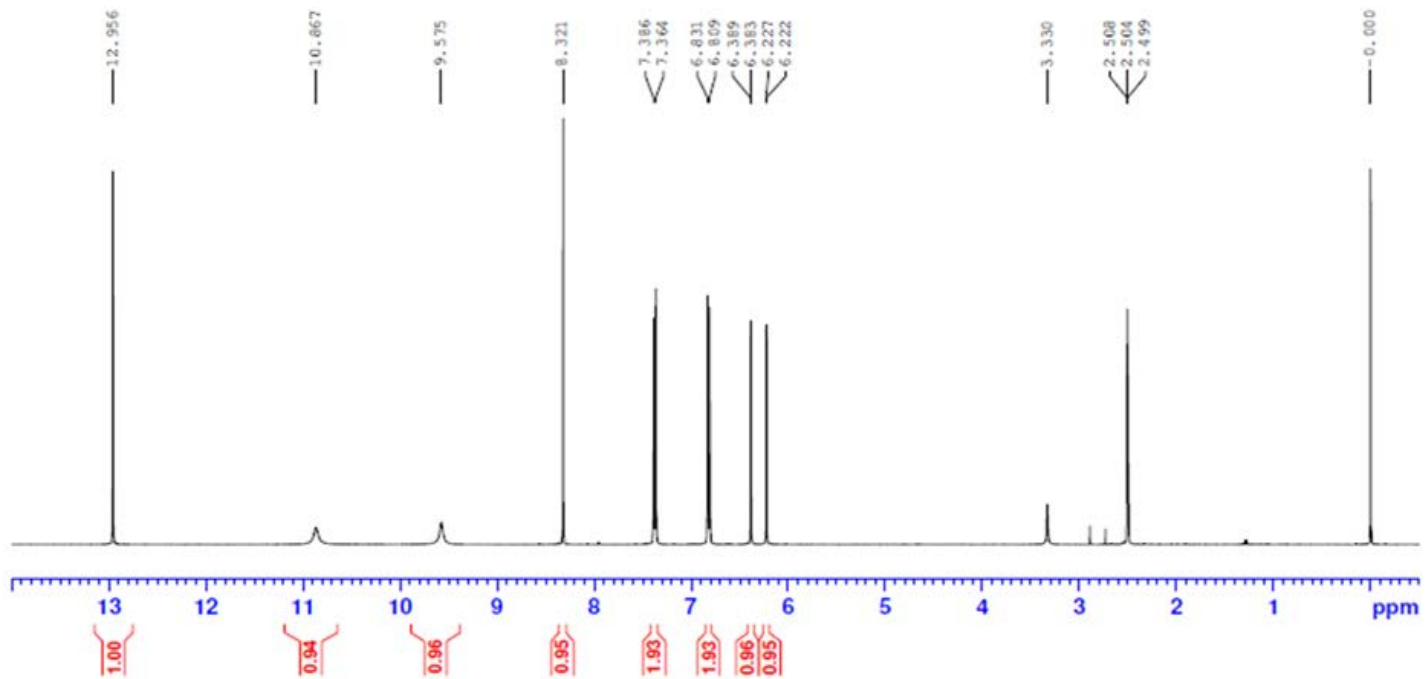


Figure 3.14. ^1H NMR of the hydroxylated product from resveratrol.

(a) resveratrol and (b) piceatannol. Product was extracted by diethyl ether from the reaction mixture and the top layer was evaporated. The residual powder and resveratrol were dissolved in DMSO- d_6 and ^1H NMR spectra were measured at 400 MHz at 25 °C. Resveratrol was dissolved in DMSO- d_6 as it was shipped from Sigma-Aldrich. ^1H NMR

spectroscopic data are stated in ppm (δ) from the internal standard (TMS, 0.0 ppm). ^1H NMR of the product was predicted as piceatannol; (400 MHz, 25 °C) δ 6.110 (t, 1H, $J = 20.$), 6.368 (d, 2H, $J = 2.0$), 6.718 (d, 1H, $J = 8.0$), 6.728 (d, olefinic H, $J = 16.4$), 6.841 (dd, 1H, $J = 2.0, 8.0$), 6.865 (d, olefinic H, $J = 16.8$), 6.954 (d, 1H, $J = 2$), 9.163 (Br s, 4H)





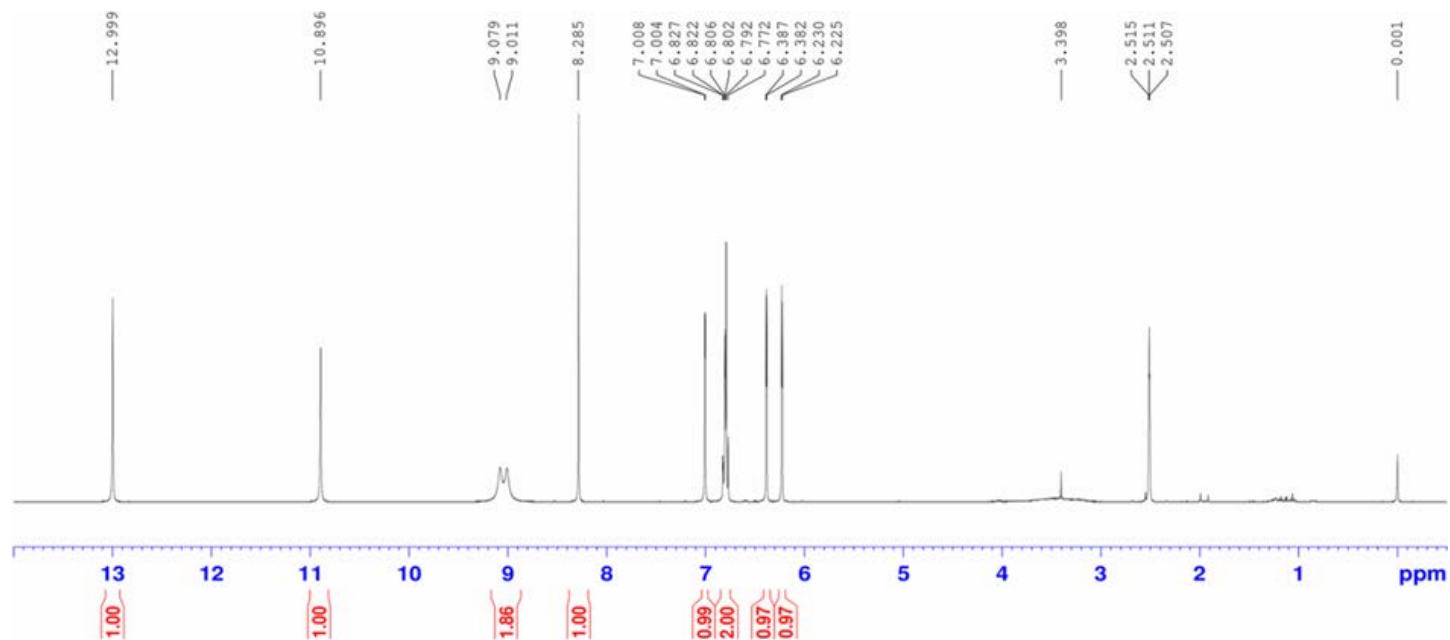
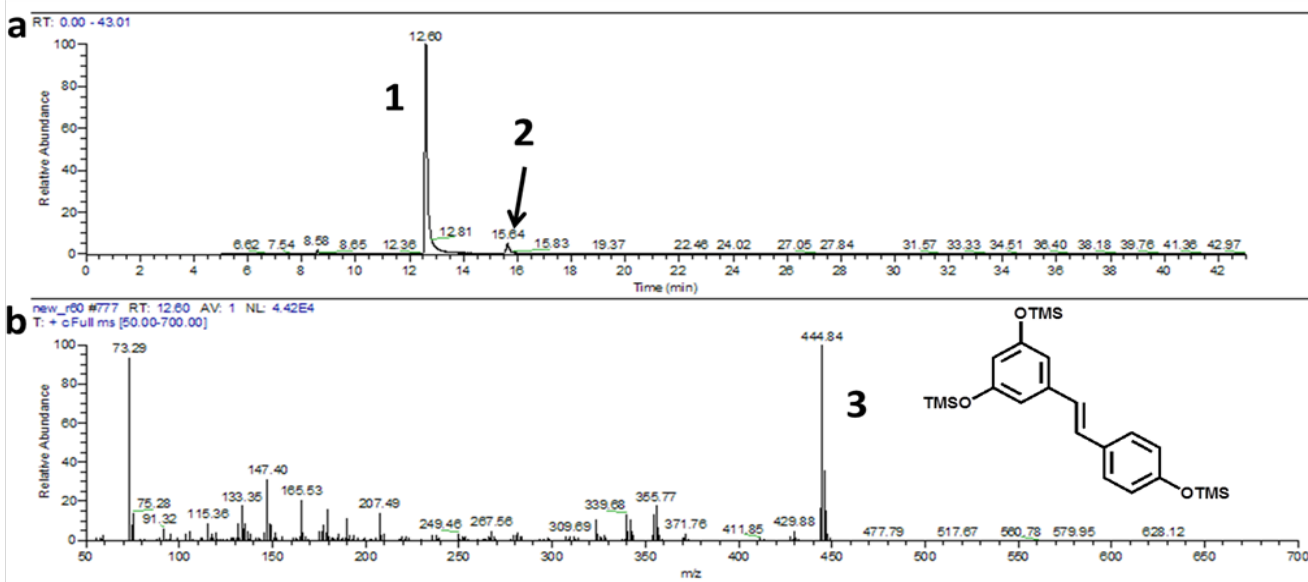


Figure 3.15. ^1H NMR of the hydroxylated product from genistein

(a) genistein and (b) orobol. Samples were extracted by diethyl ether and the top layer was evaporated. The residual powder and genistein were dissolved in DMSO- d_6 and ^1H NMR spectra were measured at 400 MHz at 25 $^\circ\text{C}$. Genistein was dissolved in DMSO- d_6 as it was shipped from Sigma-Aldrich. ^1H NMR spectroscopic data are stated in ppm (δ) from the internal standard (TMS, 0.0 ppm). ^1H NMR of the product was predicted as 3',4',5,7,-tetrahydroxyisogflavone, orobol; (400 MHz, 25 $^\circ\text{C}$) δ 6.225 (d, 1H, $J = 2.0$), 6.382 (d, 1H, $J = 2.0$), 6.772 (d, 1H, $J = 8.0$), 6.802 (dd, 1H, $J = 10, 2.0$), 7.004(d, 1H, $J = 1.6$), 8.285(s, 1H), 9.011(BRs, 1H), 9.079(BRs, 1H), 10.896(BRs, 1H), 12.999(Br s, 1H)

Sampling at 0 min



Sampling at 60 min

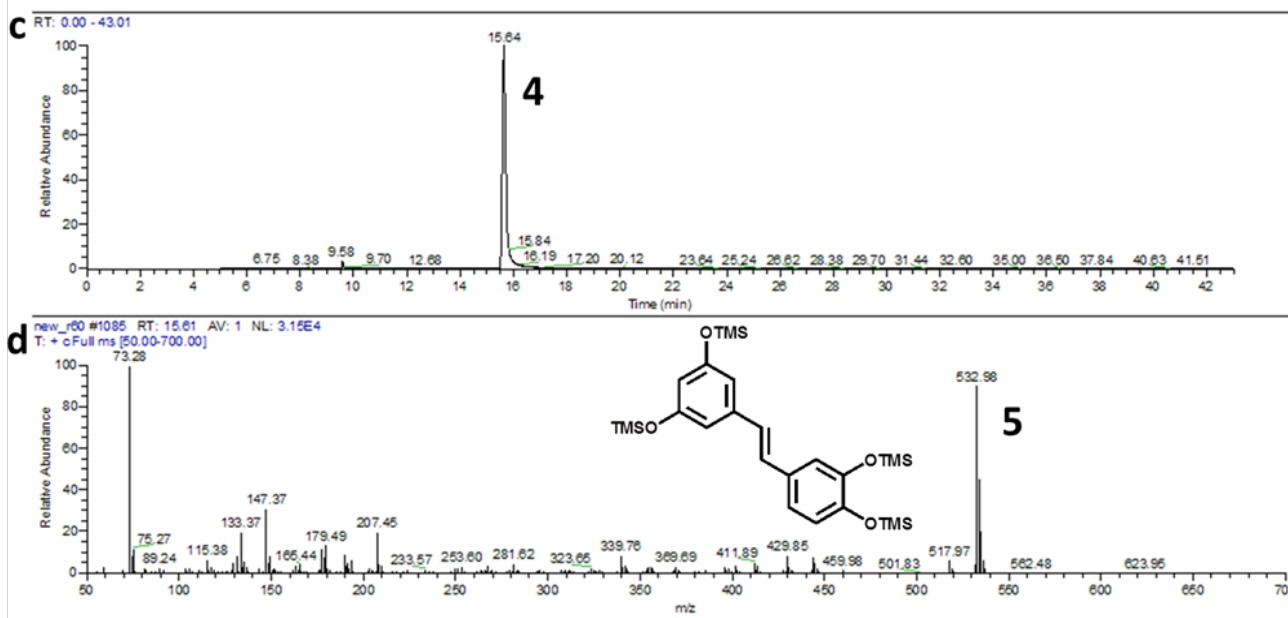
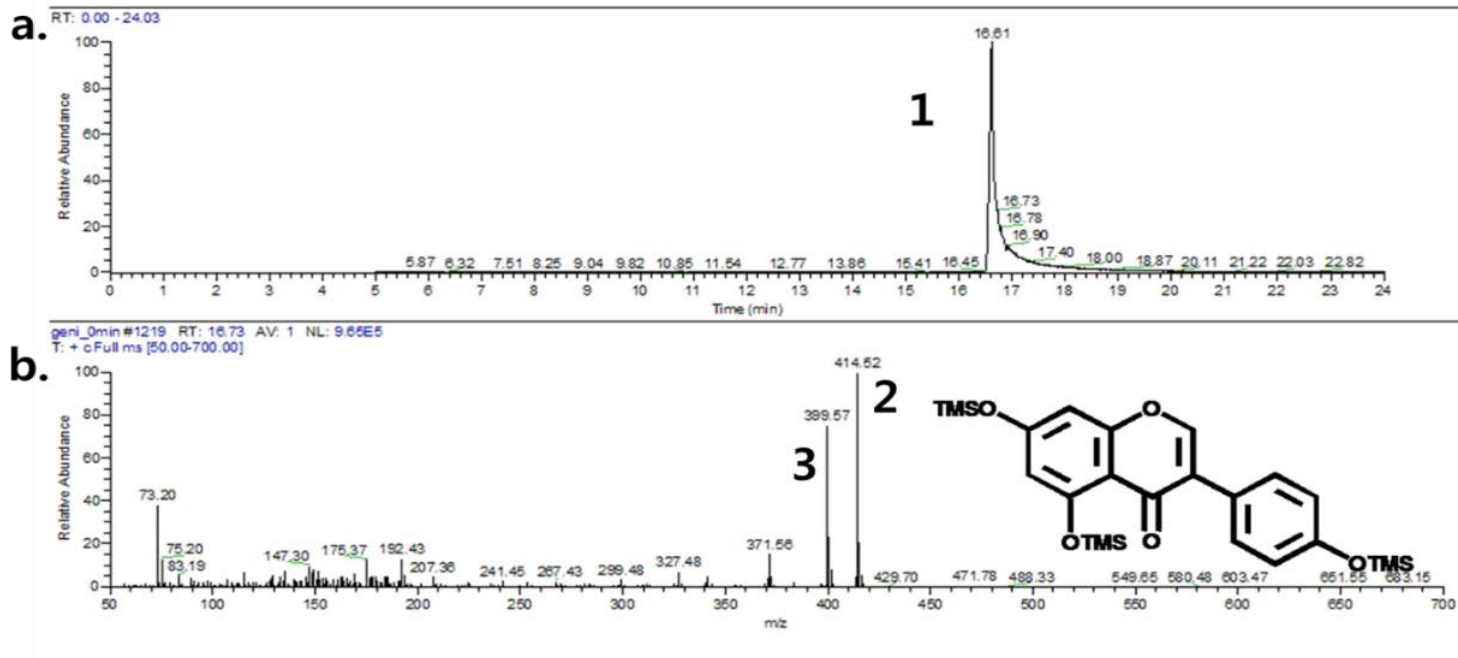


Figure 3.16. GC/MS analysis of the product from resveratrol.

Sampling was started right after the enzyme was added in the reaction. (a) and (c) show the chromatography of the sample, and (b) and (d) show the mass spectra of the peaks (1) and (4), respectively. A peak (1) at 12.60 min is resveratrol, and peaks (2) and (4) which appear at 15.64 min is piceatannol. The detected cation for piceatannol was $[M+1]^+$ ion of m/z 532.96 (5), which corresponds to the summation of four trimethylsilyl groups and piceatannol.

Sampling at 0 min



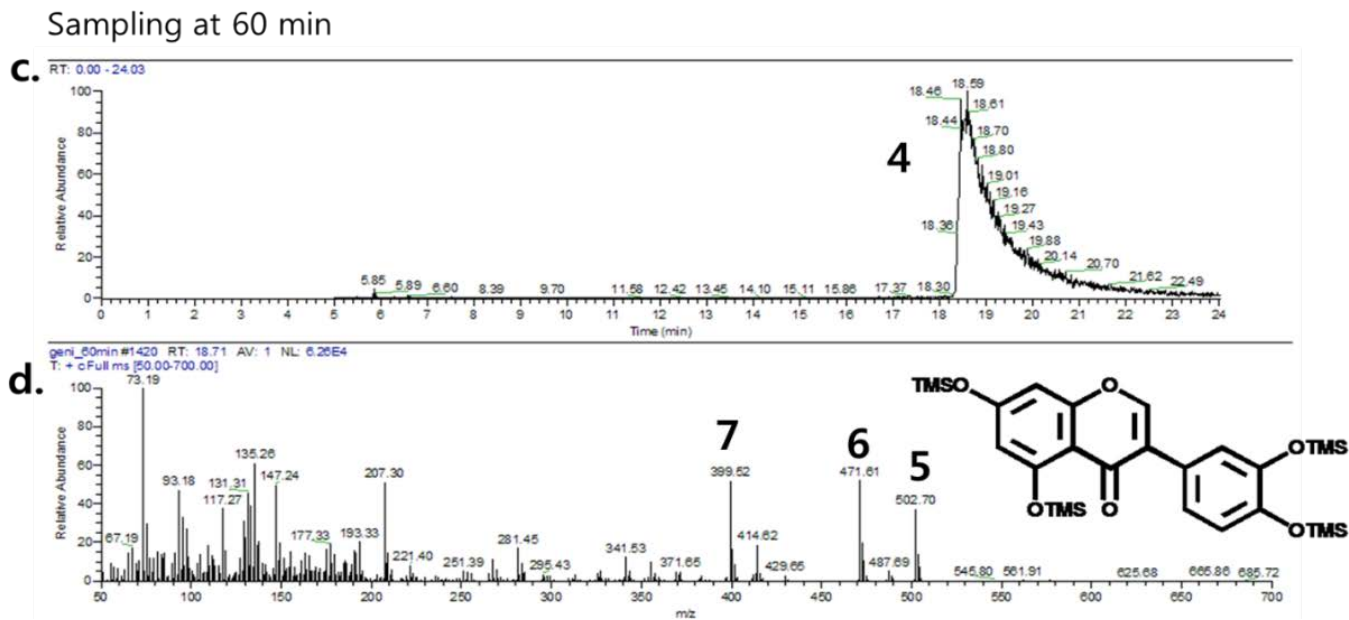


Figure 3.17. GC/MS analysis of the product from genistein.

Sampling was started right after the enzyme was added in the reaction. (a) and (c) show the chromatography of the sample, and (b) and (d) show the mass spectra of peaks (1) and (4), respectively. A peak (1) at 16.61 min is genistein and a broad peak (4) at 18.46 is orobol. The detected cation for orobol was $[M+1]^+$ ion of m/z 574.21 but only m/z 502.70 (5) was detected, which corresponds to the summation of three trimethylsilyl groups and orobol.

3.4.6 *ortho*-Hydroxylation of benzopyrone ring of isoflavones by tyrosinase; 6- and 8- hydroxylation.

In previous sections, only the 3'-hydroxylation of isoflavone (*ortho*-hydroxylation of monophenols) was subjected, but in this section, the efforts for designing Ty that in turn enable to perform *ortho*-hydroxylation of benzopyrone ring, specifically, 6- and 8- hydroxylation of isoflavones. The physiologically beneficial effects of 6- and 8- *ortho*-dihydroxy isoflavones (ODIs) are somewhat similar with 3'-ODI; however, the anti-oxidant effect is greater by repressing different paths as shown in Figure 3.18.

In this study, formononetin was selected as a starting material for produce 6- or 8-hydroxylated isoflavones. The chemical was subjected since its 4'-OH is methylated which blocks the 3'-hydroxylation. Not like elections in B ring of isoflavone, electrons in the C and A ring are stable due to its resonance structure of benzopyrone ring, more room for electrons' moving. Because of the resonance structure, the extraction of an electron from the C ring requires more energy. Therefore, the hydroxylation of 3'- position is more preferred than of 6- or 8- position of isoflavone. As the pka of the hydroxyl group of C ring is lower than B ring, the reaction is slow, and the suicide inactivation occurs more frequently which in turns requires more enzyme and additional copper ions in the reaction. The suicide inactivation mechanism is illustrated in more detail in Figure 3.19.

The separation of 6- or 8- ODI on the HPLC was not easy because of the structural similarity such as the number of hydroxy groups and molecular mass which are identical. Thus, the analysis in quantity of the products (measured by

HPLC) was not reliable (Figure 3.20). It was assumed that the first peak at retention time of 2.7 min is 8-hydroxylated product and the second peak at retention time of 3.3 min is a 6-hydroxylated product. The reaction mixture after the 24 hours of reaction contained both 6- and 8- hydroxylated formononetin, and it was confirmed by GC/MS as shown in Figure 3.21 and Figure 3.22. Unfortunately, the quantity of 8-ODI is too small to detect by GC/MS. Further identification of these materials should be continued.

Ty can produce dark pigment, melanin, from phenolic compounds by two consecutive oxidations. Using this pigment, the screening method for selecting enzymes that hydroxylate 6- or 8- position of formononetin. However, the price of the initial substrate, formononetin, is expensive for screening since the screening method requires the substrate much in quantity. As an alternative, umbelliferone was selected since its coumarin structure is also composed with benzopyrone, which is identical to the C and A ring of isoflavone. Since the oxidized umbelliferon, esculetin, could form a conjugated bond with ferric ions and exhibit greenish brown color, the color change was used for designing screening method.

The target residues for the mutation were selected based on the 3D structure of tyrosinase from *B. megaterium* after *in silico* docking simulation (AutoDock Vina) with umbelliferon and formononetin. The positions are F197, P201, N205, R209, and V218. Saturation mutagenesis of these residues is substituted to NNK codon in gene level at the same time. Since the residues are in the cluster of 20 residues, from 197th to 218th, the primers with the length of 90 base pairs designed. Total 5,000 colonies were tested firstly on umbelliferon, and those who had dark color changes were subjected to the second round of screening

on formononetin. The copper ions and ferric ions were both tested separately for comparing the ability in producing catechol derivatives and melanin. There were two colonies that changed the color of the reaction solution. The mutant was identified as V218C and F187Y/P201F. However, those mutants were also produce the mixture of 6- and 8- hydroxylated isoflavone though the ratio of the both hydroxylated products varied. However, the exact quantification is not allowed in this moment because of the structural similarity of the two products. The roles of the substituted residues should be further clarified. This incomplete study shows only the possibility of 6- or 8-position hydroxylation. It is necessary to optimize the reaction and improve the enzymes for industrial production.

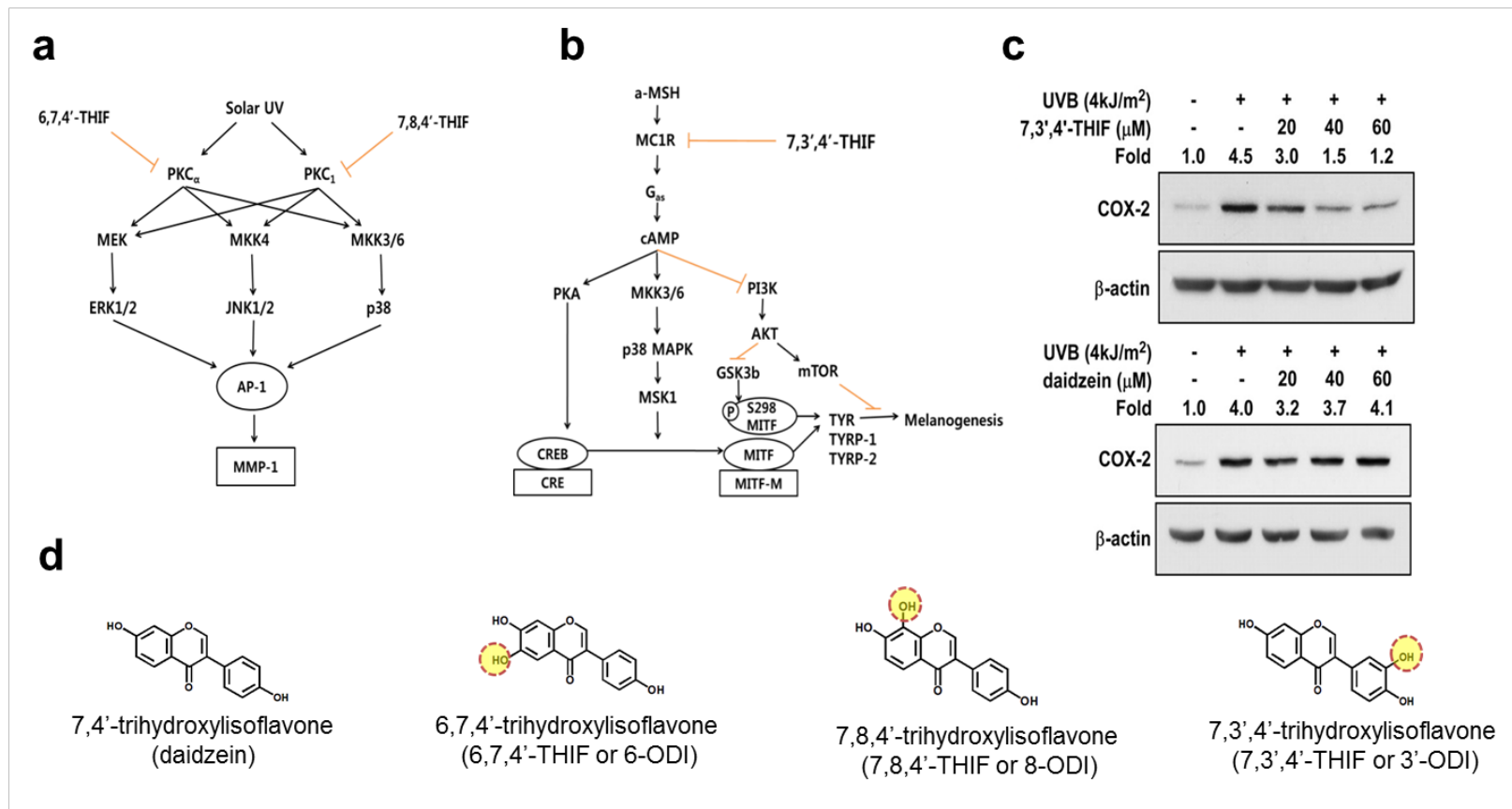


Figure 3.18. The physiological effects of catechol derivatives *ortho*-hydroxylated from daidzein

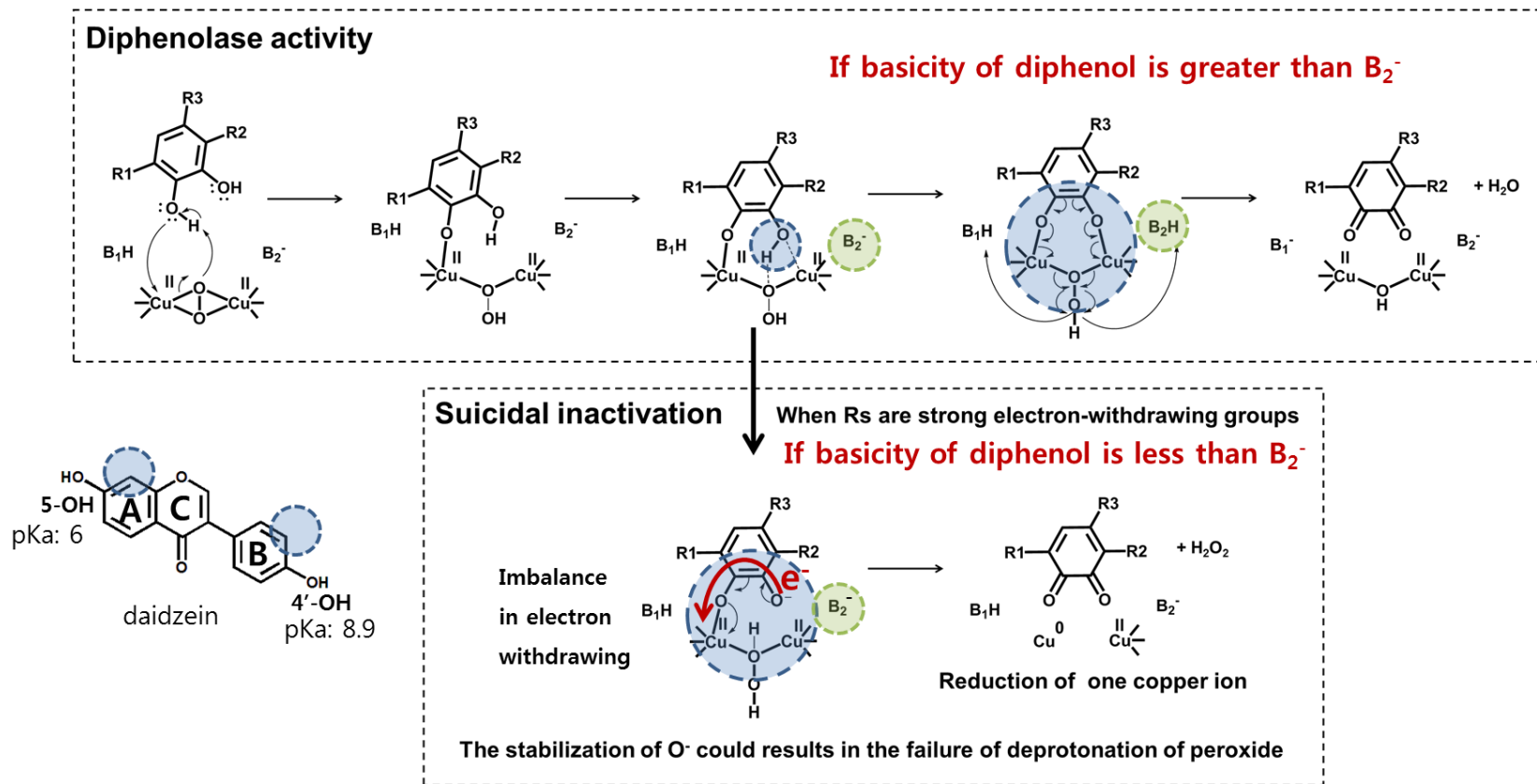


Figure 3.19. The suicide inactivation mechanism depending on the basicity of substrates

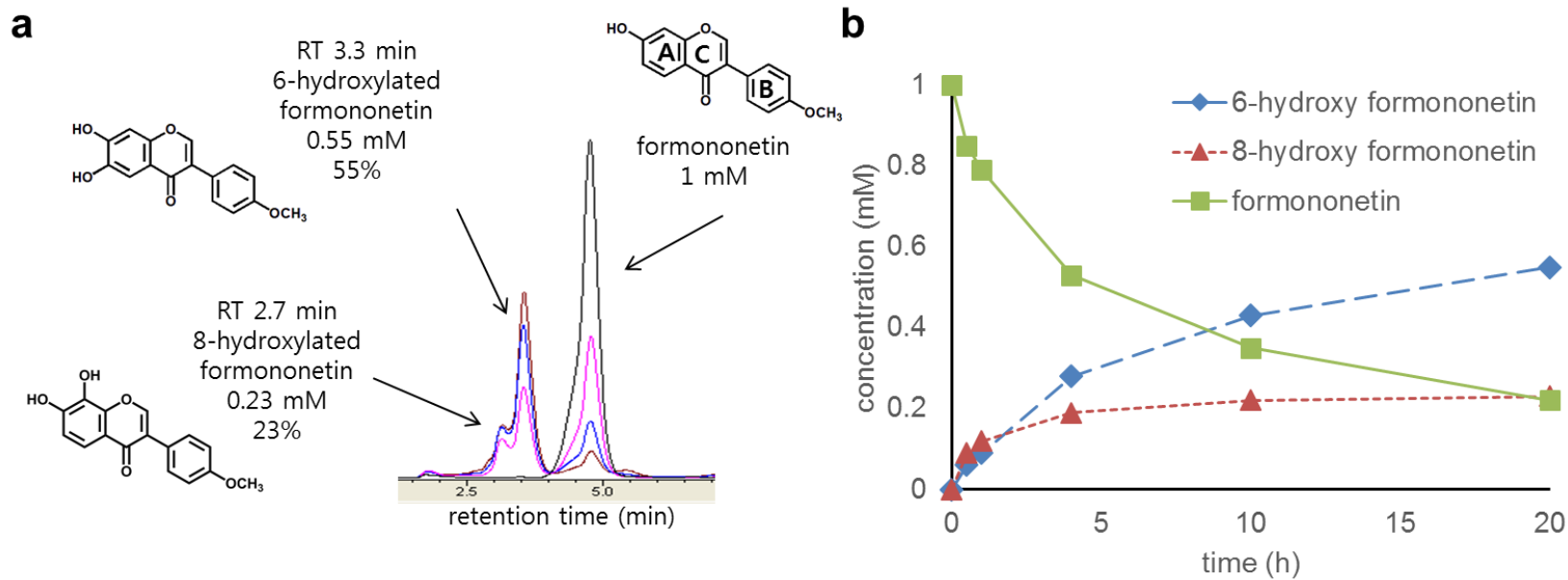
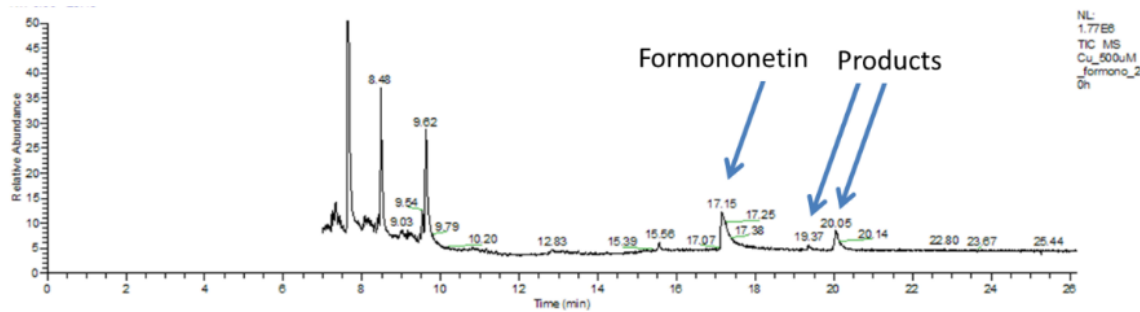
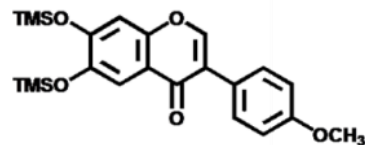
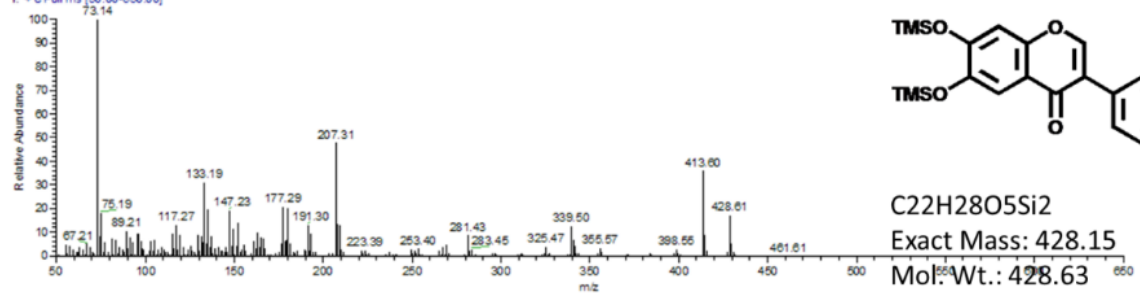


Figure 3.20. *ortho*-hydroxylation of formononetin to produce 6- or 8-hydroxylated isoflavones.



Cu_500uM_formonc_20h #1415 RT: 20.06 AV: 1 NL: 1.49E4
T: + c Full.ms [50.00-650.00]



C₂₂H₂₈O₅Si₂

Exact Mass: 428.15

Mol. Wt.: 428.63

m/e: 428.15 (100.0%), 429.15 (34.5%), 430.14

(6.7%), 430.15 (6.5%), 431.15 (2.1%)

C, 61.65; H, 6.58; O, 18.66; Si, 13.10

Figure 3.21. The full scan of the product after 20 hours of reaction

As the addition of one hydroxylation, one more TMS, which m/z is 73 is also added. Thus, more hydroxylation retained in the gas chromatography. The difference of the retention time of the 6-hydroxylated product and 8-hydroxylated product are not clearly understood yet.

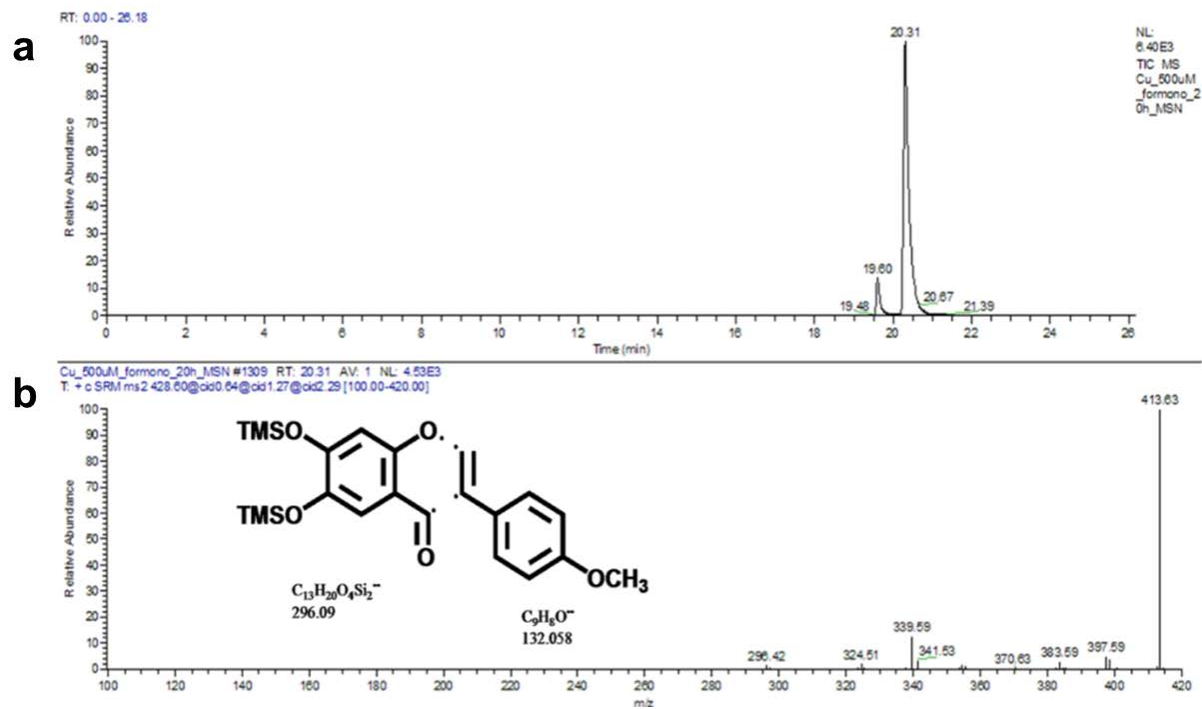


Figure 3.22. The fragmentation of 6-hydroxylated formononetin.

(a) It is the chromatography of the peaks that has 428 m/z probably thought to be 6-hydroxylated formononetin and 8-hydroxylated formononetin. The peak with the retention time of 20.31 is assumed to be 6-hydroxylated formononetin as its higher peak was observed in HPLC. (b) The fragmentation pattern shows the m/z of 296.09 which indicates the addition of one hydroxyl group in C ring.

3.4.7 Calculation of k_1 and k_2 of BM_Ty on daidzein

The continuous reaction was simplified as described in Figure 3.23 (steady-state approximation). k_1 and k_2 were obtained by substituting experimental values into the simplified equation, and the ratio of k_1 to k_2 was calculated. A, daidzein; B, 3'-ODI; C, *o*-quinone; $[B]_{ss}$, concentration of 3'-ODI at steady state; t_{ss} , time point at concentration of 3'-ODI reaching at $[B]_{ss}$; k_1 , phenolase activity; k_2 , catecholase activity

1) Rate constant of phenolase (k_1) :

$$\frac{d[A]}{dt} = -k_1[A]$$

$$[A]_t = [A]_0 e^{-k_1 t} \quad \text{----- (Eq. 1)}$$

$$\ln[A]_t = -k_1 t \ln[A]_0 \quad \text{----- (Eq. 2)}$$

2) Rate constant of diphenolase (k_2) :

At steady state,

$$\frac{d[B]}{dt} = k_1[A] - k_2[B] = 0$$

$$[B]_t = \frac{k_1}{k_2} [A]_t = \frac{k_1}{k_2} [A]_0 e^{-k_1 t} \quad \text{----- (Eq. 3)}$$

Eq. 1 can be inserted into Eq. 3. and then,

$$k_2 = \frac{k_1}{[B]_t} [A]_0 e^{-k_1 t_{ss}} \quad \text{----- (Eq. 4)}$$

Figure 3.24 are the time profiles of 1 mM of daidzein consumed and 3'-ODI produced by 130 nM of purified enzyme in 5 mL reaction at 37°C. 500 mM borate buffer at pH 9 and 5 mM of ascorbic acid were used in the reaction. k_1 , daidzein consumption rate by tyrosinase, can be obtained from Eq. 2, $\ln[\text{daidzein}]$ vs. time. The slope was obtained through in-built program of Excel (Microsoft) (Figure 3.25-a). The plot of 3'-ODI (range of 120 min to 360 min of reaction) was drawn separately, and the best fit equation of the graph was obtained by in-built program of Excel, as shown in Figure 3.25-b.

$[B]_{ss}$ and t_{ss} were calculated through the given equation after finding where the slope of a tangent line become zero. Here, $[B]_{ss}$ is 1 mM and t_{ss} is 83.74 min. The values obtained were inserted into Eq. 4 to determine k_2 , which was $7.26 \times 10^{-2} \text{ min}^{-1}$.

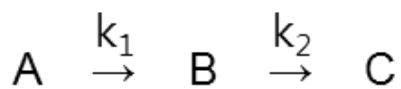
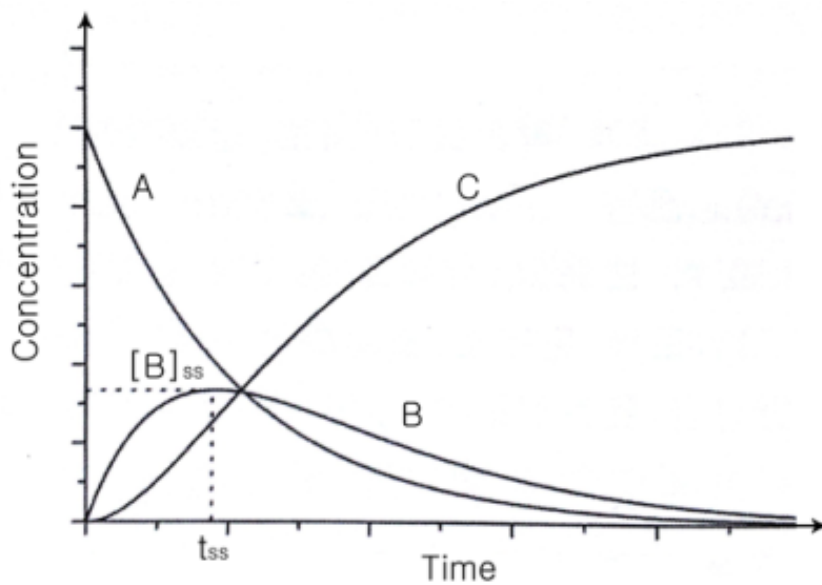


Figure 3.23. The simplified graph showing changes in the concentration of substrate, intermediate, and product.

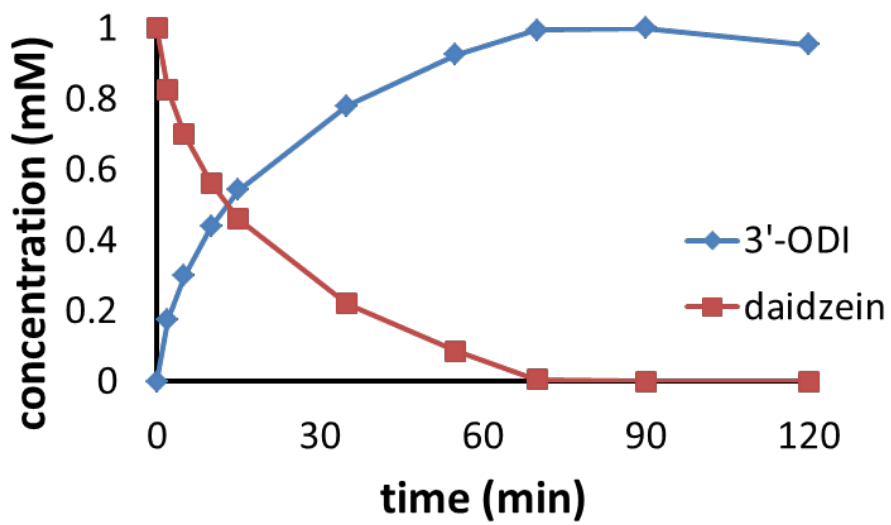
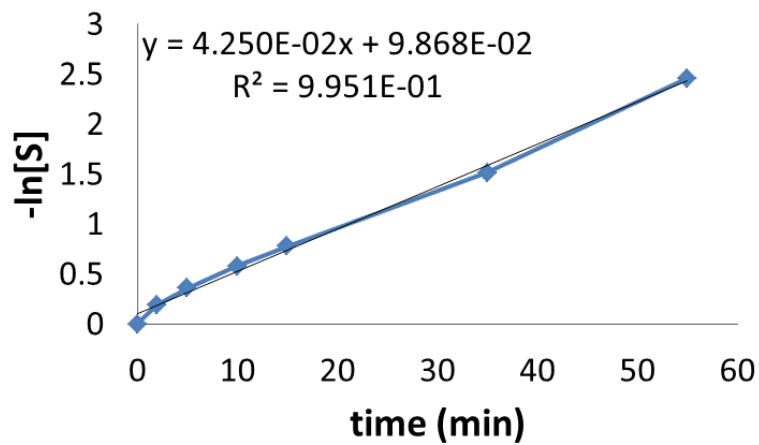


Figure 3.24. An example for calculating k_1 and k_2 .

a.



$$k_1 = 4.250 \times 10^{-2} \text{ min}^{-1}$$

b.

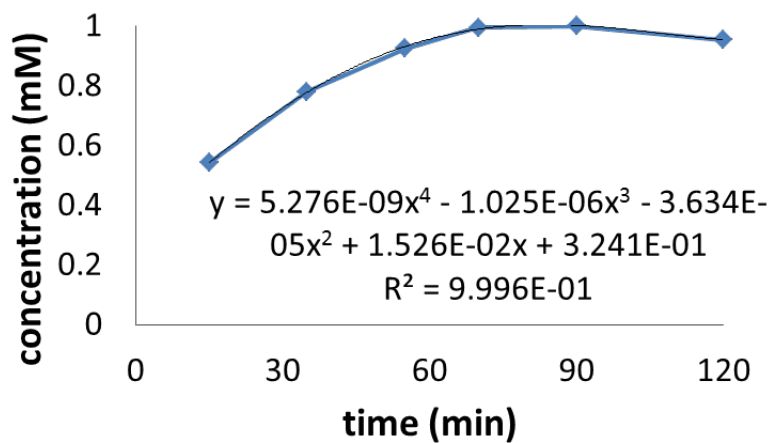


Figure 3.25. Plots for calculating k_1 and k_2

3.4.8 Calculation of oxygen transfer rate and coefficient of the 5 mL reaction in a 50 mL reactor without additional oxygen transfer.

In 5mL of 50 mM tris-HCl buffer pH 8, N₂ was blown to eliminate all oxygen at first, and then D.O. was measured after the N₂ nozzle was removed (Table 3.5).

The reaction was preceded in 50 mL Falcon tube with a diameter of 2.8mm.

$$\text{Rate of oxygen transfer} = \frac{dC}{dt} = k_{v,l} (C_{sat} - C) \quad \text{----- eq. 1S}$$

($k_{v,l}$, overall volumetric oxygen transfer coefficient; C, concentration of oxygen; C_{sat}, saturated concentration of oxygen)

Integration of eq 1S gives,

$$\ln \frac{C_{sat}-C}{C_{sat}-C_0} = -k_{v,l} \cdot t \quad \text{----- eq. 2S}$$

The overall volumetric oxygen transfer coefficient, $k_{v,l} = 0.22 \text{ min}^{-1}$

$$\text{Rate of oxygen dissolving} = \frac{dn_{aq} O_2}{dt} = \frac{V}{m.w.of O_2} \frac{dC}{dt} \quad \text{----- eq. 3S.}$$

(V, reactor volume; n_{aq} O₂, the moles of oxygen that dissolved in the reaction solution)

eq. 1S and eq. 3S can be combined to give,

$$\frac{dn_{aq} O_2}{dt} = \frac{V}{m.w.of O_2} k_{v,l} (C_{sat} - C) \quad \text{----- eq. 4S}$$

The rate of oxygen dissolving in 5mL reactor was 0.44 μmol of O₂·min⁻¹

(88 μM of $\text{O}_2 \cdot \text{min}^{-1}$ in the 5 mL solution). During the whole cell reaction (5 mL) with 500 μM daidzein (without shaking or air blowing), the amount of dissolved oxygen (D.O.) was reduced to approximately 50 μM (0.5 to 0.8 ppm) but not consumed completely, which means that the oxygen was not deficient.

3.4.9 Calculation of oxygen transfer rate and coefficient of the 400 mL reaction in a 1 L reactor with a continuous air flow rate of 12 $\text{L} \cdot \text{min}^{-1}$.

In 400 mL of 500 mM borate buffer pH 9, N_2 was blown to eliminate all oxygen at first, and then D.O. was measured with a continuous airflow rate of 12 $\text{L} \cdot \text{min}^{-1}$ (Table 3.6). The stirring bar (length: 5 cm, diameter: 1cm) was spun at 250 rpm. The integrated values (y-axis) can be inserted into eq 2S. and $k_{v,l}$ (slope) can be easily determined by trend line equation programmed as shown in Figure 3.27. The overall volumetric oxygen transfer coefficient, $k_{v,l} = 0.4637 \text{ min}^{-1}$. The rate of oxygen dissolving in 400 mL reactor with 12 $\text{L} \cdot \text{min}^{-1}$ air flow rate was 74 μmol of $\text{O}_2 \cdot \text{min}^{-1}$ (185 μM of $\text{O}_2 \cdot \text{min}^{-1}$ in 400 mL solution).

Table 3.5. Measuring D.O. for calculating oxygen transfer rate of a 50 mL reactor.

Time(min)	ppm (mg/L)	$\ln[(C_{\text{sat}}-C)/(C_{\text{sat}}-C_0)]$
0.5	0.21	0.982027183
1.5	1.69	0.834827122
2.5	3.2	0.626597031
3.5	4.32	0.394531426
4.5	5.2	0.098217828
5.5	6.41	-
6.5	6.4	-

Table 3.6. Measuring D.O. for calculating oxygen transfer rate of a 400 mL reactor.

Time (min)	ppm (mg·L ⁻¹)	ln[(C _{sat} -C)/(C _{sat} -C ₀)]
0.0	0.23	0
0.5	0.77	-0.091589396
1.0	1.67	-0.265773635
1.5	2.38	-0.428416935
2.0	2.74	-0.522235691
2.5	3.23	-0.66596725
3.0	4.10	-0.986789715
3.5	4.92	-1.42765675
4.0	5.38	-1.799896211
4.5	5.60	-2.042842389
5.0	5.75	-2.250481754
5.5	5.85	-2.417535839
6.0	5.93	-2.574721422
6.5	6.00	-2.73598957
7.0	6.10	-3.023671642
7.5	6.15	-3.205993199
8.0	6.20	-3.42913675
8.5	6.24	-3.652280302
9.0	6.27	-3.859919666
9.5	6.28	-3.939962374
10.0	6.30	-4.122283931
10.5	6.32	-4.345427482
11.0	6.35	-4.815431111
11.5	6.37	-5.326256735
12.0	6.37	-5.326256735
12.5	6.38	-5.731721843
13.0	6.38	-5.731721843
13.5	6.39	-6.424869024
14.0	6.40	-
14.5	6.40	-
15.0	6.40	-

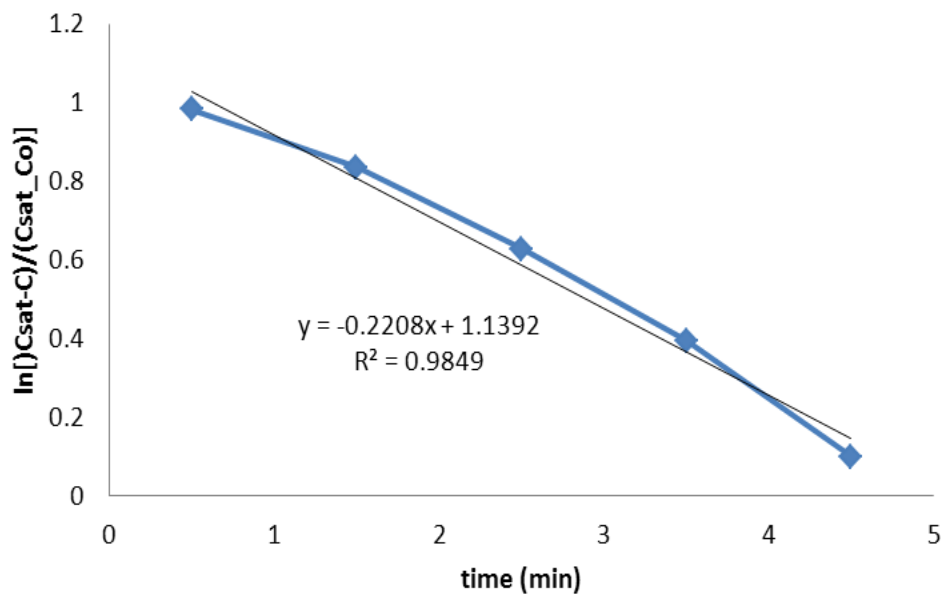


Figure 3.26. A graph for measuring $k_{v,l}$ of a 50 mL reactor

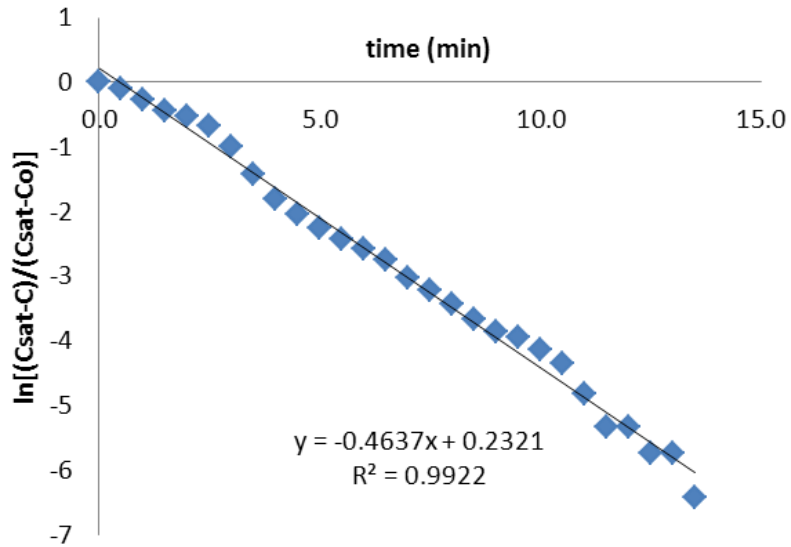


Figure 3.27. A graph for measuring $k_{v,l}$ of a 400 mL reactor.

The overall volumetric oxygen transfer coefficient, $k_{v,l}$ (slope) can be easily determined by trend line equation programmed. Thus, $k_{v,l} = 0.4637 \text{ min}^{-1}$.

3.4.10 Mass production of 3'-ODI and orobol

3.4.10.1 Enzyme expression for scale-up studies.

The experiments performed in the lab was done by using Isopropyl β -D-1-thiogalactopyranoside (IPTG) for the particular control of the over-expression of enzymes. IPTG is a strong inducer but not affordable for the industrial purpose. Thus, at the beginning of scale up studies for producing catechol derivatives, alternative inducers should be selected, which is commercially available at low price. Lactose is the original inducer of the lac operon, and is commercially available at much less price than IPTG. As shown in Figure 3.28., the expression level as the different inducers were used did not show any difference when comparing it on the SDS-PAGE gel. The concentration of the lactose in the rich media was selected among the receipt uploaded elsewhere online (Table 3.7).

After testing the lactose as an inducer, the expression level at certain time points during the culture was measured. As shown in Figure 3.29., after 9 hours of cell culture was reached at the maximum, and at that point, the cell growth was also reached the stationary phase. Thus, rest of the experiments, the cell was cultured for 9 hours with the same composition of broth at 37 °C. The agitation speed was fixed at 200 rpm, and the aeration was set at $1\text{L}\cdot\text{min}^{-1}$.

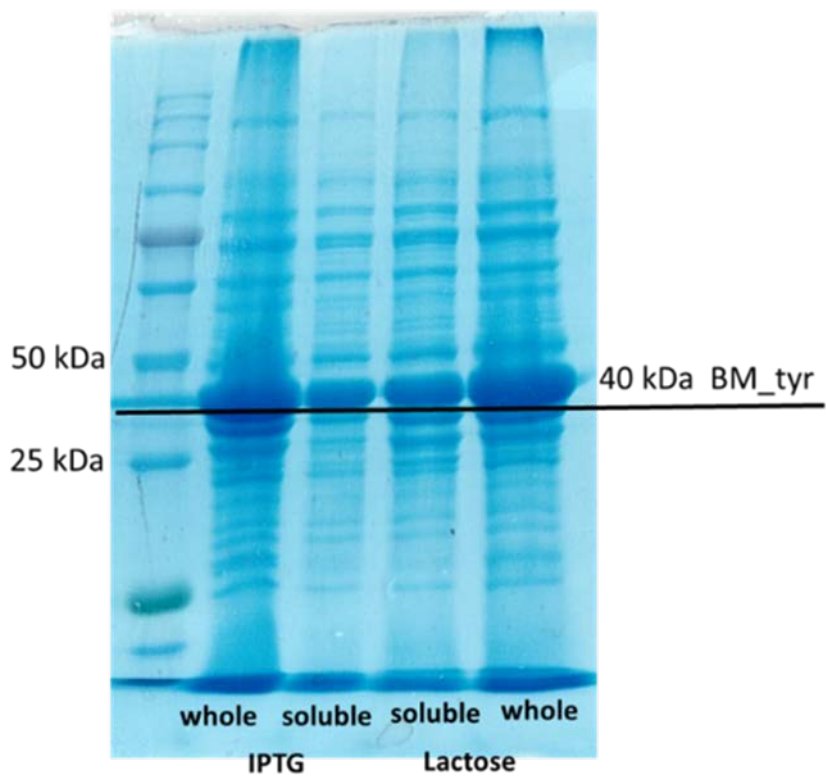


Figure 3.28. Comparison of tyrosinase as different inducers, IPTG, and lactose.

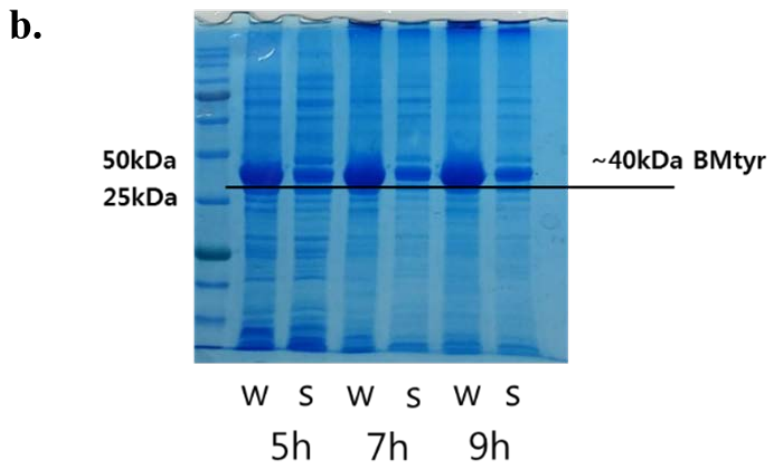
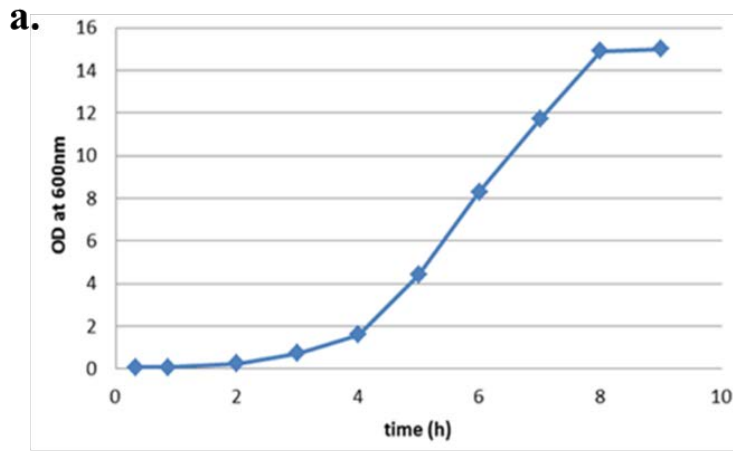


Figure 3.29. The expression level of tyrosinase at certain time periods in the lactose broth.

(a). Cell growth curve when culturing in the complex media with lactose as shown in Table 3.7. (b) The image of SDS-PAGE gel that shows the expression level of tyrosinase induced by lactose at 5, 7, and 9 hours of culturing.

Table 3.7. The composition of complex media used in this study.

Ingredient	Conc.	g·L⁻¹
Tryptone (95039-1KG-F)	1%	10
Yeast Extract	0.5%	5
Na ₂ HPO ₄ (MW=141.96)	25 mM	3.549
KH ₂ PO ₄ (MW=136.09)	25 mM	3.402
NH ₄ Cl (MW=53.49)	50 mM	2.675
Na ₂ SO ₄ (MW=142.04)	5 mM	0.71
MgSO ₄ (MW=120.37)	2 mM	0.241
Glycerol	0.5%	5
Glucose	0.05%	0.5
Lactose	0.2%	2

3.4.10.2 The optimization of the reaction conditions

Through the experiments performed on the lab scale, it was derived that the level of dissolved oxygen matters and the controlling the D.O. level was essential for this reaction. To remind again, only 170 μM of oxygen is available during the reaction, which is also derived from the lab scale reaction. As shown in Figure 3.30, L-ascorbic acid (intently used for the prevention catechols) can significantly consume the D.O. in the reaction solution. The D.O. level was monitored as the aeration was adjusted because oxygen is one crucial factor that runs the hydroxylation reaction.

After the optimizing the reaction conditions, such as the initial concentration of cell, substrate, and reducing agents as well as the conditions for the reaction, approximately, 2.7 $\text{g}\cdot\text{L}^{-1}$ (equivalent to 10 mM) was successfully converted all to 3'-ODI in an hour and a half. As shown in Figure 3.31., the turbidity of the reaction solution was changed as the reaction occurs as the product, catechol derivatives, forms the complex with boric acid and the solubility of the complex increases at the reaction. After the reaction ends, the solution became completely clear. Thus the reaction was easily monitored by nakid eyes. After identifying the product, the further scale-up studies was proceeded.

The reaction condition optimized from the 3 L reaction in the lab was ideally suited in the 18 L of reaction in 40 L reactor; however, the extraction method was not easy when scaled up. The efficient of the extraction of products with an organic solvent, ethyl acetate, was great but when handling, it is harsh and not safe. Thus, a well-equipped facility was required; however, any facility with

proper ventilation system was not available. Developing an alternative purification of the product was necessary. The studies on the purification will be discussed later this chapter.

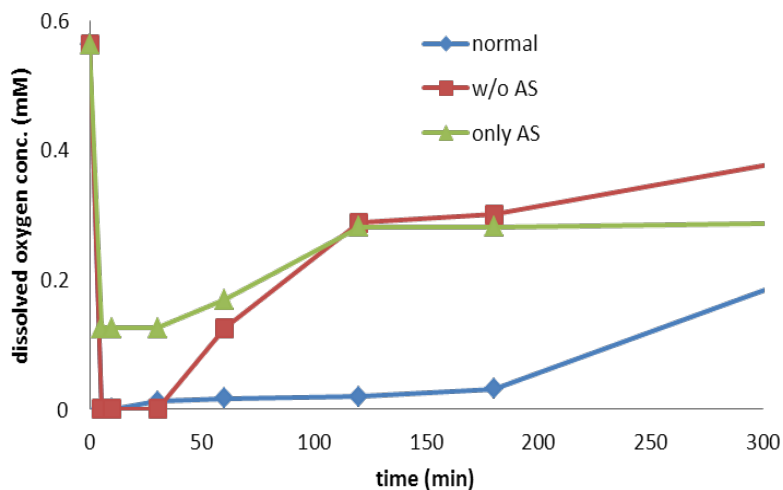
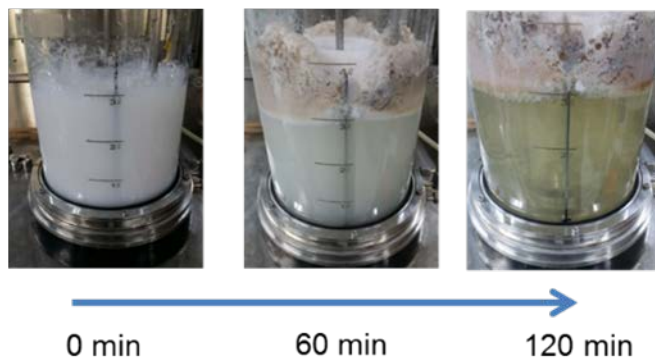


Figure 3.30. Monitoring of dissolved oxygen level during the reaction.

“Normal” represents the reaction with the substrate, L-ascorbic acid, and purified tyrosinase was given. “w/o AS” represents the reaction within the same condition except L-ascorbic acid. “only AS” represents the D.O. level of the solution with only L-ascorbic acid (2mM) was given. Only 170 μ M of oxygen is available during the reaction.

a.



b.

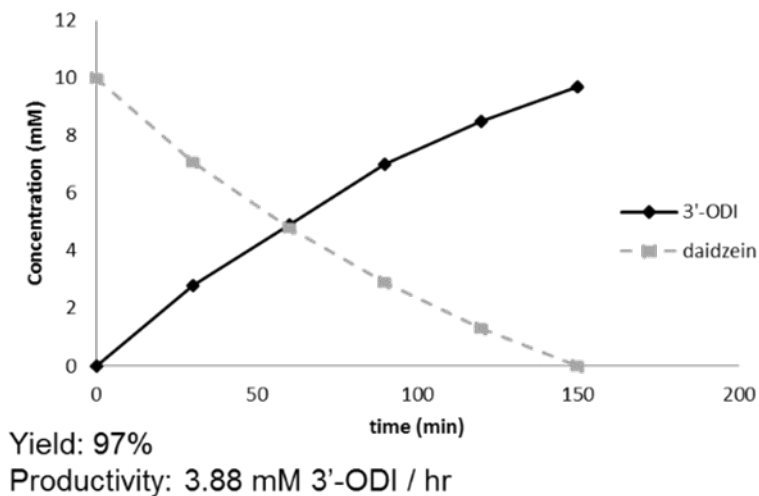


Figure 3.31. 3 L reaction of hydroxylation of daidzein with the optimized condition.

(a) The image that shows the change in turbidity of the hydroxylation of daidzein.

(b) The concentrations of daidzein and 3'-ODI measured by HPLC.

The studies beyond 300 L scale reaction were performed at Chuncheon Bioindustry Foundation where all the utilities for culturing cells, reactions, and filtering cells were equipped. However, the first trial of the reaction in 300 L was problematic from the cell culture to setting factors relating to the aeration of the reaction. First, the D.O. level as adjusting agitation speed was unexpected because of the different fin size of the turbine. Second, the substrate started to get aggregated as reaction goes since the substance is not soluble and hydrophobic. The yield of the first trial was only 22%. To get remove the by-product, melanin, several washing steps with strong acid was performed, and this affected negatively on the recovery yield which was 55%.

Furthermore, in the case of genistein, 5-hydroxy group and the ketone of C ring act as a cis-diol which has significant interaction with boron in boric acid. After addition of boric acid, the color of the solution was changed spontaneously. The problem is that the complex compound cannot diffuse across the cell membrane. The hydroxylation of genistein with the whole cell did not occur at all. Spore display of tyrosinase on the surface of Bacillus spore was performed, but the amount of the spore was not enough. Thus the lysis of cell cultured in 40 L volume was inevitable. High pressure homogenizer worked greatly but the process was slow, $30 \text{ L}\cdot\text{h}^{-1}$.

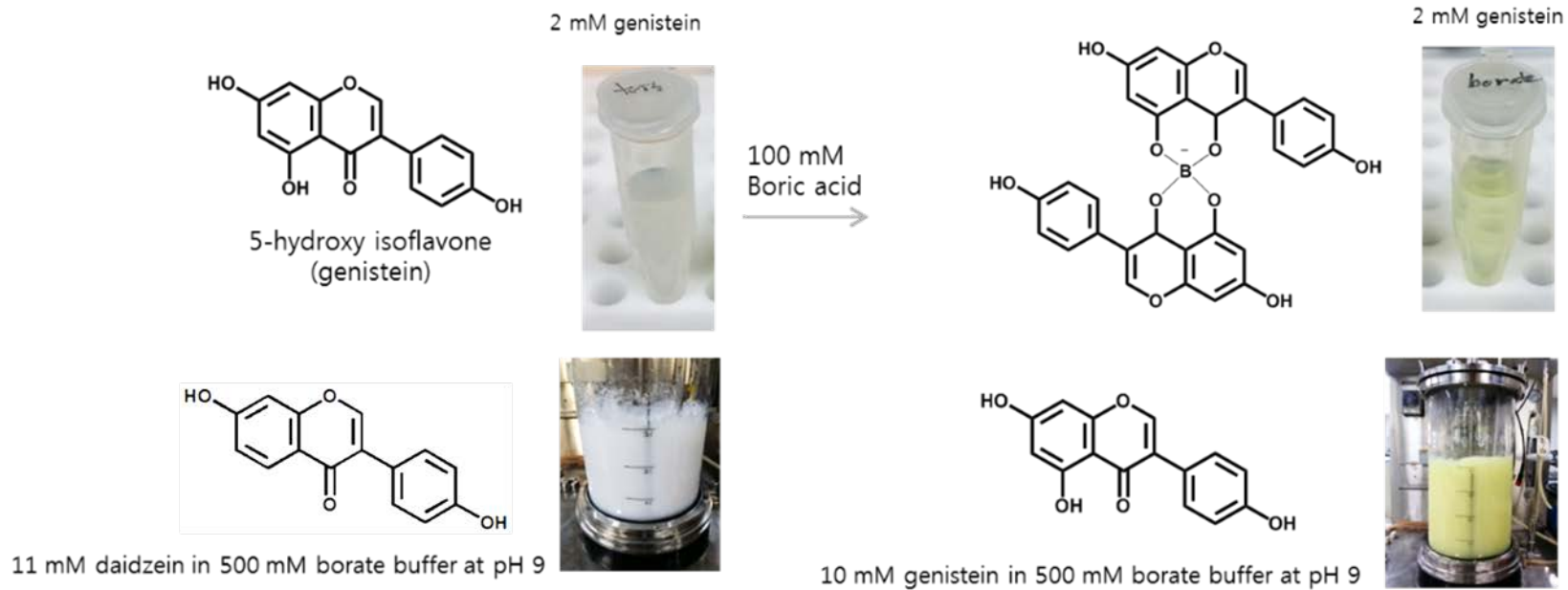


Figure 3.32. The formation of boron ester bond with genistein and boric acid.

3.4.10.3 The optimization of the purification of products.

The first extraction system was simple extraction with an organic solvent as shown in Figure 3.33. In the lab, handling few mL of organic solvent was not troublesome when refining the product; however, managing over 10 L of ethyl acetate was not safe, and thus a well-equipped facility was required. Since any facility with proper ventilation system was not available. Developing an alternative purification of the product was necessary.

Both substrate and product are insoluble isoflavones. However, it was found that only product can be made soluble when using boric acid in the reaction by leading the formation of catechol-boron complex. And after the reaction, the simple acid hydrolysis can efficiently break the bonds in complex, and precipitate the product, catechols. The procedure optimized are illustrated below in Figure 3.34. Thus, in the rest of the trials of the mass production utilized this purification method.

Unfortunately, the affinity of boric acid and piceatannol was greater than of 3'-ODI or orobol. In addition, strong acid hydrolysis for breaking boron ester bond could lead the addition of proton in the double bond between 7 and 8 position of piceatannol. Thus, alternately, the chromatography by Amberlite and washing steps using distilled water should be additionally performed for recovering piceatannol and improving the purity. The optimized steps for the refining piceatannol is illustrated below in Figure 3.35.

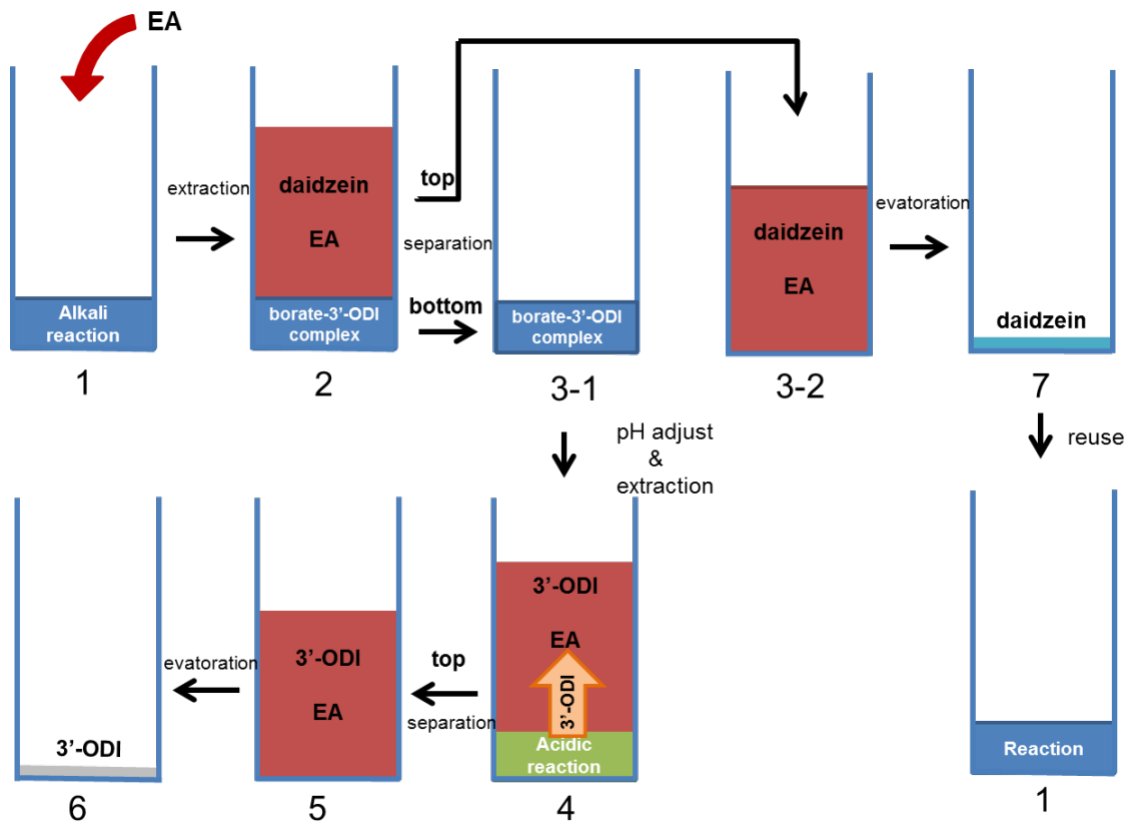


Figure 3.33. Purification with organic solvent extraction

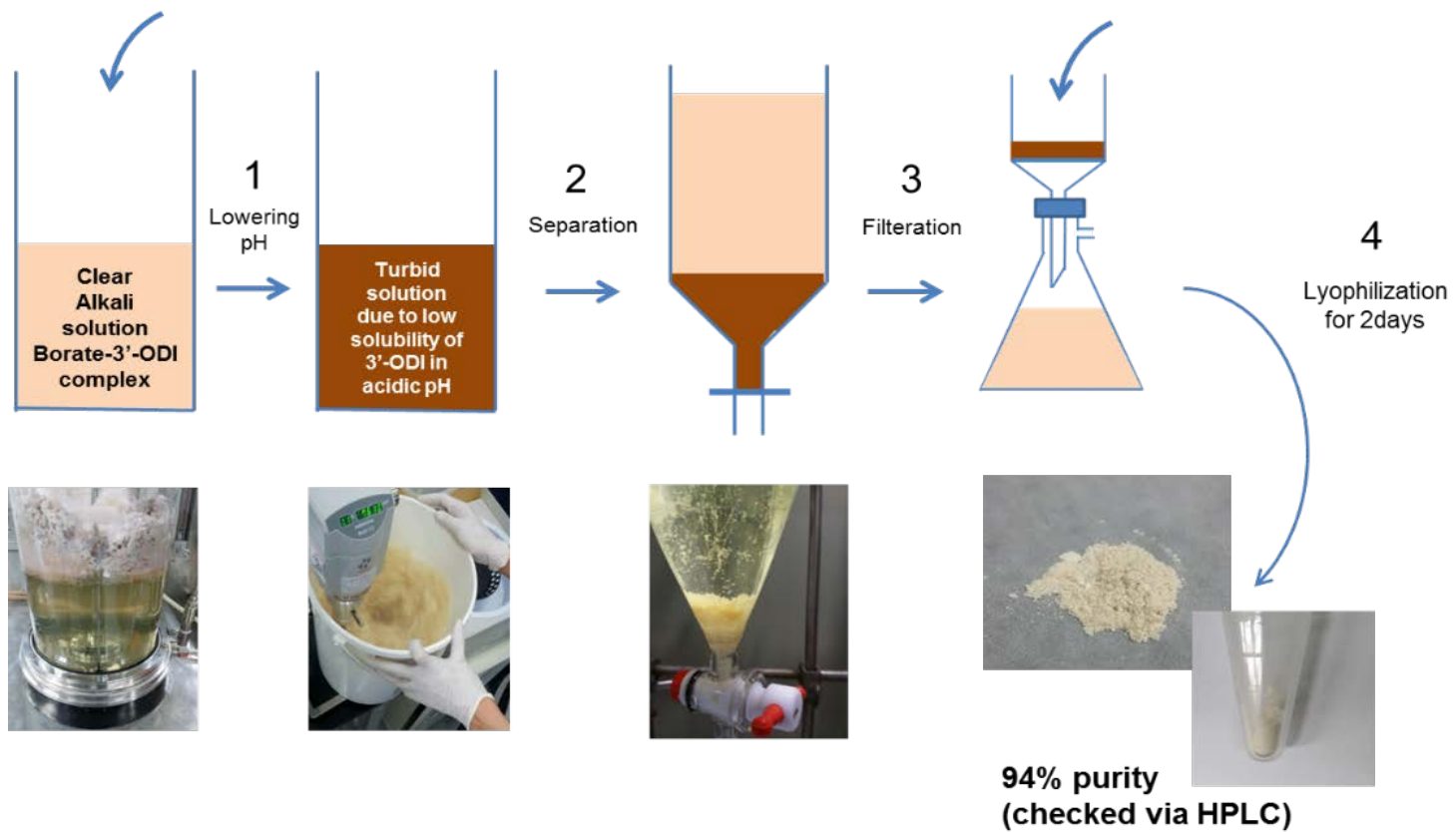


Figure 3.34. Purification by using differences in the solubility depending on pH.

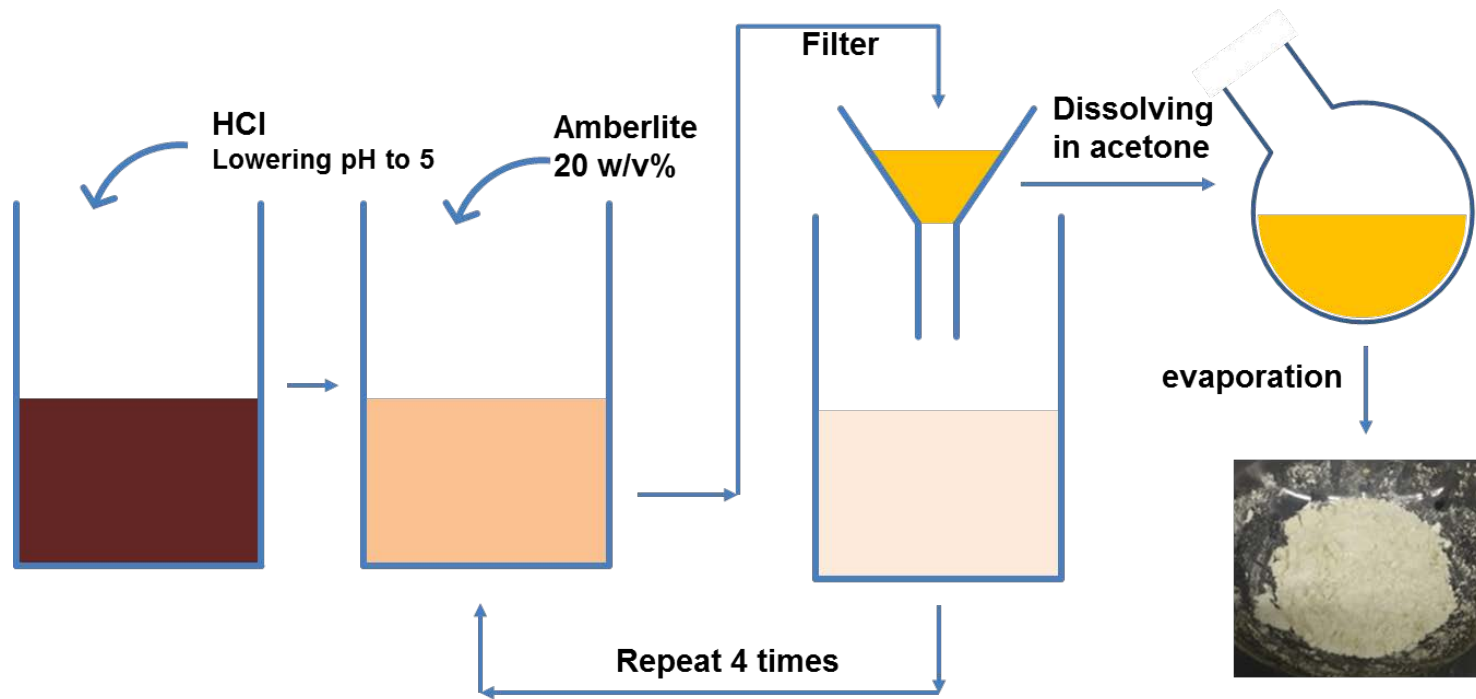


Figure 3.35. Purification of piceatannol with Amberlite.

3.4.10.4 Overall process of the mass production of catechol derivatives.

In the first trial, there were two problems arisen, one is the D.O. level as adjusting agitation speed was unexpected because of the different fin size of the turbine from the smaller reactor used for the optimization in previous studies, and another is the substrate aggregation as stated earlier. Since the materials and the rent for the facility utilized in the mass production are expensive, the number of the trials for the optimization should be minimized. Thus, the reaction was started without agitation and slightly increased as monitoring the level of D.O. And the speed of agitation was set when the D.O. started to be arisen abruptly. The excessive D.O. was regarded as not only unnecessary for the reaction but also a factor that negatively affects the reaction since it oxidizes the products. Unfortunately, there was no optimized agitation speed, but the agitation speed at which the D.O. level maintains in between 3.5 and 4 was the optimized speed. The agitation speed causing D.O. level beyond 4 leads lower in conversion yield since the excessive oxygen in the solution oxidize the product.

As a result, 3'-ODI and orobol was all converted in an hour and a half with the yield nearly at the theoretical yield. And the purity was also above 99%, which was identified by ¹HNMR, GC/MS, and HPLC. The data is identical to the analytic data in Appendix D. The overall protocols and the schematic figures for the mass production of 3'-ODI and orobol are in Figure 3.36 and Figure 3.37. Furthermore, the products, orobol and 3'-ODI were subjected for the functional ingredient of cosmetics. The both products are insoluble, but an organic solvent

that is registered in the database of the cosmetic ingredient was screened for dissolving 3 w% of the products. The material is listed as safe, and it was name as Solvent A. The name of the substance will not be specified for intellectual property protection. The formula was tested for the safety and stability, and then the prototype of the cosmetics was developed.

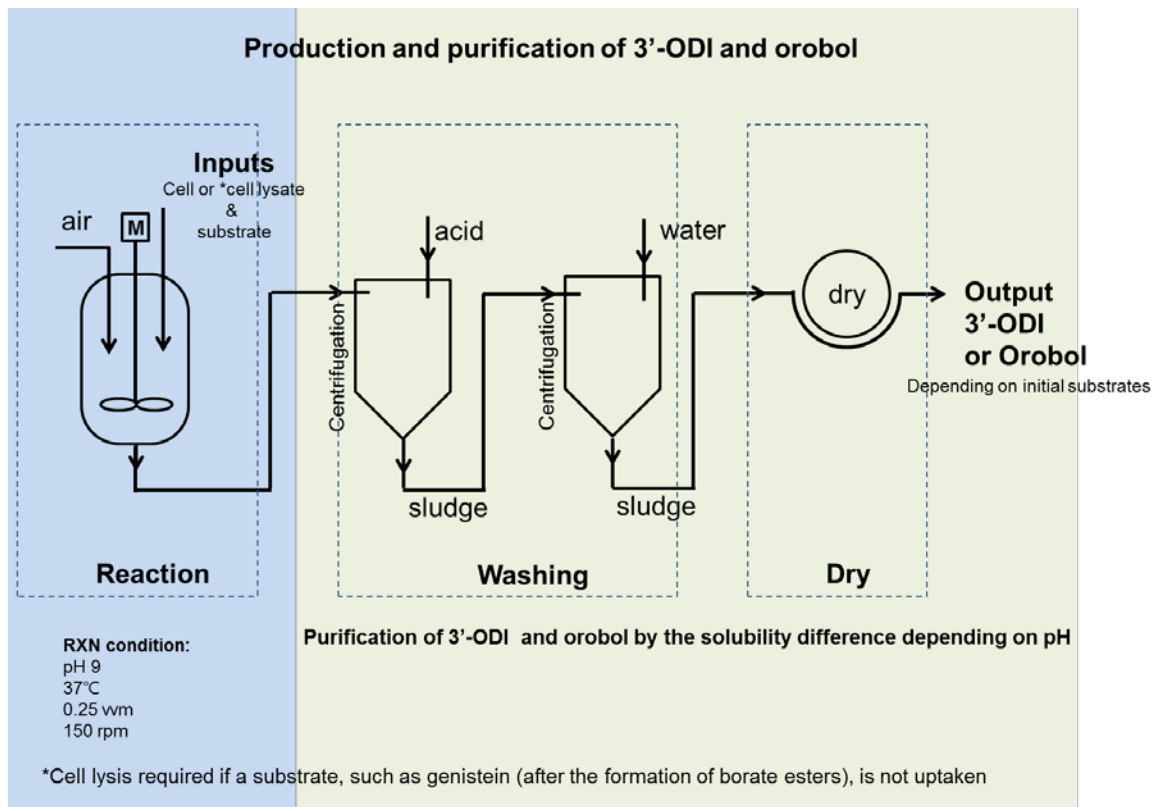


Figure 3.36. The process optimized for the production and purification of 3'-ODI and Orobol from daidzein and genistein, respectively.

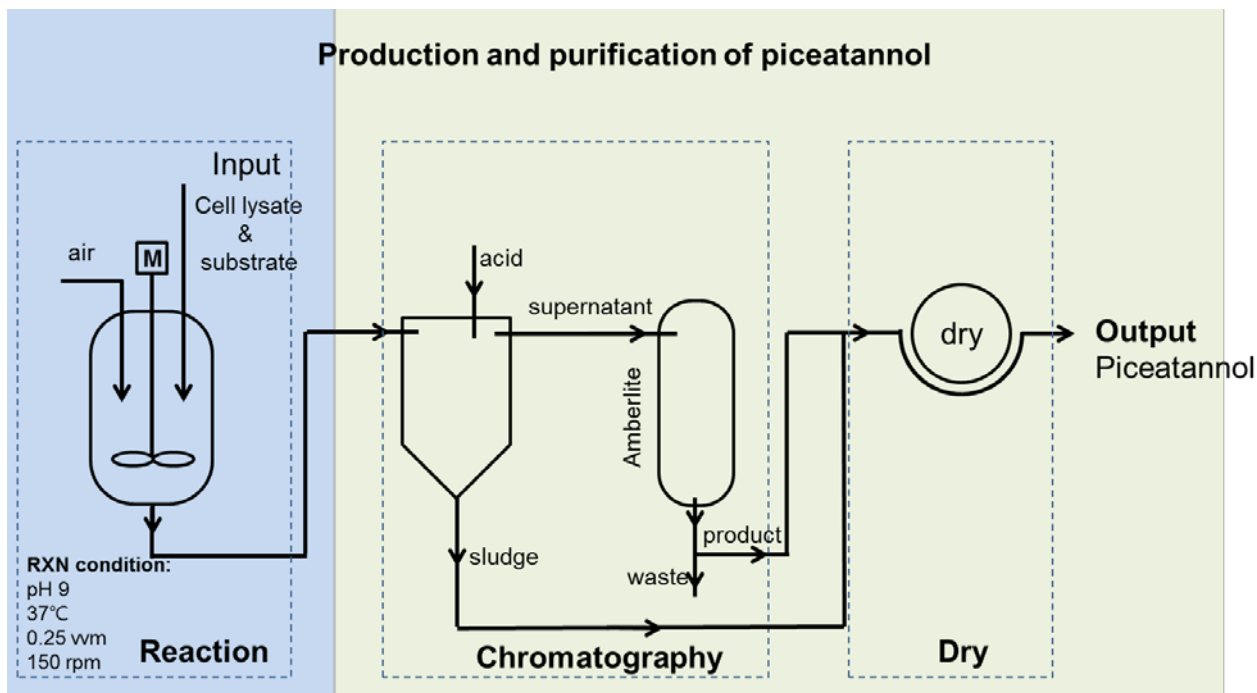


Figure 3.37. The process optimized for the production and purification of piceatannol from resveratrol.

3.5 Conclusion

The yield and productivity for 3'-ODI production was remarkably high when compared to any other *o*-hydroxylating enzymes for the B ring of isoflavonoids in the published literatures. The 100 % conversion yield of the Ty reaction at 5 mM was successfully achieved by 1) the efficient equilibrium shift of *o*-diphenolic products by the borate ester complex formation, 2) the successful completion of Ty enzyme recycling using LAA, 3) the prevention of further oxidation of *o*-diphenols to *o*-quinones using an appropriate reducing agent, and 4) the sufficient supply of oxygen.

The first critical issue in the optimization was continuous removal of the *o*-hydroxylated product from the reaction system using the optimum borate buffer to prevent further oxidations. For optimization of the reducing agents, since the reducing agents can function not only as a reagent for recycling Ty but also as an inhibitor for further oxidation, detailed understanding of the reaction mechanism is a key determinant. Moreover, the reducing agent can back-titrate *o*-quinones into *o*-diphenolic products to minimize melanin byproduct formation. Therefore, selection of the correct reducing agent is another critical issue. Although not detailed herein, reduction of the Cu²⁺ ions is an important inactivation path of Ty (Muñoz-Muñoz et al., 2010). However, such inactivation of Ty was not observed in this study.

The selectivity of the monophenolase activity over the catecholase activity of Ty was increased and the melanin formation was abolished by accurately determining the Ty reaction mechanism and optimizing the *o*-hydroxylation of monophenols. In conclusion, these results support the strong potential of tyrosinase as a monooxygenase for regio-selective *o*-hydroxylation of various monophenolis.

Chapter 4.

A novel tyrosinase from *Burkholderia thailandensis* active only at acidic pH and its application for the *ortho*-hydroxylation of monophenolic phytochemicals

4.1 Abstract

For the first time, we found that there is tyrosinase, herein, tyrosinase from *Burkholderia thailandensis*, only active at acidic pH (in the range of pH 2 to 6), yet, showed the highest catalytic efficiency ($k_{\text{cat}}/K_{\text{m}}$); 668.63 $\text{mM}\cdot\text{s}^{-1}$ to L-tyrosine, and 586.74 $\text{mM}\cdot\text{s}^{-1}$ to L-3,4-dihydroxyphenylalanine (L-DOPA) at pH 5. Interestingly, the activity was completely inactivated above pH 6. The activity of tyrosinase at acidic condition is unique since the rate-limiting step of the reaction is the deprotonation of phenolic substrates, which is more favor at neutral-to-basic pH above the pKa of monophenols. In this paper, the novel tyrosinase from *B. thailandensis* was heterologously expressed in *Escherichia coli* BL21 (DE3) and was characterized. Furthermore, we demonstrated a high potential of this enzyme for the regio-selective *ortho*-hydroxylation of monophenolic substrates to produce catechol derivatives because not only the catalytic efficiency is the highest among Tys reported so far but also the auto-oxidation of catechols by dissolved oxygen in aqueous solution could be successfully suppressed in acidic pH of 5, the optimal reaction pH of this tyrosinase from *B. thailandensis*.

Keywords: *ortho*-hydroxylation, monophenol glycosides, tyrosinase

4.2 Introduction

Tyrosinase (Ty) is one of the type III copper containing polyphenol oxidases (PPOs) that catalyzes the two-step consecutive oxidation reactions; *o*-hydroxylation of monophenols to catechols, phenolase activity (k_1), and the subsequent dehydrogenation of catechols to *o*-quinones, catecholase activity (k_2) (Goldfeder, Kanteev et al. 2013, Kanteev, Goldfeder et al. 2015). The *o*-quinone produced by Ty is unstable. Thus the non-enzymatic polymerization of *o*-quinones leading to melanin formation occurs spontaneously in the most living organisms from bacteria to humans (Kanteev, Goldfeder et al. 2015). A distinctive feature of type III copper proteins is the two copper ions ligated by six π -histidines at the active site (Ty_{deoxy}), which form (μ - η^2 : η^2 -peroxo)-dicopper(II) complex with one oxygen molecule (Ty_{oxy}) (Yoon, Fujii et al. 2009, Chiang, Keown et al. 2016, Hamann, Herzigkeit et al. 2017).

The nucleophilic attack by the hydroxyl group of the phenolic substrate on a copper ion in Ty_{oxy} initiates Ty reaction by transferring a proton from the hydroxyl group of the substrate to the peroxide group of Ty_{oxy} . And this deprotonation step of the substrate is known as the rate-limiting step of the Ty reaction (Peñalver, Rodríguez-López et al. 2003, Fenoll, Peñalver et al. 2004, Muñoz-Muñoz, Berna et al. 2012). The side-on μ - η^2 : η^2 -peroxo-bridged Cu_2O_2 of Ty_{oxy} is crucial for the both oxidations of monophenols and catechols. However, not all of the type III copper proteins, such as catechol oxidase (Cox) (Decker and Tuczec 2000, Molitor, Mauracher et al. 2016, Solem, Tuczec et al. 2016), aurone synthase (Aus) (Molitor, Mauracher et al. 2016) and hemocyanin (Hc) (Zlateva, Di Muro et al. 1996, Decker and Rimke 1998, Salvato, Santamaria et al. 1998), can

catalyze the polyphenol oxidation like Ty because of diverse neighboring residues in the active site for controlling biological events precisely (Decker and Tuczec 2000, Yoon, Fujii et al. 2009).

The regio-selective phenolase activity is one of the merits of Ty in terms of the synthesis of functional catechol-like compounds used as the pharmaceuticals and antioxidants (Goldfeder, Kanteev et al. 2014, Lee, Lee et al. 2015, Lee, Baek et al. 2016). Previous studies on the mutagenesis of bacterial Tys to increase k_1/k_2 ratio for achieving higher yield of catechols (Shuster Ben-Yosef, Sendovski et al. 2010, Goldfeder, Kanteev et al. 2013, Lee, Lee et al. 2015), and on screening optimum reducing agents to back reduce the *o*-quinones to catechols (Ros, Rodríguez-López et al. 1993, Villarama and Maibach 2005, Garcia-Molina, Munoz-Munoz et al. 2010) suggested them as suitable alternative methods of improving the yields of catechol productions. However, such approaches are somewhat limited to the improvement of the yields because the mutagenesis of Tys for increment of k_1/k_2 ratio usually resulted in diminishing enzyme activity, and the oxidation of target catechols to *o*-quinones is inevitable for a completion of Ty reaction cycle (Shuster Ben-Yosef, Sendovski et al. 2010, Goldfeder, Kanteev et al. 2013, Lee, Lee et al. 2015). Especially, the fast auto-oxidation rate of catechols by dissolved oxygen at neutral-to-basic pH abates the effectiveness of reducing agents, resulting in lower product yield (Lee, Dellatore et al. 2007, Shuster Ben-Yosef, Sendovski et al. 2010, Goldfeder, Kanteev et al. 2013). And increasing the concentration of reducing agents, such as L-ascorbic acid, could lower the pH of the reaction solution, which also negatively affects the Ty activity. One effective method for the prevention of the auto-oxidation of catechols was the introduction

of boric acid into the reaction mixture (Lee, Baek et al. 2016). By forming borate ester bonds of catechols and boric acids, the product, catechols, could be successfully protected from the auto-oxidation (Lee, Baek et al. 2016). But still, the equilibrium constant of the formation of complex is low, less than 10^{-2} M^{-2} (Lee, Baek et al. 2016), and this protection strategy is not appropriate if the separation of the excessive amount of boric acids from products is problematic.

For example, in the case of the *o*-hydroxylation of monophenol glycosides, which are more abundant and stable than aglycones in nature (Mabry, Markham et al. 1970, Le, Jang et al. 2017), such strategy of using borate buffer cannot be applicable. The hydroxyl groups of sugars in glycosides firmly hold the boric acids to form massive structures via borate monoester and diester that could disturb the substrate specificity of enzymes (Brigid Pappin 2012). Also, the borate ester bonds can be completely cleaved only at strong acidic conditions where the acid hydrolysis of glycosides may occur (Mabry, Markham et al. 1970, Brigid Pappin 2012). Therefore, screening or designing a highly active and efficient Ty with a high k_1/k_2 ratio at mild acidic condition (where the auto-oxidation is prevented) is a desirable strategy for increasing the yield of catechol productions.

Burkholderia thailandensis is a Gram-negative soil bacterium, closely related to *Burkholderia pseudomallei*, a pathogen causing melioidosis in mammalian (Haraga, West et al. 2008, Jitprasutwit, Thaewpia et al. 2010). *B. thailandensis* appears to be avirulent but the type III secretion system, a toxic delivery mechanism of infectious bacteria, could be activated specifically under acidic condition. It was reported that its secretion system could be triggered at pH 4.5 and consequently resulted in infection of human respiratory epithelial cells

(Jitprasutwit, Thaewpia et al. 2010). A gene of tyrosinase (WP_011400974), melO, was identified as the genomic sequence of *Burkholderia thailandensis* E264 was analyzed (Kim, Schell et al. 2005). The protein similarity/identity matrix obtained by pairwise sequence alignment and the cladogram of bacterial Tys show that the Ty from *B. thailandensis* (BT_Ty) has been evolved quite far from other bacterial Tys regarding the protein sequences (Figure E1). BT_Ty shows 50% sequence similarity and 39% identity with a fungal Ty from *Aspergillus oryzae* RIB40 (AO_Ty, XP_001820973.1) (Figure E1).

In this study, BT_Ty was heterologously expressed in *E. coli* and was characterized. Furthermore, we demonstrated a great potential of this enzyme for the regio-selective *ortho*-hydroxylation of monophenolic substrates to produce catechol derivatives because not only the catalytic efficiency is the highest among Tys reported so far but also the auto-oxidation of catehols by dissolved oxygen in aqueous solution could be successfully suppressed in acidic pH of 5, the optimal reaction pH of this tyrosinase,

4.3 Materials and Methods

4.3.1 Materials

Restriction enzymes and the T4 DNA ligase were from Thermo Scientific (Seoulin Bioscience Co LTD, Seongnam, Korea). DNA polymerase (Herculase II fusion DNA polymerase) was purchased from Agilent Technologies (Omicstech, Daejeon, Korea), and reagents for the genetic engineering were purchased from Invitrogen Life Technology (Seoul, Korea). All phytochemicals used in this study were purchased from Chengdu Biopurify Phytochemicals LTD (Sichuan, China). All other reagents were purchased from Sigma-Aldrich (Yongin, Korea). Tyrosinase from *Agaricus bisporus* (AB) was used as purchased from Sigma-Aldrich (Yongin, Korea, Catalog Number: T3824). *Bacillus megaterium* (ATCC 10778) and *Streptomyces avermitilis* MA4680 (ATCC 31267) were purchased from the Korean Culture Center of Microorganisms (KCCM, Seoul, Korea). *Burkholderia thailandensis* E264 (ATCC700388) was purchased from Korean Collection for Type Cultures (KCTC, Daejeon, Korea)

4.3.2 Construction of a cladogram of bacterial Tys.

A fasta file that contains all bacterial tyrosinases submitted to NCBI Reference Sequence Database (RefSeq) were downloaded from the website of National Center for Biotechnology Information (NCBI). A total of 2679 sequences was retrieved at 18th Jun 2016 by searching contents and title that contain tyrosinase

excluding a keyword, helper protein. The size of the list was reduced by CD-HIT Suit by excluding sequences that have over 90% sequence identity (Huang, Niu et al. 2010). The sequences with many gaps were removed from the list by MaxAlign 1.1 Server (Gouveia-Oliveira, Sackett et al. 2007). Alignment and phylogenetic analysis of the sequences were performed with Molecular Evolutionary Genetics Analysis (MEGA 7) (Kumar, Stecher et al. 2016). The sequences were aligned by Multiple Sequence Comparison by Log-Expectation (MUSCLE)(Edgar 2004), and the tree was drawn by maximum likelihood method based on the alignment, bootstrapping 50 times. The Newick file obtained from MEGA 7 was uploaded on Interactive Tree of Life (iTOL) for visualizing the tree (Figure 4.1) (Letunic and Bork 2016).

4.3.3 Plasmid construction

The plasmid for the recombinant tyrosinases from *B. megaterium* and *S. avermitilis* were used as previously reported (Lee, Baek et al. 2016). The plasmid for the recombinant tyrosinase from *Burkholderia thailandensis* was constructed as below. Genomic DNA was extracted from *B. thailandensis* with G-spin genomic DNA extract kit (Intron, Korea), and PCR was performed to amplify the gene of tyrosinase of *B. thailandensis*. The primers used is listed in Table 4.1. The amplified gene was digested with NcoI and HindIII and inserted into the multiple cloning sites of pET28a (Novagen, USA).

Table 4.1. The primer list for cloning tyrosinase from *Burkholderia thailandensis*

	Primer sequence (5' → 3')	Restriction enzyme site
Forward	AAAAAACCATGGGTTCCAACGTCAATGCAC	NcoI
Reverse	TTTTTAAGCTTGTCGCTCACCTCGAACTTC	HindIII

4.3.4 Expression and purification of tyrosinases

The recombinant tyrosinases from *B. megaterium* and *S. avermitilis* were expressed and purified as previously reported (Lee, Baek et al. 2016). The plasmid constructed was transformed into *E coli* BL21 (DDE3) by heat shock, and the transformed strain was selected on the Luria-Bertani (LB) agar plate with 50 µg·ml⁻¹ kanamycin. A single colony on the plate was inoculated into 5 mL of fresh LB with kanamycin. The single colony was cultured in 37 °C incubator for overnight, and 0.5 mL of the cell culture was scaled up into a 250 mL flask with 50 mL of fresh LB with kanamycin. When OD at 600 nm of the cell cultures reached approximately 0.6 at 37 °C incubator, the final concentration of 0.2 mM IPTG and 1 mM CuSO₄ were added in the culture media. The cells were continuously cultured in an incubator at 18 °C at 200 rpm for 20 hrs. The enzyme was insoluble expressed when cultivating at 37 °C after induction (Figure E10). If necessary, the expressed enzymes were Histag-purified. The concentration of purified enzymes was obtained by Bradford assay (Zor and Selinger 1996).

4.3.5 Purification of tyrosinase from *Agaricus bisporus*, mushroom tyrosinase

The lyophilized mushroom tyrosinase (AB_Ty) was purchased from Sigma-Aldrich (T3824-25KU). The purification of AB_Ty from the lyophilized powder was followed as previously reported with mild modifications (Duckworth and Coleman 1970). First, the 9.3 mg of the lyophilized powder was dissolved in 5 mL of 50 mM

sodium phosphate buffer at pH 7. 1.08 g of solid ammonium sulfate was added, and continuously stirred in an ice-cold bath. The precipitate was removed and additionally, 0.42g of ammonium sulfate was added. After centrifuging at 16000 rpm for 30 min, the precipitate was resuspended in 50 mM sodium phosphate buffer at pH 7. The solution was decolorized by calcium phosphate gel (Bio-Gel, Bio-Rad). Then, the decolorized solution was fractionated by AKTA FPLC (UPC-900; P-920; Frac-920, GE Healthcare) with size exclusion column (Hiload 16/60 Superdex 200). The fraction with tyrosinase activity (the 17th to the 20th) was fractionated again with ion exchange column (Mono Q GL 5/50) separately. The condition for the elution buffer of the first size exclusion chromatography was 300 mM of KCl in 10 mM sodium phosphate buffer at pH 7, and the flow rate was 1 mL·min⁻¹. Total 40 fractions, 5 mL each, were collected. The column was eluted with a linear gradient of 50 mM NaCl to 300 mM NaCl. The flow rate was maintained at 0.5 mL·min⁻¹. Total 22 fractions, 2 mL each, were collected. The 8th to 10th fractions showed the activities on L-tyrosine. The total of 6 mL fraction was concentrated to approximately 500 µL by the centrifugal filter with a cut-off size of 10 kDa (Amicon Ultra -15). The final concentration of the purified AB_Ty was 3.1 µM.

4.3.6 Measurement of tyrosinase activities

The kinetic values were measured by UV spectroscopy (SPECTROstar Nano, BMG LABTECH, Ortenberg, Germany). The initial rate (V_0) was determined by measuring the concentration of dopachrome at 475 nm ($\epsilon_{\text{dopachrome}} = 3600 \text{ M}^{-1} \cdot \text{cm}^{-1}$)

(Deri, Kanteev et al. 2016) at 37 °C. The reaction was held in 96-well microplate which final volume was 200 µL. The range of initial substrate (L-tyrosinase and L-dopa) was 100 µM to 1 mM, and the concentration of the Histag-purified enzyme was fixed at 100 nM. The kinetic values were obtained by regression wizard of SigmaPlot 10.0 based on the triplet set of measurements.

4.3.7 *ortho*-Hydroxylation of monophenol glycosides

The total reaction volume was set to 50 mL, and the initial substrate (monophenol glycosides) concentration was all fixed at 1 mM. The total of 100 nM BT_Ty was used in 50 mM sodium citrate buffer at pH 5. The final concentration of 2 mM L-ascorbic acid was added in the reaction for the completion of tyrosinase cycle. The additional CuSO₄ was unnecessary. After the reaction, the enzyme was inactivated by adding 20% of pure ethanol and 20% of 1 M HCl in the reaction. Before the chromatography (HPLC and LC/MS), the samples were all filtered by centrifugal filter (Amicon Ultra Centrifugal Filters, Ultracel-10K, 10,000 MWCO, Millipore)

4.3.8 HPLC and LC/MS analysis

The HPLC analysis was performed on CMB-20A (Shimadzu, Seoul, Korea) connected with a UV/Vis detector (SPD-20A) and a C18 column (SunFire™ C18, 5 µm, 4.6 x 150 mm) was used. The mobile phase A was water containing 0.1% trifluoroacetic acid, and the mobile phase B was acetonitrile. The flow rate was

fixed at $1 \text{ mL}\cdot\text{min}^{-1}$, and the concentration of mobile phase B was gradually increased from 10 % to 50% for 10 min. The detection wavelengths were 254 nm for glycitin, 258 nm for daidzin, 262nm for genistin, 320 nm for polydatin, and 320 nm for phlorizin. The same analytic conditions were applied for LC/MS except for the total flow rate and the type of C18 column. The flow rate for LC/MS was set to $400 \text{ }\mu\text{L}\cdot\text{min}^{-1}$, and Unison UK-C18 column (Imtakt USA. $3\mu\text{m}$, $3 \text{ mm} \times 75 \text{ mm}$) was used for the separation. Triple-quadrupole LC/MS (TSQ TSQ QuantumTM Access MAX Triple Quadrupole Mass Spectrometer, ThermoFisher Scientific) was used for the mass analysis of substrates and products. The vaporizer temperature was set to 300°C , and the spray voltage was set to 3.8 kV.

4.4 Result and Discussion

4.4.1 Reactivity depending on pH and measurements of kinetic parameters.

Although the biological role of BT_Ty is unknown, interestingly, the heterologously expressed BT_Ty in *Escherichia coli* BL21 (DE3) was found to be functional only in acidic condition, a pH range of 3 to 6 (Figure 4.2). The optimal pH of BT_Ty on L-tyrosine was pH 5, and the enzymatic activity of BT_Ty was completely disabled above pH 6 (Figure 4.2-b). Tys from other organisms show the catalytic activities over the broad range of pH (Figure 4.2) and usually the optimal pH of the most Tys is neutral-to-basic where the auto-oxidation of catechols are unavoidable (Zaidi, Ali et al. 2014).

BT_Ty showed the highest specific activity on both L-tyrosine, and L-3,4-dihydroxyphenylalanine (L-DOPA), as well as the high ratio of V_{\max_k1}/V_{\max_k2} (k_1/k_2), compared to the well-studied Tys, such as Ty from *Agaricus bisporus* (AB_Ty), from *Bacillus megaterium* (BM_Ty), and from *Streptomyces avermitilis* (SA_Ty) (

Table 4.2). While the k_1/k_2 ratios of other Tys are less than 0.5, the ratio of BT_Ty was 0.82, which is similar to the best mutant, specifically engineered BM_Ty (V218F) for the catechol production (Goldfeder, Kanteev et al. 2013). The high k_1/k_2 ratio with the high V_{\max} at acidic pH suggests better stabilization of catechols, herein, L-DOPA, by repression of non-enzymatic auto-oxidation of catechols. Moreover, the high Ty activity of BT_Ty, specifically k_1 , at acidic

conditions are abnormal since the late determining step of Ty reaction is the deprotonation of monophenols during the nucleophilic attack of k_1 , which is more favorable at basic pH (Espin, Varon et al. 2000, Muñoz-Muñoz, Berna et al. 2012). The Michaelis constant, K_m , of BT_Ty, was 0.59 ± 0.055 mM for L-tyrosine, and 0.83 ± 0.13 mM for L-DOPA, that is somewhat similar to the values obtained from other Tys; however, the turnover numbers, k_{cat} , of BT_ty are significantly higher than other Tys. The turnover number on L-DOPA was 487.17 s^{-1} , 4.5 times faster than of AB_Ty and more than 10 times faster than that of SA_Ty and BM_Ty. The turnover number on L-tyrosine was 397.50 s^{-1} , more than 50 times greater than other Tys. The catalytic efficiencies of BT_Ty, k_{cat}/K_m , were $668.63 \text{ mM}^{-1} \cdot \text{s}^{-1}$ for L-tyrosine, and $586.74 \text{ mM}^{-1} \cdot \text{s}^{-1}$ for L-DOPA (Table 4.2), suggesting that BT_Ty could be a proper candidate to produce catechols with high productivity and yield.

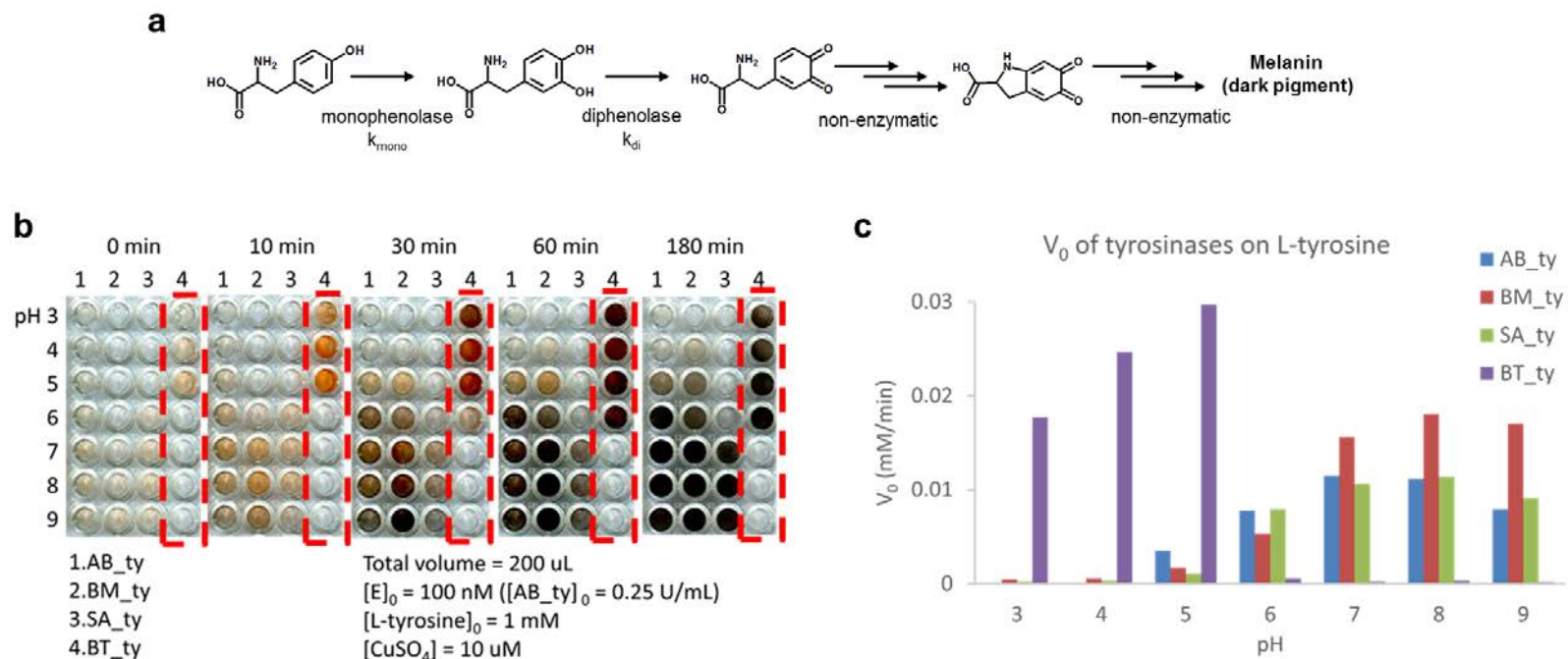


Figure 4.2. The optimal pH of Ty reaction.

(a) The general tyrosinase reaction for producing dark pigment, melanin (b) 1. Ty from *Agaricus bisporus* (AB_Ty); 2. Ty from *Bacillus megaterium* (BM_Ty); 3. Ty from *Streptomyces avermitilis* (SA_Ty); 4. Ty from *Burkholderia thailandensis* (BT_Ty). Melanin production of Tys depending on pH. The color changes (melanin production) were more evident with basicity except for BT_Ty. BT_Ty showed better activity for melanin production at acidic condition and the activity was completely disappeared when it was neutral to basic. (c) The initial oxidation rate of Tys from various organisms depending on pH. The initial rate of BT_Ty was the highest at pH 5 and dramatically decreased above the pH.

Table 4.2. Kinetic parameters of Tys

	M.W. (kDa)	substrate	V_{max} ($\mu\text{mol}\cdot\text{min}^{-1}\cdot\text{mg}^{-1}$)	K_m (mM)	k_{cat} (s^{-1})	k_{cat}/K_m ($\text{mM}\cdot\text{s}^{-1}$)	$V_{max_k1}/$ V_{max_k2}	$(k_{cat}/K_m)_{k1}/$ $(k_{cat}/K_m)_{k2}$
AB_Ty (Fenoll, Rodríguez-López et al. 2001)	44	L-tyrosine	10.8	0.25 ± 0.03	7.9 ± 0.12	31.60	0.074	0.082
		L-Dopa	145.9	0.28 ± 0.01	107.3 ± 1.45	383.21		
BM_Ty (Deri, Kanteev et al. 2016)	34	L-tyrosine	3.62 ± 0.06	0.082 ± 0.006	2.1	25.60	0.12	0.35
		L-Dopa	30.3 ± 0.6	0.24 ± 0.02	17.8	74.20		
BM_Ty mutants (V218F) (Goldfeder, Kanteev et al. 2014)	34	L-tyrosine	28.4 ± 0.7	1.4 ± 0.1	16.7	11.90	0.80	0.62
		L-Dopa	35.7 ± 7.3	1.1 ± 0.3	21	19.10		
SA_Ty (Lee, Lee et al. 2015)	33	L-tyrosine	1.05 ± 0.037	0.589 ± 0.056	0.021	0.04	0.11	0.51
		L-Dopa	9.67 ± 1.85	2.79 ± 0.79	0.19	0.07		
BT_Ty	59	L-tyrosine	404.24 ± 18.88	0.59 ± 0.055	397.5	668.63	0.82	1.14
		L-Dopa	495.42 ± 44.66	0.83 ± 0.13	487.17	586.74		

4.4.2 *ortho*-Hydroxylation of monophenol phyrochemicals by BT_Ty.

4.4.2.1 *ortho*-Hydroxylation of monophenol glycosides

The *ortho*-hydroxylation of isoflavone aglycones by BM_Ty was previously studied in our group (Lee, Baek et al. 2016) In the presence of both L-ascorbic acid and boric acid, the *ortho*-hydroxylation of resveratrol, genistein, and daidzein was successfully achieved with over 90 % conversion yield. However, such process is not appropriate for the hydroxylation of monophenol glycosides because the borate ester bonds are not easily detached from the *cis*-diols of sugar, and the strong acid hydrolysis for breaking the borate ester bonds may cause the acid hydrolysis of glycoside as well. The boric acid was not easily separated from daidzin even after the addition of 1 M HCl, and daidzin was significantly degraded when the total of 2 M HCl was added (Figure 4.3).

Besides, the substrate specificity of Ty for the glycosylated monophenols varies greatly among Tys. For instance, the MBTH (3-Methyl-2-benzothiazolinone hydrazone) color assay for measuring the oxidation rate of monophenols indicated that BM_Ty is the best Ty for the oxidation of daidzein, genistein, resveratrol, phloretin, naringenin, kaempferol, and quercetin which are all aglycones (Figure 4.4, Figure 4.10). However, the reactivity of BM_Ty on glycosides such as daidzin, glycitin, polydatin and phlorizin are much lower than that of BT_Ty (Figure 4.4). The hydroxylation of 1 mM of the four glycosides (daidzin, glycitin, polydatin and phlorizin) at acidic pH was successfully performed in an hour with >80% conversion yield (Figure 4.5). For instance, the total of 780 μ M astringin was

produced from 1 mM of polydatin in 10 min by 100 nM of BT_Ty in 50 mM sodium citrate buffer at pH 5 (the total reaction volume was 50 mL), and this is more than 10 times higher conversion yield than of the P450 BM3 (CYP102A1) mutants recently reported (Le, Jang et al. 2017). The hydroxylated products were analyzed by LC/MS, and the mass data confirmed the addition of one hydroxyl group (+16 m/z) to the initial substrates (Figure 4.6-Figure 4.9).

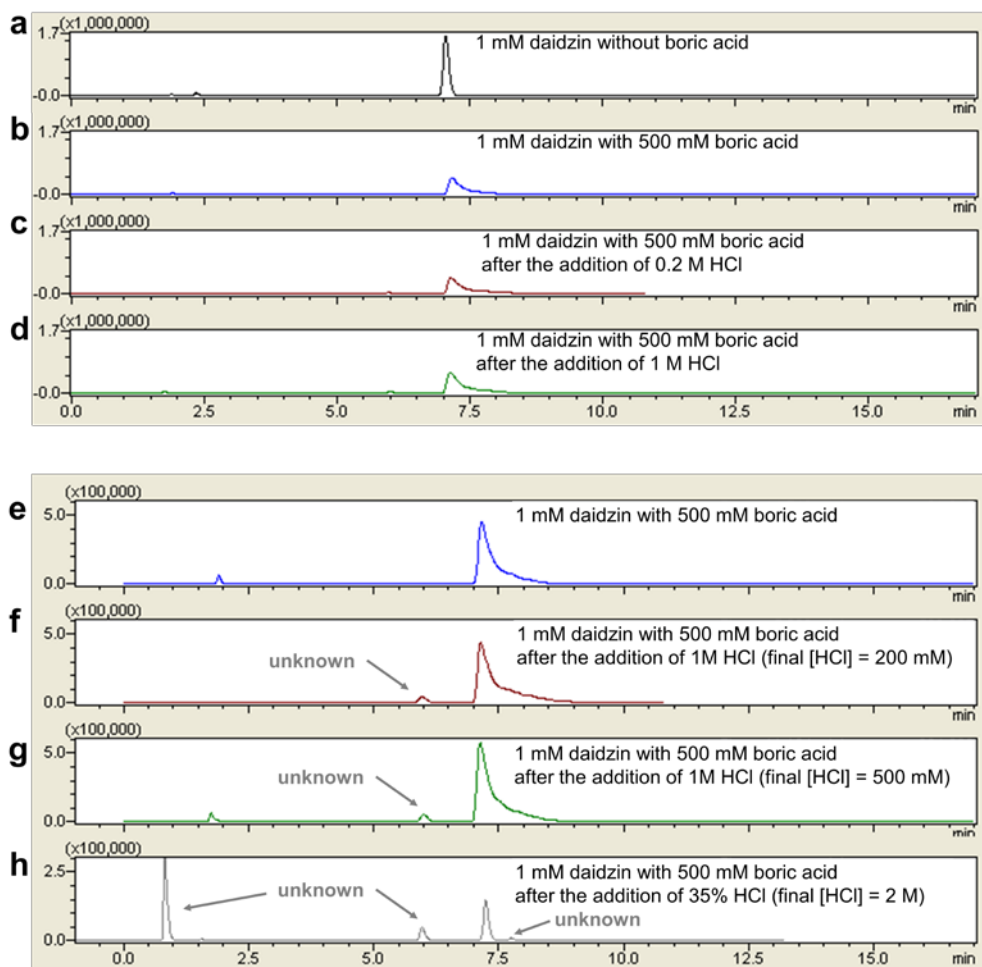


Figure 4.3. HPLC data of 1 mM daidzin in the presence of boric acid.

The final concentration of 100 μ M of daidzin was first dissolved in DMSO, and it was diluted in water or 500 mM boric acid before injection. (a) Raw data of chromatography of 1 mM daidzin. (b) Raw data of chromatography of 1 mM daidzin with 500 mM boric acid. (c) The addition of a total of 0.2 M HCl in the 1 mM daidzin solution with 500 mM boric acid was not enough to separate boric acid from daidzin. (d) Even after the addition of 1 M HCl, the daidzin was not separated from boric acid. The image labeled with (e), (f), and (g) are enlarged

images (b), (c), and (d). (h) After the addition of the final concentration of 2 M HCl in the 1 mM daidzin with 500 mM boric acid, unknown peaks were detected and the peak corresponding to daidzin fell off.

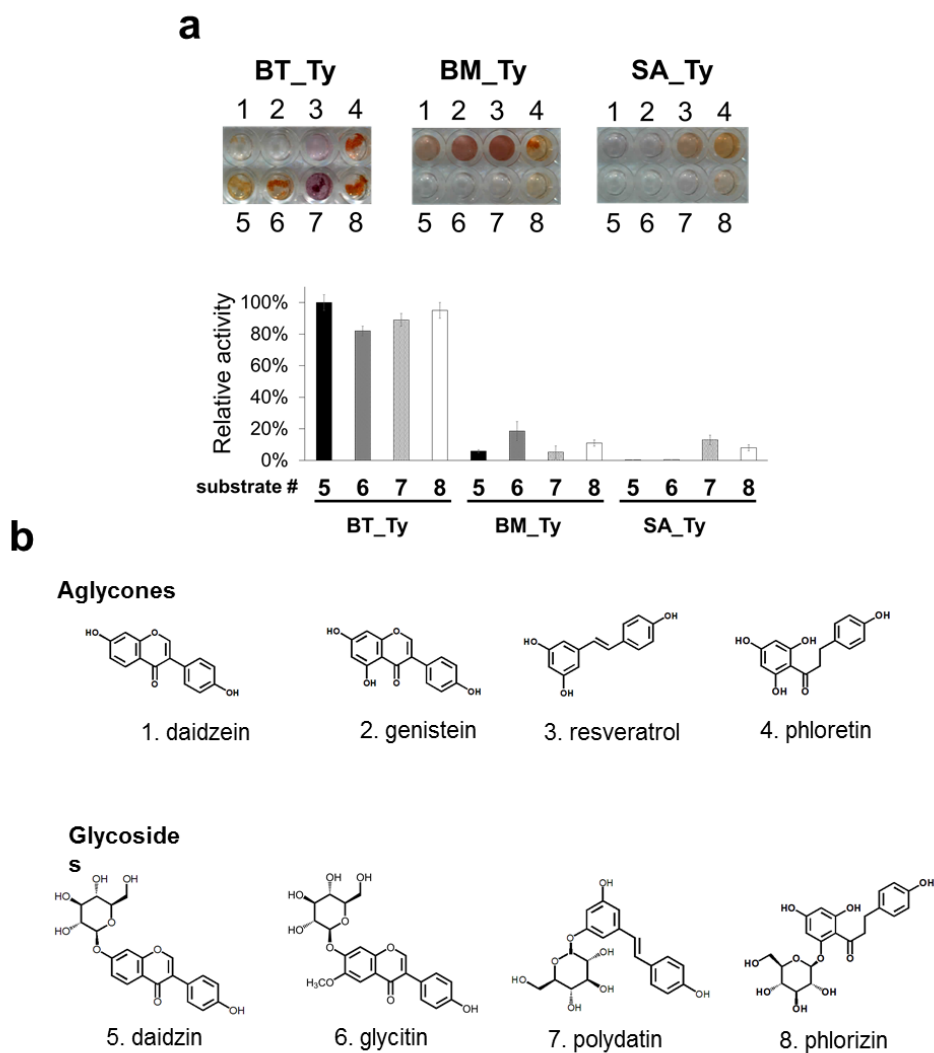


Figure 4.4. The substrate specificity of tyrosinase from different organisms.

(a) BT_Ty shows activities specifically to monophenols glycosides which is opposite to BM_Ty. Despite of similar chemical structure, the presence of one sugar moiety makes huge difference. (b) The chemical structures of monophenols used in this experiment.

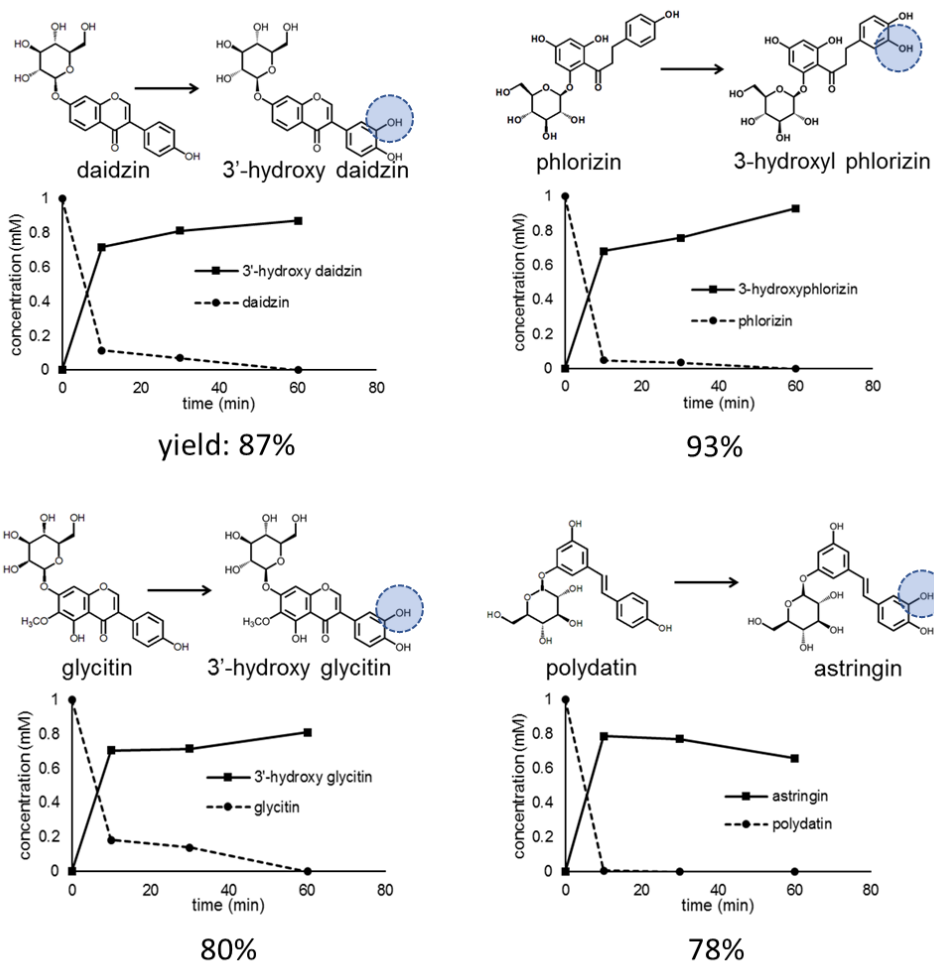


Figure 4.5. The reaction profiles of *ortho*-hydroxylation of monophenol glycosides.

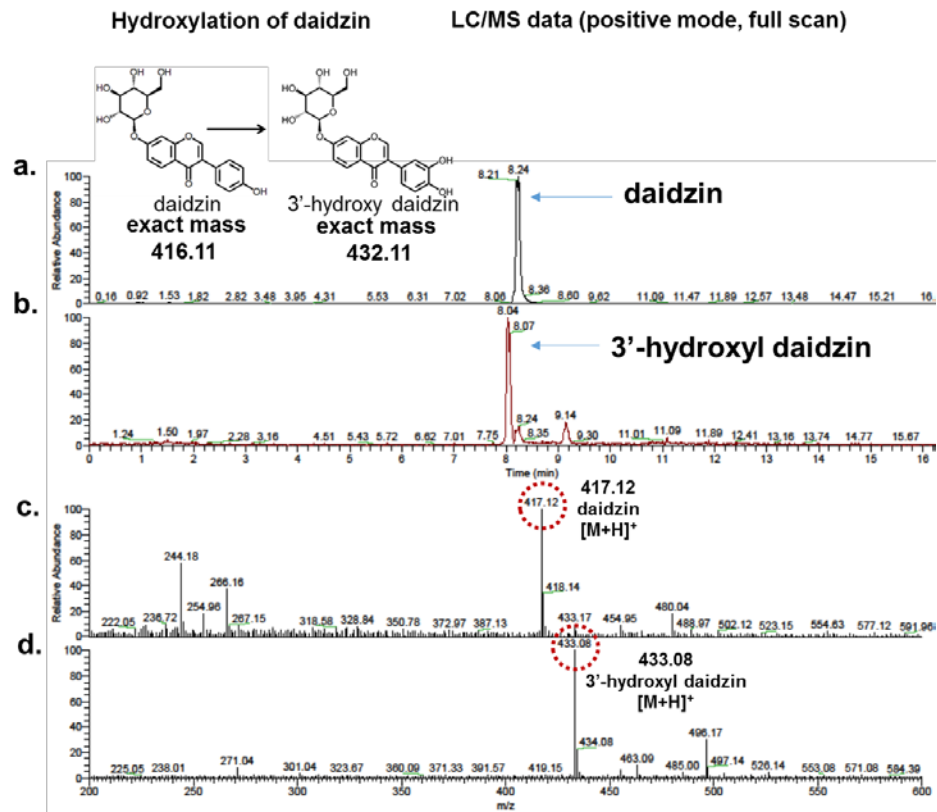


Figure 4.6. LC/MS data of the initial substrate, daidzin, and the hydroxylated product, 3'-hydroxy daidzin.

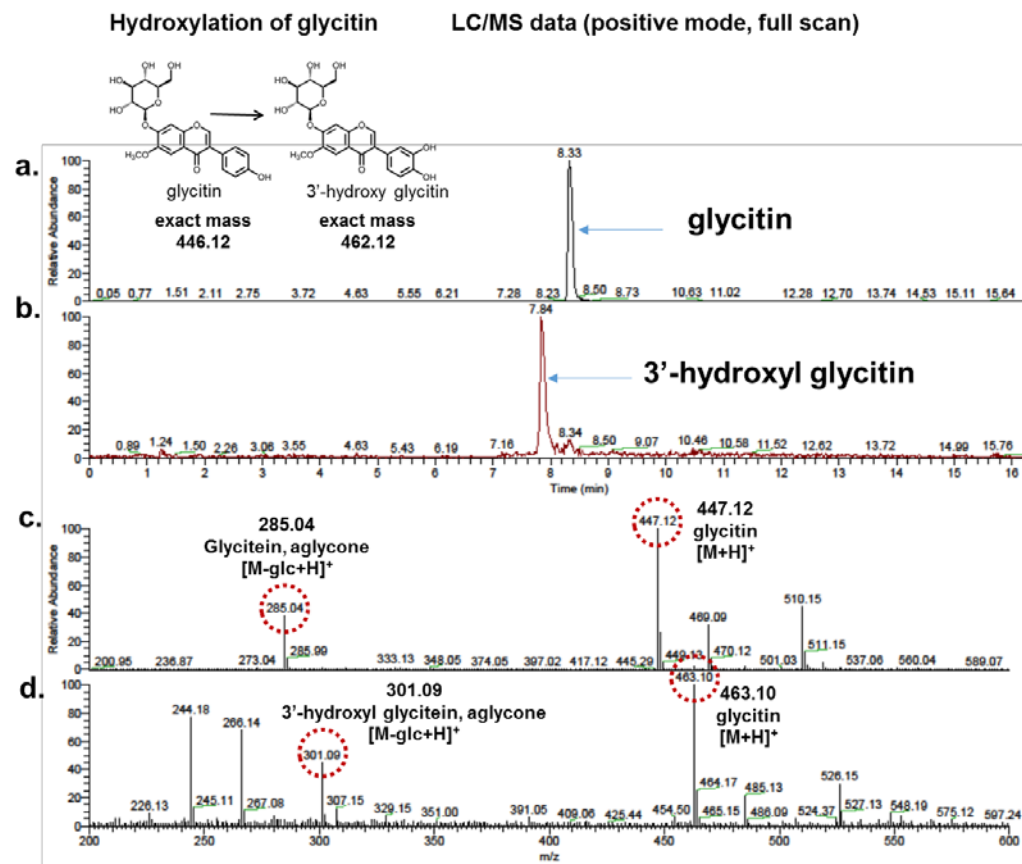


Figure 4.7. LC/MS data of the initial substrate, glycitin, and the hydroxylated product, 3'-hydroxy glycitin.

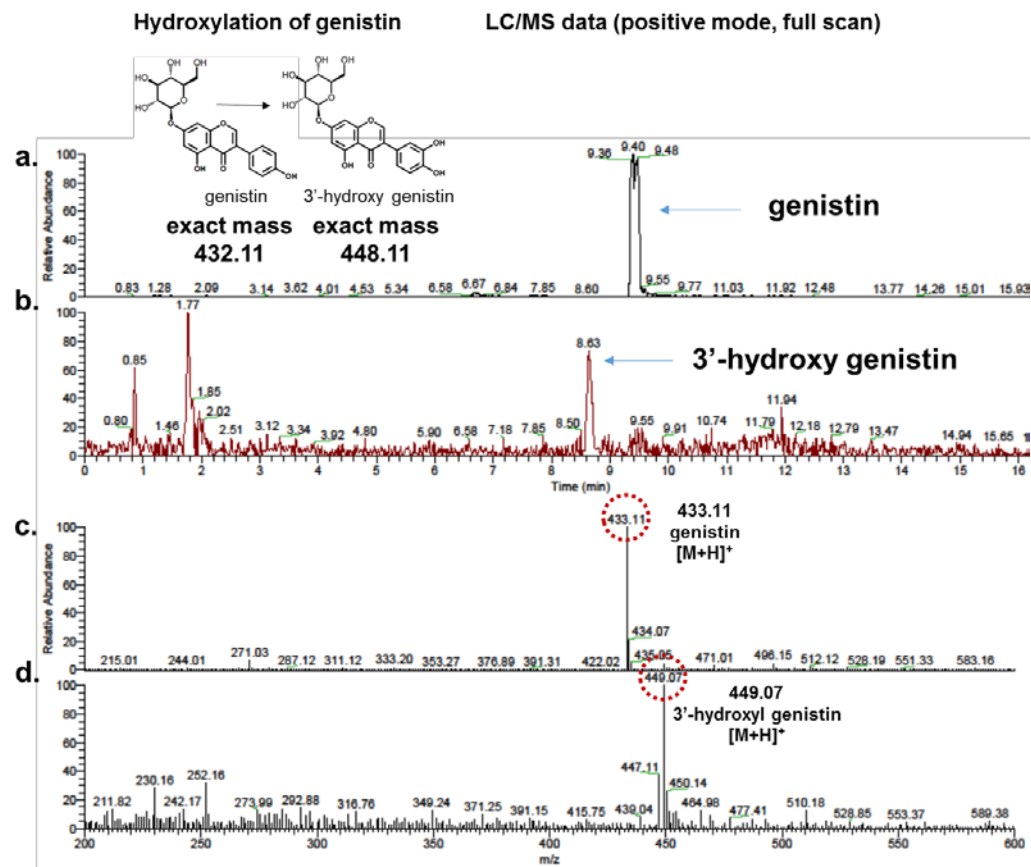


Figure 4.8. LC/MS data of the initial substrate, genistin, and the hydroxylated product, 3'-hydroxy genistin.

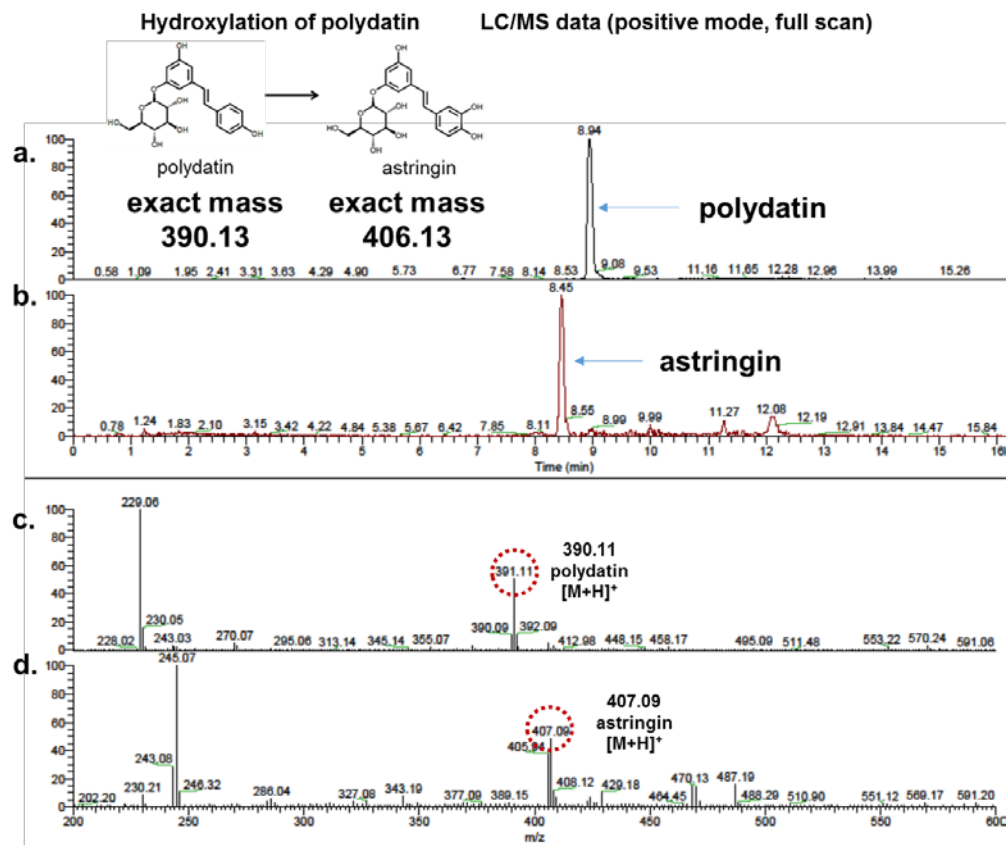


Figure 4.9. LC/MS data of the initial substrate, polydatin, and the hydroxylated product, astringin.

4.4.2.2 *ortho*-Hydroxylation of monophenol aglycones

The substrate specificity of BT_Ty seems narrow but the narrow substrate specificity is not due to the size of the tunnel to the active site. The glycosides are much bigger than aglycones but BT_Ty can take glycosides as substrate as shown in the previous section and Figure 4.4. For example, despite of structural similarity of daidzein and daidzin, the tendency of oxidation by BT_Ty were completely different. Notably, BT_Ty have activity with monophenols that have more flexibility such as resveratrol and phloretin. It seems that BT_Ty also has activity on naringenin as shown in Figure 4.10; however, the hydroxylated product was not detected in chromatography and mass analysis by HPLC and GC/MS. Only the products of resveratrol, phloretin and daidzein were clearly identified by HPLC (Figure 4.11) and GC/MS.

However, the poor solubility of aglycones matters when increasing initial substrate for producing catechol derivatives from the monophenol aglycones. For example, the daidzein is not soluble in alcohol, neither MeOH nor EtOH, the maximum concentration of initial substrate of the hydroxylation of daidzein is less than 380 μM . Usually, the reaction product flows out of the reaction system after the reaction. The reaction flow continues as the non-dissolved substrate is dissolved to participate in the reaction. However, the initial substrate was left in the reaction mixture not involving in the reaction beyond the concentration (380 μM) because the structural similarity affects the solubility of the substrate and product.

(Notice that 3'-ODI, a catechol derivative, was oxidized in basic condition but 3'-ODI stayed stable in acidic reaction mixture as shown in Figure 4.11)

Phloretin is soluble in both MeOH and EtOH, and it is found BT_Ty active in 50v/v% of MeOH but not in EtOH. (IC50 of EtOH is less than 10v/v%). The initial concentration of substrate could be increased up to 10 mM of phloretin where it reaches the saturation level of phloretin in in 50v/v% of MeOH. As a result, 8.25 mM of 3-hydroxy phloretin was produced from 10 mM phloretin in an hour. However, unfortunately, the reaction was not occurred in whole-cell reaction, and it is thought that BT_Ty is inactivated in cytoplasm where pH is maintained around 7 by systems relating to homeostasis.

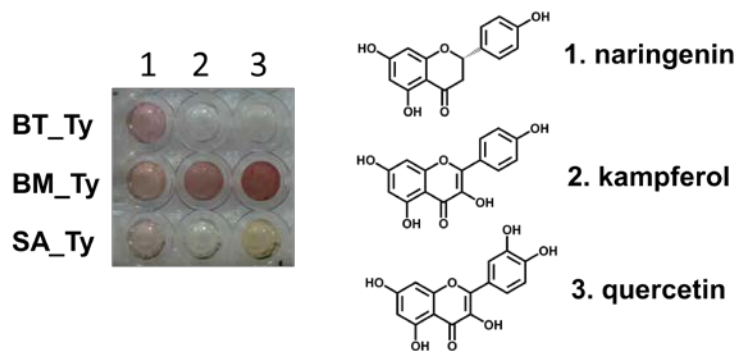


Figure 4.10. The substrate specificity of tyrosinases to naringenin, kaempferol, and quercetin.

The substrate specificity was briefly observed by the color changes as Tys oxidize the phenolic substrate. BM_Ty shows the broad substrate specificity, but BT_Ty hydroxylated only naringenin.

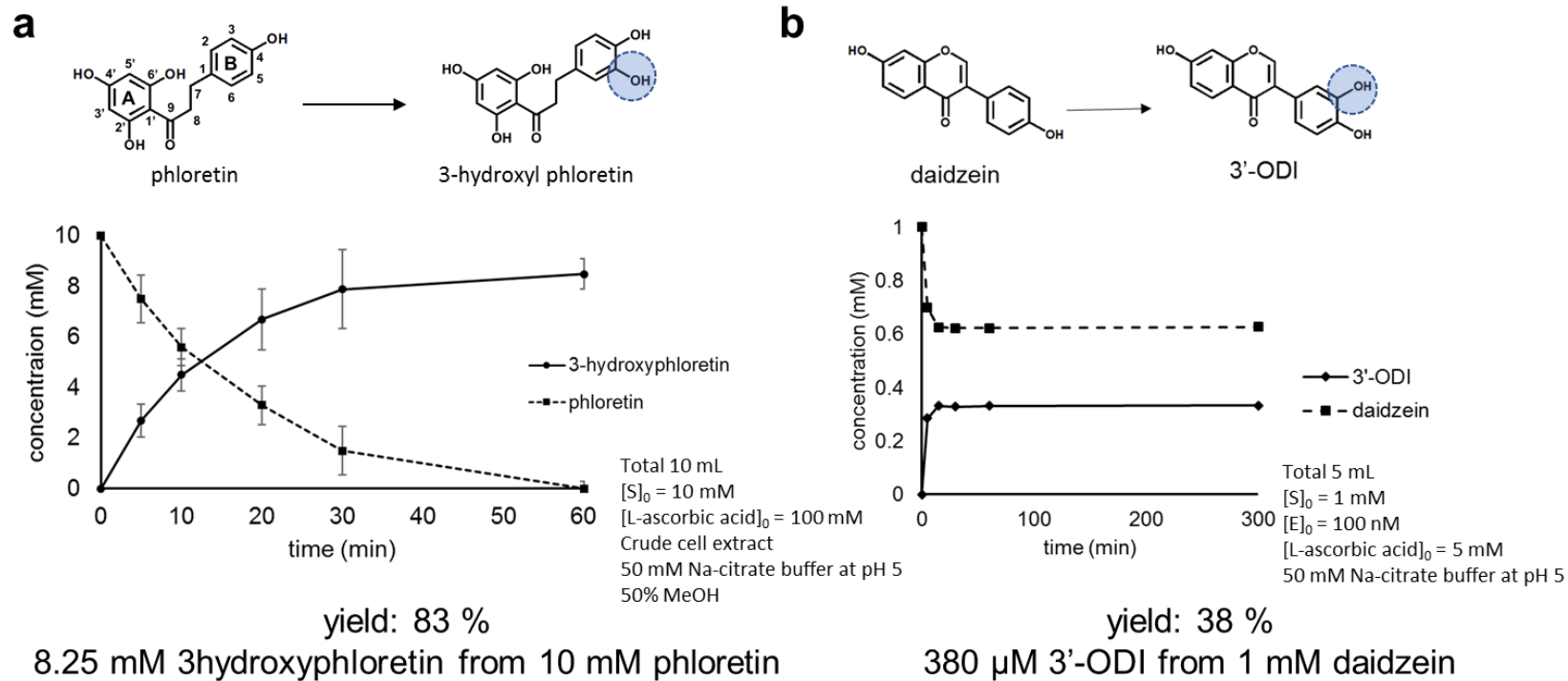


Figure 4.11. *ortho*-Hydroxylation of monophenol aglycones by BT_Ty w/o boric acid.

4.4.3 Structural analysis of BT_Ty

4.4.3.1 The morphology of BT_Ty based on the X-ray crystallography

X-ray crystallography of BT_Ty was resolved (Thanks to Prof. Kyung-Jin Kim at Kyungpook National University), and the structural analysis was performed based on the crystallography; the crystal of the enzyme was only formed at pH 4.5.

The imposed structures of the active sites and the multiple sequence alignment of 9 PPOs (Cox, Aus, and Ty) showed the well-conserved secondary structure of the active site of BT_Ty (Figure 4.12). As shown in Figure 4.12, a loop in a yellow circle is a well-conserved loop in type III copper protein though the amino acid sequences may vary. The residues on the loop were reported that they are influential for substrate binding and the k_1/k_2 ratio; for example, V218 on the loop of BM_Ty was proposed to take part in positioning of a substrate, and the V218F mutant exhibited an improved k_1/k_2 ratio (Table 4.2) (Goldfeder, Kanteev et al. 2013, Goldfeder, Kanteev et al. 2014). Furthermore, F273, an important residue for determining the substrate specificity of Aus from *Coreopsis grandiflora* (CG_Aus) is also on the loop in the same position as V218 (Figure 4.12-a) (Molitor, Mauracher et al. 2016). Especially, N307 is exactly imposed on V218 of BM_Ty and F273 of CG_Aus, and seems to make close contacts to H56 and H84, one of the core histidines that hold copper ions (Figure 4.12).

The melting temperature was measured to be 53.2 °C (Figure 4.13) which is similar to other tyrosinase; however, it was found that BT_Ty stayed in

homo-tetrameric structure at acidic pH below pH 6 (Figure 4.14). As shown in Figure 4.14-b, the result of size exclusive chromatography showed that beyond pH 6, the tetrameric configuration was not observed but only the multimeric state was observed below pH 6 where the reactivity of BT_Ty maintained, indicating that the tetrameric state of BT_Ty is important for the activity.

Furthermore, a cap domain was observed at the N-term of this enzyme. The exact starting residue for the cap domain is not clear but there exist hinge residues, forming a simple strand, pass through a side part of BT_Ty. The strand connects the cap and body domains as shown in Figure 4.15. Interestingly, the tunnel to the active site is in between the two domains; there also exist a tunnel penetrating the cap domain but the length of the tunnel is long more than 20 Å and the radius of it is less than 3 Å. If the gap between the cap and the body domain is open, then the substrate will be well accessible to the active site of BT_Ty. And the length of the path is only 2.5 Å.

In following sections, intensive structural analysis of BT_Ty was performed. To delve into the roles of the interesting side chains, the residues were substituted to alanine individually for clarifying the roles of each residue, and the activities of the mutants were observed by the initial reaction rate of dopachrome formation from L-tyrosine and by the color changes due to melanin formation.

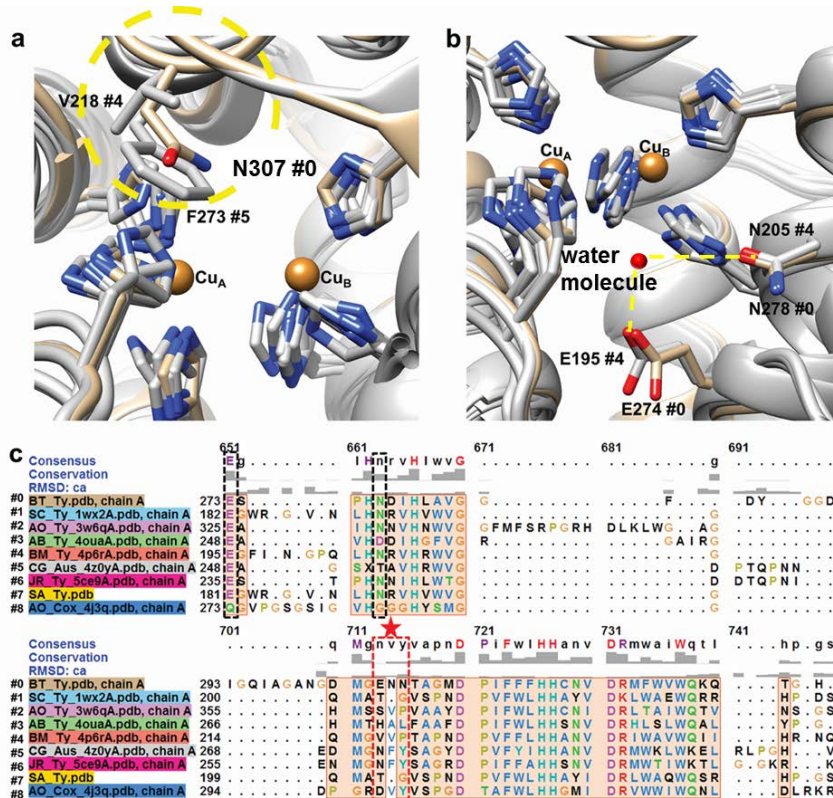


Figure 4.12. The structural comparison of type III copper containing polyphenol oxidases.

(a) The residues on the loops in the yellow circle are well known for affecting substrate specificity. N306 was found in the model of BT_Ty in that position. (b) The two residues that are known for capturing water molecule for the first phenolase activity are well positioned in the homology model of BT_Ty. (c) The multiple sequence alignment of Cox, Aus, and Ty by the secondary structure (MatchMake, in built function of Chimera 1.11.2 (Pettersen, Goddard et al. 2004)) The residues in the yellow circle is indicated in a red box, and the water capturing residues are in the two separated black boxes.

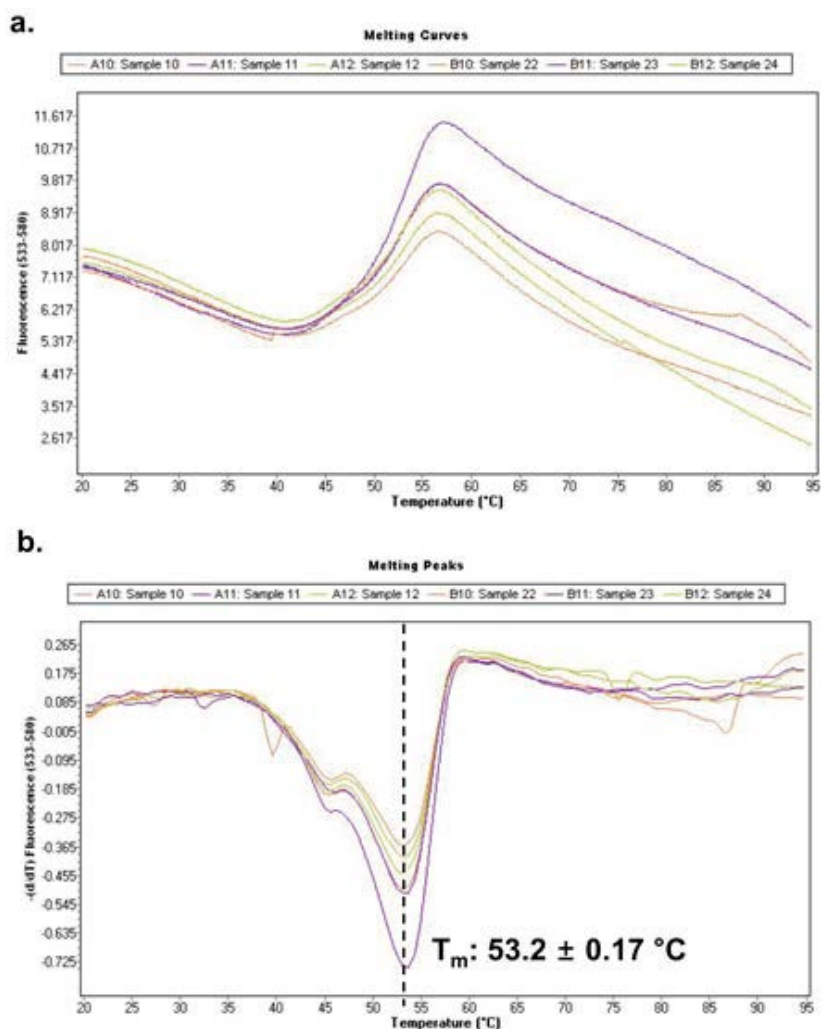


Figure 4.13. The measurement of T_m of BT_Ty.

A protein dye, SYPRO Orange dye (ThermoFischer Scientific), was used for monitoring the stability of BT_Ty depending on temperature.(Huynh and Partch 2015) LightCycler 480 II (Roche Molecular Systems Inc.) was used for controlling the temperature variation and detecting fluorescence intensity (at 568 nm).

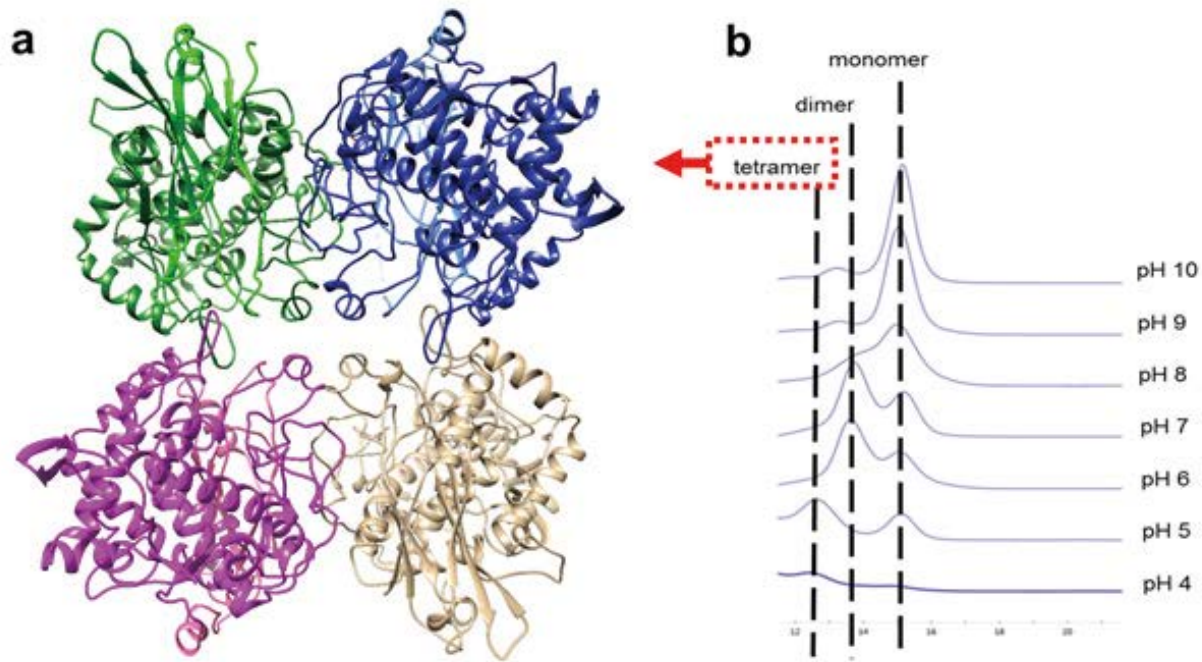


Figure 4.14. The X-ray crystallography of BT_Ty, and the result of size-exclusion chromatography depending on pH

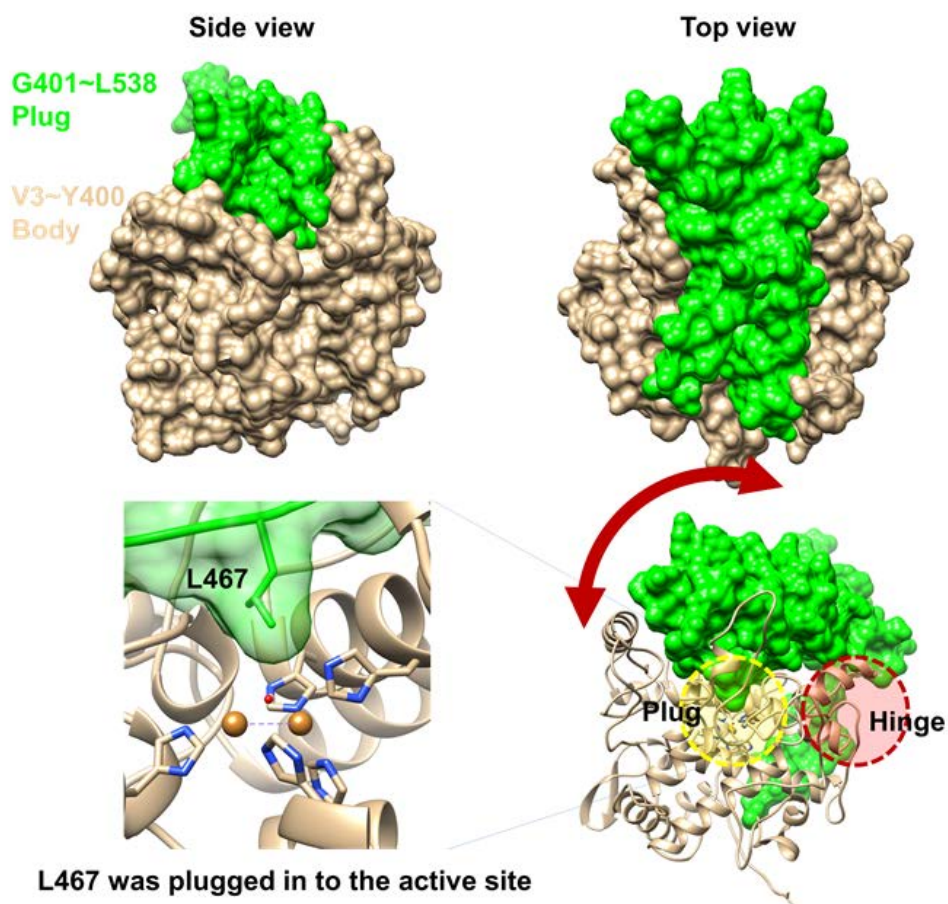


Figure 4.15. The existence of a cap domain that blocks the active site of BT_Ty.

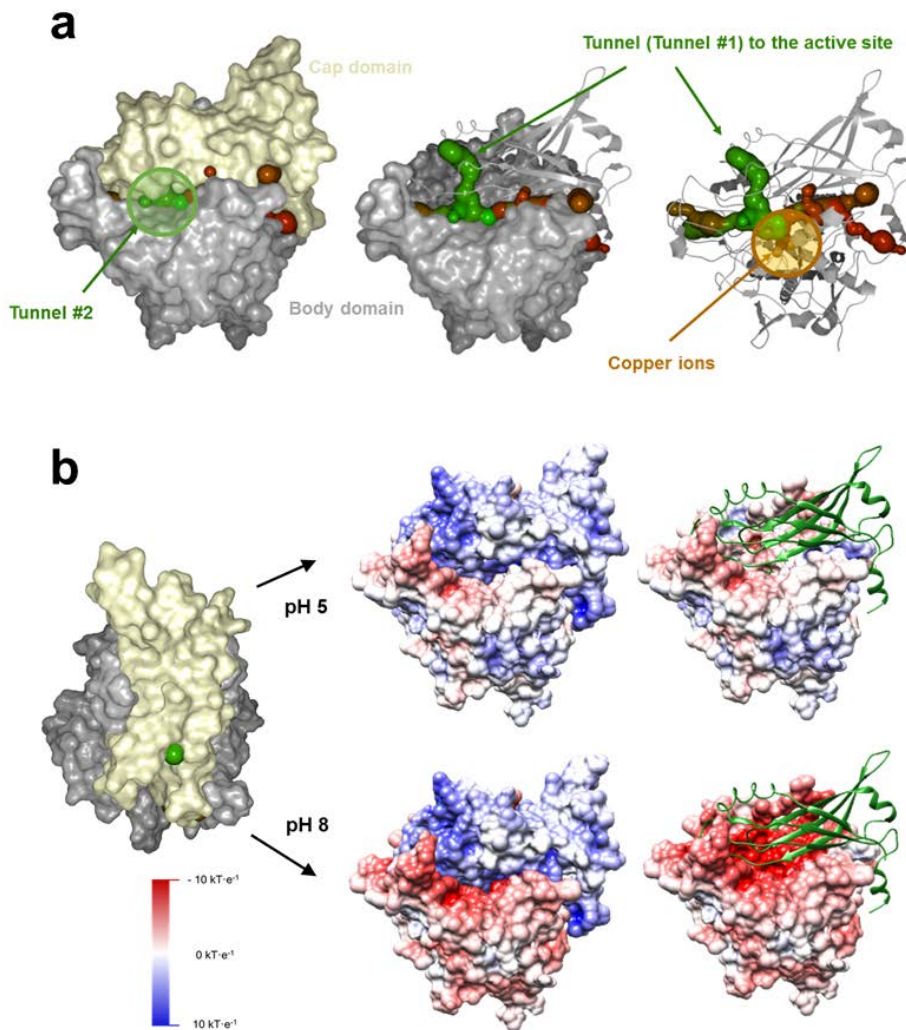


Figure 4.16. Identification of the active site, and electrostatic intra-interactions b/w cap and body domains.

(a) Prediction of tunnels to the active site of BT_Ty by CAVER Analyst ver.1.02 (b) Mapping of electrostatic intra-interactions between cap and body domains depending on pH. The calculation of electrostatic interactions was done by PDB2PQR and APBS.

4.4.3.2 Residues related to inter-interactions for maintaining the homo-tetrameric structure.

The study for expressing and characterizing the BT_Ty is novel because it is the first attempt. In addition, as stated earlier, BT_Ty has a unique homo-tetrameric structure that is not found in any of tyrosinase so far. A tyrosinase from mushroom, *A. bisporus*, AB_Ty have a dimeric structure but it is not clear if the multimeric structure is depending on pH since none of studies was found in database.

When looking closely at the structure of the enzyme, three interactions between monomers are observed. Direct interactions between Chain A and Chain C (interactions between D165 of each chain), and two interactions between Chain A and Chain B, one with the body domain of Chain B (interactions between R46.A and D74.B) and another one with the cap domain of Chain B (interactions between E344.A and R544.B) (Figure 4.17). The two inter-interactions between Chain A and Chain B are coulombic charge-based interactions since the Arg and Glu (or Asp) have opposite charges. The electrostatic interaction between Arg and Glu (or Asp) is not deeply involved in the change of pH since the protonation states of Glu and Asp are not greatly affect the intensity of charge of carboxyl group of the residues and the pKa of Arg is beyond the scope of this study which is 12.48 (Figure 4.17-b).

However, the interactions between two carboxyl group are dependent to pH since the protonated or deprotonates states of the carboxyl group affects the formation of hydrogen bond (that pulling the monomeric states together for holding the multimeric structure) and the repulsions by the two identical charges of Asp

(Figure 4.17-c). As expected, when substituting the residues stated above to alanine, the reactivity of all alanine-substituted mutants showed the significant decrease in the formation of melanin (Figure 4.18). Thus, it can be concluded that the multimeric state of BT_Ty is important for maintaining the activity of BT_Ty however, the primary reasons for requirement of multimeric states of BT_Ty for maintaining the activity is not clear. The similar tendency of other multimeric enzymes was reported previously. For example, lysine decarboxylase has a decameric structure which is also pH dependent (active only at basic pH), and inactive if the structures are divided into monomers or dimers (Kanjee, Gutsche et al. 2011).

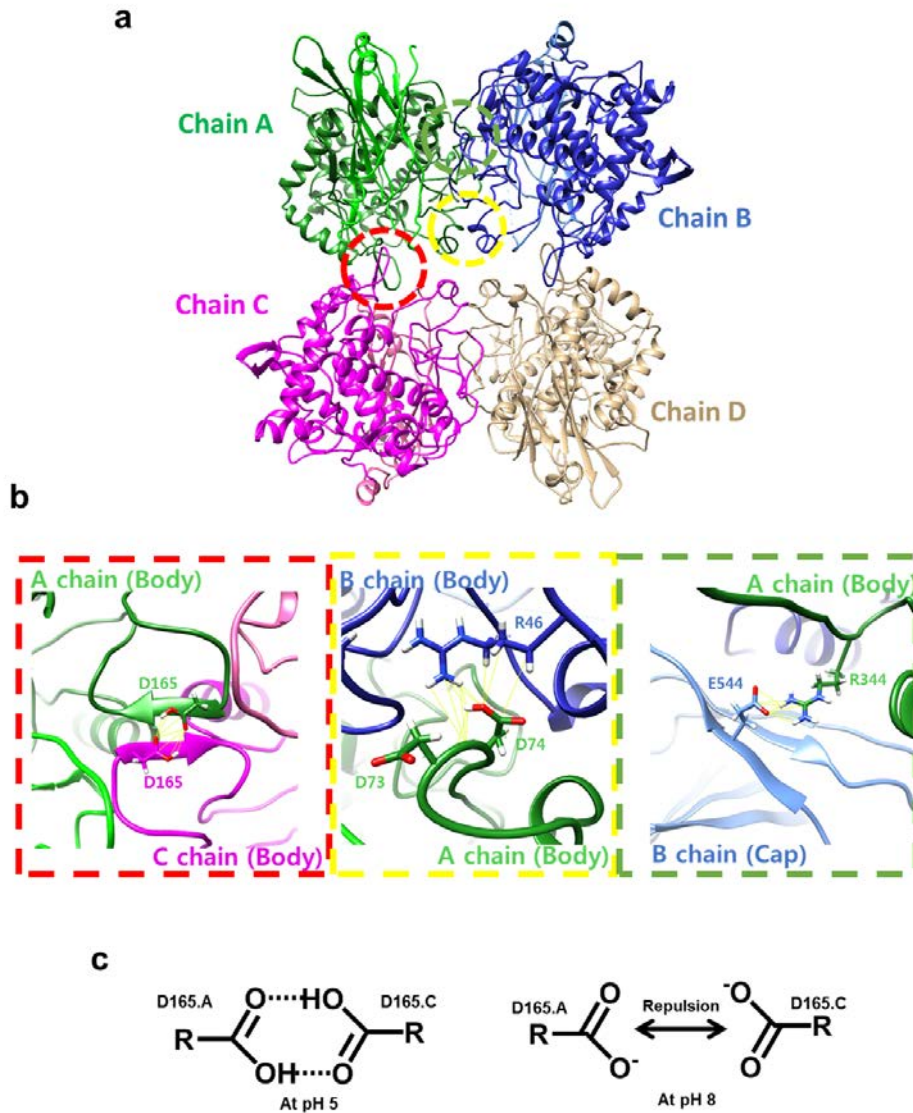
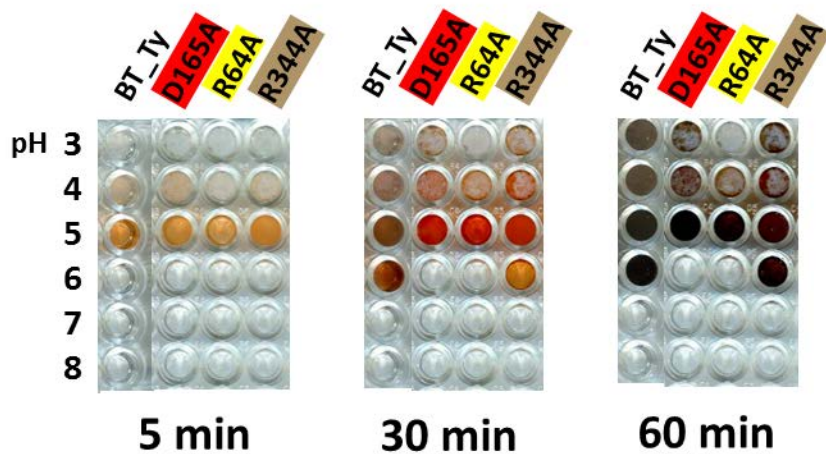


Figure 4.17. The residues that have inter-interactions for maintaining the homo-tetrameric structure.

(a) Three regions for inter-interactions b/w monomers. (b) Residues of the three major interactions. (c) Interaction and repulsion between two Asp residue (D165) depending on pH.



Total reaction volume = 200 μ L

$[S]_0 = 1$ mM

$[E]_0 = 100$ nM

$[\text{CuSO}_4] = 10$ μ M

Figure 4.18. The results of alanine scanning of residues that have inter-
interactions b/w monomers.

4.4.3.3 Residues related to intra-interactions between cap and body domains.

As stated earlier, a cap domain was observed at the N-term of BT_Ty. The exact starting residue for the cap domain is not clear but there exist hinge residues, forming a single strand which passes through the outer surface of profile of BT_Ty as shown in Figure 4.15. The a strand connects the cap and body domains as shown in Figure 4.15. Interestingly, the tunnel to the active site is in between the two domains; there also exist a tunnel penetrating the cap domain but the length of the tunnel is long more than 20 Å and the radius of it is less than 3 Å. If the gap between the cap and the body domain is open, then the substrate will be well accessible to the active site of BT_Ty. And the length of the path is only 2.5 Å.

The pI of BT_Ty is approximately 5; however, when calculating the pI based on the primary sequence of the enzyme, the cap domain is above 8.5 while the body domain is less than 5. The colorimetric mapping based on the electrostatic charge of BT_Ty is present in Figure 4.16-b. Interestingly, the charges of the interface of cap domain is dramatically changed as pH changes to pH 8 from pH 5. The interface becomes more negative at basic pH while the overall electrostatic charge of cap domains stays in a similar level since the pKa of basic residues are more than 10. Therefore, the interfaces could be closed firmly with stronger interactions between the cap and body domains at basic pH, and this could be the key mechanism for controlling the activity of BT_Ty as pH of the circumstance changes. To see the individual roles of residues, alanine scanning was performed on the residues, two arginines of the cap domain, R510 and R469, and three

residues, E306, N307, and N308 in the body domain. Asn is the amide of aspartic acid thus it is not negatively charged residue. But it is polar and has a high propensity to hydrogen bond since the amide group can donate two hydrogen bonds and the ketone can also accept hydrogen bonds. The hydrogen bonds can activate bigger dipole moment of its surround.

The substitution of E306, N307, and N308 shows increased activity above pH 5. Especially, N307A shows the activity in all pH range, and this indicates that the residue is the key residue for controlling the activity depending on pH. However, the side chain is not dependent to the changes in pH (in biological circumstance), thus, it is thought that there are other residues or water molecules that interact with N307, and synergic effects could be drawn for affecting the interactions between the cap and body domains. These residues could be the neighboring residues such as E306 and N308. Furthermore, the substitution of more than one residue among E306, N307, and N308 dramatically lost the activity. The expression level also negatively affected. Not only the total expression level was decreased but also the soluble fraction of E306A/N307A, E306A/N308A, N307A/N308A, and E306A/N307A/N308A were significantly decreased. The studies of these residues were continued in the next section, 4.4.2.4. Identifying residues related to the tyrosinase activity at acidic pH.

The substitution of arginines of the cap domains negatively affects the activity of BT_Ty. The both mutants, R469A and R510A showed decreased activity comparing to the wild-type. When expressing BT_Ty without the cap domain, the enzyme was not expressed soluble and lost its activity, indicating that the cap domain is important for maintaining the activity and stability of BT_Ty.

Interestingly, the activity partially recovered when the cap domain (expressed separately) was added in the solution where only (purified) body domain is contained. This phenomenon can certainly support the hypothesis that the cap domain is important for maintaining the activity and structural stability of BT_Ty.

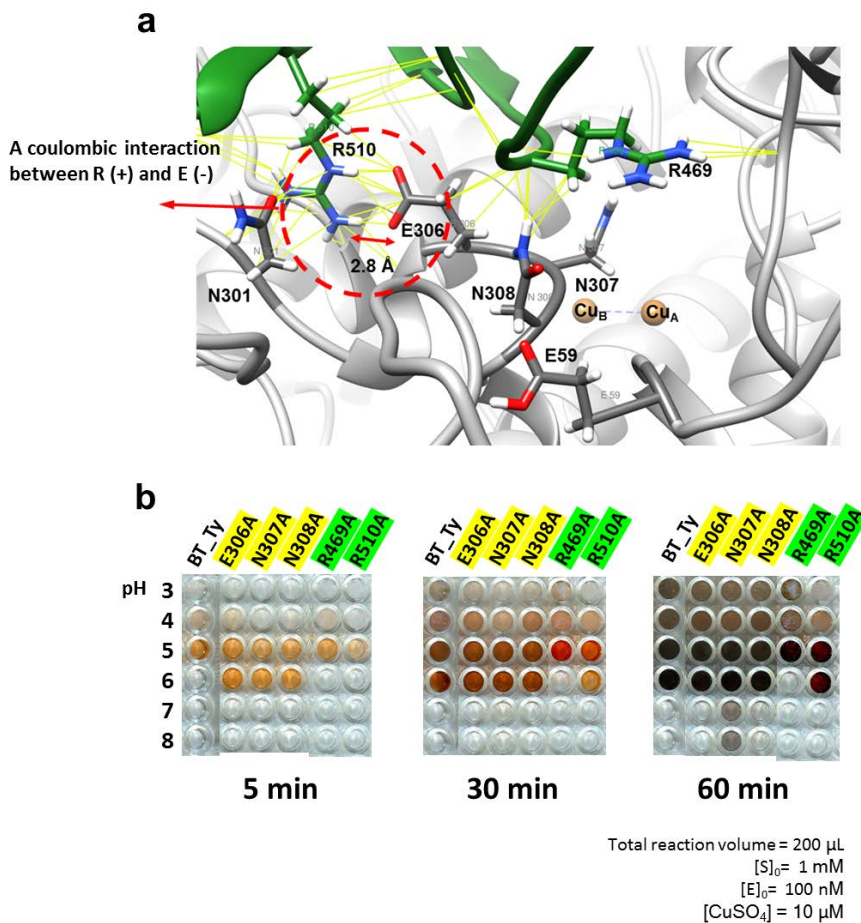
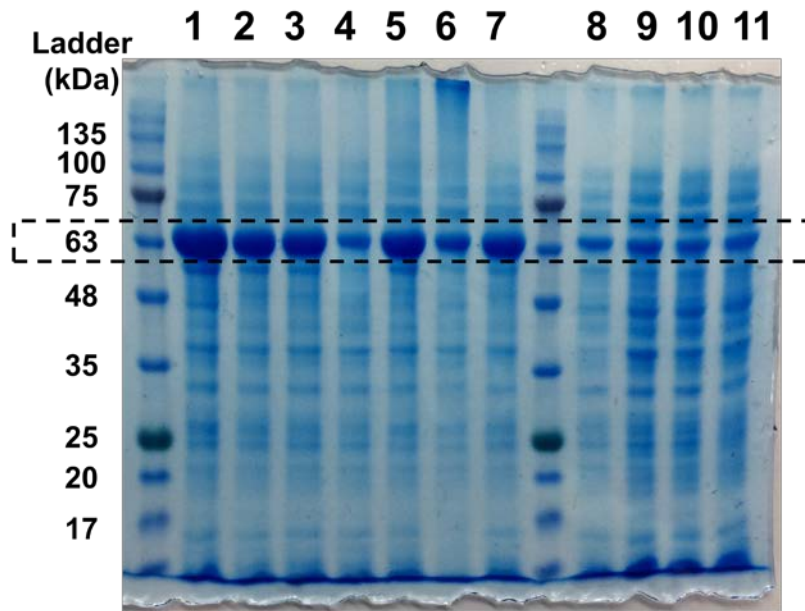


Figure 4.19. The residues that have intra-interactions b/w cap and body domains, and the result of alanine scanning on the residues.

(a) The two Arg residues, R510 and R469, of the cap domain (colored in green) have coulombic interactions to E306, E59, N307, and N308. (b) The reactivity of BT_Ty after removing the residues by alanine substitution.



1. BT_Ty (WT) 2. E58A 3. N83A 4. E305A 5. N306A 6. N307A 7. R468A
 8. N306A/ N307A 9. E305A/ N306A 10. E305A/ N307A 11. E305A/ N306A /N307A

Figure 4.20. SDS-PAGE gel images of BT_Ty mutants.

4.4.3.4 Identifying residues that enhance the Ty activity even at acidic pH.

As stated in previous section, the imposed structures of the active sites and the multiple sequence alignment of 9 PPOs (Cox, Aus, and Ty) showed the well-conserved secondary structure of the active site of BT_Ty (Figure 4.12). And, as shown in Figure 4.12, a loop in a yellow circle is a well-conserved loop in type III copper protein though the amino acid sequences may vary. Normally, hydrophobic residues such as Val and Phe were found in that position of other type III copper containing polyphenol oxidase, but Asn is in that position in case of BT_Ty. E306, N307, and N308 in that loop seems unique and especially, the amide group of N307 seems to have hydrogen bonds to the hydroxyl group of the monophenol substrate as shown in Figure 4.21.

Again, the Ty activity at low pH is disadvantageous since the rate-determining step of the initial monophenolase activity of Ty is the deprotonation of monophenols, which is more favorable at pH above its pKa, normally 8. So there should be exist residues that stabilize the deprotonated monophenols at low pH below its pKa. The stabilization could be achieved by electrostatic attractions such as hydrogen bonds. The existence of donor of hydrogen bonds around the active site could perform the role of stabilization of deprotonated monophenols. Asp, Asn and Glu are representative amino acids that could form hydrogen bonds to monophenols. Glu has a carboxyl group, and Asn also has a high propensity to hydrogen bond since the amide group can donate two hydrogen bonds. The three residues in the loop, E306, N307, and N308 were thought to be the major residues

that help deprotonation of monophenols. To see if each residue affects the entire enzyme reaction or whether the combination of residues affects the activity, each and the combination of the three residues were substituted to alanine. And the initial oxidation rates of the mutant were measured by the formation of dopachrome at different pH by UV spectroscopy.

The initial oxidation rate of BT_Ty to L-tyrosine at the optimal pH, which is 5, was $29.6 \pm 0.8 \mu\text{M}\cdot\text{min}^{-1}$. However, the reactivity decreased by more than 20% when each of three residues was substituted to alanine, and the activity was abruptly decreased or disappeared when two or three combinations of residues were substituted to alanine. (The initial oxidation rate of E306A was $23.5 \pm 1.7 \mu\text{M}\cdot\text{min}^{-1}$; of N307A was $23.9 \pm 0.9 \mu\text{M}\cdot\text{min}^{-1}$; of N308A was $23.0 \pm 1.7 \mu\text{M}\cdot\text{min}^{-1}$.) Therefore, the three residues, E306, N307, and N308 were thought to be the major residues that have hydrogen bonds to the deprotonated hydroxyl group of monophenol.

To prove the importance of the three residues for increasing Ty activity, the residues, Glu and Asn, were introduced in other Ty that has hydrophobic residue in the same positions. BM_Ty was used for the study, and the residues from M215 to A221, MGVVPTA were substituted to MGENNTA. The substitutions were done by each residue or by the combination of two or three residues. V218N, V217E/V218N, V218N/P219N and V217E/V218N/P219N mutants of BM_Ty were constructed.

But V217E/V218N/P219N mutant was not expressed at all and other mutants with combinational substitutions, V217E/V218N, V218N/P219N, lost the

activity significantly. Only the activity of V218N was increased more than 20% at the range of pH 6 to 8. Especially the initial oxidation was increased 2.8-fold at pH 6, indicating that the residue could help the deprotonation of monophenols in Ty reactions. It was expected that the ENN residues newly introduced to BM_Ty could increase the activity at lower pH (below 5); however, the all mutants lost its activity below pH 5. Each residue of the enzyme has evolved to have its proper role fixed for precisely controlling the biological function. The newly introduced Asn residue in the position (#218) slightly increased the activity but it might negatively affect the stability of the enzyme below pH 5.

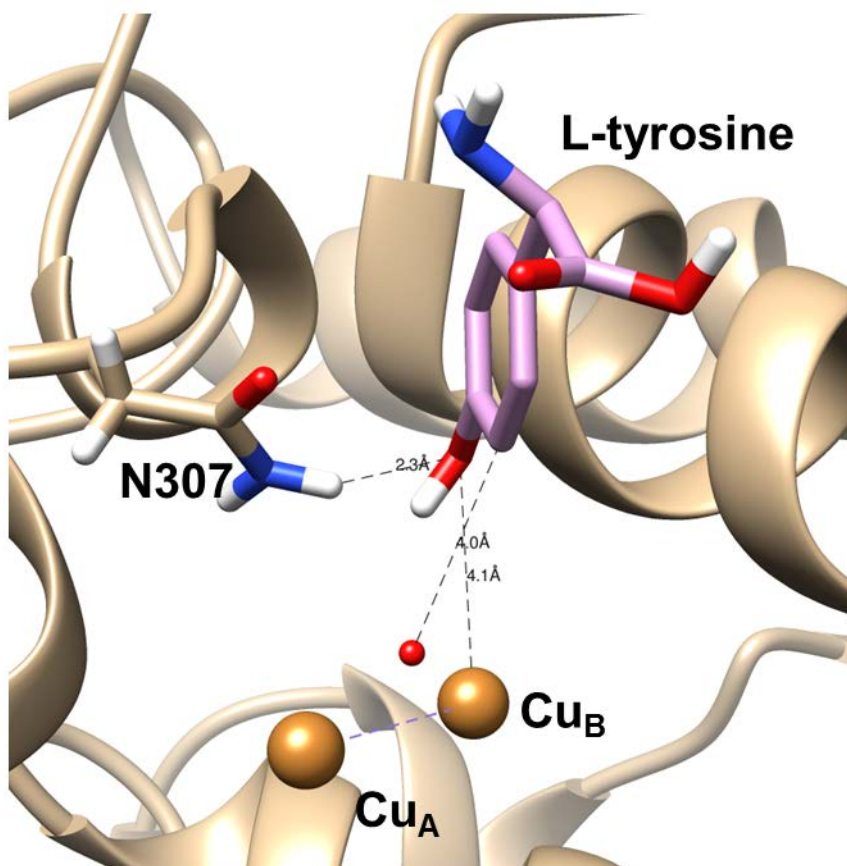


Figure 4.21. A residue that has a hydrogen bond with hydroxyl group of monophenols.

A docking simulation of BT_Ty (X-ray crystallography) and L-tyrosine by AutoDock Vina shows that the hydrophilic residue, N307, has a hydrogen bond to hydroxyl group of L-tyrosine.

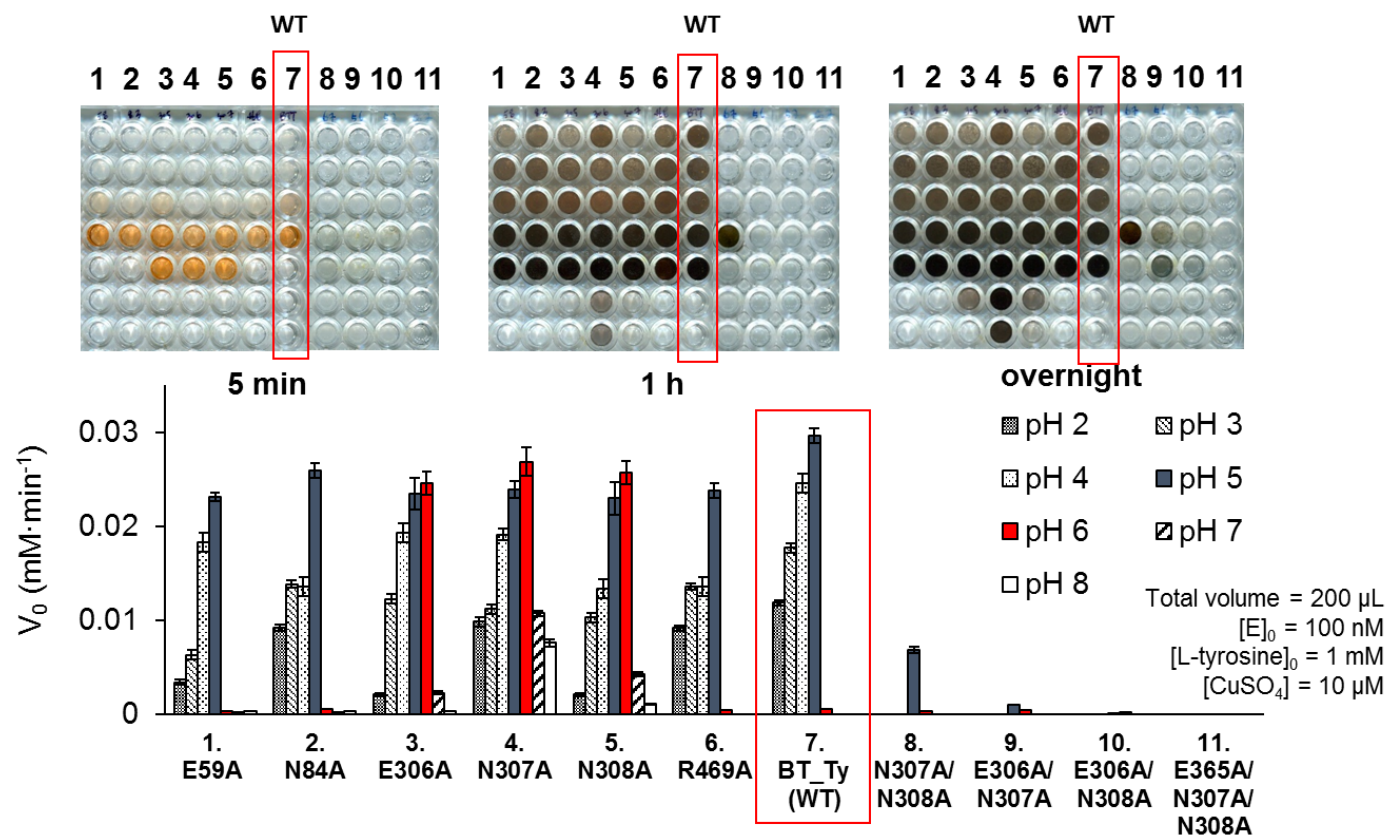


Figure 4.22. The alanine scanning of residues that have interactions to monophenol substrates.

a

BM_Ty ---- MGVVPTA
 BT_Ty ---- MG**E**NNTA

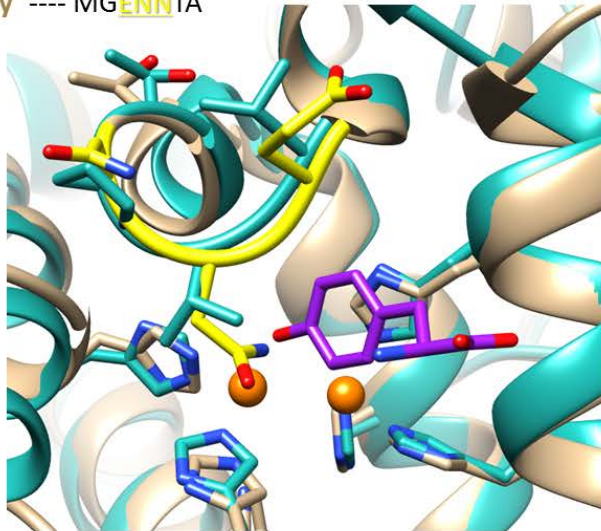
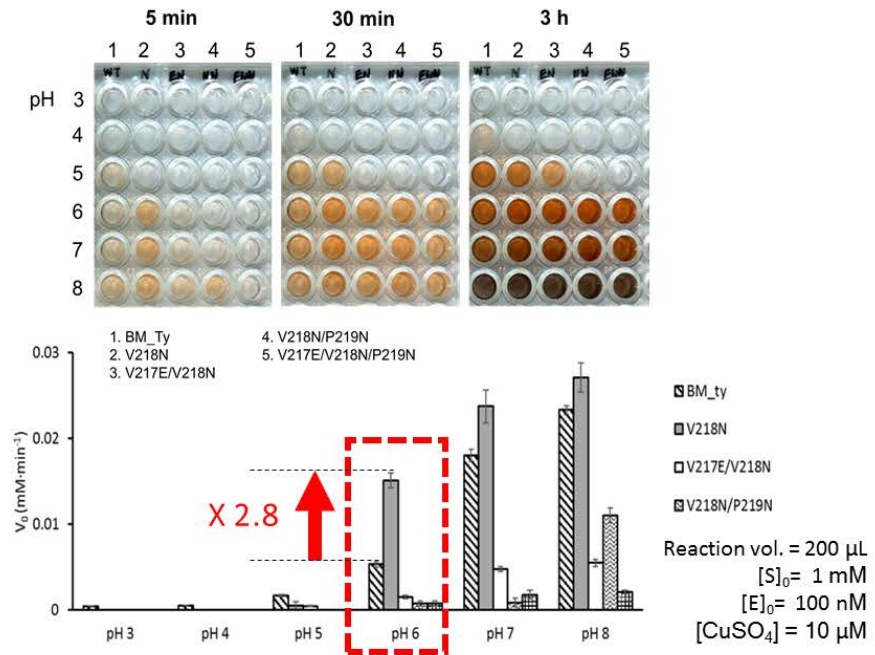
**b**

Figure 4.23. Introducing the residue, Asn, has a hydrogen bond to monophenol to other tyrosinase.

4.4 Conclusion

In this study, we first expressed and characterized the novel Ty from *B. thailandensis*, which is highly active for various monophenolic substrates at acidic pH among type III copper proteins reported so far. This Ty also has a high k_1/k_2 ratio, 0.82, in the reaction condition and it was demonstrated that these properties make BT_Ty applicable to efficient *ortho*-hydroxylation of glycoconjugate monophenols to their corresponding catechol derivatives.

However, intensive structural study of BT_Ty is not available yet because of the absence of a reliable 3D model. A template structure for homology modeling could be found through HHpred (Söding, Biegert et al. 2005) but the selected template, 3W6W, has only 20.2 % of sequence similarity with BT_Ty. We are currently in the middle of time to resolve the X-ray crystallography data of BT_Ty. And we strongly believe that understanding the structural differences of BT_Ty with other Tys could draw not only clear understanding of the mechanism of Ty activity at acidic pH (such as roles of neighboring residues in terms of the initial deprotonation of substrate) but also the strategies of enzyme engineering for enhancing the yield of the production of catechol derivatives in more detail.

Chapter 5.

**Tissue adhesive, rapid forming, and sprayable ECM
hydrogel via recombinant tyrosinase crosslinking**

5.1 Abstract

We report on a tissue adhesive hydrogel based on recombinant tyrosinase (Ty) mediated crosslinking. We tailored our adhesive hydrogels to be injectable and sprayable for use in tissue engineering and minimally invasive surgery. The adhesive hydrogels were fabricated by combining tyramine-conjugated hyaluronic acid (HA_t, 1% w/v) and gelatin (3% w/v) with novel tyrosinase from *Streptomyces avermitilis* (SA_{Ty}). The enzymatic crosslinking by SA_{Ty} was fast, with less than 30 seconds for complete gelation, and the SA_{Ty} based crosslinking significantly enhanced the physical properties and adhesive strength of the hydrogel with the native tissue samples. Furthermore, by optimizing the injection conditions, we tailored the adhesive hydrogels to be injectable and sprayable with a medical syringe and commercial airbrush nozzle, respectively. An *in vivo* analysis of the adhesive hydrogel showed a low immune modulation. The recombinant tyrosinase crosslinked hydrogel has a robust potential in tissue engineering and regenerative medicine.

Keywords: Enzymatic crosslinking, tyrosinase, *Streptomyces avermitilis*, hydrogel, minimal invasive

5.2 Introduction

Hydrogels are attractive biomaterials in regenerative biomedical applications due to their high-water content, biocompatibility and mechanical properties (Kim and Mooney 1998, Khademhosseini and Langer 2007). Recently, tissue adhesive hydrogels with a shear thinning ability have been developed for biomedical applications due to their ease of use and minimal invasiveness (Yu and Ding 2008, Ryu, Lee et al. 2011, Li, Yan et al. 2015). The criteria to ensure adhesion on the surface of biological tissues is to create enough interactions, such as ionic interaction or covalent bonds, in a wet environment (Peppas and Buri 1985, Gong 2006). In many cases, a conventional hydrogel is negatively charged (Gong 2006). However, the surface of a biological tissue has a net negative charge in physiological conditions, so there will be repulsive interactions between the tissue surface and a conventional hydrogel (Roy, Guo et al. 2015). Tissue-adhesive hydrogels, regardless of a net charge, have been extensively investigated, and a viable strategy is to create a covalent bond through phenolic groups, such as dopamine and tyramine (Lee, Messersmith et al. 2011, Li, Yan et al. 2015). Biomimetic strategies based on mussel-inspired chemistry can result in a hydrogel with tissue-adhesive properties due to the adhesive quinonic groups that are oxidized from phenolic groups (Lee, Messersmith et al. 2011). The crosslinking reactions of phenolic moieties could be initiated with chemical and enzymatic oxidation agents, such as sodium periodate (NaIO_4) and horseradish peroxidase (HRP). However, these approaches have limitations for practical applications due to the cytotoxicity and pH dependency of chemical reagents, as well as the fact that only phenol coupling is available for crosslinking. An alternative strategy,

tyrosinase (Ty) from *Agaricus bisporus* (AB_Ty) has been widely utilized for hydroxylation of phenolic moieties on macromolecules, such as gelatin (Le Thi, Lee et al. 2017), mussel protein (Hwang, Gim et al. 2007), and silk fibroin (Freddi, Anghileri et al. 2006) due to the ease of availability. Tyrosinase (Ty), a polyphenol oxidase that plays a leading role in the formation of a mussel-adhesive protein (Hwang, Zeng et al. 2010, Lee, Messersmith et al. 2011), can also oxidize phenols. First, Ty hydroxylates phenols into catechols by adding a hydroxyl group on the *ortho*-position of phenols, and this leads to the subsequent oxidation of catechols to produce quinones under physiological conditions (Decker, Dillinger et al. 2000, Lee, Baek et al. 2016). The reactive quinones promptly form covalent bonds with amines, thiols, or other phenolic moieties through non-enzymatic reactions, including oxidative phenol coupling, Michael addition, and the Maillard reaction (Chen, Embree et al. 2002, Lee, Lee et al. 2011). However, applications of AB_Ty based crosslinking have been limited due to the low degree of crosslinking as a result of the steric hinderance between AB_Ty and the macromolecules (Freddi, Anghileri et al. 2006, Hwang, Gim et al. 2007, Le Thi, Lee et al. 2017).

In this paper, we report on the design and synthesis of novel recombinant tyrosinase from *Streptomyces avermitillis* (SA_Ty) and its applications of tissue adhesive, injectable and sprayable hydrogel (Figure 5.1). The reactivity of SA_Ty to tyrosine monomer and conjugated to hydrogel was compared to widely used Ty. The model polymer, tyramine conjugated hyaluronic acid (HA_t) mixed with gelatin was evaluated in terms of its properties with SA_Ty as well as for use in surgical glue and delivery carrier of biomacromolecules.

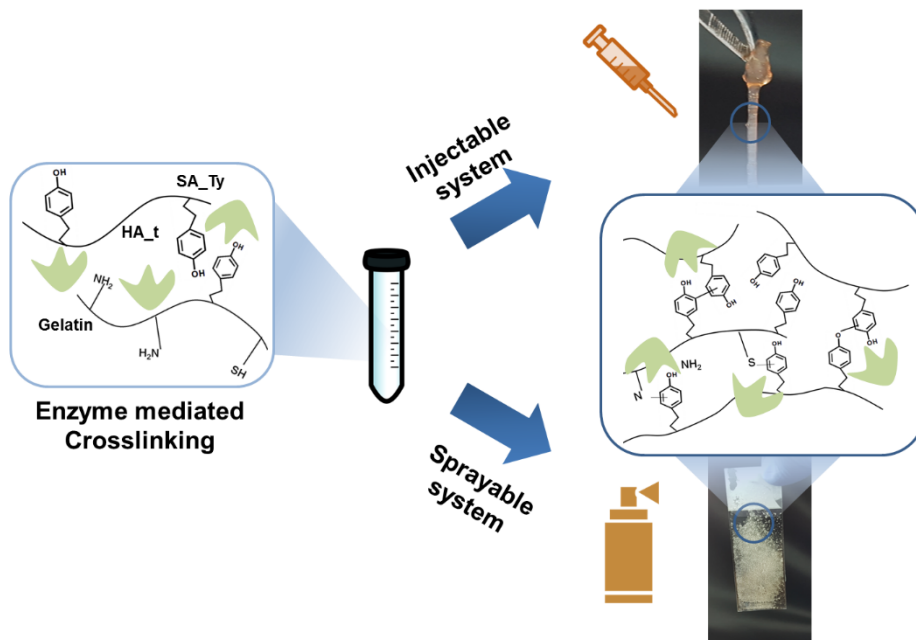


Figure 5.1. Schematic illustration of fabrication of SA_{Ty} mediated HG_{gel}.

Tyrosine group in HA_t forms covalent bond with tyrosine, amine and thiol group in gelatin via SA_{Ty}. Sol-gel transition happened within 30 s. HG_{gel} could inject through 31 G needle, and spray using commercial airbrush. This image was illustrated by Su-Hwan Kim

5.3 Materials and Methods

5.3.1 Materials

Hyaluronic acid (40 - 64 kDa) was purchased from Lifecore Biomedical, LLC (Chaska, MN). 1-Ethyl-3-(3-dimethylaminopropyl) carbodiimide hydrochloride (EDC·HCl), N-hydroxysuccinimide (NHS), tyramine hydrochloride and gelatin (from porcine skin, type A, 300 Bloom) were all purchased from Sigma-Aldrich (Yongin, Korea). Tyrosinase extracted from mushroom was used as purchased from Sigma-Aldrich (Yongin, Korea, Catalog Number: T3824-25KU). The recombinant tyrosinases from *Bacillus megaterium* and *Streptomyces avermitilis* were heterologously expressed in *Escherichia coli*. All solutions were sterilized with mixed cellulose ester membrane which cut-off size is 0.22 μm (Daihan Scientific, Korea). A commercial airbrush kit (Bluebird, ABS-130) with 0.2 mm nozzle diameter was used for spraying hydrogel.

5.3.2 Preparation of enzymes

5.3.2.1 Expression and purification of recombinant tyrosinases.

The plasmids were constructed in the previous study (Lee, Baek et al. 2016). Briefly, genomic DNA was extracted from *Bacillus megaterium* and *Streptomyces avermitilis*, and each gene of tyrosinase was amplified by PCR. The primer list is in Table 5.1. A helper protein, KP198295.1, was inserted in MCS1 of pETDuet (Novagen, USA), and the gene of *S. avermitilis* tyrosinase (SA_Ty), gi:499291317,

was inserted in MCS2. His-tag was introduced at the C-terminal of SA_Ty. Genes for *B. megaterium* tyrosinase (BM_Ty) was also amplified and inserted into the multiple cloning site of pET28a. The recombinant plasmids were transformed into *E. coli* BL21 (DE3) by heat shock. The strain was spread on a plate of Luria-Bertani (LB) agar with antibiotic selection markers (25 $\mu\text{g}\cdot\text{mL}^{-1}$ of ampicillin for pETDuet or 50 $\mu\text{g}\cdot\text{mL}^{-1}$ of kanamycin for pET28a). A colony on the plate was inoculated into 3 mL of LB broth with proper antibiotics, and the cells were cultured in an incubator at 37 °C and 200 rpm overnight. After 0.5 mL of cell culture was transferred into a 250 mL flask with 50 mL of fresh LB, the cultured cells were incubated at 37 °C and 200 rpm until the optical density at 600 nm (OD_{600nm}) of the culture media reached approximately 0.6, 0.2 mM IPTG and 1 mM CuSO₄ were added. The induced cell culture was placed in an incubator at 18 °C at 200 rpm for 20 hrs. Cell pellets were collected by centrifugation and washed with 5 mL of 50 mM tris-HCl buffer at pH 8 twice. The cell was lysed by ultra-sonication. After centrifugation at 16000 rpm for 30 min, 5 mL of the soluble fraction of crude cell soup was collected. The expressed enzymes were purified by the general His-tag purification. The final concentration of BM_Ty and SA_Ty was 12.01 μM and 10.09 μM . The concentration of purified enzymes was calculated by the general Bradford assay (Zor and Selinger 1996).

Table 5.1. A list of primers for cloning bacterial tyrosinases

Primer	Sequence (5' → 3')
SA_Ty_melC1_F	GAA CCATGG AGTTAACCCGGCGT
SA_Ty_melC1_R	GAC AAGCTT TTAATTAAACGG
SA_Ty_melC2_F	GAA CCATGG ATGACCGTACGCAA
SA_Ty_melC2_R	GAC AAGCTT GACGGTGTAGAACG
BM_Ty_F	GAT GAATTC ATGAGTAACAAGTA
BM_Ty_R	GCA GTCGAC TGAGGAACGTTTTGA

5.3.2.2 Purification of mushroom tyrosinase.

The lyophilized mushroom tyrosinase from *Agaricus bisporus* (AB_Ty) was purchased from Sigma-Aldrich (T3824-25KU). The purification of AB_Ty from the lyophilized powder was followed as previously studied (Duckworth and Coleman 1970). The 9.3 mg of the lyophilized powder was dissolved in 5 mL of 50 mM sodium phosphate buffer at pH 7. Solid ammonium sulfate, 1.08 g, was added and continuously stirred in an ice-cold bath for 1 hour. The precipitate was removed by centrifuging at 16000 rpm for 30 min. And additionally, 0.42g of ammonium sulfate was added and stirred in an ice-cold bath for 1 hour. After centrifuging at 16000 rpm for 30 min, the precipitate was dissolved in 50 mM sodium phosphate buffer at pH 7. The solution was decolorized by calcium phosphate gel (Bio-Gel, Bio-Rad). The decolorized solution was fractionated by AKTA FPLC (UPC-900; P-920; Frac-920, GE Healthcare) with size exclusion column (Hiload 16/60 Superdex 200) first and then with ion exchange column (Mono Q GL 5/50) separately. The condition for the elution buffer of the first size exclusion chromatography was 300 mM of KCl in 10 mM sodium phosphate buffer at pH 7, and the flow rate was 1 mL·min⁻¹. Total 40 fractions, 5 mL each, were collected. The 17th to 20th fraction showed the activities on L-tyrosine. Thus, the fractions were collected and injected into the second anion exchange chromatography. The column was eluted with a linear gradient of 50 mM NaCl to 300 mM NaCl. The flow rate was maintained at 0.5 mL·min⁻¹. Total 22 fractions, 2 mL each, were collected. The 8th to 10th fractions showed the activities on L-tyrosine. The total of 6 mL fraction was concentrated to approximately 500 µL by the centrifugal filter with a cut-off size of 10kDa (Amicon Ultra -15). The final

concentration of the purified AB_Ty was 3.1 μM . The concentration of purified enzymes was calculated by the general Bradford assay (Zor and Selinger 1996).

5.3.4 Measurement of the specific activity of tyrosinase.

The initial rate of tyrosinase was determined by measuring the concentration of dopachrome or adducts of quinones and MBTH, at 475 nm ($\epsilon_{\text{dopachrome}} = 3600 \text{ M}^{-1} \cdot \text{cm}^{-1}$) (Deri, Kanteev et al. 2016) or at 505 nm ($\epsilon_{\text{adduct}} = 29000 \text{ M}^{-1} \cdot \text{cm}^{-1}$) (Winder and Harris 1991) with UV-spectroscopy (SPECTROstar Nano, BMG LABTECH, Ortenberg, Germany) at 37°C. The initial concentration of substrates and the purified enzymes were all fixed at the same value as following; the reaction mixture including proper buffer system (50 mM tris-HCl buffer at pH 8 for BM_Ty and SA_Ty; 50 mM sodium phosphate buffer at pH 7 for AB_Ty), 10 μM of CuSO_4 , 200 nM of purified Tys, and the substrate (1 mM of L-tyrosine, 0.3 w/v % of gelatin or 0.2 w/v% of tyramine-substituted hyaluronic acid) was prepared in a total volume of 200 μL . The initial velocity of a tyrosinase reaction was defined as the slope of a plot of the product concentration and the reaction time.

5.3.5 Fabricating HG_gels.

5.3.5.1 Synthesis of modified HA.

The amide bonds between tyramine and carboxyl group of HA was produced by EDC/NHS coupling. Briefly, 1.0 g of HA sodium salt was dissolved in 100 mL of

distilled water, and 1.437 g of EDC, 0.863g of NHS and 1.302 g of tyramine hydrochloride were added to the solution. The solution was stirred overnight at RT. After dialysis and lyophilization, the hyaluronic acid-tyramine conjugate (HA_t) was collected. The final product was analyzed by NMR and UV spectroscopy

5.3.5.2 Preparation of HG_gels.

First, HA_t 1wt% was dissolved in buffer (50 mM tris-HCl buffer at pH 8 for BM_Ty and SA_Ty; 50 mM sodium phosphate buffer at pH 7 for AB_Ty) at 40°C, and gelatin powder 3wt% was added to the HA_t solution. After totally dissolved at 40°C water bath and sterilized by the syringe-driven filtration, 200 nM of tyrosine (also sterilized by filtration) was added to the mixture to initiate the enzymatic crosslinking of the macromolecules. The solutions were simply vortexed for homogeneous mixing, and then the reaction tubes were incubated at 37°C for 3 min. NaCl was added to reduce the viscosity of the gels when the hydrogel was used for spray coat (the concentration of NaCl was varied, and the values were specified in this manuscript where required). A commercial airbrush kit (Bluebird, ABS-130) with 0.2 mm nozzle diameter was used, and air, compressed by a standard desk built-in air compressor, was filtered through a sterilized PTFE membrane filter (Acros 50 vent filter, Pall Corporation, U.S.)

5.3.6 Characterization of the tyrosinase-mediated hydrogels.

5.3.6.1 Measurement of the swelling ratio of hydrogels.

After the tyrosinase had been added in HG_sol as stated above, 200 μL of the solution was placed in the regularly shaped acrylate mold with 8 mm diameter and 3 mm thickness. The structures in the mold are lyophilized and then immersed in distilled water at 4 $^{\circ}\text{C}$ for 24 h to reach equilibrium swelling. The swelling ratio was calculated as follows: $(W_s - W_d) \cdot W_d^{-1}$, where W_d and W_s are the weights of dry and swollen gels at equilibrium, respectively. The measurements were repeated three times.

5.3.6.2 Rheological analysis.

The mechanical properties of hydrogels were measured by a rheometer (ARES, TA Instruments, USA) using 8 mm diameter of the parallel plate. For measurements, the hydrogel samples with the defined shape of 8 mm diameter and 3 mm thickness were prepared. Each sample was placed on the ground plate of the rheometer, and the upper plate was lowered to the force of 1 gm. After identification of the linear viscoelastic region as a change of oscillatory strain at a constant frequency, the frequency sweep of the hydrogels was recorded with frequencies varying from 1 to 100 $\text{rad}\cdot\text{s}^{-1}$ at a strain of 1%. The viscosity of HG_gels after SA_tyr treatment depending on NaCl concentration was also measured by the ARES rheometer with 450 μM of gap and 100Hz of shear rate (the viscosity was monitored for 2 min with the fixed shear rate). All measurements were repeated three times.

5.3.6.3 Evaluation of gelation time of HG_gel.

The gelation time of hydrogel was evaluated using rheometer (ARES, TA instrument). The HG_sol with each tyrosinase (500 μ l) was placed between the probe (diameter: 8 mm) and rotating plate (diameter: 25 mm). The shear strain and frequency kept in 1 % and 1 Hz respectively, and measurement gap was 0.5 mm. The crossover time between storage modulus G' and loss modulus G'' was defined as gelation time.

5.3.6.4 Scanning electron microscopy (SEM) analysis.

Lyophilized hydrogels were mounted on an aluminum stage with carbon tapes. The mounted samples were sputter-coated with platinum/palladium for 110 seconds in vacuum. The image was taken with JSM-7610F Scanning Electron Microscope (JEOL USA, Inc.) at 10 μ A at 10 kV.

5.3.6.5 *In vitro* & *in vivo* HG_gels degradation.

For *in vitro* HG_gel degradation tests, HG_gel (100 μ l) was treated with collagenase type II (1 U·ml⁻¹, Worthington Bio-chemical Corp., Freehold, NJ) and hyaluronidase (1 U·ml⁻¹, Sigma-Aldrich, St. Louis, MO) in PBS respectively. PBS with enzyme was daily changed, and the sample was collected, lyophilized, and weight at day 1, 2, 3, 5, 7 (n = 4). Control group was HG_gels with no enzyme. For *in vivo* HG_gel degradation test, HG_gel (100 μ l) was injected into mouse subcutaneous tissue. Each sample with skin tissue was collected at day 7, 14, 28, and analyzed with hematoxylin and eosin (H&E) staining.

5.3.7 Biocompatibility and tissue adhesiveness.

5.3.7.1 Live/Dead assay.

C2C12 cells were cultured on the hydrogel structures (regularly shaped in acrylate mold with 8 mm diameter and 3 mm thickness) in DMEM (HyClone, Logan, Utah, USA) containing 10wt% fetal bovine serum (FBS) (Biowest, Nuaille, France), 1 wt% L-glutamine (Gibco, Grand Island, NY, USA) and 1 wt% penicillin-streptomycin (Gibco). The medium was exchanged in every two days. The cell-laden hydrogel structures were stained with Live/Dead assay reagents (Invitrogen) to quantify cell viability followed by manufacturer's instructions. Briefly, cell-laden hydrogel structures were treated with 2 μ M ethidium homodimer-1 (EthD-1) and 4 μ M calcein AM in PBS for 30 minutes.

5.3.7.2 Synthesis of fluorescein isothiocyanate (FITC) conjugated gelatin.

The covalent bond between amine in gelatin and isothiocyanate group in FITC (Sigma-Aldrich) was produced under mild conditions. Briefly, 2.6 mmol of FITC in distilled water was added to 8 % (w/v) gelatin solution for overnight at RT. After dialysis and lyophilization, the FITC conjugated gelatin was collected.

5.3.7.3 Immunofluorescence assay.

After the 3 min of enzymatic crosslinking reaction with SA_{ty}, 200 μ L of HG_{gels} (with 0.3 M NaCl) was spread on a cover glass. A thin layer of HG_{gels} on a cover

glass was soaked in sterilized deionized water (300 mL) for overnight for diluting NaCl. And C2C12 cells were cultured in the hydrogel structures as stated above. After seven days, the cell-laden hydrogel structures were fixed in 4wt% paraformaldehyde for 24 h at 4°C and washed three times with PBS for 5 minutes each. The samples were then permeabilized with 1 % (w/v) bovine serum albumin (BSA) in PBS containing 0.1 % (w/v) Triton X- 100 for 45 minutes at RT. After blocking, the samples were incubated with Alexa Fluor 594 Phalloidin (1/200 dilution) overnight at 4°C and counterstained with DAPI (1/500 dilution) for 5 minutes at RT.

5.3.7.4 Adhesion test of HG_gel to mouse skin tissue *ex vivo*.

Tissue adhesion was evaluated in Demo Lab (Anton Paar Korea) using rheometer (MCR 302, Measuring cell: P-PTD & H-PTD 200, Measuring System: PP 25, Anton-Paar, Austria). A mouse skin tissue was attached to probe and hydrogel holder (diameter: 25 mm, 20mm respectively). The hydrogel (gelatin, HA_t, HG_sol, 500 µl) with SA_Tyr was applied to mouse skin tissue on the holder and crosslinked for 5 min, and pushed by tissue probe for 5 min with 0.5 mN of normal force. The probe then pulled with the rate of 50 µm / s and collected data.

5.3.7.5 Imaging HG_gels coated on Mouse Cardiac.

After preparing HG_gels solution as mentioned above, 2 ml of HG_gel solution was mounted on airbrush kit. We used FITC-conjugated gelatin instead of gelatin to visualize HG_gels. The hydrogel solution was then ejected to mouse cardiac

tissue treated with paraformaldehyde (PFA) through the spray nozzle. The HG_gel coated mouse cardiac was analyzed via UV lamp (excitation 488 nm) and histology. Briefly, the sample was immersed into 20 % (w/v) sucrose (Sigma-Aldrich) at 4 °C overnight and transferred to cryomold with optimal cutting temperature compounds (OCT; CellPath, Powys, UK) for rapid freezing. Specimens were sectioned into 20 µm thick and analyzed by microscope.

5.3.7 Statistical analysis

All data are presented as mean \pm standard deviation (SD). Statistical significance between groups was determined by Student's t-test with * $p < 0.05$, ** $p < 0.01$, *** $p < 0.005$.

5.4 Results and Discussion

5.4.1 Structure of tyrosinase from *Streptomyces avermitilis*

The differences in amino acid sequences between SA_Ty, BM_Ty, and AB_Ty indicates that Tys are evolved diversely (Table 5.2), and it was hypothesized that the primary reason for the different efficiency in crosslinking by the tyrosinases is due to the substrate specificity of the enzymes. As shown in Figure 5.2. SA_Ty is less sterically hindered than AB_Ty or BM_Ty (Figure 5.2). The length of the tunnel of BM_Ty (predicted by CAVER Analyst 1.0) (Chovancova, Pavelka et al. 2012) is shorter than of SA_Ty; however, the loops around the active sites may hinder the accessibility of the phenolic moieties of bulky polymeric backbones. Relatively flat surface around the entrance of the active site of SA_Ty is effective to bind to phenolic moieties of macromolecules. The depth of the entrance of SA_Ty is measured to be approximately 7.6 Å (the distance between the center of the hole of the entrance and the center of the two copper ions in the homology model).

In addition, the bottleneck radius of the tunnels (CAVER prediction) of SA_Ty is 2.34 Å, the biggest among the three. The shallow depth and wide radius of the predicted tunnels are good evidence to support the reason why SA_Ty is efficient for the crosslinking reaction of macromolecules if considering the length of the phenolic substrates, which is 6.5 Å (the distance between the oxygen atom and the alpha carbon of L-tyrosine). Whereas the active site of BM_Ty and AB_Ty is located in a deep tunnel within the enzymes. The depth is more than 10 Å, where the enzymatic reactions may sterically hinder due to long polymeric backbones.

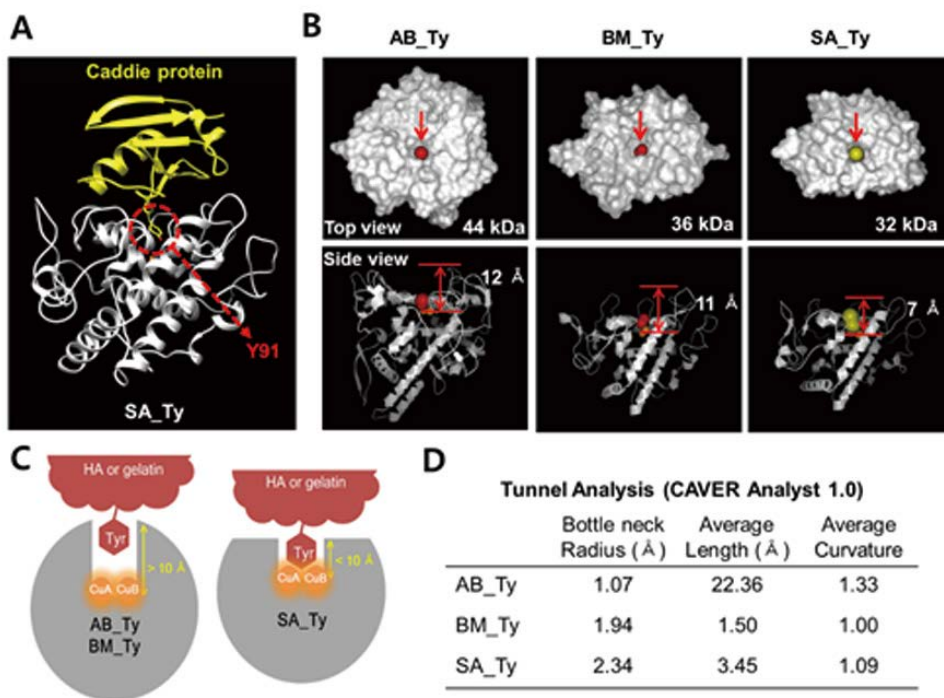


Figure 5.2. The structural comparison of tyrosinase from different organisms.

(A) A homology model of SA_Ty shows the tight interaction with the helper protein (B) The models of the active form of AB_Ty (4OUAa) and BM_Ty (3NM8a) were obtained from RCSB protein data bank. The distance between the center of the hole of the entrance and the center of the two copper ions in the visualized models by Chimera 1.11.2. (C) A schematic figure of tyrosinases. (D) The tunnel of active sites of Tys were analyzed by CAVER Analyst 1.02.

Table 5.2. Identity and similarity matrix generated by pairwise alignment.

(EMBOSS Needle, http://www.ebi.ac.uk/Tools/psa/emboss_needle/help/index-protein.html)

# of aa	identity(%) \ similarity (%)	AB_ty	BM_ty	SA_ty
576	AB_ty	-	24.6	20
297	BM_ty	16.2	-	54.3
274	SA_ty		39.7	-

5.4.2 The activities of tyrosinases from various organisms to macromolecules

The hypothesis, that the novel tyrosinase from *S. avermitilis*, SA_Ty, could be superior in terms of crosslinking macromolecules due to its flat surface, was well supported by comparing the initial rate of the oxidation reactions by the three purified tyrosinases on 100 μM of free L-tyrosine, 0.3 % (w/v) of gelatin (total 257 μM of tyrosine residues, type A, 300 g Bloom), and 0.2 % (w/v) of the tyramine-substituted hyaluronic acid (HA_t) (total 182 μM of phenolic groups, and the substitution of synthesized HA_t was confirmed by ^1H NMR and ultraviolet-visible (UV) spectrophotometry, Figure 5.4) (Figure 5.5). The initial rate, V_0 , of AB_Ty on gelatin was only $0.62 \pm 0.01 \mu\text{M}\cdot\text{min}^{-1}$ (Figure 5.6). (The concentration of monophenol moieties of the macromolecules were measured by UV spectrophotometry at 274nm where these measurements were scaled to make the molar extinction coefficient (ϵ) match the value of $1,405 \text{ M}^{-1}\cdot\text{cm}^{-1}$. And all the enzymes used in this measurement were purified, and the purity was confirmed by SDS-PAGE gel as shown in Figure 5.3)

This result can explain why the gelatin hydrogels catalyzed by AB_Ty were weak in the previous studies (Teixeira, Feijen et al. 2012, Le Thi, Lee et al. 2017). On the other hand, the V_0 of SA_Ty on the free L-tyrosine is slow, which is 6 times slower than AB_Ty, $7.94 \pm 0.25 \mu\text{M}\cdot\text{min}^{-1}$ but the activity was increased more than three times on gelatin and HA_t, $24.33 \pm 2.40 \mu\text{M}\cdot\text{min}^{-1}$ and $27.99 \pm 0.11 \mu\text{M}\cdot\text{min}^{-1}$, respectively (Figure 5.6).

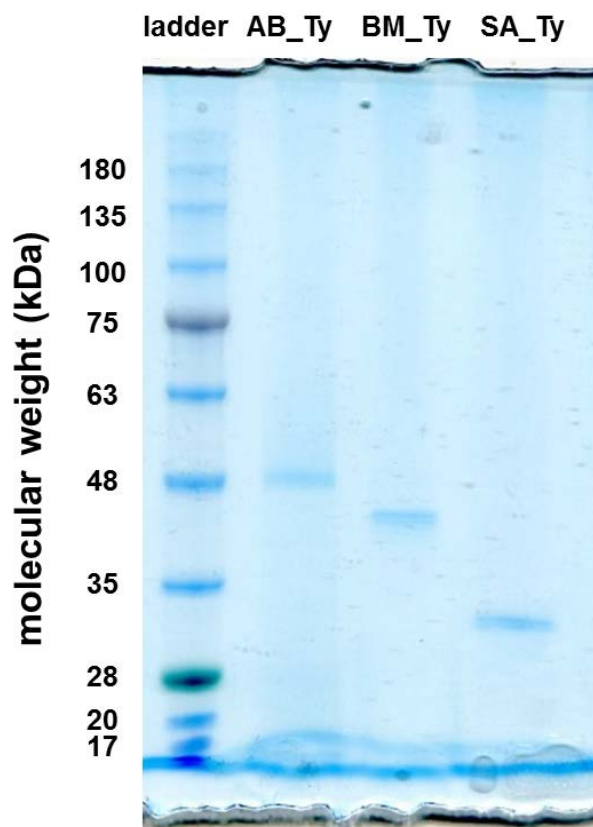


Figure 5.3. SDS-PAGE gel image of the purified tyrosinases.

The active form of AB_Ty was approximately 44kDa. The recombinantly expressed BM_Ty and SA_Ty was about 43 kDa and 33kDa, respectively.

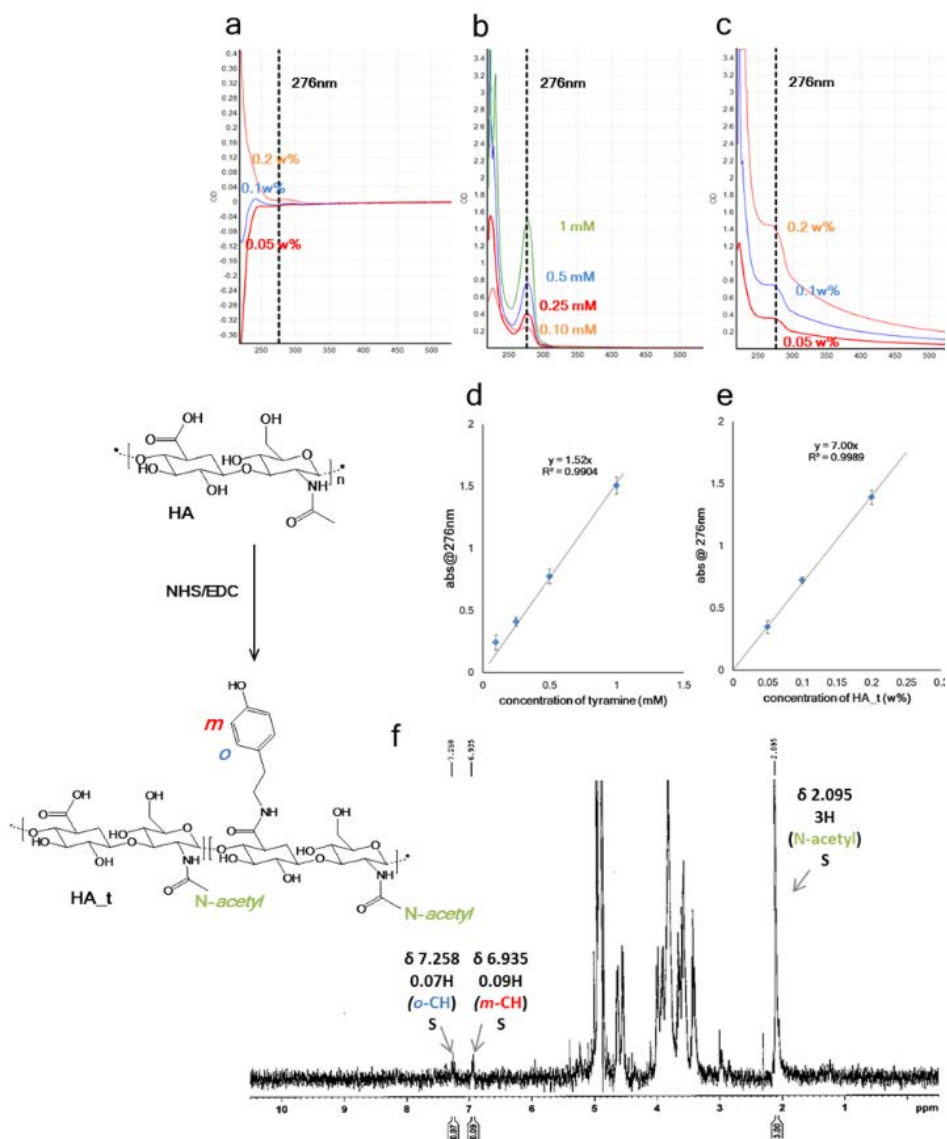


Figure 5.4. Detection of tyramine moiety on HA by UV spectroscopy and ¹H NMR.

(a) None substituted HA (1.01 - 1.80 MDa) was dissolved in 50 mM tris-HCl buffer at pH 8 (1 w%). The HA solution was diluted to 0.05 ~ 0.2 w% and loaded in a quartz cuvette (700 μ L of chamber volume; 1 cm of path length, 4science, Korea) for UV spectroscopy. No significant absorbance was detected. (b) Tyramine

hydrochloride was diluted to 0.1 ~ 1 mM, and the absorbances at 276nm were measured and plotted in (d) (The extinction coefficient of tyramine at 276 nm was $1.52 \text{ mM}^{-1}\cdot\text{cm}^{-1}$). (c) The HA_t solution was diluted to 0.05 ~ 0.2 w%, and the absorbances at 276nm were plotted (e). (f) Approximately 5 mg of HA_t was dissolved in 1mL of D₂O, and ¹H NMR spectra were measured at 400 MHz at 25°C. The ¹H NMR spectroscopic data were stated in ppm (δ) from the internal standard (TMS, 0.0 ppm). The peak at 2.095 ppm is due to the three Hs of the acetyl group of HA. Thus the integrated area of the peak was set as three Hs. The chemical shift of two H at the *ortho*-position appears around 7.258 ppm, and the two H at the *meta*-position appears around 6.935 ppm. Compared to the area of N-acetyl, the areas of Hs on tyramine were 0.07 and 0.09, respectively. Based on the integrated areas of Hs of the phenolic ring and N-acetyl group, the substitution rate of tyramine was calculated to be roughly 2.3~3.0%.

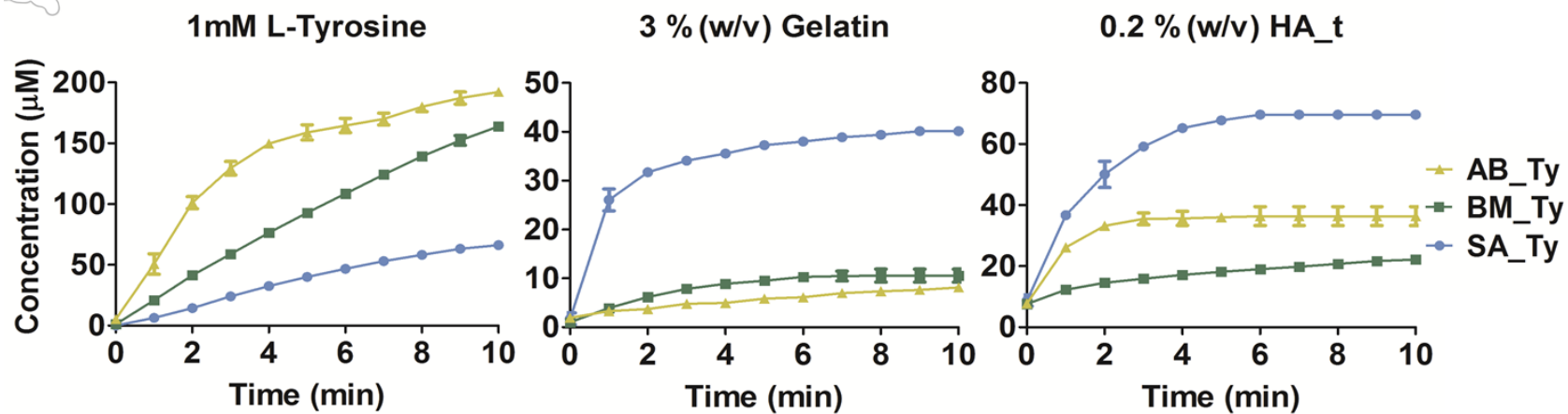


Figure 5.5. The reaction profiles of Tys on free tyrosine, gelatin, and HA_t.

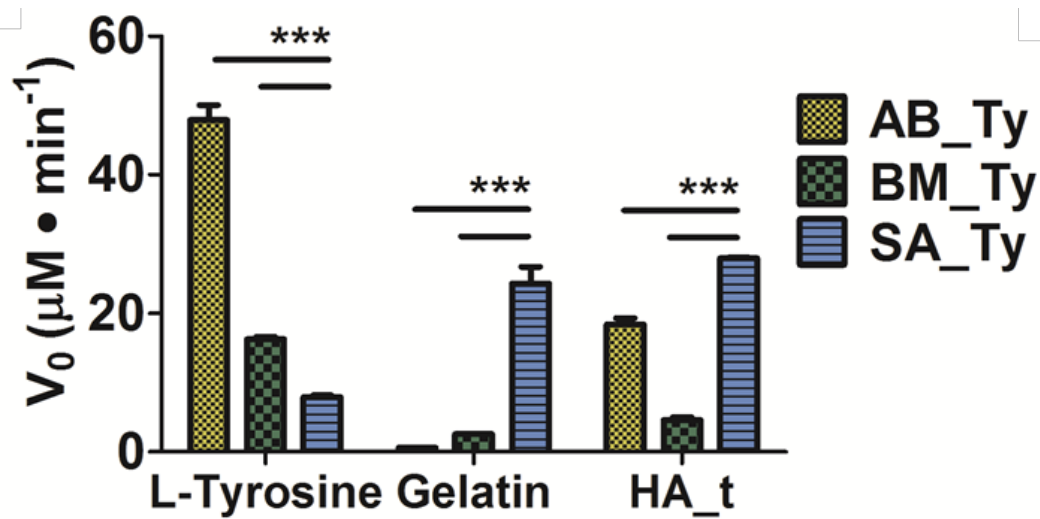


Figure 5.6. The initial oxidation rates of tyrosinase from three different organisms

5.4.3 Preparation of hydrogel

To apply the crosslinking ability of SA_Ty, the gelatin and HA_t mixture were further subjected to fabricating a biomimetic hydrogel with SA_Ty crosslinking. The final concentration of hydrogel and Ty in the reaction was all fixed in gelatin 3% (w/v) mixed with HA_t 1 % (w/v) (HG_sol), and 200 nM of the enzyme. The concentration of gelatin and HA_t was fixed at the stated concentration because the solution is easily controlled at such a concentration at room temperature (RT). Above that concentration, the solution was too viscous to pipet. When the materials were mixed according to the above composition, the solution state of the mixture, HG_sol, quickly became gelled (HG_gel). In only 30 s of the SA_Ty crosslinking reaction, 100 μ L of HG_sol gelled and did not flow down but remained intact on the cover of the 96-well plate, even when the plate had been flipped. At the same reaction time of 30 s, the color of the HG_sol crosslinked with AB_Ty changed to light brown due to oxidation, but it immediately flowed down when the plate was tilted. With relatively low concentrations (200 nM) compared to other Ty, SA_Ty easily oxidized phenolic groups in gelatin and HA_t to produce quinone groups as an advantage of its structure. Furthermore, these quinone groups coupled with each other formed polydopamine and amine and thiol groups in gelatin. So far, HG_sol mixed with SA_Ty turned to a gel state in a few seconds, and it took several hours in a sol-to-gel transition in the AB and BM_Ty groups since AB and BM_Ty has an inferior substrate specificity of the phenolic groups in macromolecules to SA_Ty.

The viscosity of the HG_gel after the addition of SA_Ty increased dramatically, and thus it was not possible to carry out pipetting (Figure 5.7). In addition, the HG_gel shaped after Ty crosslinking could not be made into its

desired shape. However, the viscosity of the HG_gel could be easily controlled by adjusting the ionic strength. By adding 0.3 M of NaCl in the HG_sol before the Ty reaction, the viscosity decreased to 0.66 Pa·s from 1.58 Pa·s (Figure 5.7). SA_Ty maintained its activity intact at 0.3 M of NaCl, and the HG_gel retained its shape as injected into phosphate buffered saline (PBS) since an excessive amount of NaCl can be easily diffused out. The HG_sol with SA_Ty turned into a gel state (HG_gel) instantly when injected into PBS through a 31 G syringe at RT (Figure 5.8, Video S1). The HG_gel injected in PBS stayed firm and was hard enough to be picked up by forceps. Interestingly, the HG_gel after SA_Ty crosslinking could be sprayed using a commercial airbrush with a nozzle diameter of 0.2 mm. Although the viscosity decreased with the salt, it was still sticky enough to coat a glass slide. The HG_sol with SA_Ty turned to aerosol through the airbrush, which has a higher surface area to volume ratio and reactivity than in the sol state. So far, the HG_sol immediately turned to HG_gel after spraying. After spraying HG_gel on the glass, the HG_gel was soaked in PBS to allow the diffusion of salt. Then, the thinly coated HG_gel could harden on the glass, which was then separated to form a thin elastic film (Figure 5.8, Video S2 & S3).

Furthermore, the sticky HG_gel was also applied as a spray coat on the surface of the mouse cardiac tissue. Before spraying, to visualize the coated hydrogel, we incorporated FITC to gelatin via EDC/NHS chemistry. The HG_gels were homogeneously coated onto the cardiac tissue. The spray process was simple when controlling and fast for deposition of the HG_gels on the surface due to the instant crosslinking by SA_Ty (Figure 5.8, d). It took only a few seconds to coat HG_gels all over the cardiac tissue. In the histological evaluation, the HG_gels were uniforml

y coated with a range of 10 to 13 μm (Figure 5.8, h). The thickness of the coated hydrogel could be regulated up to a few hundred μm by the number of times it had been sprayed. Moreover, the coated hydrogel adhered onto a superficial layer of cardiac tissue, and it would make the hydrogel stay as a thin film (Figure 5.8-h).

This simple fabrication method by injection and spraying, as shown in Figure 5.8, could imply it is a multipotent HG_gel as surgical glue and delivery carrier for biomedical and tissue engineering.

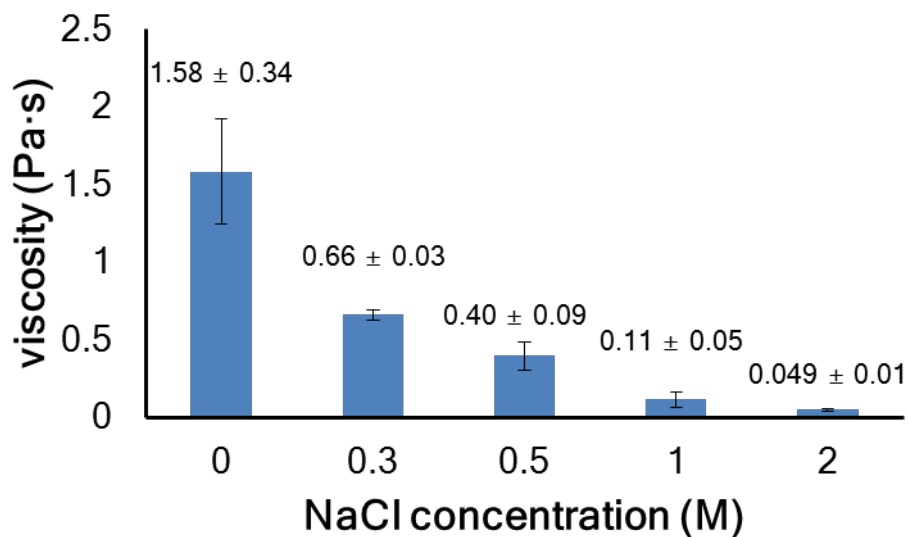


Figure 5.7. The changes in viscosity of HG_gel depending on the concentration of NaCl.

The viscosity of HG_gels after SA_tyr treatment depending on NaCl concentration was also measured by the ARES rheometer with 450 μM of gap and 100Hz of shear rate (the viscosity was monitored for 2 min with the fixed shear rate). All measurements were repeated three times.

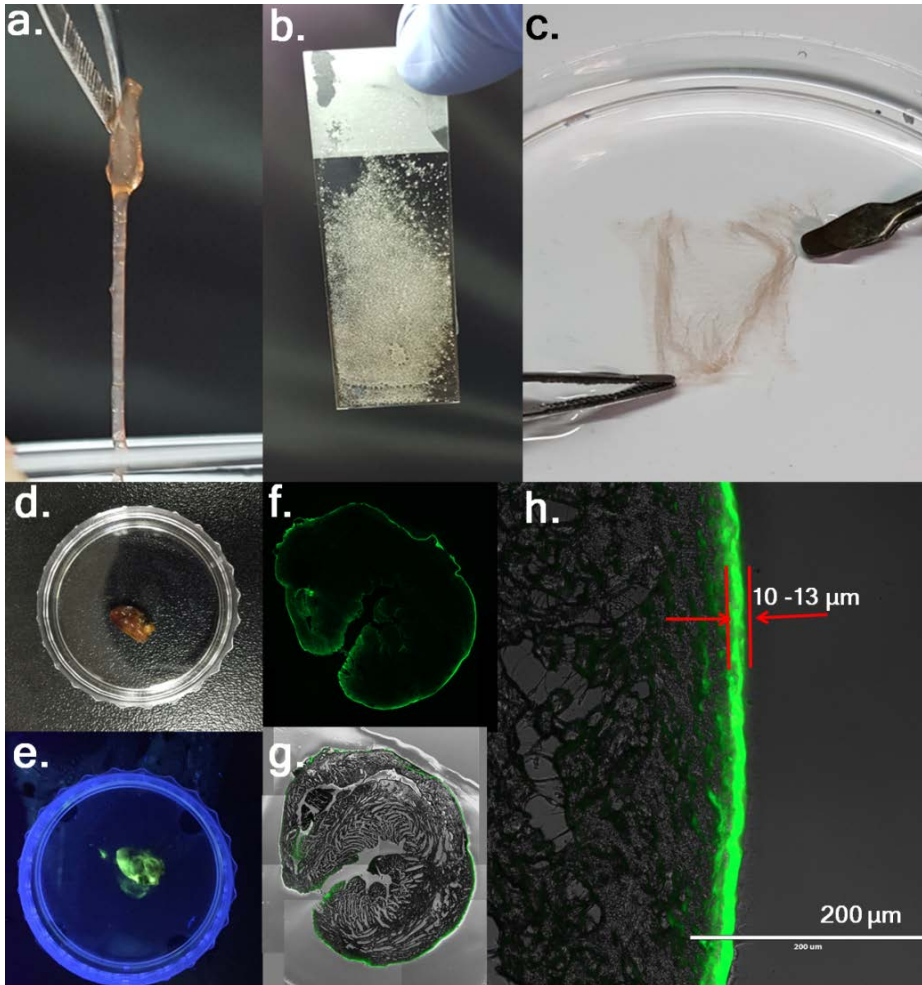


Figure 5.8. The images of HG_gel after injecting and spraying.

When HG_sol with SA_Ty was injected through 31 G needle into PBS (a) or sprayed via commercial airbrush onto slide glass (b) at RT, it turned to HG_gel immediately and stayed firmly in gel state. HG_gel fiber could be handled with forceps. (c) After diffusing NaCl out from the gel in buffered solution, an elastic thin film was made. (d-h) Images of HG_gel coating on mouse cardiac tissue *ex vivo*. The coated HG_gel (FITC tagged) was shown under 488 nm fluorescent lamp. (h) Cross section image of HG_gel coated cardiac tissue. HG_gel was coated homogeneously ranging from 10 – 13 μm .

5.4.4 Rheological studies of the cross-linked hydrogel

The reactivities of Tys on macromolecules were positively related to the mechanical properties of HG_gel. The storage modulus G' of HG_gel with BM_Ty is not distinguishable with G' of the control (Figure 5.9). HG_gels with AB_Ty showed 3.5 times increased G' and G' of the HG_gel with SA_Ty showed the highest modulus six times greater than controls. The enzymatic crosslinking of the 3 % (w/v) of gelatin solution by SA_Ty could increase the value of G' . Furthermore, we mentioned above, amine and thiol groups in gelatin would be crosslinked with tyrosine residues in HA via Michael-type additions. So, a significant synergistic effect was shown when the 1 % (w/v) of HA_t was mixed with the 3 % (w/v) of gelatin (Figure 5.9). The storage modulus G' and loss modulus G'' crossed over at 50 seconds with SA_Ty, and the sol-gel transition with AB, BM_Ty did not come within 200 seconds (Figure 5.10). The gelation time, the time at which G' and G'' intersect, showed an identical tendency when observed by plate tilting, as stated earlier.

5.4.5 Swelling and in vitro degrading properties

The swelling behavior of the HG_gel showed a reciprocal relation to mechanical properties (Figure 5.11-a). The swelling ratio of the HG_gel with AB, BM, SA_Ty showed 24.44, 34.77, and 7.52, respectively. In the SEM images, the HG_gel has a macroporous structure ranging from 200 μm to 500 μm (Figure 5.12). Furthermore, the in vitro degradation was examined in PBS in the presence of collagenase (1

$\text{U}\cdot\text{ml}^{-1}$), and hyaluronidase ($1 \text{ U}\cdot\text{ml}^{-1}$). The HG_gel gradually became degraded in both collagenase and hyaluronidase and eventually disappeared after a week (Figure 5.11-b).

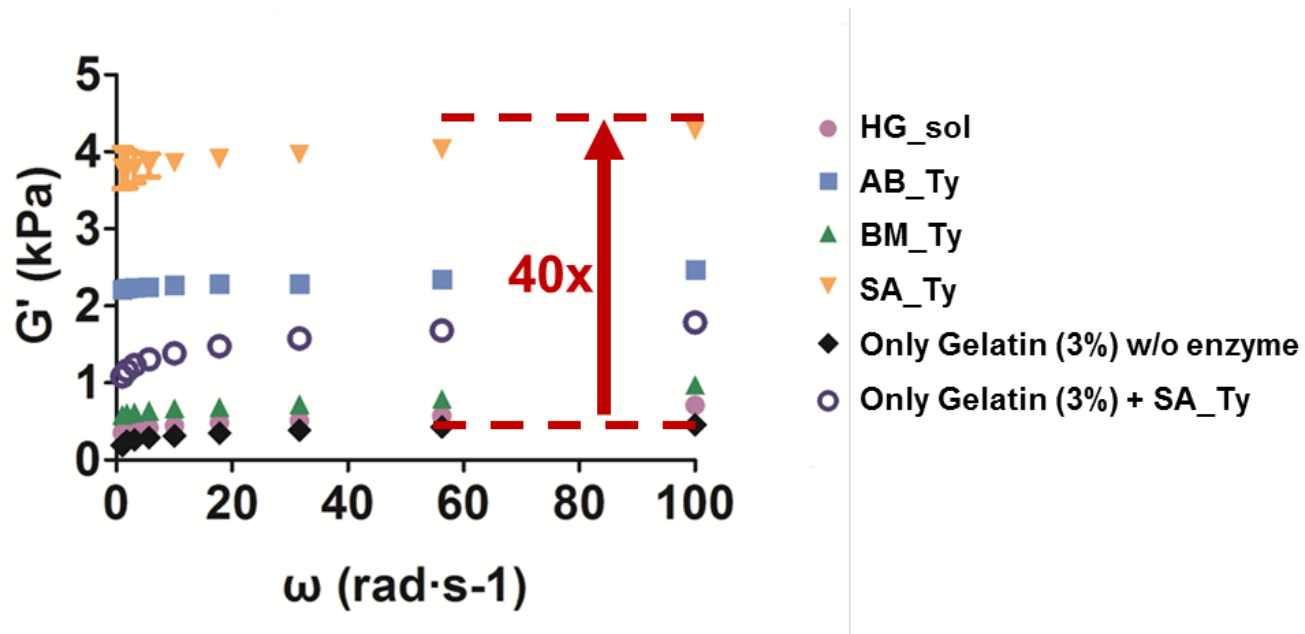


Figure 5.9. Storage modulus of gels w/ or w/o enzymatic crosslinking.

Significant improvement was observed in HG_gel with SA_Ty over 4 kPa ($n = 3$). The storage modulus increased 40 times. By the addition of *hyaluronic acid (HA), the modulus was increased twice, which indicates the mechanical properties is dependent to the density of crosslinkages. *Approximately 3% of carboxyl group of HA was substituted to tyramine.

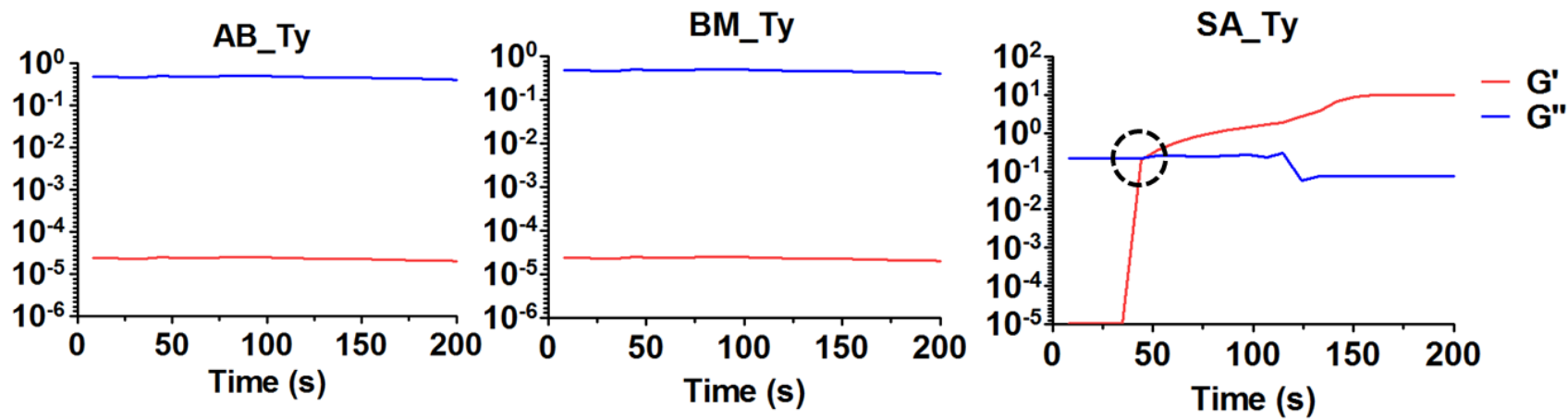


Figure 5.10. Gelation time measured by a rheometer.

When solution turned to gel state, the storage modulus (G') and loss modulus (G'') was crossover. With SA_Ty, HG_sol turned to gel within 50 s ($n = 3$).

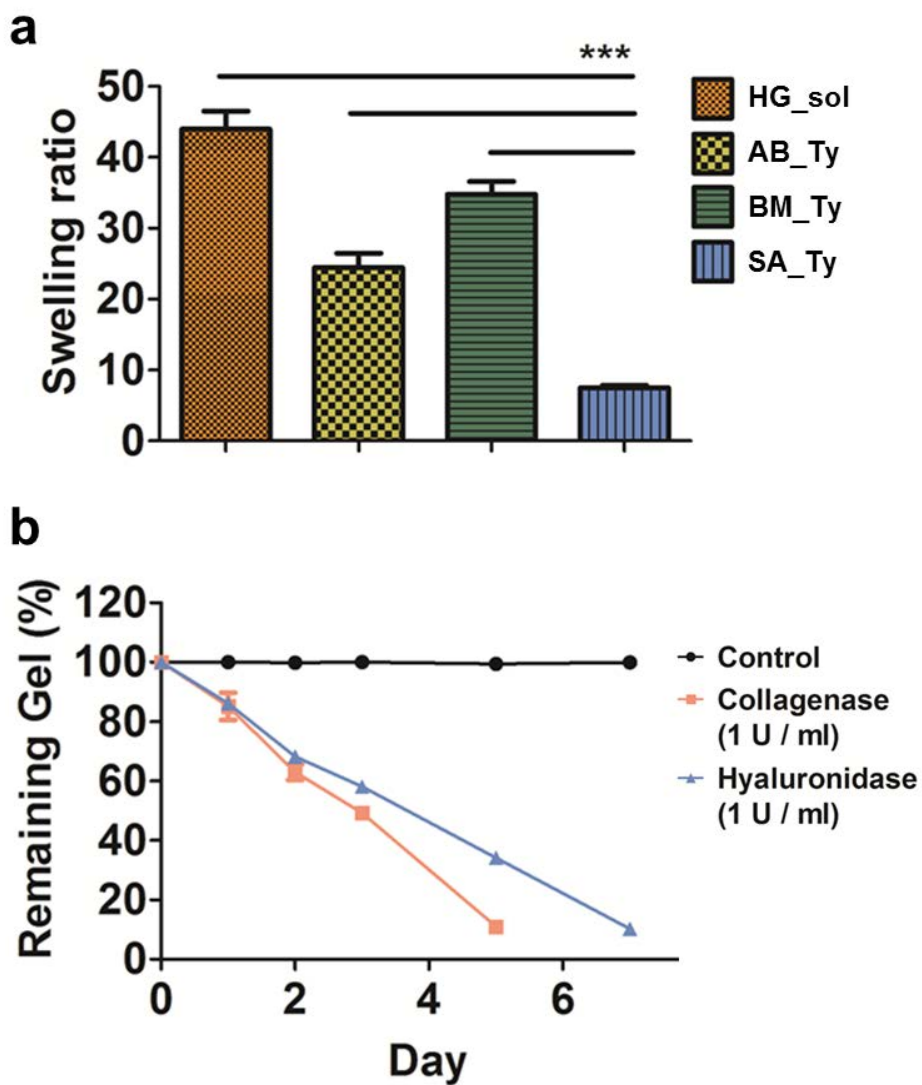


Figure 5.11. Swelling ratios of gels after crosslinking, and degrading rates of the gels.

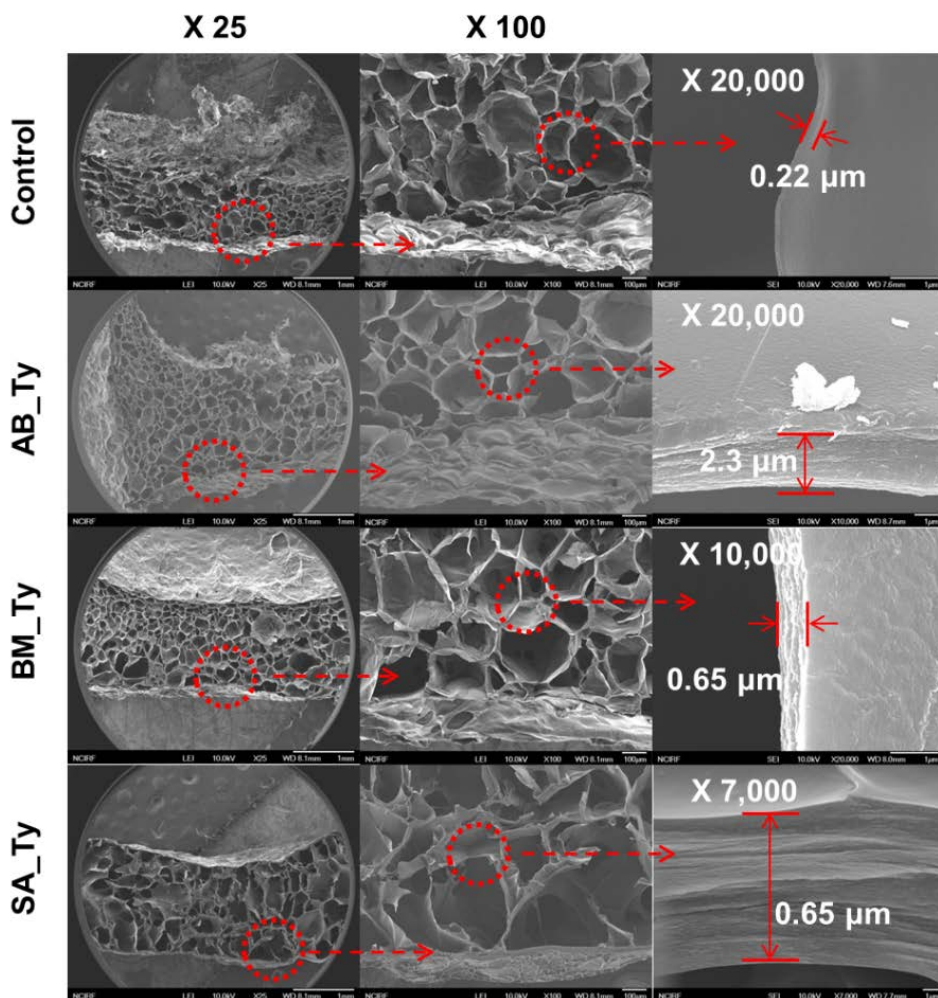


Figure 5.12. SEM images of HG_gel after tyrosinase crosslinking.

Scale bar: 1 mm (left), 100 μm (central), 1 μm (right)

5.4.6 The measurement of stickiness of HG_gel

In previous studies, the macromolecule with tyrosine residues was demonstrated to adhere to tissues after Ty reaction since the catechol quinones, oxidized from tyrosine, could form a covalent bond with thiol, amines, and other phenolic groups in native tissue (Ryu, Lee et al. 2011). To evaluate the tissue adhesion of the HG_gel, we performed a rheological tack test (Figure 5.13). The HG_gel showed tissue adhesive and ductile properties and was detached from the bottom of the mouse skin tissue after 750 s, pulling up to 37.5 mm (Figure 5.13, Video S4). Moreover, after the tack test, all of the HG_gel remained in the upper mouse skin tissue. However, the sole gelatin or HA_t, despite SA_Ty treatment, was easily detached after 120 s, pulling up to 1 mm (Figure 5.13). The adhesion work of gelatin and HA_t was 4.812 and 1.840 J·m⁻² respectively, whereas the HG_gel showed a significant increase of 21.34 J·m⁻². This is remarkable when compared to previously studied catechol-conjugated polymers, such as PAM – PAA (poly (N,N-dimethylacrylamine) with poly acrylamide) (Sudre, Olanier et al. 2012), methacrylic triblock copolymer (PMMA-PtBMA-PMMA) (Guvendiren, Messersmith et al. 2008), and poly ethylene glycol dimethacrylate (PEGDMA) (Chung, Glass et al. 2011), which have adhesion work in the range from 0.12 to 7 J·m⁻², and the well-known sticky proteins in nature, such as mussel foot proteins derived from *Mytilus californianus* and *Mytilus edulis*, have only 0.1 – 1.4 mJ·m⁻² of adhesion work (Lee, Messersmith et al. 2011). The increased storage energy in HG_gel might be due to the increased cohesive strength, the capability of the adhesive to resist rupture, after crosslinking.

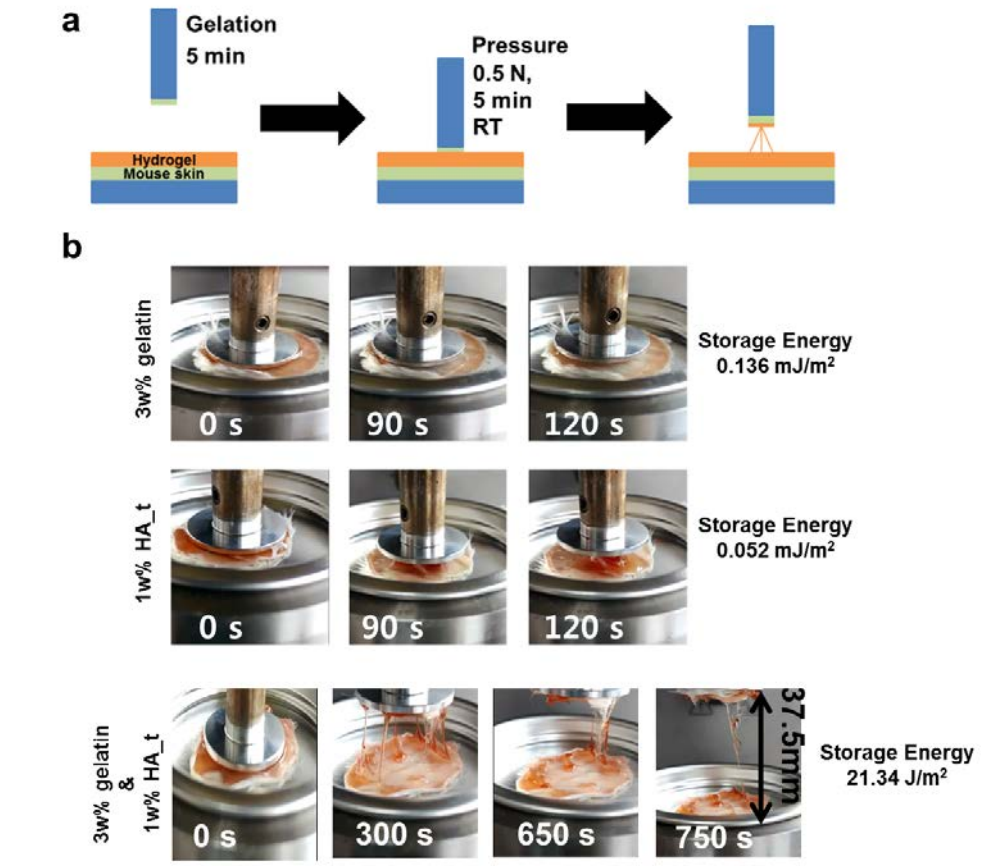


Figure 5.13. The tacking tests for measuring stickiness of gels.

(a) Schematic image of gel adhesion test to mouse skin. First, gel (500 μ l) was loaded onto hydrogel holder covered with mouse skin tissue (diameter: 25 mm) and crosslinked for 5 min. The probe with mouse skin (diameter: 20 mm) then pressured gel with 0.5 N normal force for 5 min and pulled up (rate: 50 μ m / s). (b) Image of adhesion test of gelatin 3 % (w/v) and HA_t 1 % (w/v).

5.4.7 Biocompatibility and the applications for organ coating

The HG gel supported cell growth and proliferation *in vitro* (Figure 5.14). To evaluate the *in vivo* degradation and biocompatibility, the HG_gel was injected into mouse subcutaneous space through a 31 G syringe needle. The samples were then collected and analyzed at days 7, 14, and 28 (Figure 5.15). At day 7, the fibroblast cells were infiltrated into the outer margins of the hydrogel, and the HG_gel maintained a structure without degradation. By day 14, a large number of cells infiltrated into the HG_gel, and the HG_gel has a smooth outer layer. After 28 days following the injection of the HG_gel, even though the cells were not infiltrated into the center of the HG_gel, the HG_gel had been partially replaced with vascularized connective tissue, and the outer layer of the HG_gel became rough. There was no evidence of inflammation, such as monocyte and macrophage in the peri-implant tissue, over all experiments. In general, the implanted hydrogel recruited inflammatory cells, and a foreign body reaction occurred. The peri-implant tissue then became fully degraded or replaced with connective tissue according to the cell-mediated hydrogel clearance (Anderson, Rodriguez et al. 2008). However, the HG_gel is composed of ECM derived materials and its coupling agents, SA_Ty, also an enzyme found in most living organisms. In this regard, the HG_gel was reduced and avoided inflammatory reaction and recruited native cells.

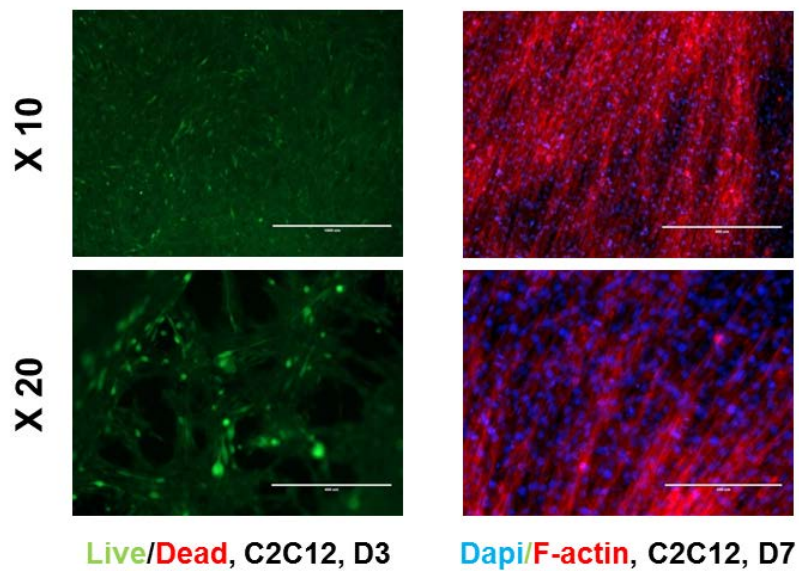


Figure 5.14. Biocompatibility test of HG_gel.

C2C12 cells were cultured onto HG_gel and performed Live / Dead assay at day 3 and F-actin staining at day 7 (counter staining: Dapi) (Scale bar: 500 μm (X 10), 200 μm (X 20)).

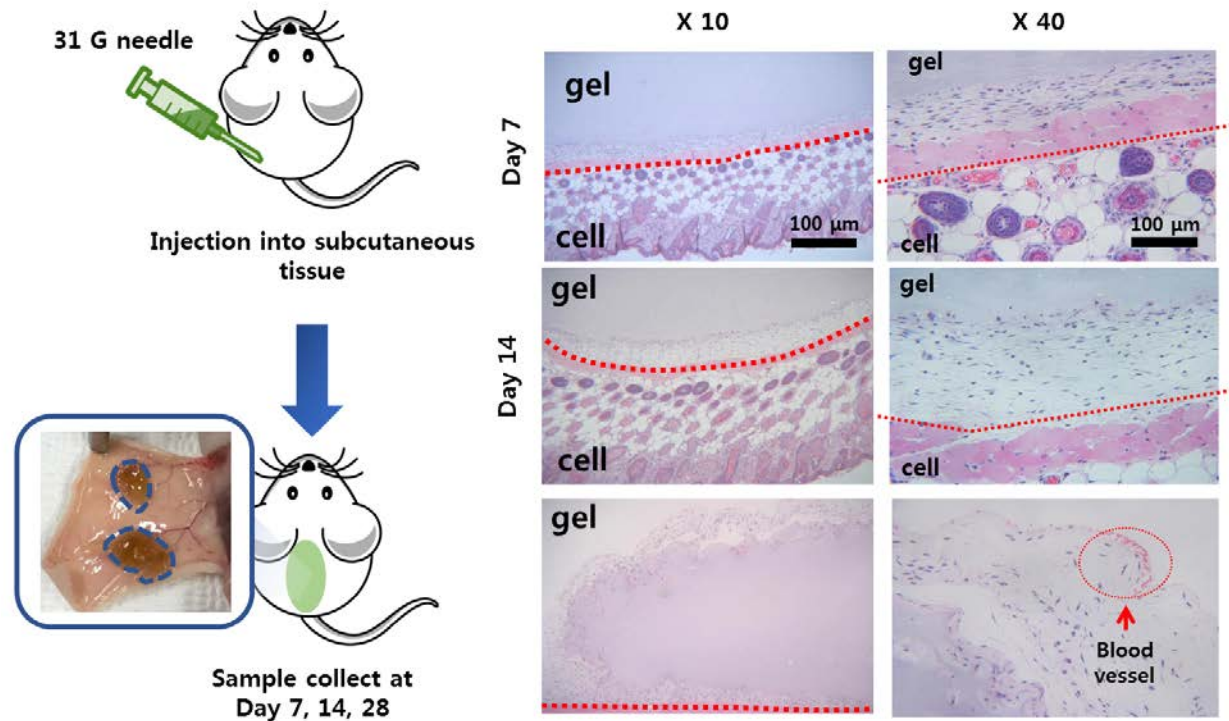


Figure 5.15. Histological evaluation of in vivo degradation and stability of HG_gel.

HG_gel (100 μ l) was injected into mouse subcutaneous tissue using 31 G needle and harvested at day 3, 7, 14, 28. H&E staining image was cross section of HG_gel integrated with native skin.

5.4.8 List of supplementary videos (Links to Google Drive)

Video S1. Injectable HG_gel. The video is available at a link below

<https://drive.google.com/open?id=0B72Kp6enpyKjUI9WN0RKejd2SDA>

Video S2. Sprayable HG_gel with a commercial airbrush. The video is available at a link below

<https://drive.google.com/open?id=0B72Kp6enpyKjX1NvR3V4UIA2WjQ>

Video S3. Detached HG_gel after spraying onto a slide glass. The video is available at a link below

<https://drive.google.com/open?id=0B72Kp6enpyKjOWsxUFILOFZFcjg>

Video S4. Adhesion test of HG_gel (speed: 16 X). The video is available at a link below

<https://drive.google.com/open?id=0B72Kp6enpyKjcFV5RmUwLTThhM0k>

5.5 Conclusion

In conclusion, we utilized a novel Ty from *S. avermiltillis* which has a proper structure to oxidize phenolic groups on macromolecules instantly, and it allows the gelatin-HA based system to be crosslinked for injectable or sprayable use. The structure of the SA_Ty, with a flat, wide and shallow entrance to the active site when compared to other tyrosinases from mushroom or *Bacillus*, broadens the substrate specificity and enhances the activity of SA_Ty on the macromolecules. SA_Ty successfully accelerated the HG_gel hardening within 30 seconds through a permanent covalent bond between the catecholquinone and amine, thiol, and other phenolic groups. The SA_Ty endowed HG_gel with high mechanical properties and tissue adhesive function. This strategy to form fast injectable/sprayable hydrogels was widely applicable to in situ hydrogels, incorporating phenolic groups in a biopolymer. In addition, the HG_gel could be developed as a robust tool for surgical glue and localized delivery of cells or biomacromolecules, with the advantage of a tissue adhesive and cell recruiting function in vivo. The HG_gel was demonstrated to be homogeneously coated on mouse cardiac tissue ex vivo through a commercial airbrush, and it has 10 ~ 13 μm of thickness with a short jetting. It stayed firmly due to its adhesive properties. Overall, the tissue adhesive, injectable and sprayable hydrogel with a newly developed Ty offers robust potential to develop surgical glue and delivery carrier in the field of biomedical and tissue engineering.

Chapter 6.

Designing elastin-like polypeptide for introducing functionalities into ECM hydrogels

6.1 Abstract

A set of elastin-like polypeptides (ELPs) was expressed and purified to emulate the tyrosinase-mediated covalent bonds between ELPs and/or biomaterials used in Chapter 5, such as gelatin, and tyramine-conjugated hyaluronic acid. Specifically, the goals of our protein design were, first, to generate ELPs that would have covalent bonds crosslinked by tyrosinase in the possible ELP body–ELP body and ELP body–other macromolecules, and, second, to create ELPs that would have interfacial interactions by binding to reduced graphene oxide (rGO). Firstly, the modification of the guest residue in the body part of ELP, the degree of crosslinkage of hydrogel was increased. After incorporating Tyr residue in the body part of ELP, the ELP, VY12V20NNCN, which contains 5 mol% of Tyr residues, increased the degree of crosslinkages of HG_gel made by gelatin and tyramine-conjugated hyaluronic acid, and as a result, the mechanical strength (G') of the gel was significantly increased. Furthermore, it was shown that the Tyr residue introduced into the ELP body could be hydroxylated to sticky DOPA residue by the simple enzymatic treatment. Secondly, introducing a functionality, a graphene binding sequences, at the C-term of ELP could offer the conductivity to the hydrogel by incorporating the nature of graphene. Through this study, the great potent of ELP was demonstrated by showing that the ELPs can be used as an crucial factor for offering functionality in ECM hydrogel along with more density of crosslinkages.

Keywords: Elastin-like polypeptide, reduced graphene oxide, ELP hydrogel

6.2 Introduction

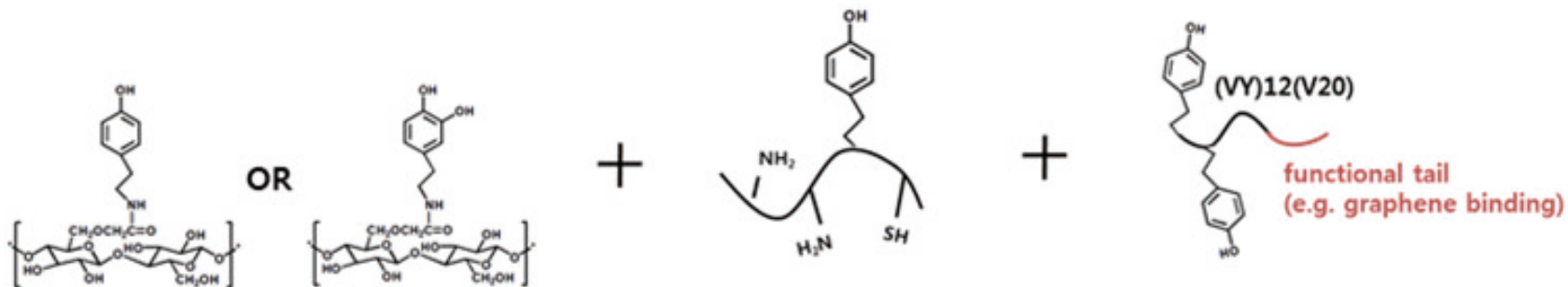
Elastin-like polypeptide (ELP) is an artificial peptide designed, being modeled after the tropoelastin of mammals. A part of the tropoelastin is composed of a repeated sequence of (VPGVG)_n. The artificial ELP takes the repeating sequences with a guest residue at the 4th position of its basic pentapeptide sequence. So, the general sequence for the ELP is (VPGXG)_n, where X is called the guest residue. In Chapter 5, a simple method for fabricating a sticky hydrogel composed of gelatin and tyramine-conjugated hyaluronic acid was presented, and the hydrogel after crosslinking by SA_Ty showed the improved mechanical properties. This study has been further developed to give functionality to the existing fabrication method for the sticky hydrogel present in Chapter 5 by the addition of ELP that contains tyrosine residue and a functional group in its tail part, C-term of the sequence.

The brief schematic figure is in Figure 6-1. The modified carbohydrate and gelatin were the materials subjected in Chapter 5. To remind again, briefly, polysaccharides, such as chitosan and cellulose, are robust and have great ability to hold water molecules, which is important in making hydrogels. Gelatin, a hydrolyzed collagen, has flexibility and elasticity that sugar does not have so that it can compensate for the lack of such properties of the carbohydrate. The two materials are fascinating in terms of supporting the structure against the force exerted by cells when proliferating and migrating. However, the two substances are not suitable for imparting functionality to the gel because it is impossible to make fine-tuning works.

On the other hand, ELP can be genetically designed at the DNA level, and

thus, head (N-term), guest residues, tail (C-term), and the length of the protein could be precisely adjustable. Moreover, its nature of inverse transition states depending on temperature is a unique feature, and it makes the purification process very simple. The general process of purification is called, “inverse transition cycle (ITC),” and the simplified procedure is illustrated in Figure 6.3. ELP is soluble below a melting temperature and precipitated above the melting temperature, which is inverse, when comparing to other substances. The transition states of the ELP is changed at $T_m \pm 1^\circ\text{C}$. It is because of the residues are highly hydrophobic. As the movement of water and hydrophilic attack get stronger, the tendency of aggregation due to hydrophobic intra-interaction get stronger as well.

By using the properties of ELP, tremendous studies relating ELP hydrogels or hybrid materials of inorganic materials and ELP were reported previously. However, none of studies offer the method for making ELP hydrogel crosslinked by tyrosinase. In this study, Tyr residues were introduced as a guest residue for increasing the crosslinking density, and a functionality such as graphene binding was introduced in the tail part of the ELP with an expectation that the newly designed ELP can improve the mechanical properties of hydrogel (like resilin, an elastic protein found in insects which naturally has di- or tri-tyrosine linkages), and could offer a functionality to hydrogel.



Modified Carbohydrate

- Robustness
- Hydrogen bonds for holding water

Gelatin

- Elasticity
- Cell bindings sites

ELP with functional tail

- More crosslinkages
- Elasticity
- Functional tale
- Genetical modification

Figure 6.1. The schematic figure of three building blocks of fabricating functional hydrogel.

6.3 Materials and Methods

6.3.1 Nomenclature

The ELP body were composed of repeating sequences of the form $[(VPGVG)_l(VPGXG)_m(VPGVG)_n]_k$ where X was either valine (V) and tyrosine (Y) in this study. “l, m, n” is the number of repeats, and “k” is total pentapeptide numbers. The backbones were named after the one letter amino acid code corresponding to the X position followed by the number of elastin-like pentapeptides in the sequence. For example, VY10 corresponds to the sequence $[(VPGVG)(VPGYG)]_5$. The names and the corresponding sequences constructed in this study are listed in Table 6.2. The method for designing ELP was reprinted from a previous article with permission for this thesis (Wang, Lee et al. 2011)

6.3.2 Construction of plasmids for expressing ELPs

Cloning was performed in *E. coli* DH5a. DNA sequences corresponding to the sequences for VV, VY, and YV were created by annealing and ligation of synthetic oligonucleotides listed in Table 6.1. The oligonucleotides were ligated into a pJ54 derived vector (DNA 2.0, Menlo Park, CA), prepared by digestion with *Bam*HI and *Bsa*I or *Bpi*I and *Bsa*I. In a typical round of cloning, the ELP insert was prepared by digestion with *Bam*HI and *Bsa*I and the ELP vector was prepared with *Bam*HI and *Bsa*I. The products were ligated by T4 DNA Ligase and transformed into *E. coli*. Cloning rounds were repeated until the target sequences were generated. The

ELP sequences were transferred into Eco31I digested, modified pET28a containing specific N-terminal and C-terminal DNA sequences such as NN, CN, and CGo listed in Table 6.1. The modified vectors were created by ligation of oligonucleotides into NcoI and *Bam*HI digested pET28a. All enzymes used in this study were purchased from Thermo Scientific. But FastDigest restriction enzyme was not used because of its instability for usages, especially BsaI and BpiI. Normal restriction enzyme worked greatly for this study.

Table 6.1. Primer list for N-term head and C-term tail groups of ELP

Primer name	Sequences 5'→3'
NN4_F	CATGAGCGGCGTTGGCGTCCTGAGACC
NN4_R	GTGACCAGTGGGTCTCAGGACGCCAACGCCGCT
CN4_F	CACTGGTCACGGTCTCGGTCCCGGGTTAATAA
CN4_R	GATCTTATTAACCCGGGACCGAGACC
CGo_F	CATGAGCGGCGTTGGCGTCCTGAGACC
CGo_R	GTGACCAGTGGGTCTCAGGACGCCAACGCCGCT
VV_F	GTCCCAGGTGTGGGCGTACCGGGCGTTGGT
VV_R	GGACACCAACGCCCGGTACGCCACACCTG
YV_F	GTCCCAGGTGTGGGCGTACCGGGCGTTGGT
YV_R	GGACGCCAACGCCAGGAACGCCGTAACCCG
VY_F	GTCCCAGGTGTGGGCGTGCCGGGTACGGC
VY_R	GGACGCCGTAACCCGGCACGCCACACCCG

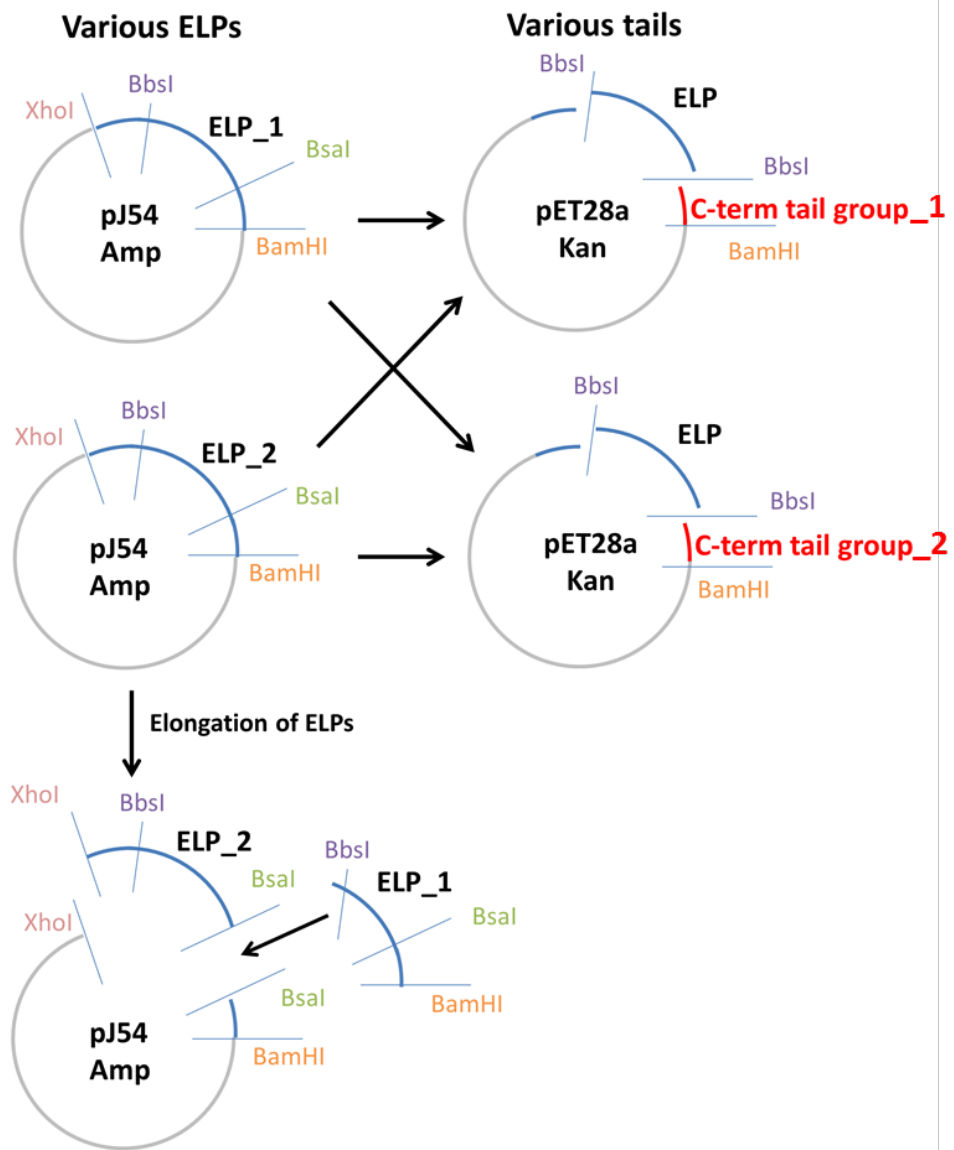


Figure 6.2. Schematic figure of constructing plasmid for ELP elongation and C-term tail group.

6.3.3 Expression of ELP in *E. coli* and purification by ITC

The expression method was followed as previously reported with minor modification (Wang, Lee et al. 2011), and the method for expressing ELP was reprinted from a previous article with permission for this thesis (Wang, Lee et al. 2011). The ELP plasmids were transformed into *E. coli* BL21 (DE3) for expression. ELP expression was performed in a flask of Terrific Broth supplemented with 30 $\mu\text{g}\cdot\text{mL}^{-1}$ kanamycin with shaking at 225 rpm and 37 °C for 24 h. The cells were isolated by centrifugation, resuspended in 10 mM Tris-Cl, 2 mM EDTA, pH 8.0 and lysed by ultra-sonication. The cell lysate was centrifuged at $30000 \times g$ for 30 min and the soluble fraction was mixed with poly(ethlyeneimine) (PEI $M_w \sim 750000$, Sigma-Aldrich) to form a 0.5% PEI solution. The PEI solution was centrifuged at $20000 \times g$ for 15 min and the supernatant was subjected to 3–4 rounds of inverse transition cycling for purification. NaCl or ammonium sulfate was used as the precipitating salt and resuspension was performed in distilled water, during each round. The proteins were dialyzed into deionized water then lyophilized.

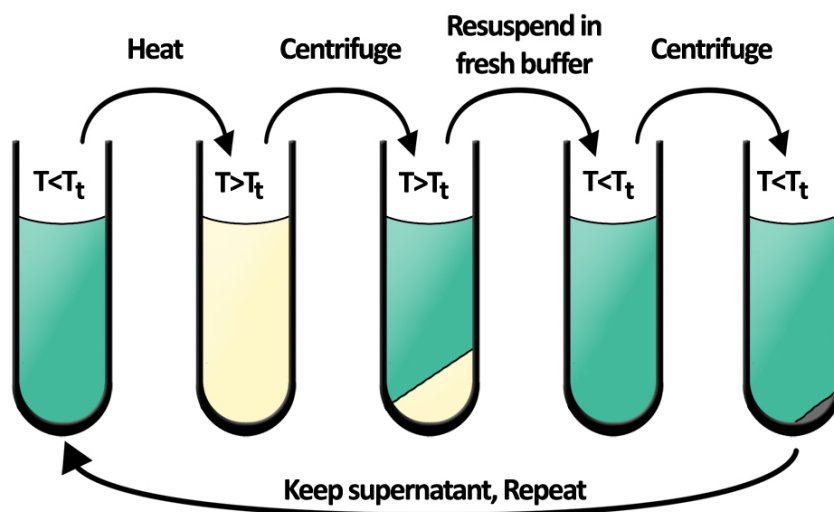


Figure 6.3. Schematic figure of inverse transition cycling for purifying ELPs

By using the reversible transition of ELP as temperature changes. The inverse transition cycling in short, ITC is a simple method for purifying ELPs. The figure was illustrated by Eddie Wang

6.3.4 Preparation of the ECM hydrogel, HGE_gel (HG_gel + ELP)

The procedure of preparing HGE_gel was followed as the method for preparing HG_gel as stated in Chapter 5. Briefly, HA_t 1wt% was dissolved in buffer (50 mM tris-HCl buffer at pH 8 for BM_Ty and SA_Ty; 50 mM sodium phosphate buffer at pH 7 for AB_Ty) at 40°C, and gelatin powder 3wt% was added to the HA_t solution. After totally dissolved at 40°C water bath and sterilized by the syringe-driven filtration, purified tyrosine (also sterilized by filtration) was added to the mixture to initiate the enzymatic crosslinking of the macromolecules. And then the temperature was cooled down to 18°C. After cooling down the temperature, ELP was added. The solutions were simply vortexed for homogeneous mixing, and then the reaction tubes were incubated at 18°C for overnight.

6.3.5 Hydroxylation of Tyr residue of VY24V20

The purified ELP was dissolved in 500 mM boric acid at pH 9 at ice-cold water bath, and 50 mM of L-ascorbic acid was added in the solution. 200 nM of SA_Ty was added and incubated at 18°C for overnight. After the reaction, 50 mM of EDTA solution was added for stopping the reaction. The solution was placed in a dialysis tubing and all the salt used in this reaction was changed to distilled water for three days in a cold room. After dialysis, the modified ELP was lyophilized. The modification was confirmed by the color change of ELP solution in the

presence of ferric ions depending on pH.

6.3.6 Preparation of mussel mimicking ELP hydrogel

The lyophilized ELP (2w/w%) was dissolved in distilled water, and 1 mM of ferric ions were added in the solution. And the pH was adjusted by adding 6M of NaOH or 35% HCl.

6.3.7 Synthesis of reduced graphene oxide (rGO)

The procedure for synthesis of reduced graphene oxide was followed as previously reported (Abdolhosseinzadeh, Asgharzadeh et al. 2015). The size of graphite was 325 mesh, which is equivalent to approximately 40 μM . Briefly, 1 g of graphite flakes was added to 50 mL concentrated sulfuric acid while stirring in an ice-water bath. 3 g potassium permanganate was gradually added by maintaining the temperature at ice bath. Then, the suspension was stirred at room temperature for 25 min followed by 5 min sonication in an ultrasonic bath. After repeating the stirring-sonication process for 12 times, the reaction was quenched by the addition of 200 mL distilled water. An extra 2h ultrasonic treatment was carried out. After adjusting the pH at ~6 by the addition of 1M sodium hydroxide solution, the suspension was further sonicated for 1 h. 10 g L-ascorbic acid was dissolved in

100 mL distilled water and then was slowly added to the exfoliated graphite oxide suspension at room temperature. The reduction was performed at 95 °C for 1 h. The resultant black precipitates were simply filtered by cellulose filter paper and further were washed with a 1M hydrochloric acid solution and distilled water to neutral pH. Finally, the filtrate was freeze-dried to obtain rGO powder.

6.3.8 Preparation of rGO hydrogel and a thin rGO film.

The total of 2 mg·ml⁻¹ of each rGO and VY24V20NNCN was mixed and dissolved in distilled water. And the solution was placed in a refrigerator overnight. The unbinding rGO particle was removed by pipetting supernatant to transfer it to a clean tube. The supernatant (rGO bound to ELP) was also insoluble but homogeneously dispersed in solution. The supernatant was placed in 30°C, and let it precipitate again. And at this time, the precipitate was collected for removing unbinding ELP dissolved in supernatant. This repeated twice for removing both unbinding proteins and rGO particles. After the washing the rGO-ELP composite, the rGO-ELP was lyophilized and redissolved in a cold 50 mM tris-HCl buffer at pH 8. And tyrosinase reaction was performed at 18°C for overnight. After the reaction, the rGO-ELP composite became aggregated and lumped in one piece.

6.4 Results and Discussion

6.4.1 Expression and purification of ELPs.

A set of elastin-like polypeptides (Table 6.2) was synthesized to emulate the covalent bonds between ELPs and/or the materials used in Chapter 5 such as gelatin, and tyramine-conjugated hyaluronic acid. Specifically, the goals of our protein design were, first, to generate ELPs that would have covalent bonds crosslinked by tyrosinase in the possible ELP body–ELP body and ELP body–other macromolecule and, second, to create ELPs that would have interfacial interactions by binding to reduced graphene oxide (rGO). To generate synthetic proteins with the desired interactions, a series of ELP genes were synthesized via a seamless, iterative cloning method that is akin to previously implemented techniques as shown in Figure 6.2 and Figure 6.3 (Wang, Lee et al. 2011). The ELP body sequences were transferred to expression vectors containing the desired N- and C-terminal sequences in-frame. The proteins were expressed, purified via the ITC method (Figure 6.3) and purified. The ELPs purified for this study was listed in Table 6.2.

VY24V20NNCN and VY24V20NNCGo were successfully expressed in *E. coli*. The T_m of both ELPs was 16°C, indicating the tail part, the graphene binding sequences does not affect the T_m of ELP. The both ELP contains only 5 mol% of Tyr residues. However, the hydrophobic guest residues in X position results in lowering transition temperature and may negatively affect to the solubility of ELPs when changed to a tyrosine residue. Thus, more concentration of tyrosine residue in the ELP was impossible. In addition, increasing ELP length, n , also results in

lowering transition temperature, and may negatively affect to the solubility of ELPs. ELP and gelatin should stay in the same gel phase for maximizing the mechanical strength.

Table 6.2. The list of ELPs expressed and purified in this study

ELP body	# of AAs	Sequence of amino acid	mol%
V60	300	(VPG <u>V</u> G) ₆₀	-
V120	600	(VPG <u>V</u> G) ₁₂₀	-
Y60	300	(VPG <u>Y</u> G) ₆₀	Y, 20%
V20Y24V20	320	(VPG <u>V</u> G) ₂₀ (VPG <u>Y</u> G) ₂₄ (VPG <u>V</u> G) ₂₀	Y, 7.5%
VY24V20	220	(VPGVGVPG <u>Y</u> G) ₁₂ (VPG <u>V</u> G) ₂₀	Y, 5%
Tails	# of AAs	Sequence of amino acid	
NNCN	11	MSGVG^ <u>ELP-BODY</u> ^VPGVG_	
NNCGo	12	MSGVG^ <u>ELP-BODY</u> ^EPLQLKM_	

6.4.2 VY24V20 as a crosslinker of ECM hydrogel, HG_gel

ELPs synthesized and expressed for this study are listed in Table 6.2. Tyr residues are inserted in the position of guest residue for having crosslinkages within ELPs or with gelatin and other polymers so that the ELPs stay stable in the hydrogel. Also, more degree of crosslinking can be allowed by Tyr residues introduced in the body part of ELP, and this dense crosslinking could improve the mechanical property of the hydrogel.

After incorporating ELP, VY12V20NNCN, into gelatin and hyaluronic acid, the mechanical strength of the gel was measured by rheometer. The addition of 0.05 w% ELP with 5 mol % Y guest residues increase storage module to 6 kPa which is three times higher than control. However, more than 0.1 w% of ELPs negatively affected the storage moduli of the hydrogels (Figure 6.4). It was because of that ELP that are not crosslinked with other material could negatively affect to the lattice of the whole material. The unbound ELP or ELP inclusions crosslinked itself could be impurity point defects as not homogeneously mixed with other material. This may cause the formation of pores, cracks, phase separation because the immiscible ELP can be foreign inclusions. Thus, the optimal concentration of guest residues and other macromolecules should be drawn and used for the further applicational studies.

Unfortunately, the ELP with 20 mol % of Tyr residues was not purified by ITC. Currently, the purification method is being optimized by addition of surfactant during the purification. The hydrophobic guest residues in X position results in lowering transition temperature and may negatively affect to the solubility of ELPs

when changed to a tyrosine residue. Thus, more concentration of tyrosine residue in the ELP was problematic. In addition, increasing ELP length, n , also results in lowering transition temperature, and may negatively affect to the solubility of ELPs. ELP and gelatin should stay in the same gel phase for maximizing the mechanical strength. The melting temperature of ELP and the mechanical strength could not be estimated by its sequences. Therefore, design of various ELPs, the actual synthesis and characterizations should be carried out to finish this project.

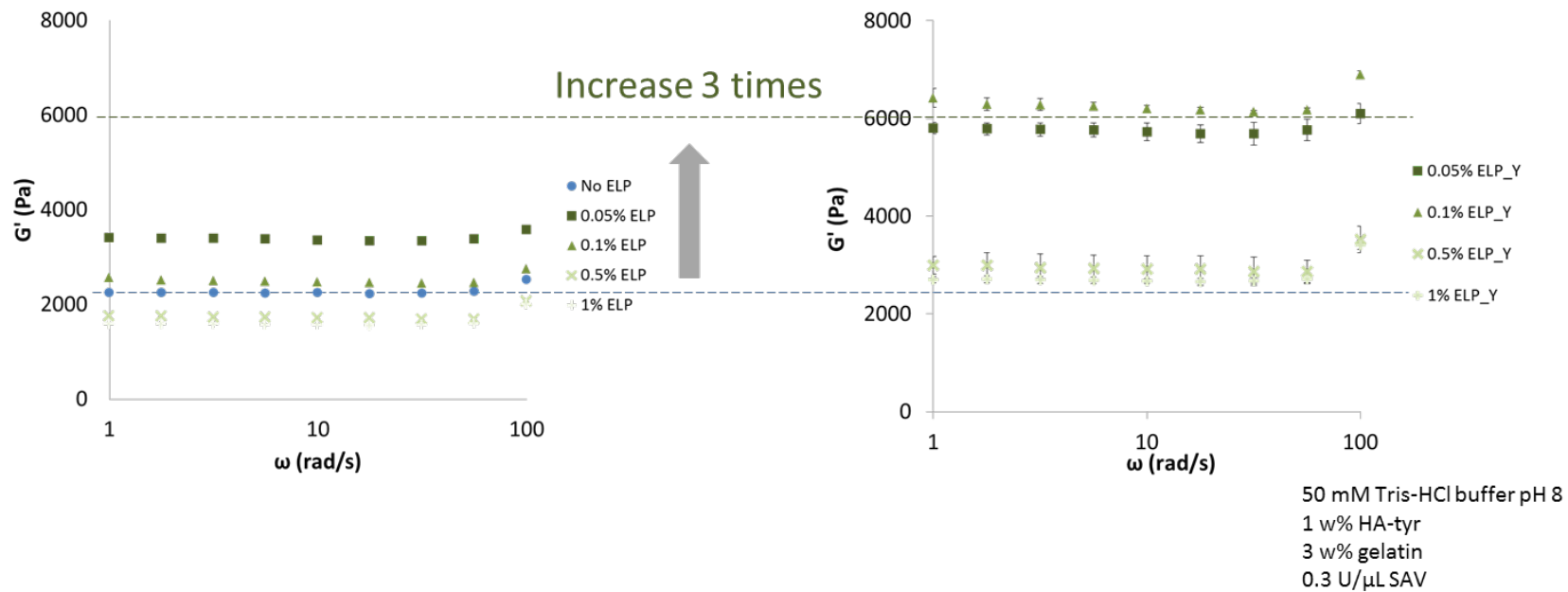


Figure 6.4. Rheology test of gelatin-hyaluronic acid hydrogel incorporating ELPs.

6.4.3 Introducing DOPA moiety into gelatin and VY24V20 for mimicking the mussel foot protein

Interestingly, the ELPs with tyrosine residue was hydroxylated and became DOPA, which catecholic moiety can form conjugated bonds to ferric ions reversibly. The states of formation changed as pH shift while normal ELP not hydroxylated was not shown this property. The image of the ELP gel is shown in Figure 6.5. After incubating the ELP with tyrosinase overnight, the gel became sticky and showed elasticity. It has been demonstrated that when a part of the gel was pulled up, it stretched like a thread. The color became dark after the tyrosinase reaction, and this is regarded of the reaction relating to melanin production as aromatic ring can absorb light of various wavelengths when tightly gathering by crosslinkages between bodies of ELPs. The phase transition was occurred reversibly as pH changed. However, high amount of salt that was used for pH adjustment, made ELP aggregated. The aggregated ELP was back to the initial state as the salts were removed by dialysis. The measurement of mechanical properties of this mussel mimicking ELP was not able because that the ELP hydrogel was fragile not enough to be shaped, and the G' of this gel was not distinguishable to distilled water used for adjusting base line of rheological measurements. However, through this study, it was shown that the Tyr residue introduced into ELP could be hydroxylated to have sticky DOPA residue by the simple enzymatic treatment.

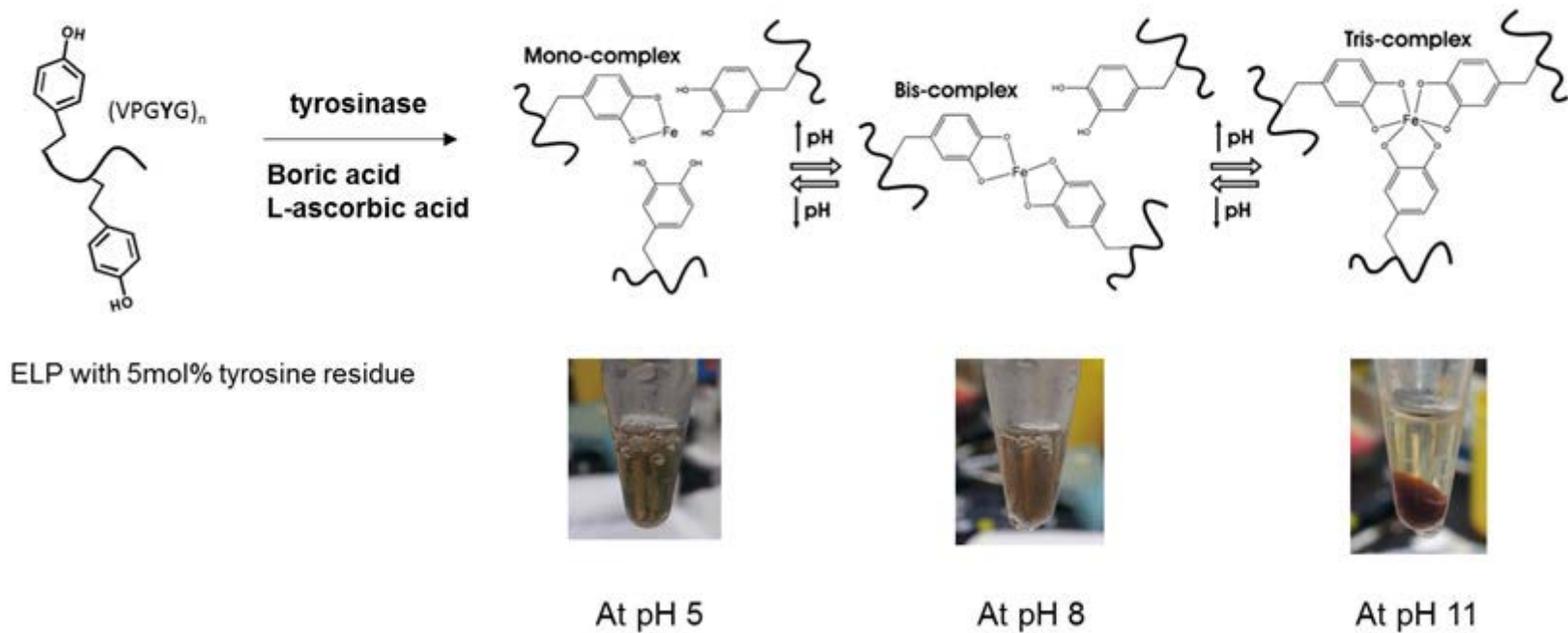


Figure 6.5. The image of ELP gel containing DOPA residues as pH changes in the presence of ferric ions

6.4.4 Synthesis of rGO, and fabrication of rGO-ELP hydrogel.

Reduced graphene oxide (rGO) was synthesized from graphite with 325 mesh which is equivalent to approximately 40 μM . The method for synthesis rGO was followed as previously reported, a simplified Hummers method (Abdolhosseinzadeh, Asgharzadeh et al. 2015). The synthesized rGO was characterized on powder XRD for confirmation as shown in Figure 6.6. The graphene oxide (GO) shows high intensity at 12.0 degree (which is not appear in this data) while reduced graphene oxide (rGO) show a broad peak at 25 degrees. This indicates that all exfoliated graphite (after this process, graphite becomes GO) reduced to rGO successfully.

The evidence that the ELP with graphene binding sequence could be indirectly shown by adding rGO-ELP in the immiscible mixture of ethyl acetate and water. rGO is completely hydrophobic thus not soluble in water while GO has a moiety that interacts with water. As shown in Figure B9, GO seems to form a thin layer between the interface of water and ethyl acetate, and the rGO appears to be deposited on the bottom. Since the ELP is soluble in water, rGO-ELP acted as a surfactant. As shown in Figure 6.7, the interface of water and ethyl acetate disappeared when rGO-ELP was added. The rGO-ELP gel shows the intact inverse transition state as temperature changes. The gel was dissolved at low temperature and get gelled after increasing temperature above 16 $^{\circ}\text{C}$, which is the T_m of ELP used (VY12V20NNCGO).

Furthermore, a thin film could be fabricated after washing the rGO-ELP with EtOH several times for dehydration. After injecting the gel on a glass plate

and waiting for complete evaporation of EtOH, a thin film was made on the glass. This composite material was conductible, which resistance was approximately 40 k Ω . The conductivity was shown only when water is entirely evaporated. However, after dehydration, the film was fragile and lost its elasticity. Unfortunately, the elasticity was not recovered once it was soaked in distilled water again. It was assumed that the inter-interactions between materials (probably crosslinked by SA_Ty) were broken due to the external physical force exerted to the film, and not self-recovered by itself.

Through this study, a method for fabrication graphene hydrogel was present. And this study demonstrated that ELP could be incorporated when a functionality should be introduced such as RGD (cell binding residues), gold binding sequences, bone morphogenetic proteins (BMPs) binding sequences, etc. Further studies should be followed for supporting the idea that the ELPs can be used as an crucial factor for offering functionality in ECM hydrogel along with more density of crosslinkages.

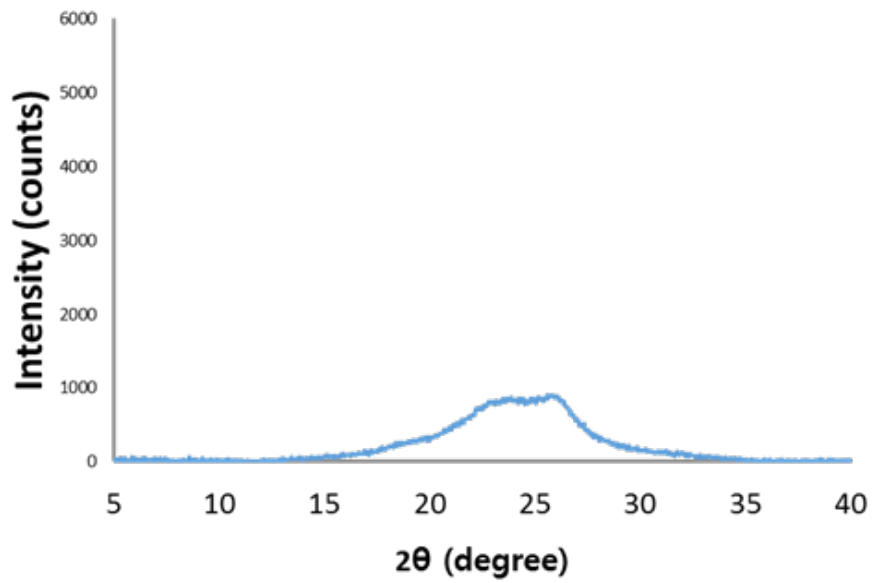


Figure 6.6. The result of powder X-ray diffraction.

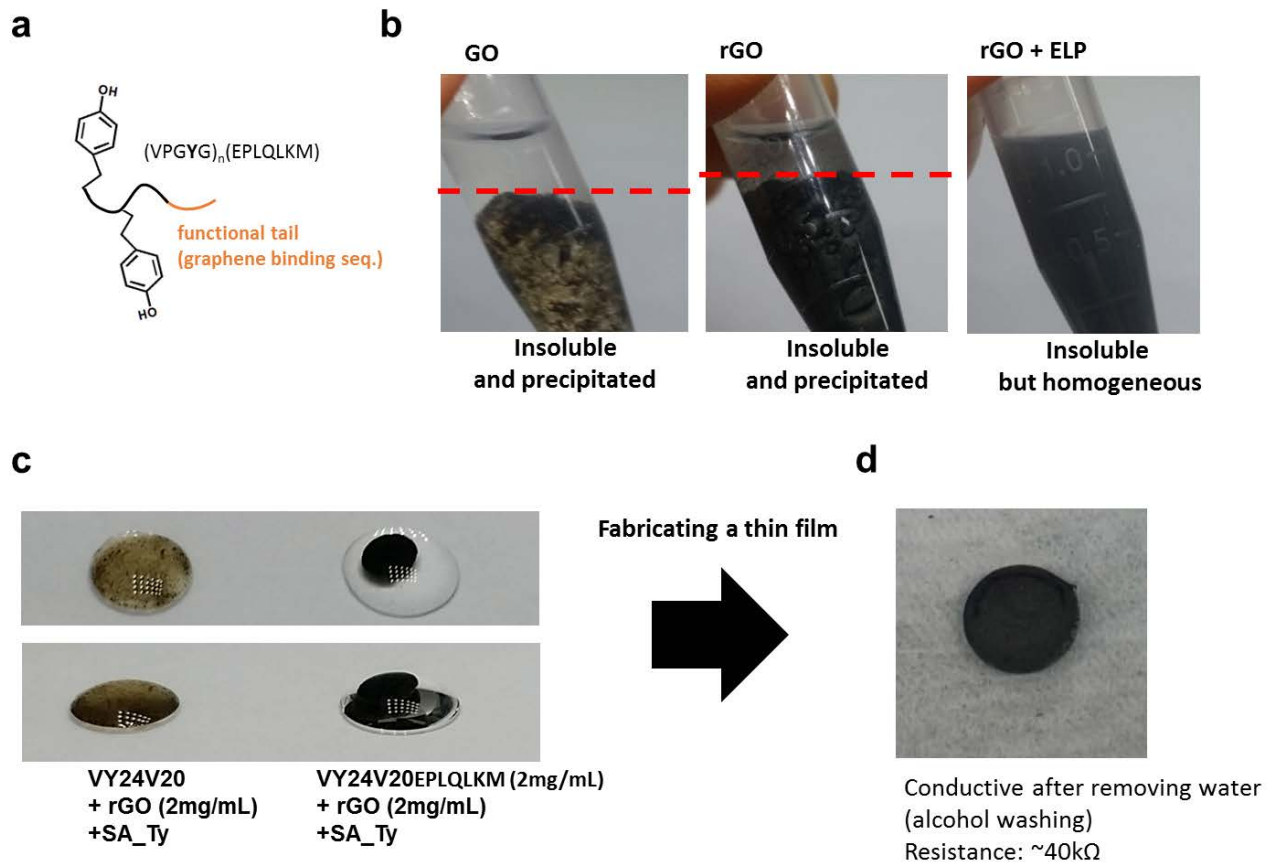


Figure 6.7. The images of the rGO-ELP hydrogel.

6.5 Conclusion

A set of elastin-like polypeptides was synthesized to emulate the covalent bonds between ELPs and/or the materials used in Chapter 5 such as gelatin, and tyramine-conjugated hyaluronic acid. Specifically, the goals of our protein design were, first, to generate ELPs that would have covalent bonds crosslinked by tyrosinase in the possible ELP body–ELP body and ELP body–other macromolecule and, second, to create ELPs that would have interfacial interactions by binding to reduced graphene oxide (rGO). To generate synthetic proteins with the desired interactions, a series of ELP genes were synthesized via a seamless, iterative cloning method. And this is one of great merit for using ELP as a functional factor since it can be genetically modified for fine tuning.

First, the modification of the guest residue in the body part of ELP, the degree of crosslinkage of hydrogel was increased. After incorporating Tyr residue in the body part of ELP, the ELP, VY12V20NNCN, increased the degree of crosslinkages of HG_gel made by gelatin and hyaluronic acid, and as a result, the mechanical strength (G') of the gel was significantly increased. The addition of 0.05 w% ELP with 5 mol % Y guest residues increase storage module to 6 kPa which is three times higher than control. Furthermore, it was shown that the Tyr residue introduced into the ELP body could be hydroxylated to have sticky DOPA residue by the simple enzymatic treatment.

Secondly, introducing a functionality, a graphene binding sequences, at the C-term of ELP could offer the conductivity to the hydrogel. Through this study, a method for fabrication graphene hydrogel was present. And this study

demonstrated that ELP could be incorporated when a functionality should be introduced such as RGD (cell binding residues), gold binding sequences, bone morphogenetic proteins (BMPs) binding sequences, etc. Further studies should be followed for expanding the idea that the ELPs can be used as an crucial factor for offering functionality in ECM hydrogel along with more density of crosslinkages.

Chapter 7.

Overall Conclusion

7.1 From the design of reaction paths to the mass production of functional catechol derivatives

The reactivity of tyrosinase regarding the oxidation of monophenols are superior to other oxidases, such as cytochrome P450 and tyrosine hydroxylase, which require unaffordable cofactors, NAD(P)H or tetrahydrobiopterin. However, there are three major issues in the production of catechol derivatives from monophenols by one-step reaction of tyrosinase. The first issue is the inseparable second oxidation of tyrosinase that oxidizes the target products, catechol derivatives. Second, catechols are easily oxidized not only by tyrosinase but also by dissolving oxygen at neutral-to-basic pH in aerobic condition. The optimum pH of tyrosinases, except tyrosinase from *B. thailandensis*, is basic and the oxygen is crucial for activating tyrosinase since it is also an oxygenase that extracts electrons from the substrate and reducing oxygen to water. Third, the product, catechol derivatives, produced by tyrosinase in this thesis, are ironically the inhibitors of tyrosinase. Thus, product inhibition, as well as the suicide inactivation, matters through the all reactions.

The reactions are not separated and the second catecholase activity is faster than the first hydroxylation, making it difficult to get the intermediate products, the catechol derivatives we want. To prevent the intermediate products, catechols, from being oxidized by the enzyme, it is necessary to remove the products from the reaction system as the reaction processes, which in turn deactivates the enzyme because the seamless circulation of three different states of tyrosinase, *deoxy-*, *oxy-*, *met-*tyrosinase, only maintains the continuous enzymatic activity of tyrosinase, and the two oxidation reactions are the paths for their circulation.

At the beginning of this study, much effort had been exerted on the enzyme engineering of tyrosinase for designing and screening novel tyrosinase mutants that could resolve all the limitations tyrosinase has. In Chapter 2, intensive site saturation mutagenesis on 15 residues in 8 Å from copper ions was performed, and more than 2,700 colonies were evaluated. However, the effect of the addition of reducing agent was much greater than the best mutant, I41Y, screened. Therefore, the direction of the research was shifted more toward studying reducing agent and its regenerating system. At first, NAD(P)H regenerating system was incorporated in whole cell bioconversion of resveratrol to piceatannol; however, still the addition of oxidized cofactor (NAD⁺) was expensive, and the concentration is limited in cytoplasm since the cofactor is being used in everywhere in cell metabolism.

Formic acid, hydroxylamine, L-ascorbic acid were all possible alternatives. However, for formic acid to be used at an effective concentration, the reaction solution became too acidic and inhibited the activity of tyrosinase. In the case of hydroxylamine, the amine group, a nucleophile, spontaneously have covalent bonds with quinone by the conjugate addition. Although the concentration of quinone is low, the rate of quinone formation will be shifted faster as the reaction rate of quinone and hydroxylamine increases.

L-ascorbic acid is one of the well-known inhibitors of tyrosinase reaction. But it was realized that ascorbic acid is only involved in the non-enzymatic process of melanin process after intensive studies of the mechanism. As shown in Chapter 3, it was proved that the ascorbic acid does not act as an inhibitor of the oxidation reaction of tyrosinase but a circulator of tyrosinase reaction by reducing *met-*

tyrosinase to *deoxy*-tyrosinase for the first time. The use of L-ascorbic acid was innovative since the reducing agent could achieve not only back-reducing oxidized catechols but also activating *met*-tyrosinase.

To remind again, briefly, the solution for resolving the three limitations suggested in this thesis was the addition of two bypass reactions. One is the protection of the arene diol of catechols by inducing the formation of borate ester bonds with boron, and another is the reduction of *met*-tyrosinase instead of catechols that are removed from the reaction system by the boron ester bonds. The addition of boric acid brought up another positive effect in the reaction, which is the increase in the solubility of phenolic compounds, both substrate, and product. The phenolic substrate subjected in this thesis are insoluble; however, the product, catechols, becomes soluble when binding to boric acid. Thus, the progress of the reaction was easily monitored by the turbidity.

The reducing agent used in this thesis is an L-ascorbic acid which is commercially available in affordable price compared to NAD(P)H. The strategy was also applicable in the mass production of orobol and 3'-ODI, which are found in fermented soy product in limited quantity. Since the boron-catechol complex are soluble while the separated catechols are insoluble, the refining process of the product was simple and easy. The acid hydrolysis for breaking boron ester bonds, washing step for removing additives and neutralization are the only steps for the purification. The purity of all the products were over 99%. The quantity of enzymes (whole cell reaction), additives, and aeration were optimized and developed sequentially several times in 6 L, 70 L and 500 L reactor, and, as a result, 1.27 kg of 3'-ODI and orobol was produced from 1.2 kg of daidzein and genistein

in one hour through 400 L reaction. The price of the both substances is over \$2,000/mg (based on the searching in SciFinder). The method demonstrated in this thesis is the only method that produces 3'-ODI and orobol in kg scale so far.

Though the target products were produced in kg scale with the optimized method, still, industrial and economical commercialization of these catechol derivatives somewhat lacks in the initial concentration used in the current reaction, which is $3 \text{ g}\cdot\text{L}^{-1}$. Beyond the concentration, the formation of boron ester bonds between boron and catechols are restricted since the concentration of boric acid is already reached at the saturated level. The dissociation constant of the complex is low, less than one. Thus the formation is unfavorable. Consequently, unbound catechols were oxidized spontaneously by tyrosinase and dissolved oxygen. Furthermore, this protection strategy is not appropriate when the separation of the excessive amount of boric acids from the product is problematic as present in Chapter 4.

Thus, the discovery of the novel tyrosinase from *B. thailandensis* is one of the valuable outcomes of this thesis. Its reactivity at acidic pH is abnormal but useful in the production of catechol derivatives since the auto-oxidation is prevented successfully. However, the solution for reducing met-tyrosinase is still defective. It should be accompanied by a quantification of the reducing power and screening for a substance with higher reducing power with much less dissociation constant than the currently used L-ascorbic acid should be followed.

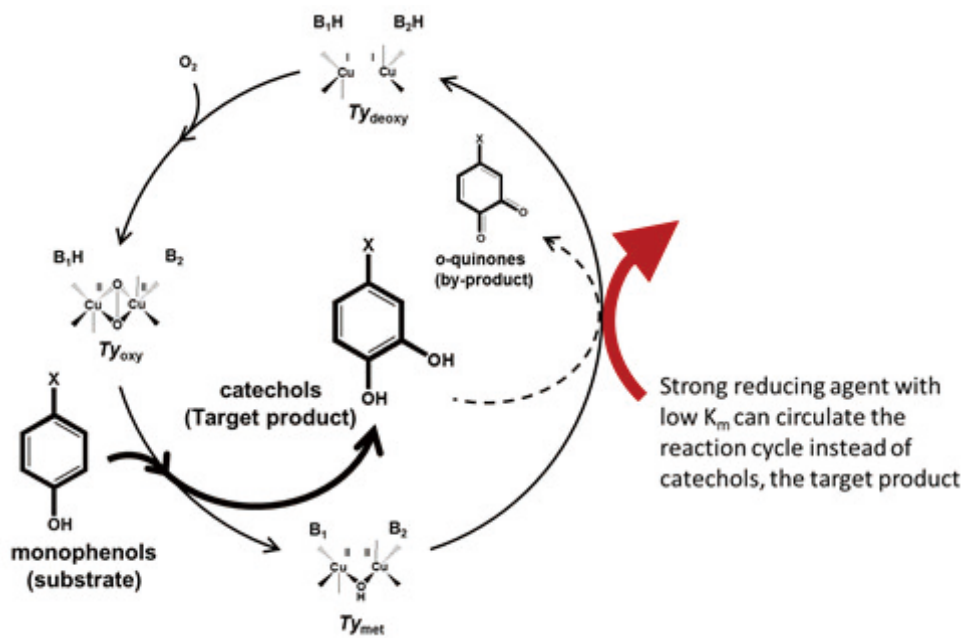


Figure 7.1. A simplified reaction scheme for efficient *ortho*-hydroxylation by tyrosinase.

7.2 Expanding the scope of target products and searching novel tyrosinase with different substrate specificity.

Unlike chemical catalysts, one of the great advantages of enzymes is substrate specificity that can distinguish small differences in chemistry. Even enzymes with the same mechanism may have different substrate specificities and should be used differently depending on the target substance. One attempt tried for expanding the scope of this project was searching a novel tyrosinase. Firstly, Subgrouping Automata, an algorithm (developed by prof. Joo-Hyun Seo) based on the pairwise sequence alignments of primary sequences were used for categorizing the tyrosinase submitted in the database of National Center for Biotechnology Information (NCBI). However, unfortunately, the algorithm is not applicable for tyrosinase because the conserved domain of tyrosinase is not consistent resulting in unreliable alignment results due to too many gaps between the aligned sequences.

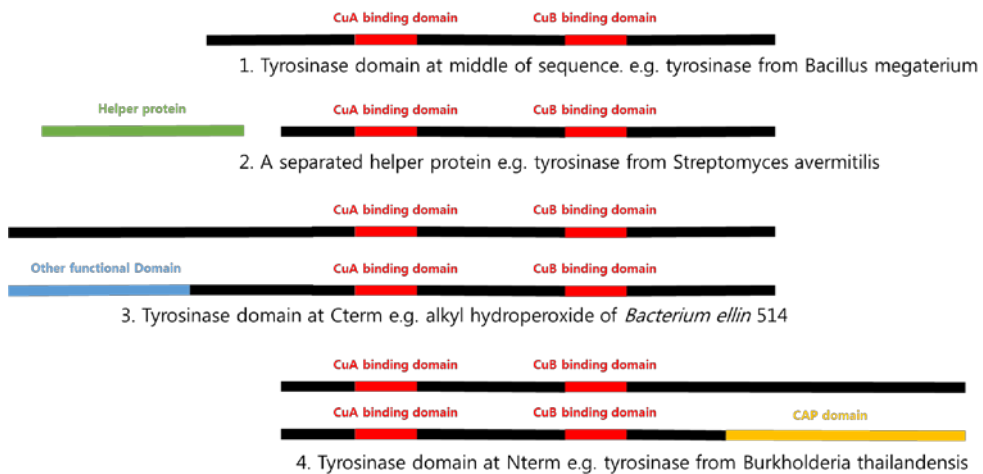


Figure 7.2. The position of tyrosinase domain.

The position and length of the domains vary depending on origins, which make it difficult to perform multiple sequence alignment. The Cterm or Nterm extended domains are probably the residues that control the substrate specificity for controlling the biological roles.

There is more than 2,000 bacterial tyrosinase withdrawn from NCBI. The sequences were all collected and organized omitting similar sequence with over 90% identity. After trimming the unnecessary sequences, for instance, sequences with too many gaps that cause inaccuracy of alignment, 499 bacterial tyrosinase remained for analysis. As shown in Figure 7.2, there are 6 groups that specified by the sequence alignment. The first goal was to clone and express the enzymes in each group and to examine their characteristics, but it was not easy to obtain the strains. To be honest, it seemed entirely fortunate to be able to find a new enzyme in some way, and the project is not completed unless all the enzymes in each group are characterized and unless the general features of each group are not identified. However, predicting substrate specificity of enzymes based on primary sequences are practically impossible unless the accurate 3D structure is resolved. Figure 7.4 shows the structures of monophenols that are subjected in this thesis; however, not all of the substances were successfully hydroxylated. An approximate prediction of which residues around the active site is involved in substrate binding is possible with *in silico* docking simulation; however, unfortunately, the docking simulation still does not clearly predict enzyme-ligand binding.

Only bacterial tyrosinase has been the subject of cloning because of easy accessibility of gDNA. The tyrosinase from *B. thailandensis* has a structure similar to that of hemocyanin and can be considered to provide a stepping stone to look at the evolutionary relationship between tyrosinase and hemocyanin further between all type III copper proteins by identifying the roles of residues allow the specific functions of each enzyme.

Substrate specificity may vary not only depending on whether the

substrate is bound but also depending on the substrate, even if the reaction is due to the same mechanism. The tendency of hydroxylation on B ring (phenolic group) and A ring (benzopyran ring) of isoflavone was distinctly different. An uncompleted study on this matter is written in Appendix. An in which contains the trials of enzymatic engineering for 6- or 8- hydroxylation of daidzein, and formononetin. The rate of hydroxylation on the benzopyran ring is much slower than on the phenolic group, and showed a higher frequency of suicide inactivation. The addition of extra copper ions could resolve the suicide inactivation, but still, it could be a matter when it comes to the mass production. The current concentration studied with the benzopyran ring is less than 1 mM. The suicide inactivation is because the electrons extracted from substrates end up reducing copper ions of the active site not reducing the oxygen molecule bound in between of the copper ions. The reason can be the rings with more space for electrons' stable staying or with electron-withdrawing groups have a strong tendency for keeping electrons inside the structure, consequently, increasing the acidity of peroxo moiety of the dicopper-peroxo complex when binding to the substrate. It is hypothesized that the greater acidity of peroxo group than neighboring residues or water is crucial for the mechanism of suicide inactivation. The possible solution can be lower the pH of the solution, and positioning the acidic residues around the active site.

The pI of tyrosinase from *B. thailandensis* is approximately 5.5, which means plenty of acidic residues are available, and the enzyme is active in acidic condition. The use of this tyrosinase in the reaction could overcome the limitation; however, the substrate specificity does not allow the reaction. Recently, the structure of the tyrosinase from *B. thailandensis* was resolved with the thankful

help of the team of prof. Kyung Jin Kim at Kyungpook National University. The research on this enzyme is still in the process, and, hypothetically, the reaction at acidic condition could overcome the inactivation once the substrate specificity of the enzyme is broadened to benzopyran ring, for instance, formononetin.

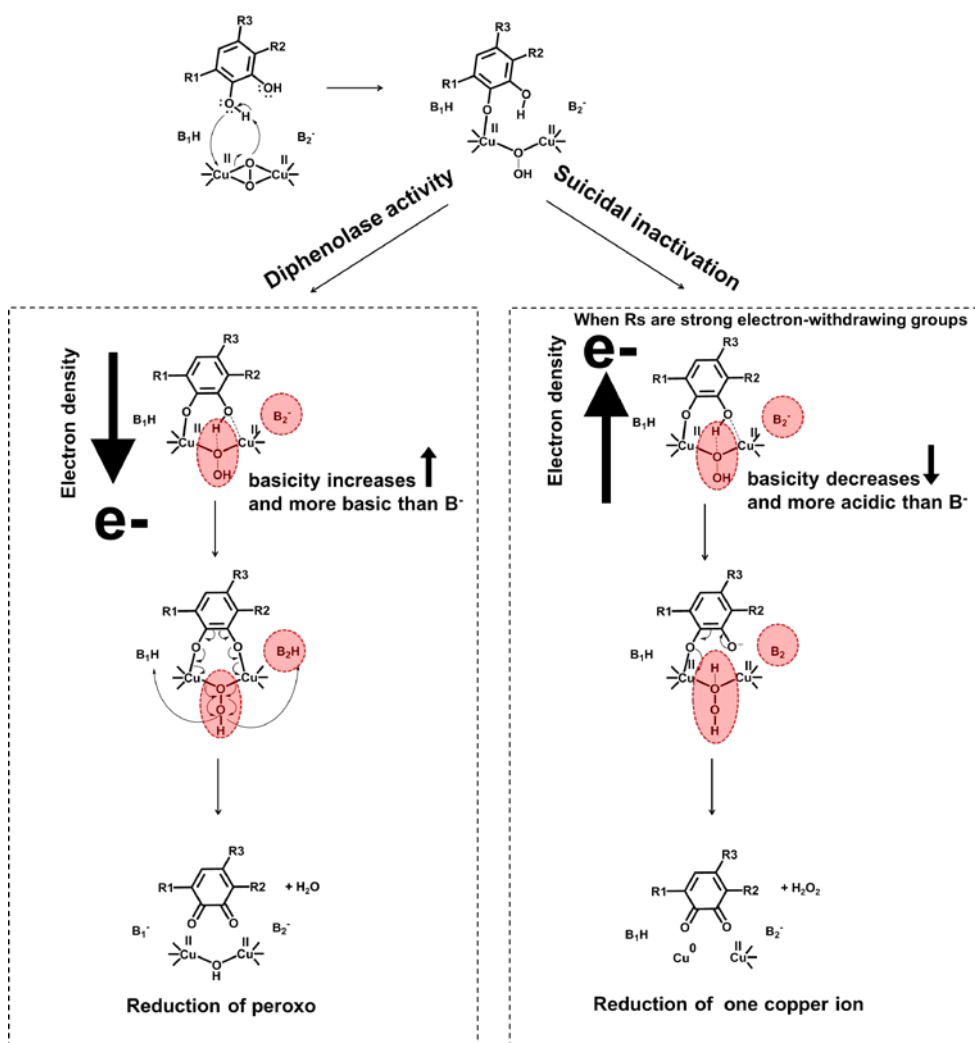


Figure 7.3. The hypothetical reasons for the suicide inactivation

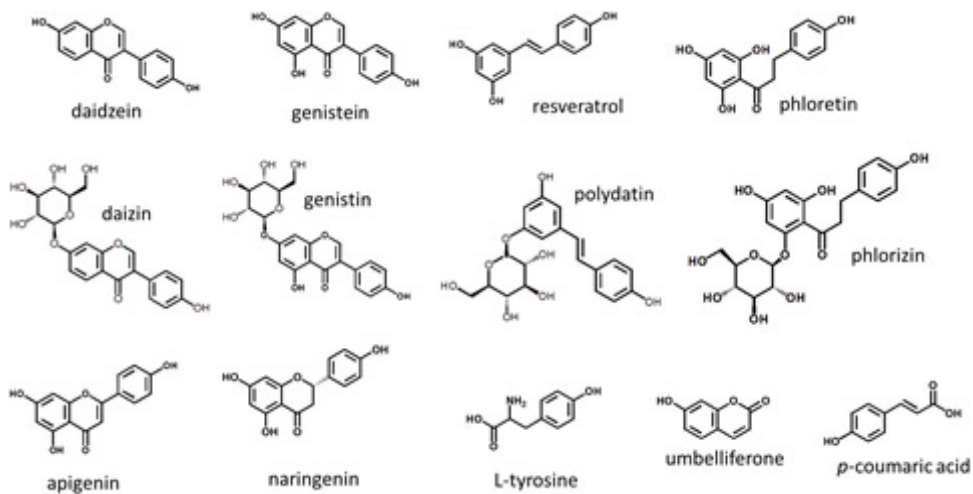


Figure 7.4. Chemicals subjected in this thesis for the substrate of *ortho*-hydroxylation

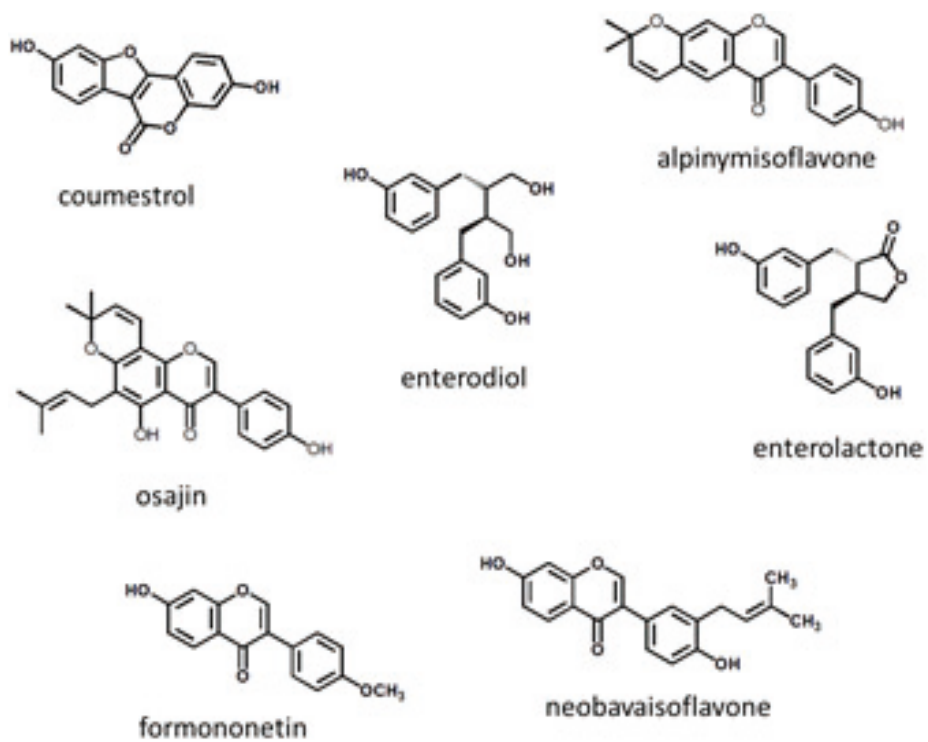


Figure 7.5. Possible substrates for *ortho*-hydroxylation by tyrosinase

7.3 Enzymatic crosslinking for fabricating hydrogels and polymerization for producing dark pigments.

Again, the substrate specificity is one of the great advantages of enzymes that can distinguish small differences in chemistry. Even enzymes with the same mechanism may have different substrate specificities and should be used differently depending on the target substance. The accessibility of free small substance with a phenolic group such as L-tyrosine to the enzyme differs from the L-tyrosine on the macromolecules such as gelatin. Through the studies for previous chapters, it was found that tyrosinase from *Streptomyces avermitilis* has a flat surface that is evolved for binding to a helper protein. Thus, the new tyrosinase from *S. avermitilis* was brought up for resolving the steric hindrance when crosslinking macromolecules; the main reason makes mushroom tyrosinase inefficient when it comes to oxidize phenolic group on macromolecules.

Overall, this thesis clearly shows that the origin or structures of tyrosinases should be considered depending on the purpose and type of substrate. This is a well-known fact, but, this fact has been overlooked much in many previous types of research. Through this study, it shows the superiority of this tyrosinase from *S. avermitilis* in crosslinking, and many researchers will use this enzyme or work to find similar enzymes that have a flat surface and shallow tunnel to the active site.

Moreover, it was also well-known that gelatin differs in melting point with ionic strength. The melting point of gelatin is above the room temperature thus it is hard to handle at room temperature. The physiological concentration of NaCl was dramatically effective in decreasing the viscosity of gelatin. And the

addition of a small amount of salt enabled the injection and spray of the sticky gel.

Unfortunately, the tacking force of this gel did not improve compared to conventional gelatin gels. It was assumed that the adhesion by catechol residues appears to be weaker than the adhesion by hydrogen bonds. This is because the substitution rate of the catechol moiety is low, but it seems to be pointless to make it higher. This is because the further introduction of monophenol-type moieties to introduce more catechol-like moieties significantly reduces the water solubility of the material. Although the tacking force is not improved, the gel was still sticky and showed greatly increased mechanical properties in terms of storage modulus (strength) and adhesion work (stickiness). Especially, the adhesion work of this stick hydrogel was remarkable, which is $21.34 \text{ J}\cdot\text{m}^{-2}$, compared to previously studied catechol-conjugated polymers including mussel foot proteins, which in the range of 0.12 to $7 \text{ J}\cdot\text{m}^{-2}$.

The strategy to form fast injectable/sprayable hydrogels present in this thesis was widely applicable to in situ hydrogels, incorporating phenolic groups in a biopolymer. Also, the HG_gel could be developed as a robust tool for surgical glue and localized delivery of cells or biomacromolecules, with the advantage of a tissue adhesive and cell recruiting function in vivo. The HG_gel was demonstrated to be homogeneously coated on mouse cardiac tissue ex vivo through a commercial airbrush, and it has $10 \sim 13 \mu\text{m}$ of thickness with a short jetting. It stayed firmly due to its adhesive properties. Overall, the tissue adhesive, injectable and sprayable hydrogel with a newly developed Ty offers robust potential to develop surgical glue and delivery carrier in the field of biomedical and tissue engineering.

Reference

- Abdolhosseinzadeh, S., H. Asgharzadeh and H. Seop Kim (2015). "Fast and fully-scalable synthesis of reduced graphene oxide." Scientific Reports **5**: 10160.
- Anderson, J. M., A. Rodriguez and D. T. Chang (2008). "Foreign body reaction to biomaterials." Semin Immunol **20**(2): 86-100.
- Bijelic, A., M. Pretzler, C. Molitor, F. Zekiri and A. Rompel (2015). "The Structure of a Plant Tyrosinase from Walnut Leaves Reveals the Importance of "Substrate-Guiding Residues" for Enzymatic Specificity." Angew Chem Int Ed Engl **54**(49): 14677-14680.
- Bisignano, G., A. Tomaino, R. L. Cascio, G. Crisafi, N. Uccella and A. Saija (1999). "On the In-vitro Antimicrobial Activity of Oleuropein and Hydroxytyrosol." Journal of Pharmacy and Pharmacology **51**(8): 971-974.
- Bisignano, G., A. Tomaino, R. Lo Cascio, G. Crisafi, N. Uccella and A. Saija (1999). "On the in-vitro antimicrobial activity of oleuropein and hydroxytyrosol." J Pharm Pharmacol **51**(8): 971-974.
- Brighid Pappin, M. J. K., Todd A. Houston (2012). Boron-Carbohydrate Interactions, Carbohydrates - Comprehensive Studies on Glycobiology and Glycotechnology.
- Bright, H. J., B. J. Wood and L. L. Ingraham (1963). "Copper, tyrosinase, and the kinetic stability of oxygen." Ann N Y Acad Sci **100**: 965-976.
- Brown, R. S., K. B. Male and J. H. Luong (1994). "A substrate recycling assay for phenolic compounds using tyrosinase and NADH." Anal Biochem **222**(1): 131-139.
- Cabanes, J., S. Chazarra and F. Garcia-Carmona (1994). "Kojic acid, a cosmetic

- skin whitening agent, is a slow-binding inhibitor of catecholase activity of tyrosinase." J Pharm Pharmacol **46**(12): 982-985.
- Carlson, B. W. and L. L. Miller (1985). "Mechanism of the oxidation of NADH by quinones. Energetics of one-electron and hydride routes." Journal of the American Chemical Society **107**(2): 479-485.
- Chen, T., H. D. Embree, E. M. Brown, M. M. Taylor and G. F. Payne (2003). "Enzyme-catalyzed gel formation of gelatin and chitosan: potential for in situ applications." Biomaterials **24**(17): 2831-2841.
- Chen, T., H. D. Embree, L. Q. Wu and G. F. Payne (2002). "In vitro protein-polysaccharide conjugation: tyrosinase-catalyzed conjugation of gelatin and chitosan." Biopolymers **64**(6): 292-302.
- Chiang, L., W. Keown, C. Citek, E. C. Wasinger and T. D. P. Stack (2016). "Simplest Monodentate Imidazole Stabilization of the oxy-Tyrosinase Cu₂O₂ Core: Phenolate Hydroxylation through a Cu^{III} Intermediate." Angewandte Chemie International Edition **55**(35): 10453-10457.
- Choi, K. Y., E. Jung, D. H. Jung, B. P. Pandey, H. Yun, H. Y. Park, R. J. Kazlauskas and B. G. Kim (2012). "Cloning, expression and characterization of CYP102D1, a self-sufficient P450 monooxygenase from *Streptomyces avermitilis*." Febs j **279**(9): 1650-1662.
- Choi, K. Y., E. O. Jung, H. Yun, Y. H. Yang, R. J. Kazlauskas and B. G. Kim (2013). "Development of colorimetric HTS assay of cytochrome p450 for ortho-specific hydroxylation, and engineering of CYP102D1 with enhanced catalytic activity and regioselectivity." Chembiochem **14**(10): 1231-1238.
- Chovancova, E., A. Pavelka, P. Benes, O. Strnad, J. Brezovsky, B. Kozlikova, A.

- Gora, V. Sustr, M. Klvana, P. Medek, L. Biedermannova, J. Sochor and J. Damborsky (2012). "CAVER 3.0: a tool for the analysis of transport pathways in dynamic protein structures." PLoS Comput Biol **8**(10): e1002708.
- Chung, H., P. Glass, J. M. Pothen, M. Sitti and N. R. Washburn (2011). "Enhanced adhesion of dopamine methacrylamide elastomers via viscoelasticity tuning." Biomacromolecules **12**(2): 342-347.
- Decker, H., R. Dillinger and F. Tucek (2000). "How Does Tyrosinase Work? Recent Insights from Model Chemistry and Structural Biology." Angewandte Chemie International Edition **39**(9): 1591-1595.
- Decker, H. and T. Rimke (1998). "Tarantula hemocyanin shows phenoloxidase activity." J Biol Chem **273**(40): 25889-25892.
- Decker, H. and F. Tucek (2000). "Tyrosinase/catecholoxidase activity of hemocyanins: structural basis and molecular mechanism." Trends Biochem Sci **25**(8): 392-397.
- Deri, B., M. Kanteev, M. Goldfeder, D. Lecina, V. Guallar, N. Adir and A. Fishman (2016). "The unravelling of the complex pattern of tyrosinase inhibition." Scientific Reports **6**: 34993.
- Duckworth, H. W. and J. E. Coleman (1970). "Physicochemical and kinetic properties of mushroom tyrosinase." J Biol Chem **245**(7): 1613-1625.
- Edgar, R. C. (2004). "MUSCLE: multiple sequence alignment with high accuracy and high throughput." Nucleic Acids Research **32**(5): 1792-1797.
- Espin, J. C., R. Varon, L. G. Fenoll, M. A. Gilabert, P. A. Garcia-Ruiz, J. Tudela and F. Garcia-Canovas (2000). "Kinetic characterization of the substrate

- specificity and mechanism of mushroom tyrosinase." Eur J Biochem **267**(5): 1270-1279.
- Fairhead, M. and L. Thöny-Meyer (2012). "Bacterial tyrosinases: old enzymes with new relevance to biotechnology." New Biotechnology **29**(2): 183-191.
- Fenoll, L. G., M. J. Peñalver, J. N. Rodríguez-López, P. A. García-Ruiz, F. García-Cánovas and J. Tudela (2004). "Deuterium isotope effect on the oxidation of monophenols and o-diphenols by tyrosinase." Biochemical Journal **380**(Pt 3): 643-650.
- Fenoll, L. G., J. N. Rodríguez-López, F. García-Sevilla, P. A. García-Ruiz, R. Varón, F. García-Cánovas and J. Tudela (2001). "Analysis and interpretation of the action mechanism of mushroom tyrosinase on monophenols and diphenols generating highly unstable o-quinones." Biochimica et Biophysica Acta (BBA) - Protein Structure and Molecular Enzymology **1548**(1): 1-22.
- Festa, R. A. and D. J. Thiele (2011). "Copper: an Essential Metal in Biology." Current biology : CB **21**(21): R877-R883.
- Freddi, G., A. Anghileri, S. Sampaio, J. Buchert, P. Monti and P. Taddei (2006). "Tyrosinase-catalyzed modification of Bombyx mori silk fibroin: grafting of chitosan under heterogeneous reaction conditions." J Biotechnol **125**(2): 281-294.
- Garcia-Molina, F., J. L. Munoz-Munoz, M. Garcia-Molina, P. A. Garcia-Ruiz, J. Tudela, F. Garcia-Canovas and J. N. Rodriguez-Lopez (2010). "Melanogenesis inhibition due to NADH." Biosci Biotechnol Biochem **74**(9): 1777-1787.

- Goldfeder, M., M. Kanteev, N. Adir and A. Fishman (2013). "Influencing the monophenolase/diphenolase activity ratio in tyrosinase." Biochimica et Biophysica Acta (BBA) - Proteins and Proteomics **1834**(3): 629-633.
- Goldfeder, M., M. Kanteev, N. Adir and A. Fishman (2013). "Influencing the monophenolase/diphenolase activity ratio in tyrosinase." Biochim Biophys Acta **1834**(3): 629-633.
- Goldfeder, M., M. Kanteev, S. Isaschar-Ovdat, N. Adir and A. Fishman (2014). "Determination of tyrosinase substrate-binding modes reveals mechanistic differences between type-3 copper proteins." Nat Commun **5**: 4505.
- Gong, J. P. (2006). "Friction and lubrication of hydrogels—its richness and complexity." Soft matter **2**(7): 544-552.
- Gouveia-Oliveira, R., P. W. Sackett and A. G. Pedersen (2007). "MaxAlign: maximizing usable data in an alignment." BMC Bioinformatics **8**: 312.
- Guvendiren, M., P. B. Messersmith and K. R. Shull (2008). "Self-assembly and adhesion of DOPA-modified methacrylic triblock hydrogels." Biomacromolecules **9**(1): 122-128.
- Hamann, J. N., B. Herzigkeit, R. Jurgeleit and F. Tuzcek (2017). "Small-molecule models of tyrosinase: From ligand hydroxylation to catalytic monooxygenation of external substrates." Coordination Chemistry Reviews **334**: 54-66.
- Haraga, A., T. E. West, M. J. Brittnacher, S. J. Skerrett and S. I. Miller (2008). "Burkholderia thailandensis as a Model System for the Study of the Virulence-Associated Type III Secretion System of Burkholderia

- pseudomallei." Infection and Immunity **76**(11): 5402-5411.
- Hazra, B., R. Sarkar, S. Bhattacharyya and P. Roy (2002). "Tumour inhibitory activity of chicory root extract against Ehrlich ascites carcinoma in mice." Fitoterapia **73**(7-8): 730-733.
- Hazra, B., R. Sarkar, S. Bhattacharyya and P. Roy (2002). "Tumour inhibitory activity of chicory root extract against Ehrlich ascites carcinoma in mice." Fitoterapia **73**(7-8): 730-733.
- He, L., D. E. Fullenkamp, J. G. Rivera and P. B. Messersmith (2011). "pH responsive self-healing hydrogels formed by boronate-catechol complexation." Chem Commun (Camb) **47**(26): 7497-7499.
- Hernandez-Romero, D., A. Sanchez-Amat and F. Solano (2006). "A tyrosinase with an abnormally high tyrosine hydroxylase/dopa oxidase ratio." Febs j **273**(2): 257-270.
- Hoffmann, A., C. Citek, S. Binder, A. Goos, M. Rubhausen, O. Troeppner, I. Ivanovic-Burmazovic, E. C. Wasinger, T. D. Stack and S. Herres-Pawlis (2013). "Catalytic phenol hydroxylation with dioxygen: extension of the tyrosinase mechanism beyond the protein matrix." Angew Chem Int Ed Engl **52**(20): 5398-5401.
- Huang, Y., B. Niu, Y. Gao, L. Fu and W. Li (2010). "CD-HIT Suite: a web server for clustering and comparing biological sequences." Bioinformatics **26**(5): 680-682.
- Huynh, K. and C. L. Partch (2015). "Current Protocols in Protein Science: Analysis of protein stability and ligand interactions by thermal shift assay." Current protocols in protein science / editorial board, John E. Coligan ... [et al.]

79: 28.29.21-28.29.14.

- Hwang, D. S., Y. Gim, H. J. Yoo and H. J. Cha (2007). "Practical recombinant hybrid mussel bioadhesive fp-151." Biomaterials **28**(24): 3560-3568.
- Hwang, D. S., H. Zeng, A. Masic, M. J. Harrington, J. N. Israelachvili and J. H. Waite (2010). "Protein- and metal-dependent interactions of a prominent protein in mussel adhesive plaques." J Biol Chem **285**(33): 25850-25858.
- Ismaya, W. T., H. J. Rozeboom, A. Weijn, J. J. Mes, F. Fusetti, H. J. Wichers and B. W. Dijkstra (2011). "Crystal structure of *Agaricus bisporus* mushroom tyrosinase: identity of the tetramer subunits and interaction with tropolone." Biochemistry **50**(24): 5477-5486.
- Iyanagi, T. and I. Yamazaki (1970). "One-electron-transfer reactions in biochemical systems. V. Difference in the mechanism of quinone reduction by the NADH dehydrogenase and the NAD(P)H dehydrogenase (DT-diaphorase)." Biochim Biophys Acta **216**(2): 282-294.
- Jitprasutwit, S., W. Thaewpia, V. Muangsombut, A. Lulitanond, C. Leelayuwat, G. Lertmemongkolchai and S. Korbsrisate (2010). "Effect of acidic pH on the invasion efficiency and the type III secretion system of *Burkholderia thailandensis*." J Microbiol **48**(4): 526-532.
- Kanjee, U., I. Gutsche, E. Alexopoulos, B. Zhao, M. El Bakkouri, G. Thibault, K. Liu, S. Ramachandran, J. Snider, E. F. Pai and W. A. Houry (2011). "Linkage between the bacterial acid stress and stringent responses: the structure of the inducible lysine decarboxylase." The EMBO Journal **30**(5): 931.
- Kanteev, M., M. Goldfeder and A. Fishman (2015). "Structure-function

- correlations in tyrosinases." Protein Sci **24**(9): 1360-1369.
- Khademhosseini, A. and R. Langer (2007). "Microengineered hydrogels for tissue engineering." Biomaterials **28**(34): 5087-5092.
- Kim, B. S. and D. J. Mooney (1998). "Development of biocompatible synthetic extracellular matrices for tissue engineering." Trends Biotechnol **16**(5): 224-230.
- Kim, H. S., M. A. Schell, Y. Yu, R. L. Ulrich, S. H. Sarria, W. C. Nierman and D. DeShazer (2005). "Bacterial genome adaptation to niches: divergence of the potential virulence genes in three Burkholderia species of different survival strategies." BMC Genomics **6**: 174.
- Kim, Y.-J. and H. Uyama (2005). "Tyrosinase inhibitors from natural and synthetic sources: structure, inhibition mechanism and perspective for the future." Cellular and Molecular Life Sciences CMLS **62**(15): 1707-1723.
- Kumar, S., G. Stecher and K. Tamura (2016). "MEGA7: Molecular Evolutionary Genetics Analysis Version 7.0 for Bigger Datasets." Mol Biol Evol **33**(7): 1870-1874.
- Land, E. J., C. A. Ramsden and P. A. Riley (2007). "The mechanism of suicide-inactivation of tyrosinase: a substrate structure investigation." Tohoku J Exp Med **212**(4): 341-348.
- Larrosa, M., F. Tomás-Barberán and J. Espín (2004). "The grape and wine polyphenol piceatannol is a potent inducer of apoptosis in human SK-Mel-28 melanoma cells." European Journal of Nutrition **43**(5): 275-284.
- Larrosa, M., F. A. Tomas-Barberan and J. C. Espin (2004). "The grape and wine polyphenol piceatannol is a potent inducer of apoptosis in human SK-

- Mel-28 melanoma cells." Eur J Nutr **43**(5): 275-284.
- Le, T.-K., H.-H. Jang, H. T. H. Nguyen, T. T. M. Doan, G.-Y. Lee, K. D. Park, T. Ahn, Y. H. Joung, H.-S. Kang and C.-H. Yun (2017). "Highly regioselective hydroxylation of polydatin, a resveratrol glucoside, for one-step synthesis of astringin, a piceatannol glucoside, by P450 BM3." Enzyme and Microbial Technology **97**: 34-42.
- Le Thi, P., Y. Lee, D. H. Nguyen and K. D. Park (2017). "In situ forming gelatin hydrogels by dual-enzymatic cross-linking for enhanced tissue adhesiveness." Journal of Materials Chemistry B **5**(4): 757-764.
- Lee, B. P., P. B. Messersmith, J. N. Israelachvili and J. H. Waite (2011). "Mussel-Inspired Adhesives and Coatings." Annu Rev Mater Res **41**: 99-132.
- Lee, B. P., P. B. Messersmith, J. N. Israelachvili and J. H. Waite (2011). "Mussel-inspired adhesives and coatings." Annual review of materials research **41**: 99-132.
- Lee, D. E., K. W. Lee, S. Byun, S. K. Jung, N. Song, S. H. Lim, Y. S. Heo, J. E. Kim, N. J. Kang, B. Y. Kim, G. T. Bowden, A. M. Bode, H. J. Lee and Z. Dong (2011). "7,3',4'-Trihydroxyisoflavone, a metabolite of the soy isoflavone daidzein, suppresses ultraviolet B-induced skin cancer by targeting Cot and MKK4." J Biol Chem **286**(16): 14246-14256.
- Lee, H., S. M. Dellatore, W. M. Miller and P. B. Messersmith (2007). "Mussel-Inspired Surface Chemistry for Multifunctional Coatings." Science (New York, N.Y.) **318**(5849): 426-430.
- Lee, K. W., A. M. Bode and Z. Dong (2011). "Molecular targets of phytochemicals for cancer prevention." Nat Rev Cancer **11**(3): 211-218.

- Lee, N., E. J. Kim and B.-G. Kim (2012). "Regioselective Hydroxylation of trans-Resveratrol via Inhibition of Tyrosinase from *Streptomyces avermitilis* MA4680." ACS Chemical Biology **7**(10): 1687-1692.
- Lee, N., S.-H. Lee, K. Baek and B.-G. Kim (2015). "Heterologous expression of tyrosinase (MelC2) from *Streptomyces avermitilis* MA4680 in *E. coli* and its application for ortho-hydroxylation of resveratrol to produce piceatannol." Applied Microbiology and Biotechnology **99**(19): 7915-7924.
- Lee, S.-H., K. Baek, J.-E. Lee and B.-G. Kim (2016). "Using tyrosinase as a monophenol monooxygenase: A combined strategy for effective inhibition of melanin formation." Biotechnology and Bioengineering **113**(4): 735-743.
- Lee, S. H., Y. Lee, S.-W. Lee, H.-Y. Ji, J.-H. Lee, D. S. Lee and T. G. Park (2011). "Enzyme-mediated cross-linking of Pluronic copolymer micelles for injectable and in situ forming hydrogels." Acta biomaterialia **7**(4): 1468-1476.
- Letunic, I. and P. Bork (2016). "Interactive tree of life (iTOL) v3: an online tool for the display and annotation of phylogenetic and other trees." Nucleic Acids Res **44**(W1): W242-245.
- Li, L., B. Yan, J. Yang, L. Chen and H. Zeng (2015). "Novel mussel-inspired injectable self-healing hydrogel with anti-biofouling property." Adv Mater **27**(7): 1294-1299.
- Lin, Y. and Y. Yan (2014). "Biotechnological production of plant-specific hydroxylated phenylpropanoids." Biotechnol Bioeng **111**(9): 1895-1899.

- Lo, Y. L., W. Wang and C. T. Ho (2012). "7,3',4'-Trihydroxyisoflavone modulates multidrug resistance transporters and induces apoptosis via production of reactive oxygen species." Toxicology **302**(2-3): 221-232.
- Mabry, T. J., K. R. Markham and M. B. Thomas (1970). The Aglycone and Sugar Analysis of Flavonoid Glycosides. The Systematic Identification of Flavonoids. Berlin, Heidelberg, Springer Berlin Heidelberg: 23-32.
- Maeda, H., Y. Fujii and Y. Mihashi (2008). "Diol-substituted boron complexes of dipyrrolyl diketones as anion receptors and covalently linked 'pivotal' dimers." Chem Commun (Camb)(36): 4285-4287.
- Masuda, T., K. Momoji, T. Hirata and B. Mikami (2014). "The crystal structure of a crustacean prophenoloxidase provides a clue to understanding the functionality of the type 3 copper proteins." Febs j **281**(11): 2659-2673.
- Matoba, Y., T. Kumagai, A. Yamamoto, H. Yoshitsu and M. Sugiyama (2006). "Crystallographic evidence that the dinuclear copper center of tyrosinase is flexible during catalysis." J Biol Chem **281**(13): 8981-8990.
- Mauracher, S. G., C. Molitor, R. Al-Oweini, U. Kortz and A. Rompel (2014). "Latent and active abPPO4 mushroom tyrosinase cocrystallized with hexatungstotellurate(VI) in a single crystal." Acta Crystallogr D Biol Crystallogr **70**(Pt 9): 2301-2315.
- Miean, K. H. and S. Mohamed (2001). "Flavonoid (Myricetin, Quercetin, Kaempferol, Luteolin, and Apigenin) Content of Edible Tropical Plants." Journal of Agricultural and Food Chemistry **49**(6): 3106-3112.
- Miean, K. H. and S. Mohamed (2001). "Flavonoid (myricetin, quercetin, kaempferol, luteolin, and apigenin) content of edible tropical plants." J

Agric Food Chem **49**(6): 3106-3112.

Mirica, L. M., M. Vance, D. J. Rudd, B. Hedman, K. O. Hodgson, E. I. Solomon and T. D. Stack (2005). "Tyrosinase reactivity in a model complex: an alternative hydroxylation mechanism." Science **308**(5730): 1890-1892.

Molitor, C., S. G. Mauracher and A. Rompel (2016). "Aurone synthase is a catechol oxidase with hydroxylase activity and provides insights into the mechanism of plant polyphenol oxidases." Proc Natl Acad Sci U S A **113**(13): E1806-1815.

Muñoz-Muñoz, J. L., J. Berna, M. d. M. García-Molina, F. Garcia-Molina, P. A. Garcia-Ruiz, R. Varon, J. N. Rodriguez-Lopez and F. Garcia-Canovas (2012). "Hydroxylation of p-substituted phenols by tyrosinase: Further insight into the mechanism of tyrosinase activity." Biochemical and Biophysical Research Communications **424**(2): 228-233.

Munoz-Munoz, J. L., F. Garcia-Molina, R. Varon, P. A. Garcia-Ruiz, J. Tudela, F. Garcia-Canovas and J. N. Rodriguez-Lopez (2010). "Suicide inactivation of the diphenolase and monophenolase activities of tyrosinase." IUBMB Life **62**(7): 539-547.

Nov, Y. (2012). "When second best is good enough: another probabilistic look at saturation mutagenesis." Appl Environ Microbiol **78**(1): 258-262.

Palavicini, S., A. Granata, E. Monzani and L. Casella (2005). "Hydroxylation of phenolic compounds by a peroxodicopper(II) complex: further insight into the mechanism of tyrosinase." J Am Chem Soc **127**(51): 18031-18036.

Park, J.-S., H. Y. Park, D. H. Kim, D. H. Kim and H. K. Kim (2008). "ortho-

- Dihydroxyisoflavone derivatives from aged Doenjang (Korean fermented soy paste) and its radical scavenging activity." Bioorganic & Medicinal Chemistry Letters **18**(18): 5006-5009.
- Park, J. S., D. H. Kim, J. K. Lee, J. Y. Lee, D. H. Kim, H. K. Kim, H. J. Lee and H. C. Kim (2010). "Natural ortho-dihydroxyisoflavone derivatives from aged Korean fermented soybean paste as potent tyrosinase and melanin formation inhibitors." Bioorg Med Chem Lett **20**(3): 1162-1164.
- Park, J. S., H. Y. Park, D. H. Kim, D. H. Kim and H. K. Kim (2008). "ortho-dihydroxyisoflavone derivatives from aged Doenjang (Korean fermented soy paste) and its radical scavenging activity." Bioorg Med Chem Lett **18**(18): 5006-5009.
- Peñalver, M. a. J., J. N. Rodríguez-López, P. A. García-Ruiz, F. García-Cánovas and J. Tudela (2003). "Solvent deuterium isotope effect on the oxidation of o-diphenols by tyrosinase." Biochimica et Biophysica Acta (BBA) - Proteins and Proteomics **1650**(1-2): 128-135.
- Peppas, N. A. and P. A. Buri (1985). "Surface, interfacial and molecular aspects of polymer bioadhesion on soft tissues." Journal of Controlled Release **2**: 257-275.
- Pettersen, E. F., T. D. Goddard, C. C. Huang, G. S. Couch, D. M. Greenblatt, E. C. Meng and T. E. Ferrin (2004). "UCSF Chimera--a visualization system for exploratory research and analysis." J Comput Chem **25**(13): 1605-1612.
- Piotrowska, H., M. Kucinska and M. Murias (2012). "Biological activity of piceatannol: leaving the shadow of resveratrol." Mutat Res **750**(1): 60-82.

- Pizer, R. and L. Babcock (1977). "Mechanism of the complexation of boron acids with catechol and substituted catechols." Inorganic Chemistry **16**(7): 1677-1681.
- Ramsden, C. A. and P. A. Riley (2014). "Tyrosinase: the four oxidation states of the active site and their relevance to enzymatic activation, oxidation and inactivation." Bioorg Med Chem **22**(8): 2388-2395.
- Rolff, M., J. Schottenheim, H. Decker and F. Tuczek (2011). "Copper-O₂ reactivity of tyrosinase models towards external monophenolic substrates: molecular mechanism and comparison with the enzyme." Chem Soc Rev **40**(7): 4077-4098.
- Ros, J. R., J. N. Rodríguez-López and F. García-Cánovas (1993). "Effect of L-ascorbic acid on the monophenolase activity of tyrosinase." Biochemical Journal **295**(Pt 1): 309-312.
- Ross, P. K. and E. I. Solomon (1990). "Electronic structure of peroxide bridged copper dimers of relevance to oxyhemocyanin." Journal of the American Chemical Society **112**(15): 5871-5872.
- Roy, C. K., H. L. Guo, T. L. Sun, A. B. Ihsan, T. Kurokawa, M. Takahata, T. Nonoyama, T. Nakajima and J. P. Gong (2015). "Self-Adjustable Adhesion of Polyampholyte Hydrogels." Advanced materials **27**(45): 7344-7348.
- Ryu, J. H., Y. Lee, W. H. Kong, T. G. Kim, T. G. Park and H. Lee (2011). "Catechol-Functionalized Chitosan/Pluronic Hydrogels for Tissue Adhesives and Hemostatic Materials." Biomacromolecules **12**(7): 2653-2659.

- Söding, J., A. Biegert and A. N. Lupas (2005). "The HHpred interactive server for protein homology detection and structure prediction." Nucleic Acids Research **33**(Web Server issue): W244-W248.
- Salvato, B., M. Santamaria, M. Beltramini, G. Alzuet and L. Casella (1998). "The enzymatic properties of Octopus vulgaris hemocyanin: o-diphenol oxidase activity." Biochemistry **37**(40): 14065-14077.
- Seeger, M., M. Gonzalez, B. Camara, L. Munoz, E. Ponce, L. Mejias, C. Mascayano, Y. Vasquez and S. Sepulveda-Boza (2003). "Biotransformation of natural and synthetic isoflavonoids by two recombinant microbial enzymes." Appl Environ Microbiol **69**(9): 5045-5050.
- Sendovski, M., M. Kanteev, V. S. Ben-Yosef, N. Adir and A. Fishman (2011). "First structures of an active bacterial tyrosinase reveal copper plasticity." J Mol Biol **405**(1): 227-237.
- Sendovski, M., M. Kanteev, V. Shuster Ben-Yosef, N. Adir and A. Fishman (2010). "Crystallization and preliminary X-ray crystallographic analysis of a bacterial tyrosinase from Bacillus megaterium." Acta Crystallogr Sect F Struct Biol Cryst Commun **66**(Pt 9): 1101-1103.
- Shuster Ben-Yosef, V., M. Sendovski and A. Fishman (2010). "Directed evolution of tyrosinase for enhanced monophenolase/diphenolase activity ratio." Enzyme and Microbial Technology **47**(7): 372-376.
- Solem, E., F. Tucek and H. Decker (2016). "Tyrosinase versus Catechol Oxidase: One Asparagine Makes the Difference." Angew Chem Int Ed Engl **55**(8): 2884-2888.

- Solomon, E. I., P. Chen, M. Metz, S.-K. Lee and A. E. Palmer (2001). "Oxygen Binding, Activation, and Reduction to Water by Copper Proteins." Angewandte Chemie International Edition **40**(24): 4570-4590.
- Springsteen, G. and B. Wang (2002). "A detailed examination of boronic acid–diol complexation." Tetrahedron **58**(26): 5291-5300.
- Sudre, G., L. Olanier, Y. Tran, D. Hourdet and C. Creton (2012). "Reversible adhesion between a hydrogel and a polymer brush." Soft Matter **8**(31): 8184-8193.
- Tarkhanova, I. G., M. G. Gantman, A. O. Chizhov and V. V. Smirnov (2010). "Conjugated oxidation of thiols and amines in the presence of copper complexes." Reaction Kinetics, Mechanisms and Catalysis **101**(2): 267-278.
- Teixeira, L. S., J. Feijen, C. A. van Blitterswijk, P. J. Dijkstra and M. Karperien (2012). "Enzyme-catalyzed crosslinkable hydrogels: emerging strategies for tissue engineering." Biomaterials **33**(5): 1281-1290.
- Villarama, C. D. and H. I. Maibach (2005). "Glutathione as a depigmenting agent: an overview." Int J Cosmet Sci **27**(3): 147-153.
- Wada, S., H. Ichikawa and K. Tatum (1995). "Removal of phenols and aromatic amines from wastewater by a combination treatment with tyrosinase and a coagulant." Biotechnol Bioeng **45**(4): 304-309.
- Wada, S., H. Ichikawa and K. Tatum (1993). "Removal of phenols from wastewater by soluble and immobilized tyrosinase." Biotechnol Bioeng **42**(7): 854-858.
- Wang, E., S.-H. Lee and S.-W. Lee (2011). "Elastin-like Polypeptide Based

- Hydroxyapatite Bionanocomposites." Biomacromolecules **12**(3): 672-680.
- Winder, A. J. and H. Harris (1991). "New assays for the tyrosine hydroxylase and dopa oxidase activities of tyrosinase." Eur J Biochem **198**(2): 317-326.
- Wu, Z., F. A. Fernandez-Lima and D. H. Russell (2010). "Amino acid influence on copper binding to peptides: cysteine versus arginine." J Am Soc Mass Spectrom **21**(4): 522-533.
- Xu, D.-Y. and Z. Yang (2013). "Cross-linked tyrosinase aggregates for elimination of phenolic compounds from wastewater." Chemosphere **92**(4): 391-398.
- Yamazaki, S. and S. Itoh (2003). "Kinetic evaluation of phenolase activity of tyrosinase using simplified catalytic reaction system." J Am Chem Soc **125**(43): 13034-13035.
- Yoon, J., S. Fujii and E. I. Solomon (2009). "Geometric and electronic structure differences between the type 3 copper sites of the multicopper oxidases and hemocyanin/tyrosinase." Proceedings of the National Academy of Sciences **106**(16): 6585-6590.
- Yu, L. and J. D. Ding (2008). "Injectable hydrogels as unique biomedical materials." Chemical Society Reviews **37**(8): 1473-1481.
- Zaidi, K. U., A. S. Ali, S. A. Ali and I. Naaz (2014). "Microbial Tyrosinases: Promising Enzymes for Pharmaceutical, Food Bioprocessing, and Environmental Industry." Biochemistry Research International **2014**: 16.
- Zlateva, T., P. Di Muro, B. Salvato and M. Beltramini (1996). "The o-diphenol oxidase activity of arthropod hemocyanin." FEBS Lett **384**(3): 251-254.
- Zor, T. and Z. Selinger (1996). "Linearization of the Bradford protein assay increases its sensitivity: theoretical and experimental studies." Anal

Biochem **236**(2): 302-308.

국문 초록

구리를 조효소로 사용하는 폴리페놀 산화제인 티로시나아제는 멜라닌 합성에 관여하는 주요 효소이며, 박테리아에서 포유류까지 대부분의 생물체에서 찾을 수 있다. 포유동물의 털과 두족류의 먹물 등에서 찾을 수 있는 어두운 색소들이 티로시나아제에 의해 합성된 멜라닌의 대표적인 예가 되겠다. 자연 착색은 페놀형 소분자, 예를 들어 필수 아미노산 중 하나인 L-타이로신으로부터 연속적인 두 번의 산화 반응을 통해 불안정한 퀴논형물질로 전환되는 것을 시작으로, 아민기나 또 다른 페놀형 물질과의 고분자 중합반응에 의해 형성된다. 그러므로, 이 산화 효소에 대한 이전의 연구들은 주로 피부 미백 및 과일 갈변 방지를 목적으로 하는 착색 반응 억제제를 찾는 데 초점이 맞추어 졌다. 반면, 이 효소를 산업적 가치가 있는 촉매로 개발하기 위한 연구는 상대적으로 많이 부족한 실정이다.

본 논문에서는 기능성 카테콜 형 구조 물질 생산과 고분자 가교 반응을 위한 티로시나아제의 연속적 두 산화 반응의 조절 및 그의 응용 기술에 대해 제안하고 있다. 간략히 말하자면, 반응 진행 중 변화하는 세 가지 다른 티로시나아제의 형태를 조절하여, 연속적인 두 산화 반응을 분리하거나 촉진하는 방법을 제시한다. 따라서, 본 연구의 내용은 티로시나아제의 두 가지 다른 산화 반응과 그 응용처에 따라 크게 두 가지 주제로 나눌 수 있다.

첫 번째 주제는 두 연속적 산화 반응 중, 일차 수산화 반응만을 이용하는 기술개발로, 멜라닌 부산물의 생산에 관여하는 이차 산화반응의 선택적 억제 연구에 관한 것이다. 이 첫 번째 연구 주제의 응용처는 기능성 카테콜형 유도체를 생산하기 위한 모노페놀의 위치-선택적 오르토-수산화 반응에 초점을 두고 있다. 이렇게 생산된 카테콜 형 구조 물질은 뛰어난 항산화성, 항알레르기성, 항암 효과를 가지고 있어, 식품 첨가물, 화장품 성분 및 제약 시장에서 높은 가치가 있다. 첫 번째 주제는 이 논문의 제 2장, 3장 및 4장에 걸쳐 기술 되고 있다. 이 세 장들은 티로시나아제의 두 번째 산화반응을 억제하기 위한 반응 경로 설계, 신규 티로시나아제 탐색 및 변이주 제작 등의 내용을 담고 있다.

결론적으로, 오르토-수산화 모노페놀계 식물화학물의 생산을 실험실 규모의 효소 공학으로 시작하여 대량 생산(400L 반응)까지 완성시켰으며, 약 1.2 kg의 오르토-수산화 이소플라본인 3'-ODI와 orobol을 $3.17 \text{ g} \cdot \text{L}^{-1} \cdot \text{h}^{-1}$ 의 생산성으로 합성하였다. 이 반응에 대한 총 수율(전환율 및 회수율 모두 고려)은 99% 이상으로 거의 이론적인 값에 도달했으며, 생성물은 99% 이상의 순도로 매우 순수하게 회수되었다. 또한, 이 방법은 범용적으로 적용될 수 있어, phloretin, resveratrol, naringenin, apigenin, daidzin, polydatin, glycitin, genistin 등과 같은 다양한 페놀계 식물 화학 물질의 오르토-수산화 반응에 적용 가능하다는 것이 증명되었다.

두 번째 주제는 멜라닌 형성에 관여하는 이차 산화 반응의 효율

을 높여 고분자 상 모노페놀 잔기의 산화 반응을 촉진하는 것으로, 고분자 가교 및 중합반응을 유도하는 기술개발에 관한 것이다. 본 연구를 통해 상기 연구 주제는, 생체 고분자 유래 물질로부터 하이드로겔을 제조하고 최소 침습적 치료를 위한 분사/주사 가능 점착성 하이드로겔의 개발로 발전되었다. 이차 산화 반응을 억제하기 위한 이전 장들(제 2장, 3장, 4장)과는 달리, 제 5장과 6장은 고분자의 효소 가교결합을 위한 티로시나아제의 활성 촉진 연구 및 가교 밀도를 높이기 위한 가교제(예, elastin-like polypeptide) 생산 연구가 수반되었다. 티로시나아제의 가교 반응에 관한 선행연구들은 대부분 구매 가능한 *Agaricus bisporus*(버섯) 유래 티로시나아제를 사용하였으며, 버섯 티로시나아제와 고분자 사이의 입체적 장애에 기인하여 낮은 가교 결합력을 보였다.

이전 장들에 대한 연구를 통해, *Streptomyces avermitilis* 유래 티로시나아제는 도움 단백질에 쉽게 붙기 위해 평평한 표면을 갖게 진화됐음을 알았고, 따라서 *S. avermitilis* 유래 티로시나아제가 고분자 가교시 발생하는 입체 장애를 해결하기 위한 해결책으로 제시되었다. 제 5장에서는 *S. avermitilis* 유래 티로시나아제의 가교 반응을 통한 하이드로겔(젤라틴과 히알루론산 바탕)의 제조 방법이 제시되었고, 저장 탄성률(강도)과 점착성이 크게 향상되었음을 확인하였다. 특히 이렇게 개발된 하이드로겔의 점착성은 $21.34 \text{ J} \cdot \text{m}^{-2}$ 로 측정되었으며, 이전에 연구된 홍합 발 단백질을 포함한 catechol-conjugated polymer($0.12 \sim 7 \text{ J} \cdot \text{m}^{-2}$)와 비교 시 세배 이상 향상된 값을 알 수 있었다. 제 6장에서

는 상기 개발된 젤의 가교비율을 높이고 기능성을 부여 하기 위해, 포유류 유래 tropoelastin 모사 elastin-like polypeptide(ELP)를 새로 디자인 하여 도입하였다. 5 mol%의 티로신 잔기가 도입된 ELP를 0.5w% 젤에 포함 시켜 가교 시킨 결과, 두배 이상 향상된 저장탄성(6kPa)을 갖게 되었다.

티로시나아제는 다른 효소들에 비해 상대적으로 안정적이고 빠른 산화 반응을 수반하고 있어 산업적 가치가 매우 높다고 판단된다. 하지만, 멜라닌 부산물 생성, 분리되지 않은 두 산화 반응, 제한된 가용성에 기인하여 실질적인 산업적 이용이 제한되고 있는 것이 현실이다. 본 논문은 티로시나아제의 두 산화 반응과 유래에 따른 구조 분석을 깊이 있게 다루고 있으며, 상기 제시된 문제점을 효과적으로 해결하는 방안을 제시하고 있다. 또한 일차 수산화 반응과 이차 산화 반응의 성공적인 예시를 제공하고 있으므로, 본 연구를 통해 개발된 티로시나아제의 반응법 및 신규 티로시나아제가 위치 특이적 수산화/산화 반응의 산업적 응용에 범용적으로 적용될 수 있다고 판단된다.

주요어: 티로시나아제, 위치특이적 수산화반응, 오르토-수산화반응, 수산화 이소플라본, 3' -오디아미, 오로볼, 하이드로겔, 효소가교, 멜라닌합성 억제

학번: 2012-23296

